



University of
Salford
MANCHESTER

Behaviour of Single Batter Piles and Pile Groups Under Lateral Soil Movement in Sand

Osamah Salim Abdulkareem Al-Salih

School of Computing, Science & Engineering
University of Salford
UK

Submitted in Partial fulfilment of the Requirements of
Degree of Doctor of Philosophy

2019

Table of Contents

Table of Contents	i
List of Figures.....	vi
List of Tables	xii
List of Publications	xiii
Acknowledgements	xiv
Declaration.....	xv
Abbreviations	xvi
Dedication	xxi
Abstract.....	xxii
Chapter 1 Introduction.....	1
1.1 Background	1
1.2 Batter piles.....	4
1.3 Problem statement	5
1.4 Aim and objectives.....	6
1.5 Contribution to knowledge.....	7
1.6 Outline of thesis	8
Chapter 2 Literature Review	9
2.1 Introduction	9
2.2 Piles subjected to horizontal soil movement	9
2.2.1 Experimental studies.....	9
2.2.2 Theoretical studies	23
2.3 Research review on batter pile	29
2.3.1 Experimental tests.....	29
2.3.2 Analytical studies.....	36
2.4 Summary	39
Chapter 3 Experimental Apparatus and Test Procedures	43
3.1 Introduction	43

3.2	Experimental apparatus	44
3.3	Experimental testing box.....	44
3.4	Design of the testing box.....	44
3.5	Lateral loading system	46
3.6	Sand properties.....	47
3.7	Model piles.....	47
3.8	Data acquisition system.....	50
3.8.1	Strain gauges:.....	50
3.8.2	LVDT (Linear variable differential transformer)	50
3.8.3	Electronic tiltmeter.....	50
3.8.4	Load cell.....	51
3.8.5	Data logger.....	51
3.9	Calibration of piles	51
3.10	Model pile cap	53
3.11	Soil preparation.....	55
3.12	Pile installation	56
3.13	Experiment procedure.....	60
3.14	Sign convention	61
3.15	Data analysis and processing	63
3.15.1	Numerical differentiation.....	63
3.15.2	Numerical integration	64
3.16	Spreadsheet program for data processing.....	65
3.17	Testing programme.....	65
3.18	Summary.....	68
Chapter 4 Experimental Results of Single Batter Pile Tests.....		69
4.1	Introduction	69
4.2	Repeatability.....	71
4.3	Tests for single piles subjected to rectangular soil movement profiles.....	72

4.3.1	Free-head tests on a 16 mm diameter pile (RSF16, 0°)	72
4.3.2	Influence of embedded length	75
4.3.3	Effect of batter angle (RSF16, β)	79
4.3.4	Limiting soil pressure profile	85
4.3.5	Effect of pile location in the testing box (boundary effect)	90
4.3.6	Influence of pile head fixity (RSL16, β)	94
4.3.7	Influence of pile diameter (RSF20, β) & (RSF25, β)	95
4.4	Tests for single batter piles subjected to triangular soil movement profile (TSF16, β)	99
4.4.1	Experimental results with density (γ_s) = 14.7 kN/m ³	99
4.4.2	Experimental results with density (γ_s) = 15.2 kN/m ³	100
4.4.3	Experimental results with density (γ_s) = 15.7 kN/m ³	101
4.5	Summary of single piles subjected to triangular soil movement	102
4.6	Comparison of pile responses obtained from different soil movement profiles (RSF16, 0°) & (TSF16, 0°)	103
4.6.1	Tests with $\beta = 0^\circ$	103
4.7	Summary	105
4.7.1	Rectangular soil movement profile	105
4.7.2	Triangular soil movement profile	106
Chapter 5 Experimental Results of Pile Group Tests		107
5.1	Introduction	107
5.2	Setup of pile group testing programme	109
5.3	Effect of pile groups arrangement	111
5.3.1	Results for (VVL) batter pile group configuration test	111
5.3.2	Results for (VBL, BVL and BBL) configuration tests	115
5.4	Effects of pile spacing	121
5.5	Effect of pile cap	124
5.6	Group effect	125

5.6.1	Group factors	125
5.6.2	Effect of pile groups arrangement on the group factors	125
5.6.3	Effect of pile spacing on the group factors	126
5.6.4	Effect of pile cap on the group factors.....	126
5.6.5	Group factors from previous study	128
5.7	Summary	129
Chapter 6 Three-Dimensional Finite Element Analysis.....		130
6.1	Introduction.....	130
6.2	Description of the computer program	130
6.3	PLAXIS 3D Introductory limitations.....	131
6.4	PLAXIS embedded pile	132
6.5	Pile-soil interaction	133
6.6	The influence of coefficient R_{inter} on the behaviour of the pile-soil interaction 137	
6.7	Skin resistance and base resistance (pile bearing capacity)	139
6.8	Finite element simulation of test results.....	141
6.8.1	Material modelling.....	141
6.8.2	Numerical analysis for standard test RSF16,0°.....	144
6.8.3	Numerical results for standard test RSF16,0°	152
6.8.4	Numerical analysis of test RSL16, 0°	154
6.8.5	Numerical analysis of test (RSF20, 0°) and (RSF25, 0°).....	155
6.9	Numerical analysis for the batter pile group tests.....	156
6.9.1	Numerical analysis of test VVL.....	156
6.9.2	Numerical analysis of test BBL	161
6.10	Parametric studies.....	164
6.10.1	Effect of Young's modulus.....	165
6.10.2	Effect of dilatancy angle of sand	166
6.10.3	Effect of soil friction angle	167

6.10.4	Effect of strength reduction factor (R_{inter})	168
6.10.5	Effect of pile cross-sectional.....	170
6.10.6	Effect of L_m/L_s on batter pile response with different values of batter angles (β).....	171
6.11	Limitations of PLAXIS program.....	173
6.12	Summary.....	174
Chapter 7	Conclusions and Recommendations for Future Work.....	176
7.1	Conclusions	176
7.1.1	Experimental work.....	176
7.1.2	Numerical work	179
7.2	Suggestions for future research	179
7.3	Concluding remarks	180
References		182
Appendix A	Pile Group Test Results.....	192
Appendix B	Pile Group Test Results.....	235

List of Figures

Fig. 1.1 Schematic illustration of lateral loading of piles: (a) Active-pile-loading; (b) Passive pile-loading (Cubrinovski & Ishihara, 2007).....	1
Fig. 1.2 Piles subjected to lateral forces resulting from soil movement (Miao, 2005)..	2
Fig. 1.3 Types of batter piles (Rao, 1994)	4
Fig. 1.4 A batter pile undergoing lateral soil movement	5
Fig. 1.5 Collapse of 13-storey building in China (Khudeira, 2010)	6
Fig. 2.1 Schematic view of the test equipment (Matsui et al., 1982).....	10
Fig. 2.2 Relationship between lateral force acting on a pile and soil displacement (Matsui et al., 1982).....	10
Fig. 2.3 Overview of experimental apparatus (Poulos et al., 1995).....	11
Fig. 2.4 Large-scale laminar shear box design (Tsuchiya et al, 2001)	12
Fig. 2.5 Model test setup (Pan et al., 2002a).....	13
Fig. 2.6 Configuration of centrifuge model (Leung et al., 2003).....	14
Fig. 2.7 Procedure of single pile installation and loading (Miao, 2005)	15
Fig. 2.8 Normalised p-y curve for Test S-1 and S-2 (Miao, 2005).....	15
Fig. 2.9 Normalised p-y curves for Test G-1 (Sh = 3D) and G-2 (Sh = 6D) (Miao, 2005)	16
Fig. 2.10 Effects of number pf piles on group factor F_m (Miao, 2005)	16
Fig. 2.11 Tests on piles subjected to a uniform lateral soil movement together with different axial load (Guo and Ghee, 2006)	17
Fig. 2.12 Testing apparatus for the model pile group tests (Guo and Ghee, 2006)	17
Fig. 2.13 Response of pile A and B (Group 1x2) (Guo and Ghee, 2006)	18
Fig. 2.14 Test setup (Lee and Chiang, 2007).....	18
Fig. 2.15 Load test setup (White et al., 2008).....	19
Fig. 2.16 The geometry of pile group investigated (Ersoy and Yildirim, 2014)	20
Fig. 2.17 Measured lateral displacement versus depth (adopted from Kalteziotis et al., 1993)	21
Fig. 2.18 Measured lateral soil movement profiles (Ong et al., 2003)	22
Fig. 2.19 Averaged measured pile and soil displacements with time (Smethurst and Powrie, 2007).....	23
Fig. 2.20 Method of De Beer and Wallays (De Beer and Wallays, 1972).....	24

Fig. 2.21 Stabilising piles in a row through plastically deforming ground (Ito and Matsui, 1975)	24
Fig. 2.22 Failure modes of rigid piles (Viggiani, 1981)	26
Fig. 2.23 Failure modes of flexible piles (Viggiani, 1981).....	26
Fig. 2.24 Schematic view of the in-flight pile installation equipment for single batter pile tests in the centrifuge (Zhang et al., 1999).....	32
Fig. 2.25 Influence of pile batter on pile resistance (Zhang et al., 1999)	33
Fig. 2.26 Experimental box (Manoppo, 2010).....	34
Fig. 2.27 Schematic sketch of experimental set up for cyclic lateral load tests (Prabha and Boominathan, 2010).....	34
Fig. 2.28 Experimental setup (Singh and Arora, 2017)	36
Fig. 2.29 Comparison of lateral load-deflection curves of batter pile at different batter angles (Rajashree and Sitharam, 2001).....	37
Fig. 2.30 Comparison of lateral load-deflection curve for different batter angles at n = 600 cycles (Rajashree and Sitharam, 2001).....	37
Fig. 3.1 Schematic diagram of testing box (a) Elevation view and (b) Top view	45
Fig. 3.2 Testing box	46
Fig. 3.3 Triangular and rectangular loading blocks	47
Fig. 3.4 Motor and screw jack	47
Fig. 3.5 Gradation curve of the sand.....	48
Fig. 3.6 Direct shear box test	48
Fig. 3.7 Schematic diagram of a pile subjected to rectangular and triangular loading block.....	49
Fig. 3.8 LVDT.....	51
Fig. 3.9 Electronic tiltmeter	51
Fig. 3.10 Load cell	51
Fig. 3.11 Data logger	51
Fig. 3.12 Strain gauges calibration	53
Fig. 3.13 Setup for Strain gauges calibration.....	53
Fig. 3.14 The details and dimensions of the pile cap.....	55
Fig. 3.15 Wooden tamping hammer	56
Fig. 3.16 The installation guide of batter pile.....	57
Fig. 3.17 Angle meter	58
Fig. 3.18 Final view of the instrumented batter pile to testing (free-head pile test)....	58

Fig. 3.19 Details of aluminium frame used for a fixed-head pile test	59
Fig. 3.20 Final view of the instrumented pile prior to testing (fixed-head pile test) ...	59
Fig. 3.21 Testing procedure of single pile test.....	60
Fig. 3.22 Pile behaviour based on beam theory (Qin, 2010)	62
Fig. 3.23 Numerical integration for calculating pile rotation and displacement	65
Fig. 3.24 Batter pile setup for lateral soil movements	67
Fig. 3.25 Types of 2x1 pile group configurations.....	67
Fig. 4.1 Bending moment distributions from the "standard" test, $\beta= 0^\circ$	73
Fig. 4.2 Response of the 16 mm diameter pile in terms of shear force, soil reaction, pile rotation and pile deflection at $L_m/L_s = 150/150$	74
Fig. 4.3 The effect of L_s on bending moment for a fixed L_m (150 mm)	76
Fig. 4.4 The effect of L_m on bending moment for a fixed L_s (150 mm)	76
Fig. 4.5 The relationship between maximum bending moment and dimensionless embedded length (L_e).....	77
Fig. 4.6 The relationship between normalised maximum bending moment and dimensionless embedded length (L_e)	79
Fig. 4.7 Bending moment profiles for different batter angles (β).....	80
Fig. 4.8 Bending moment of batter pile for different values of (β) and (U_x), $d_{max} = 200$ mm	81
Fig. 4.9 Influence of pile batter angle on M_{max} of piles with different U_x	82
Fig. 4.10 Shear force profiles with different values of β , $U_x = 25$ mm	84
Fig. 4.11 Soil reaction profiles with different values of β , $U_x = 25$ mm	84
Fig. 4.12 Pile rotation profile with different values of β , $U_x = 25$ mm.....	84
Fig. 4.13 Pile deflection profile with different β , $U_x = 25$ mm.....	84
Fig. 4.14 Maximum bending moment (M_{max}) against maximum shear force (F_{max}) relationship for single batter piles tests conducted at ratios of $L_m/L_s=150/150$...	85
Fig. 4.15 Typical soil reaction profiles showing the p_{max} in moving (L_m) and stable (L_s) layer	86
Fig. 4.16 Maximum soil pressure in L_m for tests with $L_m/L_s = 150/150$, $U_x =30$ mm.	87
Fig. 4.17 Normalised ($P - U_x$) curve for a single batter piles embedded in sand (moving layer).....	88
Fig. 4.18 Maximum soil pressure in L_s for tests with $L_m/L_s = 150/150$, $U_x =30$ mm ..	89
Fig. 4.19 Normalised "P - U_x " curve for a single batter piles embedded in sand (stable layer)	89

Fig. 4.20 Location of a model batter pile in the testing box	91
Fig. 4.21 Responses of the piles tested at different locations in the testing box, $\beta=0^\circ$	92
Fig. 4.22 Responses of the piles tested at different locations in the testing box, ($\beta=$ +10°).....	93
Fig. 4.23 M_{\max} vs (U_x) with different values of (d_s) at $\beta = 0^\circ$ and $+10^\circ$	93
Fig. 4.24 M_{\max} vs d_s with two values of β	94
Fig. 4.25 Bending moment profile for a fixed-head pile along the pile shaft, $\beta= 0^\circ$...	95
Fig. 4.26 Bending moment profile for a fixed and free head batter pile with different values of β , $U_x = 25$ mm	95
Fig. 4.27 Bending moment profiles of 16, 20 and 25 mm diameter piles	96
Fig. 4.28 M_{\max} against pile diameter at different values of (β).....	97
Fig. 4.29 Normalised M_{\max} vs pile diameter, $\beta = 0^\circ$	98
Fig. 4.30 M_{\max} vs pile diameter with different values of β	98
Fig. 4.31 Pile head deflection vs soil displacement (U_x).....	98
Fig. 4.32 Responses of batter piles subjected to triangular soil movement profile with different values of β , $\gamma_s = 14.7$ kN/m ³	100
Fig. 4.33 Responses of batter piles subjected to triangular soil movement profile with different values of β , $\gamma_s = 15.2$ kN/m ³	101
Fig. 4.34 Responses of batter piles subjected to triangular soil movement profile with different values of β , $\gamma_s = 15.7$ kN/m ³	102
Fig. 4.35 M_{\max} vs γ (kN/m ³) with different values of β , $U_x= 25$ mm	103
Fig. 4.36 M_{\max} vs β with different values of sand densities, $U_x= 25$ mm.....	103
Fig. 4.37 Responses batter pile subjected to two types soil movement profiles.....	104
Fig. 5.1 Schematic diagram showing group test setting up	109
Fig. 5.2 The final view of the pile group prior to testing with different configurations	110
Fig. 5.3 Measured moments at each strain gauge during test	111
Fig. 5.4 Bending moment profiles, test (VVL configuration)	112
Fig. 5.5 Shear force profiles, test (VVL configuration).....	113
Fig. 5.6 Soil reaction profiles, test (VVL configuration).....	114
Fig. 5.7 Rotation profiles, test (VVL configuration)	114
Fig. 5.8 Deflection profiles, test (VVL configuration)	115
Fig. 5.9 Moment profiles for (2×1) batter pile groups with different configurations	117

Fig. 5.10 Shear force profiles for (2 × 1) batter pile groups with different configurations	117
Fig. 5.11 Soil reaction profiles for (2 × 1) batter pile groups with different configurations	118
Fig. 5.12 Rotation profiles for (2 × 1) batter pile groups with different configurations	118
Fig. 5.13 Deflection profiles for (2 × 1) batter pile groups with different configurations	119
Fig. 5.14 M_{max} for capped-head two-piles with different configurations	120
Fig. 5.15 Cap displacement versus box displacement for (2 × 1) batter pile groups with different configurations.....	120
Fig. 5.16 The effect of pile spacing on the pile response of 2×1 pile group (BVL) ..	123
Fig. 5.17 Cap displacement versus box displacement at different values of (S), for BVL configuration and $\beta = -10^\circ$	123
Fig. 5.18 Bending moments for free single vertical pile (standard test), free and capped two-batter pile, (BVF & BVL)	124
Fig. 6.1. Schematic of embedded pile in 3D mesh and elastic zone around embedded pile (Brinkgreve et al., 2013)	133
Fig. 6.2 Embedded pile element denoted by the solid line within a 10-node tetrahedral soil element (PLAXIS 3D, 2013).....	134
Fig. 6.3 Shear resistance and tip resistance (PLAXIS 3D, 2013)	135
Fig. 6.4 Node model for the pile-soil interaction (Dao, 2011)	138
Fig. 6.5 3D geometry and boundary conditions for standard test.....	145
Fig. 6.6 Typical 3D soil element (10-Node Tetrahedrons) used in the model (PLAXIS 3D Reference Manual, 2013).....	147
Fig. 6.7 Different densities of mesh coarseness generated in PAXIS 3D.....	149
Fig. 6.8 The effect of mesh density on the pile response.....	151
Fig. 6.9 Predicted and measured bending moments for the standard single vertical pile test (RSF16, 0°).....	152
Fig. 6.10 Predicted and measured pile responses for the standard test (RSF16, 0°)..	153
Fig. 6.11 Predicted and measured bending moments for the fixed -headed single vertical pile test	154
Fig. 6.12 Predicted and measured bending moments for 20 mm and 25 mm diameter single vertical pile tests	155

Fig. 6.13 The geometry of a 3D FEM analysis for test VVL	157
Fig. 6.14 PLAXIS 3D mesh before and after FEM analysis	158
Fig. 6.15 Visualization of pile responses at the end of analysis, $U_x = 30$ mm.....	159
Fig. 6.16 Measured versus predicted piles responses of test VVL at $U_x = 30$ mm, s=3D.....	161
Fig. 6.17 The geometry of a 3D FEM analysis for test BBL, $\beta = \pm 10^\circ$	162
Fig. 6.18 Measured Vs. predicted piles responses of test BBL ($\beta = \pm 10^\circ$) at $U_x = 30$ mm, s=3D.....	164
Fig. 6.19 The effect of Young's modulus on the pile response	166
Fig. 6.20 The effect of dilatancy angle of sand on the pile response.....	167
Fig. 6.21 The effect of soil friction angle on the pile response	168
Fig. 6.22 Effect of strength reduction factor (R_{inter}) on the pile response.....	169
Fig. 6.23 Effect of pile cross-sectional on the pile response	170
Fig. 6.24 Response of the 16 mm diameter pile with different L_m/L_s ratio	172
Fig. 6.25 Variation of maximum bending moment with L_m/L_s for different values of soil displacement at: (a) $\beta = 0^\circ$, (b) $\beta = +10^\circ$, (c) $\beta = +20^\circ$, (d) $\beta = -10^\circ$, (e) $\beta = -$ 20°	173

List of Tables

Table 2.1 Summary of previous studies on Piles subjected to horizontal soil movement and batter piles under lateral loading	41
Table 3.1 Properties of the model sand.....	49
Table 3.2 Pile dimensions and material properties	50
Table 4.1 Tests conducted on single batter and vertical piles.....	70
Table 4.2 Effect of error in test data on M_{max}	71
Table 4.3 Details of each test on a single free-head pile of 16 mm diameter.....	75
Table 4.4 Maximum bending moments from test series 1 and 2.....	77
Table 4.5 Comparisons of different behaviours of single vertical and batter piles	82
Table 4.6 Tests conducted to study the boundary effect of the testing box.....	90
Table 5.1 Tests conducted on piles in a group.....	108
Table 5.2 Summary of group factors Pile	127
Table 5.3 Summary of group factors from previous study	128
Table 6.1 Values for R_{inter} proposed by Waterman (2006)	138
Table 6.2 Values of proportional factor (m), (Poulos, 1989).....	143
Table 6.3 Surface boundary fixities for moving ground.....	145
Table 6.4 Sand soil properties in PLAXIS 3D.....	146
Table 6.5 Pile properties in PLAXIS 3D	146
Table 6.6 Calculation phases	148
Table 6.7 Results for different densities of mesh generation.....	150
Table 6.8 Summary of pile cap input parameters used in PLAXIS 3D.....	156
Table 6.9 Different sand properties used in parametric study	165
Table 6.10 PLAXIS 3D models with ($\beta = 0^\circ, \pm 10^\circ$ and $\pm 20^\circ$) at different ratio of L_m/L_s Moving.....	171

List of Publications

Journal papers

Osamah Al-Salih & Sabbagh, T. T. (2018). Model tests on single batter piles subjected to lateral soil movement. *Research Journal of Applied Sciences, Engineering and Technology* 16(1), 24-29.

Toma Sabbagh, T., Al-Salih, O., & Al-Abboodi, I. (2019). Experimental investigation of batter pile groups behaviour subjected to lateral soil movement in sand. *International Journal of Geotechnical Engineering*, 1-12.

Conference papers

Osamah Al-Salih, Sabbagh, T. T. & Wisam Alawdi. (2018). Experimental investigation of single batter pile behaviour subjected to lateral soil movement. 2nd International Conference on Structural and Civil Engineering (ICSCE), University of Lisbon, Portugal, September 26-28, 2018.



Paper under consideration

Osamah Al-Salih & Sabbagh, T. T. (Effect of Lateral Soil Movement on Batter Pile Groups in Sand with different configurations). *International Journal of Geotechnical Engineering*.

Acknowledgements

I would like thank Allah (God) for giving me the patience, the knowledge and the strength to finish this work.

My deepest gratitude goes to my supervisor, Dr. Tahsin Toma Sabbagh for his for his support, encouragement and trust shown to me during the course of this study. His valuable effort and time dedicated to this research are appreciated. Without him, the thesis progress would have been more difficult.

The research scholarship and financial support granted by the Iraqi Ministry of Higher Education and Scientific Research and their representative Iraqi Cultural Attaché for offering this opportunity to finish my PhD here in the UK, and to make this research a reality and success are acknowledged. I also wish to thank The University of Basrah and The College of Engineering for providing this scholarship.

Sincere thanks are also extended to the technicians of the Soil Mechanic Laboratory especially Mr. Philip Latham and Mr. Anthony Burrage. Also, I would like to thank the School of computing, science and engineering, Slaford University, for their help and support during my PhD journey.

At the same time, I would like to thank Dr. Ihsan Qasim Al-abboodi for his invaluable assistance in conducting the experiments. Also, many thanks go to my friends, postgraduate students, now some of them graduated, Dr. Ammar Jasim, Mr. Wesam Abed Ali, Dr. Adel Ahmed and Dr. Jawad Abed for making this journey of a lifetime more exciting, smooth, and meaningful.

Last but definitely not least. I would like to thank, my father, and in loving memory of my mother, and my brothers. Special thanks to my wife Agharid, my sons Mustafa, Aliridha, Mujtaba and my beautiful daughter Fatima. This research won't be completed without their love and support from such a great family.

Osamah Alsalih

Declaration

This thesis is submitted to the University of Salford rules and regulations for the award of a PhD degree by research. While the research was in progress, some research findings were published in refereed journals papers prior to this submission.

The researcher declares that no portion of the work referred to in this thesis has been submitted in support of an application for another degree of qualification of this, or any other university or institution of learning.

Osamah Salim Abdulkareem Al-Salih

Abbreviations

A_f	effective surface area of the pile shaft
A_p	area of pile
B_{max}	maximum base resistance
BB	Both - Batter
BS	British Standard
BV	Batter -Vertical
c	cohesion of soil
C_c	coefficient of curvature
c_{inter}	cohesion of the embedded interface which is linked to the strength properties of the adjacent soil.
C_u	coefficient of uniformity
c_u	undrained shear strength of the soil
D	outer diameter of the pile cross section
D_i	inner diameter of the pile cross section
D_{10}	effective size
D_2	edge to edge spacing between two piles
D_{50}	mean grain size
D_r	sand relative density
ds	distance between the pile location and shear box boundary
E_{cap}	pile cap Young's modulus
E_p	Young's modulus of the pile
$E_p Z_p$	conversion factor
E_s	soil Young's modulus
q_f	unit friction resistance at any depth z
f_i	shear force at point i

F_m	group factor in terms of maximum bending moment
F_p	group factor in terms of ultimate soil pressure
F_s	factor of safety
F_{tip}	the force at the pile tip
I_p	moment of inertia of the pile
$E_p I_p$	for pile bending rigidity
$[K]^{skin}$	material stiffness matrix of the interface
K	effective earth pressure coefficient
K_n and K_t	elastic normal stiffness of the embedded interface element in horizontal directions
K_o	lateral earth pressure coefficient at rest
K_p	coefficient of passive earth pressure
K_s	elastic shear stiffness of the embedded interface element
K_{tip}	the material stiffness matrix of the spring element at the pile tip
L_m	depth of moving layer
L_s	depth of stable layer depth
L_e	pile embedded length ($= L_s + L_m$)
L_p	Pile length
LVDT	linear variable differential transformer
m	proportional factor of $E_s = mz$ relationship
M	bending moment of the pile at the strain gauge locations
M_{+max}	maximum positive bending moment
m_i	bending moment at point i
M_{max}	maximum absolute bending moment
M_{-max}	maximum negative bending moment
$M_{g(max)}$	absolute value of maximum bending moment for a pile in a group

$M_{sv(max)}$	maximum bending moment of the 'standard' single vertical pile
M_y	Yield bending moment
N_p	the lateral capacity factor
N_{pile}	pile bearing capacity
N_q	bearing capacity factor
p_i	soil reaction (lateral force per unit length) at point i
p_{max}	maximum soil reaction
P_{max}	maximum soil pressure, (= maximum soil reaction / pile diameter)
P_p	Rankine's passive earth pressure
p_{pile}	perimeter of the pile section
P_u	ultimate soil pressure
P_{ui}	ultimate soil pressure P_u for a pile in the group
P_{us}	ultimate soil pressure P_u for a single isolated vertical pile
q'	effective vertical stress at the level of pile tip
R_{inter}	strength reduction factor for the interface
Q_f	pile skin resistance
q_f	unit friction capacity at any depth
q_p	unit base resistance at pile tip
R^2	coefficient of determination
R_{inter}	strength reduction factor
rv	relative variation (%)
r_2 & r_1	first and second measured maximum bending moment of two tests
s	centre to centre spacing between two piles
t	wall thickness of pile
$\{t\}^{skin}$	force at the integration points
t_s	shear stress due to friction between pile and the soil

t_t and t_n	normal stress due to lateral displacement of the pile
T_{\max}	shear resistance along the pile
$T_{\text{bot},\max}$	maximum skin resistance at pile tip
$T_{\text{top},\max}$	maximum skin resistance at pile head
U_x	box displacement
u_s^p	pile movement in axial direction
u_n^p, u_t^p	pile movement in lateral direction
u_s^s	soil movement in axial direction
u_n^s, u_t^s	soil movement in lateral direction
$u_{\text{tip}}^p - u_{\text{tip}}^s$	the relative displacement vector between the soil and the pile at the foot
VB	Vertical-Batter
VV	Vertical-Vertical
y_1	pile cap deflection
y_i	pile deflection at point i
z	depth below soil surface
Z_p	elastic section modulus of the pile cross section
α	coefficient of linear fit of $M_{\max} = \alpha F_{\max}$ relationship
γ_{cap}	Pile cap unit weight
γ_p	pile unit weight
γ_s	soil unit weight
γ_{sat}	saturated unit weight of soil
γ_{unsat}	unsaturated unit weight of soil
\emptyset_{inter}	soil–pile friction angle
$\{\Delta u_{\text{rel}}\}^{\text{skin}}$	relative displacement vector between the soil and the pile
Δz	subintervals for dividing the pile length
δ_i	pile displacement at point i

δ_0	pile displacement at soil surface
δ_{tip}	pile displacement at soil surface
ε	measured strain
\emptyset	angle of internal friction of soil
θ_i	pile rotation at point i
θ_0	rotation of the pile at soil surface
θ_{tip}	pile rotation at soil surface
ν_s	soil Poisson's ratio
σ	flexural stress
ψ	soil dilatancy angle

Dedication

Dedication

I dedicate this piece of research to soul my father, brother and sister, to mother for her blessing, brothers, wife and my lovely kids Mustafa, Fatimah, Aliridha and Mujtaba.

Abstract

Piles are commonly subjected to induced loads from nearby construction activities such as approach embankments, excavation, tunnelling and moving slopes. To better understand the mechanism of this complicated soil-pile interaction problem, a comprehensive experimental and numerical program were carried out to investigate the behaviour of batter pile foundations embedded in sandy soil when subjected to lateral soil movements.

In the experimental work, a series of model tests on single batter pile subjected to a soil movement profile (triangular or rectangular) was performed to study the effect of a number of parameters on the behaviour of single batter pile. In addition, the lateral responses were investigated on a group of batter piles of different configurations: Batter-Vertical (VB), Vertical-Batter (VB), Both Vertical (VV) and Both Batter (BB). The effect of centre to centre pile spacing (S) was also investigated. The results from the single pile tests show that, the maximum bending moment induced in a single batter pile was found to be dependent on, among other factors, batter angle, pile embedded length, distance between the batter piles location and soil movement source, pile diameter, profile of soil movement, sand density and the pile head fixity condition. Regardless of the value of batter angle, the bending moment profile was a single curvature. The largest value of maximum bending moment was observed for the negative batter pile while vertical pile results showed lower value, however, the lowest value was recorded for the positive batter pile. For the pile group tests; the behaviour of the individual piles in a group are significantly affected by the pile spacing, pile head conditions and the pile group arrangement. It was also shown that the group effect might either increase or decrease the maximum bending moment, depending on the above-mentioned influencing factors.

Numerical analyses with the three-dimensional finite element method were performed using PLAXIS 3D software with "embedded pile" feature to predict and compare the results from the single batter piles and pile groups tests in sand. In all the predictions, the numerical analysis was shown to be able to predict the experimental results reasonably well. Result of parametric studies indicated that Young's modulus and friction angle were among the parameters that had the greater effect on batter pile

behaviour, in particular the lateral displacement and bending moments of piles. Other less influential parameters were the interface properties between the pile and the soil, dilation angle, the density of finite element mesh and the pile cross-sectional shapes.

In summary, through the numerical and experimental outcomes, it is hoped that the current study provides an important understanding and clear indications of how both soil and pile parameters are affecting the behaviour of batter pile and batter pile groups subjected to lateral soil movements.

Chapter 1

Introduction

1.1 Background

Pile foundations can be subjected to direct external lateral loads applied at the head of the pile or pile cap, for example wind loading on a high-rise building or piles in bridge abutments. This type of loading is called “active” loading and the piles subjected to these loadings are known as “active piles” (Fig. 1.1a). However, there are many cases piles are subjected to indirect loads due to the lateral movement of the surrounding ground. This type of loading is called “passive” loading, and piles subjected to these loadings are called “passive piles” (Fig. 1.1b).

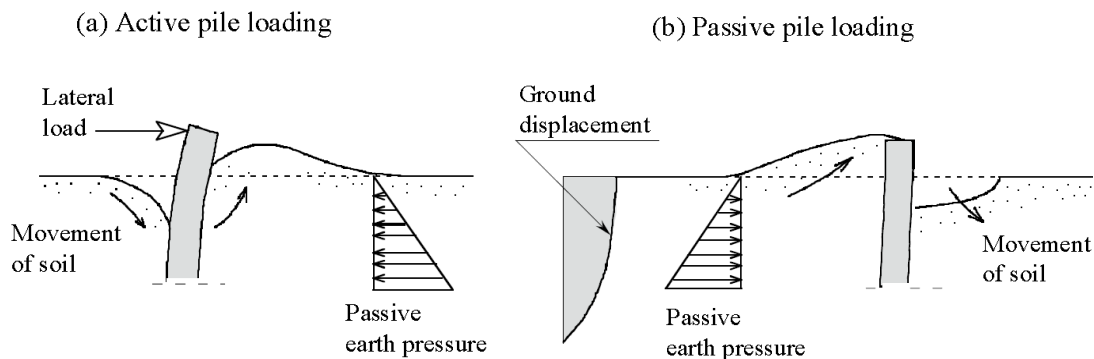
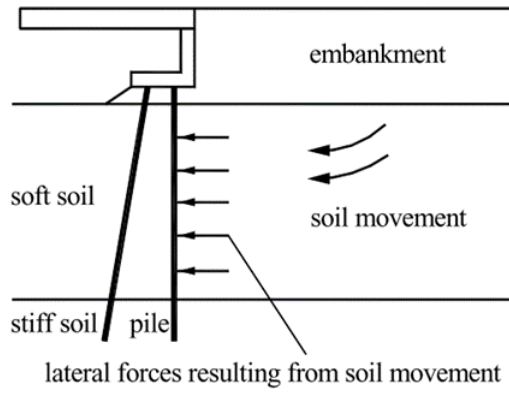
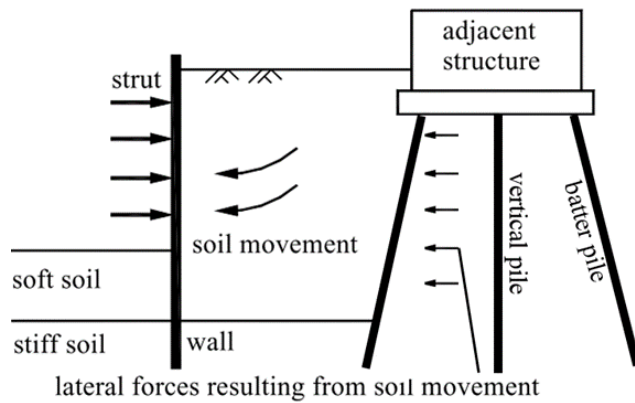


Fig. 1.1 Schematic illustration of lateral loading of piles: (a) Active-pile-loading; (b) Passive pile-loading (Cubrinovski & Ishihara, 2007)

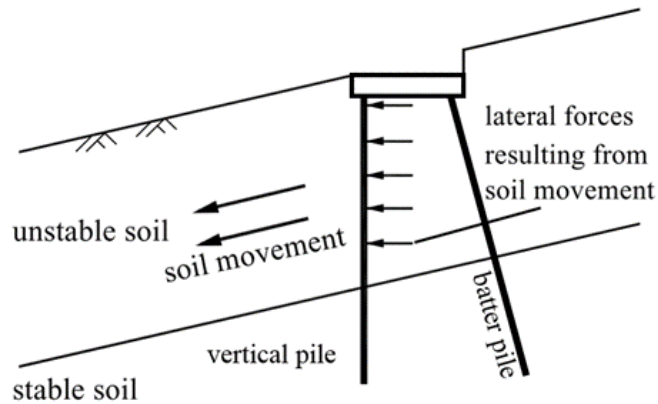
In many cases piles are not designed primarily to sustain lateral soil movements although such movements may occur, examples being piles supporting bridge abutments adjacent to approach embankments, existing pile foundations adjacent to pile driving or excavations, and pile foundations in moving slopes. On the other hand, piles may be purposely designed to restrain soil movements when they are used to stabilize unstable slopes or potential landslides. Fig. 1.2 shows some typical cases for piles subjected to lateral forces resulting from soil movements.



(a) Embankment



(b) Excavation



(c) Unstable slope

Fig. 1.2 Piles subjected to lateral forces resulting from soil movement (Miao, 2005)

A number of methods have been developed for analysing laterally loaded piles. Generally, they can be classified into one or more of the following categories: analytical solutions (Guo and Lee, 2001); the load transfer approach ($p \sim y$ curves) (Reese and Van Impe, 2001); boundary element methods (Poulos and Davis, 1980); and finite difference and finite element methods (Randolph, 1981). Recent analyses have tended to concentrate on numerical methods, in particular, the three-dimensional finite element methods. The importance of incorporating interface elements to simulate possible slippage and separation between the pile and soil, and capturing the soil nonlinearity using advanced models, has been widely recognized (Karthigeyan et al., 2006; Gatmiri et al, 2011; Byrne et al, 2015).

Predicting the behaviour of piles subjected to lateral loading arising from horizontal soil movement is a more complicated issue as free-soil movement cannot be easily and accurately estimated. Great efforts have been made to clarify the responses of vertical piles under different situations through physical modelling, and analytical and numerical analysis. Among these are studies on:

- piles supporting bridge abutments or piles adjacent to an embankment (De Beer and Wallays, 1972; Springman et al., 1994; Bransby and Springman, 1997; Ellis and Springman, 2001; Jeong et al. 2004; Karim (2013);
- piles used for slope stabilisation (Ito and Matsui, 1975; Ito et al., 1982; Viggiani, 1981; Poulos, 1973, 1995; Chow, 1996; Cai and Ugai, 2003);
- single piles and pile groups subjected to excavation-induced soil movements in sand (Finno et al., 1991; Leung et al., 2000, 2003) and clay (Leung et al., 2003; Ong et al., 2004; Ilamparuthi and Madhumathi 2011; Ng et al. (2017);
- lateral load and its effects on pile foundations through centrifuge experiments (Lee and Chiang, 2007; Choudhury et al., 2008; Yoon and Ellis, 2009); and
- full-scale tests (De Beer, 1977; Finno et al. 1991; Ashford et al., 2006; Juirnarongrit and Ashford et al., 2006; Smethurst and Powrie, 2007).

1.2 Batter piles

Batter or inclined piles are piles driven at an angle with the vertical to resist large lateral force from winds, water waves, soil pressures, and impacts (Meyerhof & Yalcin, 1993). Their distinct advantage over vertical piles is that they transmit the applied lateral loads partly in axial compression and/or tension rather than only through shear and bending, while vertical piles carry lateral loads through shear and bending. Thus, batter piles offer larger stiffness and lateral bearing capacity than vertical piles of the same dimensions and material (Giannakou et al. 2010). Accordingly, batter piles are usually used as foundations for bridge piers and abutments, oil production platforms, under tall chimneys, anchored bulkheads, high retaining walls, high rise buildings, high-pile wharfs and transmission towers.

According to their direction of inclination, batter piles are classified into positive batter piles which are inclined against the loading direction and negative batter piles which are battered toward the loading direction (Rao, 1994), see (Fig. 1.3)

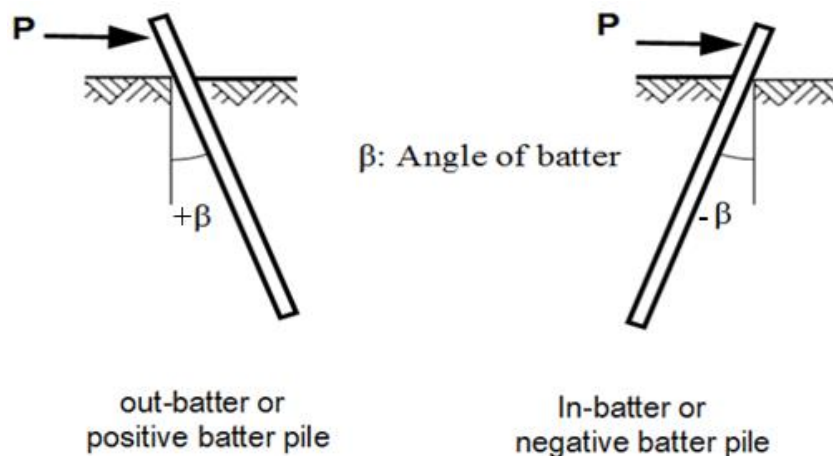


Fig. 1.3 Types of batter piles (Rao, 1994)

1.3 Problem statement

The situation of a batter pile subjected to lateral soil movements is shown in Fig. 1.4. In this situation, soil mass is divided into a moving layer and a stable layer. The pile portion in the upper part is subjected to lateral soil movement, whereas the pile portion in the lower part is subjected to lateral loading transmitted from the upper pile portion. Fig. 1.4b shows that the soil surrounding the pile at any depth is at equilibrium under the initial stress state before the soil starts moving. Once the soil begins moving, the stress in soil surrounding the pile will change from the initial state to a new equilibrium state. This results in the development of lateral forces on the batter pile shafts. These lateral forces may induce bending moments and deflections in batter piles (Leung et al., 2003; Miao et al., 2006). In extreme cases, they might lead to two problems in the pile foundations:

- Serviceability problem due to additional lateral deformation of the piles.
- Structural failure of the piles when the yield bending moment is reached.

For example Fig. 1.5 shows one of the most famous damage caused by horizontal soil movement which is the collapse of 13-storey building in China in 2009 under nearby surcharge loading and excavation works (Khudeira 2010). The collapse was due to rotating/overturning and falling on its side.

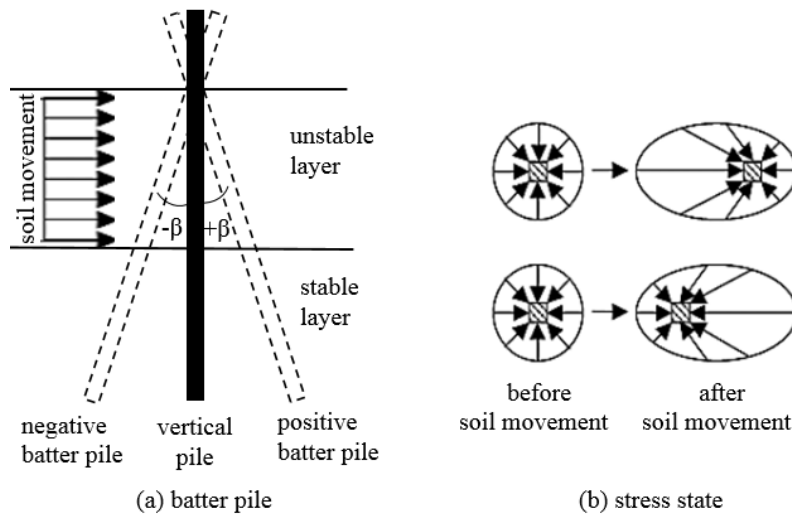


Fig. 1.4 A batter pile undergoing lateral soil movement

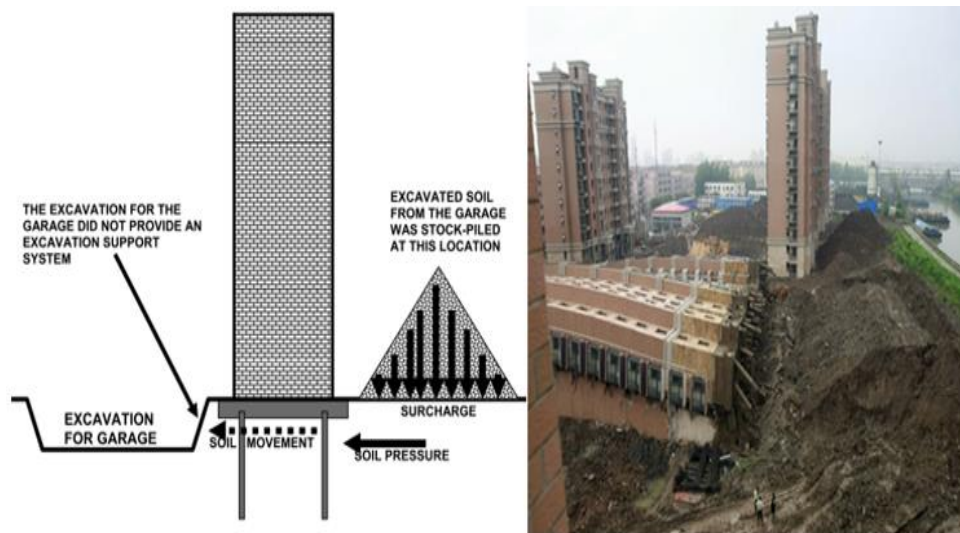


Fig. 1.5 Collapse of 13-storey building in China (Khudeira, 2010)

1.4 Aim and objectives

As previously mentioned, lateral soil movements can induce additional bending moments, shear forces and deflections in the pile. Excessive soil movements may also cause distress or failure. Therefore, the main aim of this study is to investigate the behaviour of single batter piles, single vertical pile and pile groups embedded in sandy soil when subjected to lateral soil movements.

This research project involves extensive experimental model tests and three-dimensional finite element analyses. A complete programme has been carried out to investigate the effect of a number of parameters which are believed to have influence on the behaviour of batter piles in sand. In order to achieve the aim mentioned above, the following objectives are followed:

- Gathering significant information and documenting the works that have been done to date by studying a wide literature review regarding the subject of piled foundations subjected to lateral loads.
- Conducting full experimental testing programme on instrumented model single batter piles and piles group (instrumented with strain gauges) embedded in sandy soil and subjected to lateral soil movement. Parameters that are believed to affect batter pile behaviour such as: batter angle, sand density, pattern of soil movement, thickness of moving soil mass, batter pile diameter pile head fixity conditions, pile spacing and the arrangement of piles in a group were

investigated. The behaviour of batter single piles and pile group were identified in terms of bending moments, shear forces and pile deflections measured by certain instrumentations.

- Use of the experimental results to test the ability of PLAXIS 3D to predict the response of single batter piles, including the zero-batter pile (i.e. vertical pile) and pile groups subjected to lateral soil movements. Once the comparison was achieved, then a parametric study was performed to determine the effects of some other factors such as soil Young's modulus and interface properties.
- Use of the PLAXIS 3D program to perform historical case studies in order to a) test the ability of the computer program to predict full scale test data; b) investigate the sensitivity of the associated parameters needed for input and provide some guidelines for the choice of these parameters in practical use; c) to extract useful information regarding both soil behaviour and pile behaviour from the field tests.

1.5 Contribution to knowledge

To date, a large number of studies (theoretical and experimental in the field or laboratory projects) in the literature have been carried out to investigate the behaviour of single vertical piles or pile group subjected to lateral (active and/or passive) loads. Also, the problem of batter piles subjected to vertical, horizontal and inclined active load has attracted a considerable amount of research work as mentioned in the literature review (see Chapter 2). However, there are limited studies (especially on the experimental side) related to the behaviour of batter pile subjected to lateral passive load due to surrounding soil movement and such behaviour is still not well understood.

Generally, the behaviour of batter piles subjected to lateral soil movements is influenced by many factors, such as the pile head fixity conditions and batter angles. Therefore, further investigation by the experimental and numerical studies are required to provide insight into the influence of different parameters on the batter pile response, in terms of lateral deflection, the shear force and the bending moment distributions along the pile shaft. Therefore, based on the experimental and numerical results, it is hoped that the current study may lead to a better understanding of the response of batter pile under lateral loads due to lateral soil movement and to achieve a better knowledge related to this problem.

1.6 Outline of thesis

The outline of this thesis is briefly described below:

Chapter 1 (Introduction): gives a brief introduction of the existing problems and outlines the main purposes of this research work.

Chapter 2 (Literature Review): presents a critical review of the research work which has been done, including theoretical and experimental work.

Chapter 3 (Experimental Apparatus and Test Procedures): describes the set-up of the experimental apparatus, and the testing procedures and programmes for single piles and pile groups.

Chapter 4 (Experimental Results of Single Batter Pile Tests): presents and discusses test results of single batter pile model tests.

Chapter 5 (Experimental Results of Pile Group Tests): presents the experimental results of pile group tests and interpretation of the results.

Chapter 6 (Three-Dimensional Finite Element Analysis): presents comparisons between the experimental results and the theoretical predictions by PLAXIS 3D program. Additional investigations of the related parameters were also presented.

Chapter 7 (Conclusions and Recommendations for Future Work) present major findings from this research work and gives some recommendations and suggestions for future research.

Chapter 2

Literature Review

2.1 Introduction

The important findings of researches corresponding to this study is reviewed in this Chapter. These researches will be divided into two categories: (1) Piles subjected to horizontal soil movement and (2) batter piles under lateral loading, as these are the main focus of this research. This is followed by a summary of these studies (refer to Table 2.1).

2.2 Piles subjected to horizontal soil movement

Considerable research work has been carried out to understand the response of passive piles under various situations through experimental modelling (laboratory and field tests) and analytical approaches on theoretical piles subjected to horizontal soil movement.

2.2.1 Experimental studies

2.2.1.1 Laboratory tests

In this thesis, the behaviour of batter piles subjected to lateral soil movement is investigated through model tests and therefore it is worthwhile to review the previous experimental research that has been conducted in this area. Laboratory studies directly addressing the response of either single vertical piles or pile groups due to lateral soil movement have been investigated extensively either by using centrifuge modelling techniques or small-scale laboratory model tests.

Matsui et al. (1982) carried out a series of model tests on piles in a row due to lateral soil movement to check the validity of the theoretical equations presented by Ito and Matsui (1975). A commercial clay was used in the tests as well as sand. The schematic view of the test equipment is shown in Fig. 2.1. The internal dimensions of the container box are 60 mm long by 30 mm wide by 30 mm deep. Circular piles with diameters of 20 mm, 30 mm and 40 mm and a length of 300 mm were used in the tests. Piles in a row were set at the centre of the container box and the pile diameter as well as the pile

spacing could be changed. Based on the experimental results, it was found that the relationship between the lateral force acting on a pile and the soil displacement could be represented by a bi-linear curve with an inflection point (see Fig. 2.2). It was also found that the ultimate pressure could be approximately estimated as 1.6 times the theoretical lateral pressure based on the theory of Ito and Matsui (1975).

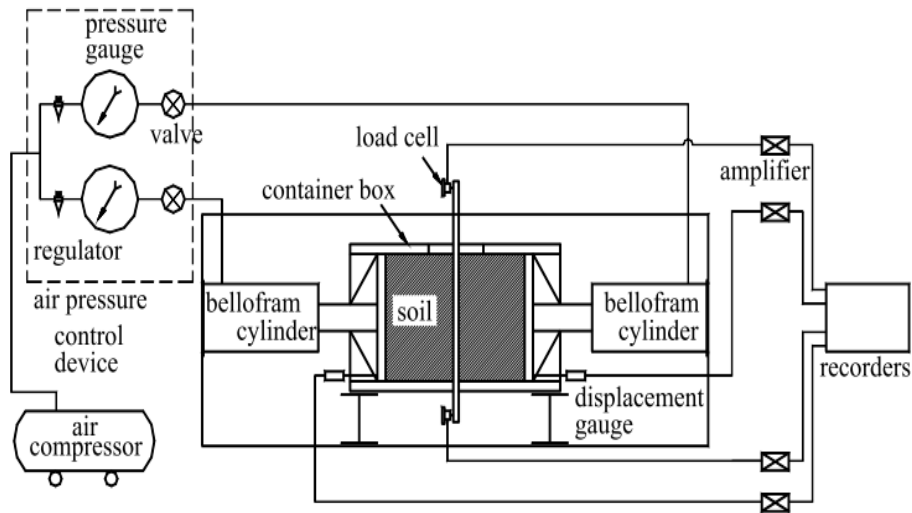


Fig. 2.1 Schematic view of the test equipment (Matsui et al., 1982)

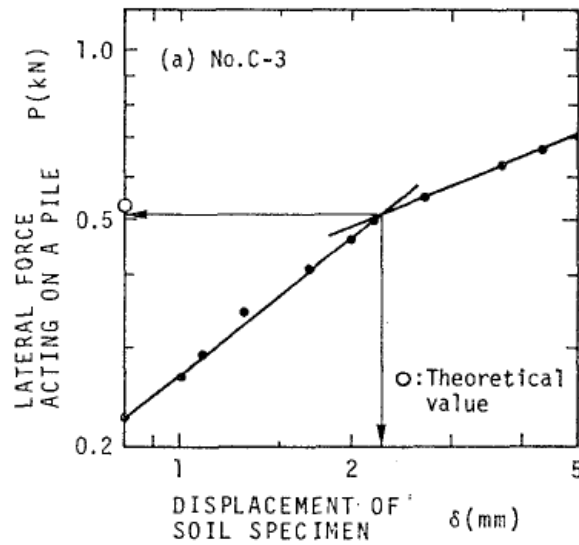


Fig. 2.2 Relationship between lateral force acting on a pile and soil displacement

(Matsui et al., 1982)

A series of small-scale laboratory tests on single instrumented model piles embedded in calcareous sediments undergoing lateral movement were reported by Poulos et al. (1995). The main part of the test apparatus consisted of a testing vessel, made of steel sheet with dimensions of 450 mm wide, 565 mm long and 700 mm deep as shown in Fig. 2.3. The vessel was equipped with steel plates capable of rotating and creating a triangular soil movement profile. Instrumented aluminium piles with different diameters of 25 mm, 35 mm and 50 mm were used. It was found that the bending moment increased with increasing soil movement, but the rate of increase reduced, especially when the soil surface movement was greater than 50mm. Also, under a constant soil density, the maximum pile bending moment was dependent on (1) the pile head fixity condition, (2) the ratio of pile embedded length in the upper moving soil layer to the pile length in the lower stable soil layer and (3) pile diameter and pile stiffness.

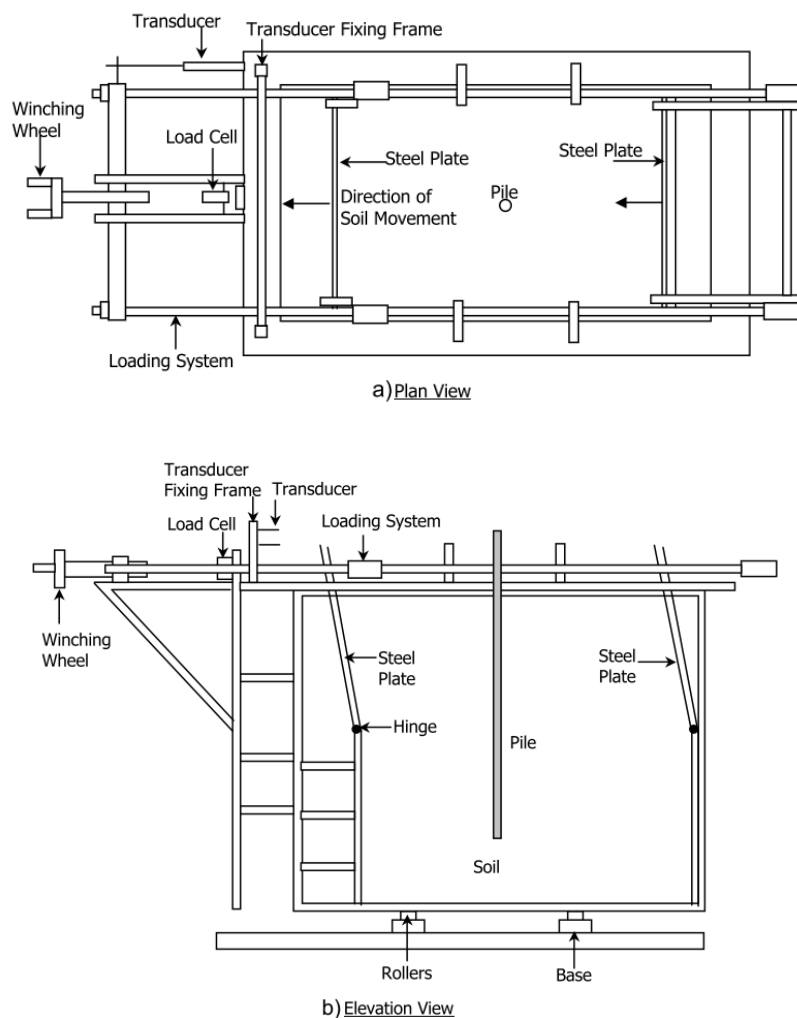


Fig. 2.3 Overview of experimental apparatus (Poulos et al., 1995)

Poulos et al, (1997) used the same apparatus to further investigate the behaviour of pile groups subjected to a linearly varying distribution of lateral soil movements with depth. For piles in a row, the maximum bending moment was found to decrease with decreasing pile spacing and was not significantly affected by either the number of piles or the pile head condition. On the other hand, for two piles in a line, each pile had a different behaviour. In the case of free-head piles, the “near” pile had a larger M_{max} (maximum bending moment) than the “far” pile and the single pile. In the case of piles with pile cap, the shape of the bending moment profiles was different from that of the single pile. The piles experienced relatively large negative bending moments in the upper part of the pile due to the restraint of the pile cap.

A number of years later, a large-scale laminar shear box was developed by Tsuchiya et al. (2001) to carry out a series of instrumented piles embedded in silica sand, subjected to various profiles of lateral soil movement (the configuration of the experimental apparatus is shown in Fig. 2.4. The influence of the lateral ground movements on the behaviour of a pile and their failure patterns were investigated; the tests indicated that the strain distribution of the pile was clearly affected by the profile of the lateral soil movements. This shear box also has the ability to impose both axial load and lateral soil movement simultaneously to the pile

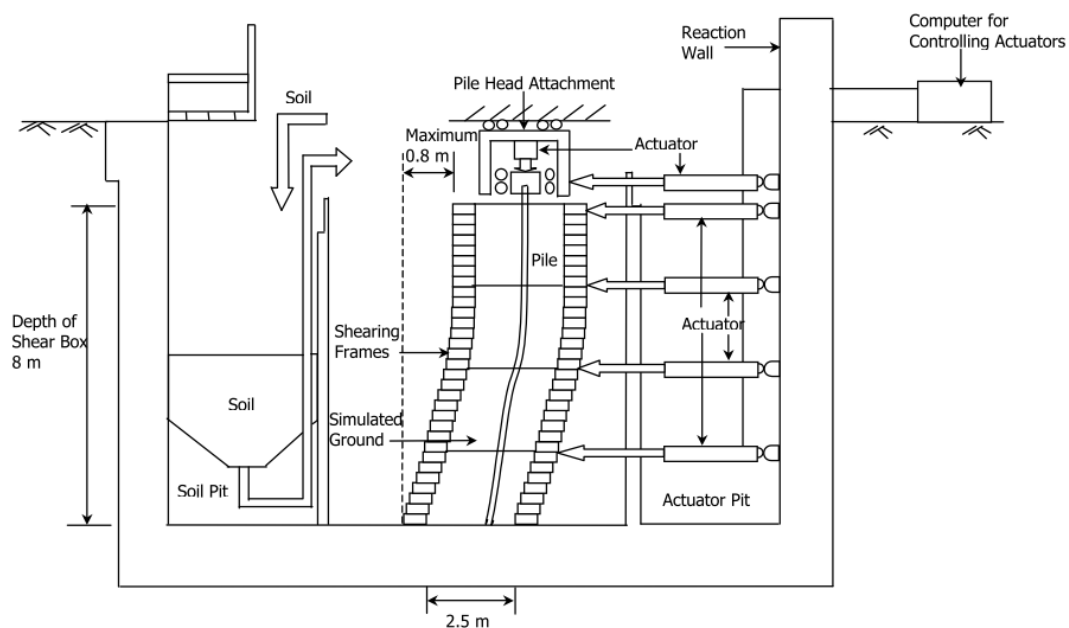


Fig. 2.4 Large-scale laminar shear box design (Tsuchiya et al, 2001)

Pan et al (2002a) performed a series of laboratory model tests in soft clay to investigate the behaviour of coupled piles subjected to lateral soil movements “passive” piles, and to determine the ultimate soil pressure acting on the pile shaft. The schematic view of the test equipment is shown in Fig. 2.5. Two piles in a row centre-to-centre “joining” line being perpendicular to the direction of the applied soil movements and in a line centre-to-centre “joining” line being in the direction of the applied soil movements were considered. The ultimate soil pressures along the pile shaft for two piles in a row and in a line with pile spacings of three and five times the pile width B (20 mm) were lower than those for single passive piles. Group effects still existed even with a pile spacing of $5B$ for coupled piles in a row and in a line. Group factors decrease as pile spacing decreases for piles in a row. The test results also indicated that different distributions of limiting soil pressures along the pile shaft were developed for the single and coupled passive piles.

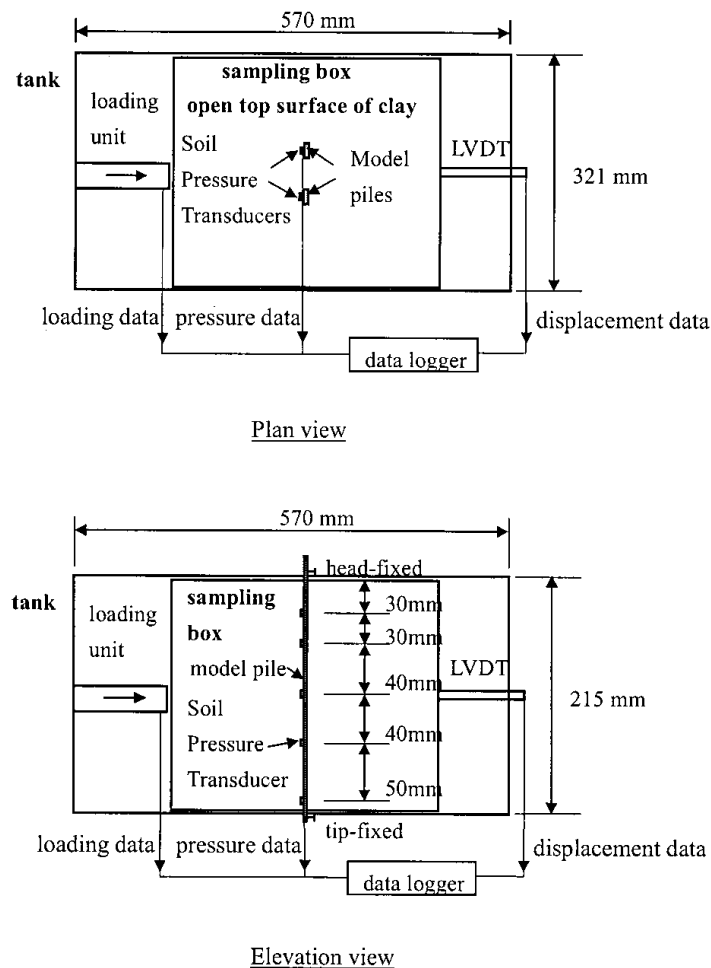


Fig. 2.5 Model test setup (Pan et al., 2002a)

Leung et al (2003) carried out a series of centrifuge model tests on free-head and capped-head pile groups consisting of 2, 4 and 6 piles located adjacent to deep excavation in dry sand as shown in Fig. 2.6. The model piles were fabricated from hollow square aluminium tubes with an outer width of 9.53 mm and an inner width of 6.35 mm. The pile length embedded in sand was 250 mm, and the final model excavation depth was 90 mm with a total wall embedment of 160 mm. It was found that when two free-head or capped-head piles with the centre-to-centre spacing of $3.2D$ (D is the pile diameter) were arranged in a row parallel to the retaining wall at a distance of $5D$, the interaction effect between piles was insignificant. When two piles were arranged in a line perpendicular to the wall, the existence of a front pile reduced the detrimental effect of excavation-induced soil movement on the rear pile. For free-head 4-pile or 6-pile groups, the induced bending moment decreased as the number of piles increased.

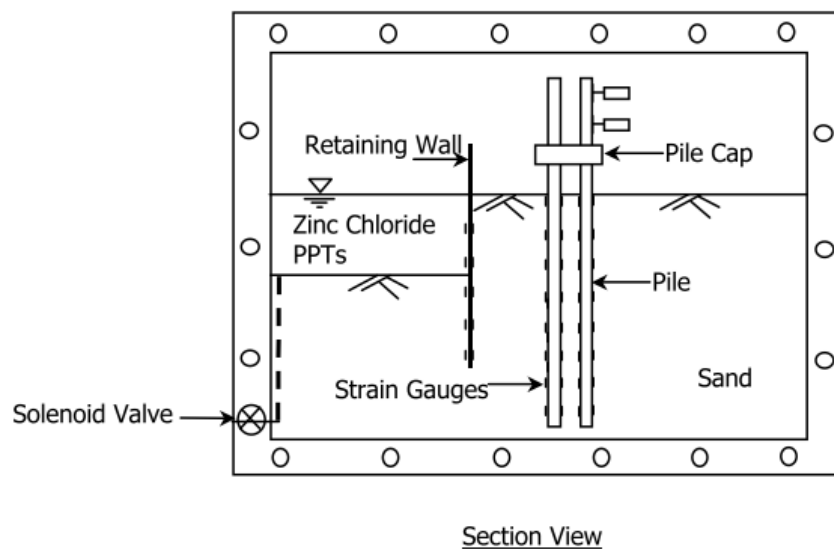


Fig. 2.6 Configuration of centrifuge model (Leung et al., 2003)

Miao (2005) carried out experimental studies to investigate the behaviour of single piles and pile groups embedded in soft clay when subjected to lateral soil movements as shown in Fig. 2.7. The main part of the test apparatus consisted of a testing vessel made of stainless-steel plates of 16 mm thickness, and was 570 mm long, 322 mm wide and 165 mm high (internal dimensions). For single pile tests, the results showed that the pile shape had some effects on the ultimate soil pressure. The ultimate soil pressure for a square pile (S-2) was 12% higher than that for a circular pile (S-1), see Fig. 2.8. For pile group tests, the ultimate soil pressure acting on an individual pile within a group was different from that of a single pile. The ultimate soil pressures for individual piles

in a group were generally smaller than those of single piles. The ultimate soil pressures acting on an individual pile within a group differed with different piles spacing (S_h), see Fig. 2.9, numbers of piles and arrangements of the piles. There was an obvious trend that the pile group factor in terms of the ultimate soil pressures for the whole group, reduced with an increased number of piles (see Fig. 2.10), and increased with increasing pile spacing.

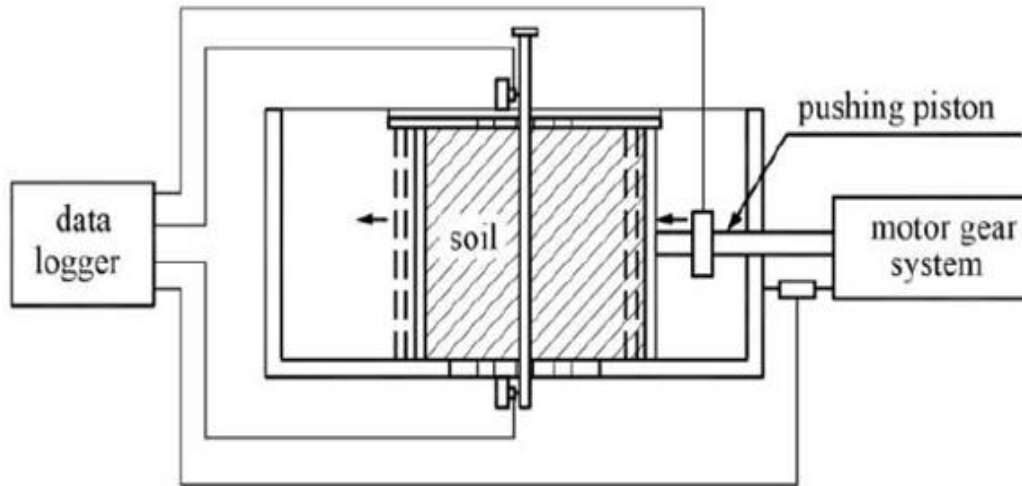


Fig. 2.7 Procedure of single pile installation and loading (Miao, 2005)

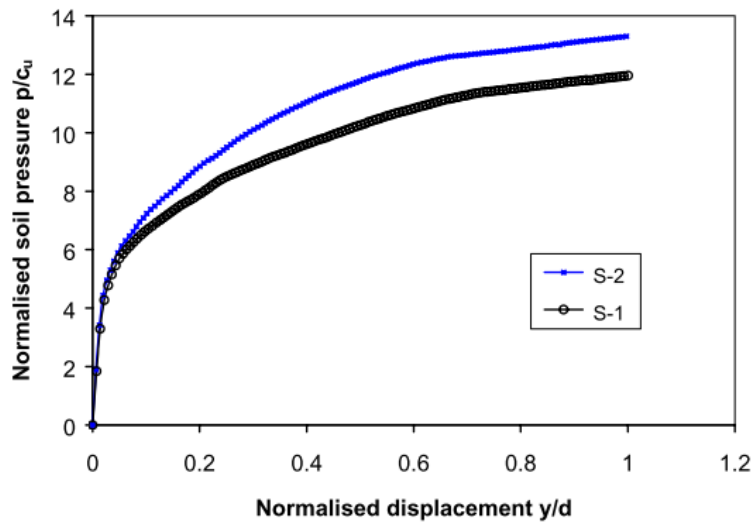


Fig. 2.8 Normalised p-y curve for Test S-1 and S-2 (Miao, 2005)

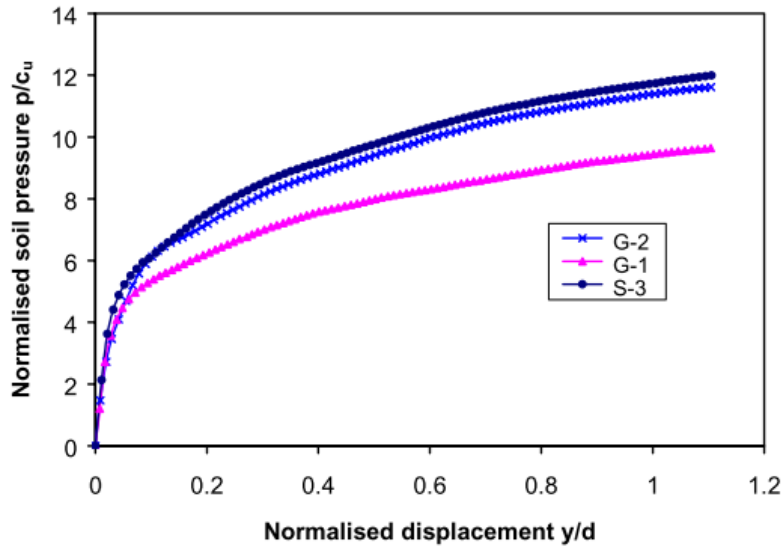


Fig. 2.9 Normalised p-y curves for Test G-1 ($Sh = 3D$) and G-2 ($Sh = 6D$) (Miao, 2005)

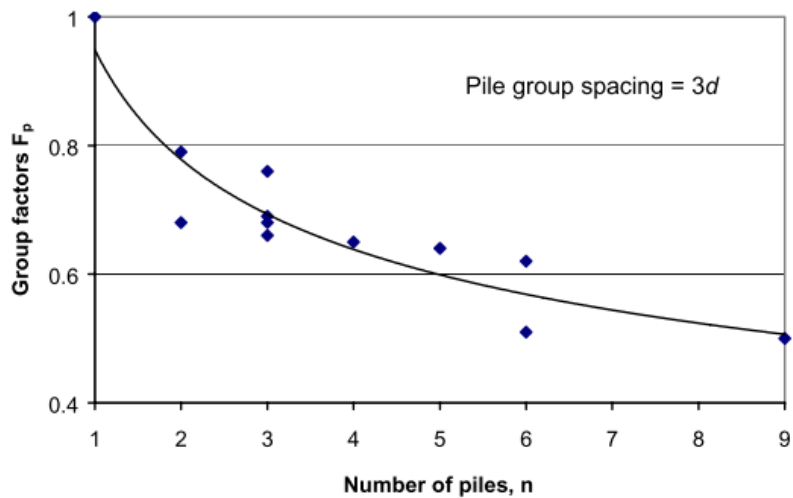


Fig. 2.10 Effects of number of piles on group factor F_m (Miao, 2005)

Guo and Ghee (2006) conducted a comprehensive series of model tests on instrumented piles (aluminium tubes with 1200 mm in length and 32 mm in outer diameter) embedded in dry sand to investigate the response of a piles due to lateral soil movement and axial load, as summarized in Fig. 2.11. The group pile tests were conducted using a shear apparatus, see Fig. 2.12. It has internal dimensions of 100 mm by 100 mm, and 80 mm in height. The upper box for sliding depth L_m is movable, which consists of a

number of 25 mm thick square laminar aluminium frames. It allows a desired number of the frames to be moved together by a rectangular loading block. Based on the experimental results, it was found that, when the model pile groups subjected to simultaneously a uniform lateral soil movement and axial load imposed on the pile cap, observed decrease in bending moment, shear force and soil reaction in the pile, see Fig. 2.13.

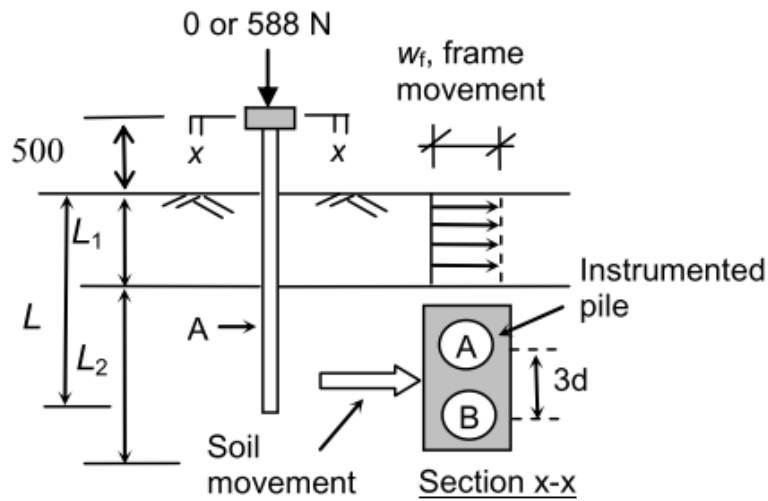


Fig. 2.11 Tests on piles subjected to a uniform lateral soil movement together with different axial load (Guo and Ghee, 2006)

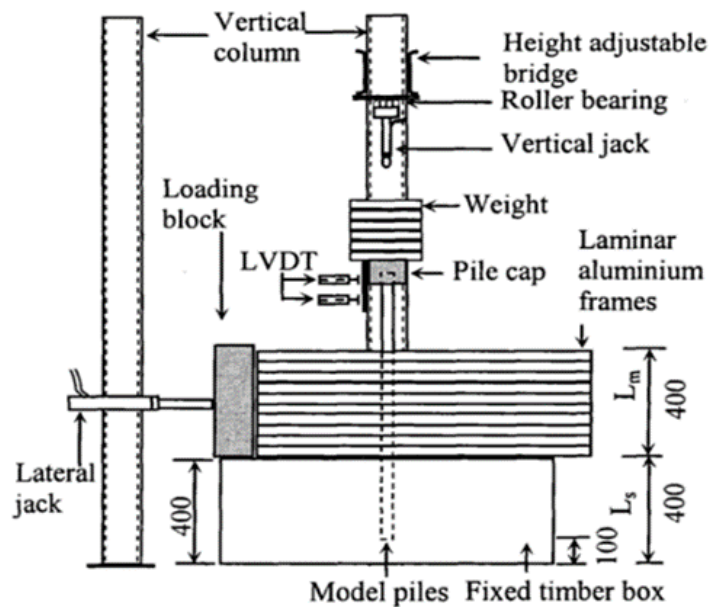


Fig. 2.12 Testing apparatus for the model pile group tests (Guo and Ghee, 2006)

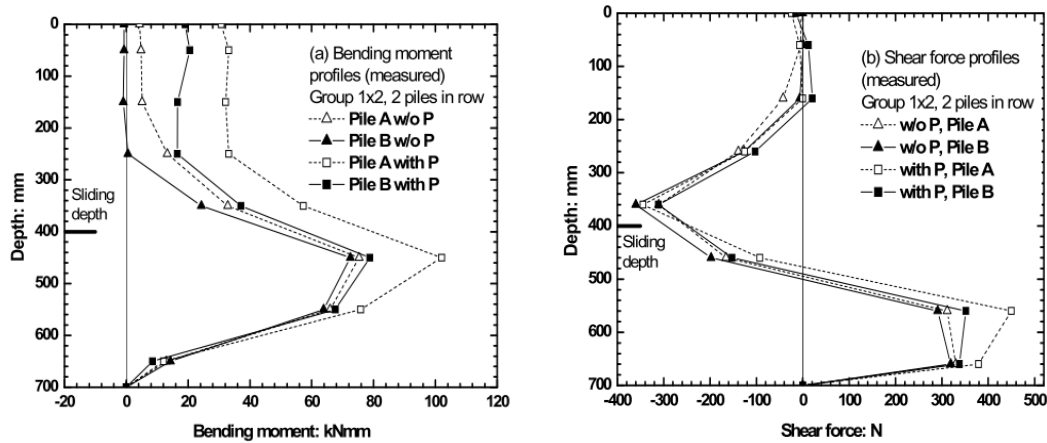


Fig. 2.13 Response of pile A and B (Group 1x2) (Guo and Ghee, 2006)

Lee and Chiang (2007) carried out a series of centrifuge model tests on piles in saturated sandy ground to investigate responses of single piles under various working loads to nearby tunnelling using, see Fig. 2.14. Two instrumented piles located at various distances from tunnels with various diameters used to measure bending moments induced on piles, as a result it is observed that the depth ratio, which is the ratio of pile length to the distance from pile tip to the horizontal axis of the tunnel, as a result it is observed that the depth ratio. It is also noticed that shallow tunnelling near a long pile induces both positive and negative bending moments, whereas deeper tunnelling induces large negative bending moments.

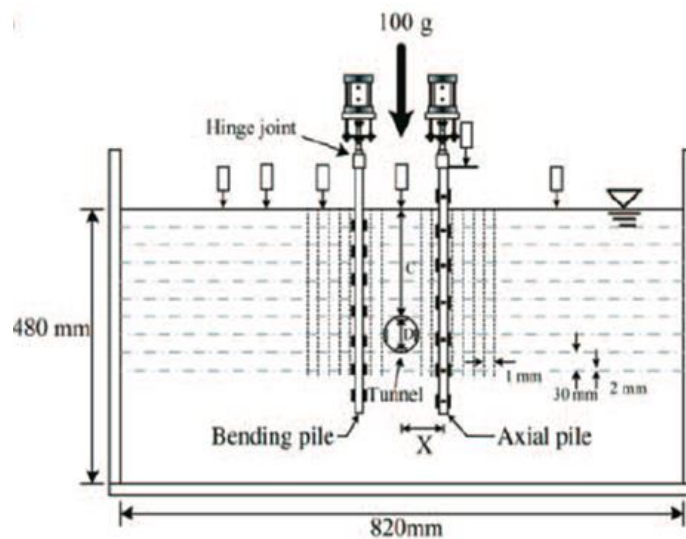


Fig. 2.14 Test setup (Lee and Chiang, 2007)

White et al. (2008) investigated the response of slender, drilled piles under relative soil-pile lateral displacement. Large scale load tests were carried out in which piles were drilled through a box into fixed ground and then lateral pressure was applied to the movable part of the box as shown in the Fig. 2.15. They used composite piles consist of cementations grout with steel bar in the centre of the pile. Three types of soil were used in the tests. Using the experimental results, pressure-displacement curves were drawn from laboratory shear strength tests. It is found that the maximum bending moment occurred at depths ranged from 2.7 to 5.4 times pile diameters under the base of sliding layer.

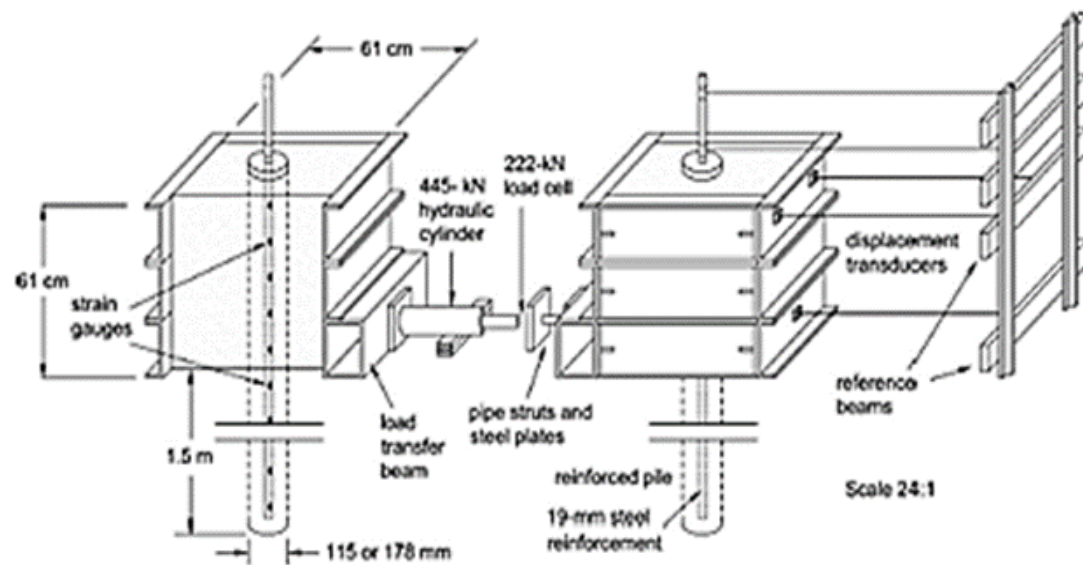


Fig. 2.15 Load test setup (White et al., 2008)

Qin (2010) performed extensive model tests by using the same apparatus was developed by Guo and Ghee (2006) to investigate the response of piles subjected to lateral soil movement. The study discussed the effect of source of lateral soil movement on the behaviour of a single pile. The pile was installed at three locations to the loading side where lateral soil movement was generated by using a triangular or rectangular loading block to simulate corresponding soil movement profiles. The test results were presented in terms of the development of maximum bending moment, maximum shear force and pile deflection at ground surface with soil movement and their distribution along the pile with depth. The effect of the distance on the maximum bending moment was obvious. The maximum bending moment reduced with increased distance between piles and the source of lateral soil movement.

Ersoy and Yildirim (2014) observed the behaviour of vertical piles installed to increase slope stability under lateral soil movement by model tests conducted in a specially built large scale shear box Fig. 2.16. A laboratory model tests were carried out on sandy soil slopes stabilised with piles. A row of four 800 mm long aluminium pipes with a diameter of 35 mm and wall thickness of 5 mm were used. Pile heads were connected to each other by means of an aluminium beam. Single row was subjected to loading due to lateral soil movement. Deformations and bending moments developed in the pile sections were measured by strain gauges attached at different points along the pile lengths. The results showed that the maximum bending moment values along the pile section below the sliding surface increase as the relative density of sand decreases. The distribution of bending moment in the pile group demonstrates that the maximum moment on Pile 1 is higher than Pile 3.

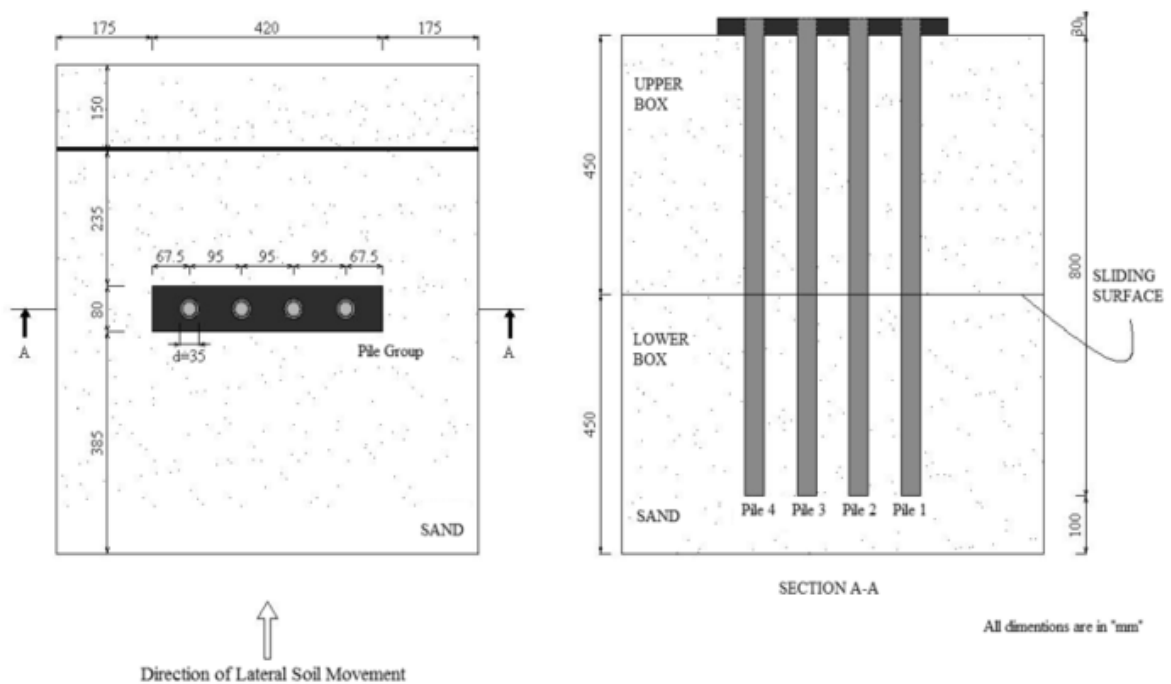


Fig. 2.16 The geometry of pile group investigated (Ersoy and Yildirim, 2014)

Recently, Al-abboodi and Sabbagh (2017) designed and fabricated an experimental apparatus, which allows lateral soil movements and vertical load to be applied simultaneously on a pile. This apparatus was used to investigate the influence of axial loads, sand density and the depth of moving soil on the lateral behaviour of piled raft under progressively moving sand and the depth of moving soil on the lateral behaviour of piled raft under progressively moving sand. It is found that the above parameters

play an important role in the response of piled foundations. The value of soil displacement at which the measured moment reaches its ultimate value decreases as axial loads increase. Peak displacement of the raft has been found to be a function of soil density.

2.2.1.2 Field tests

The existing field tests on piles subjected to lateral soil movements can be classified into three categories:

- 1) lateral soil movements induced by an unstable slope;
- 2) lateral soil movements induced by deep excavation activities adjacent to the piled foundation;
- 3) lateral soil movements induced by the construction of an embankment at the soil surface adjacent to the piles.

In order to study the lateral reaction of piles in slope stabilisation problems, Kalteziotis et al. (1993) investigated the lateral soil displacement profile with depth using in-soil inclinometers at two locations as shown in Fig. 2.17. The profile of soil displacement with time along the soil depth in a region in between piles had a triangular shape, while in a location (uphill) the slope rather shows approximately a block sliding of the soil mass (uniform or trapezoidal displacement).

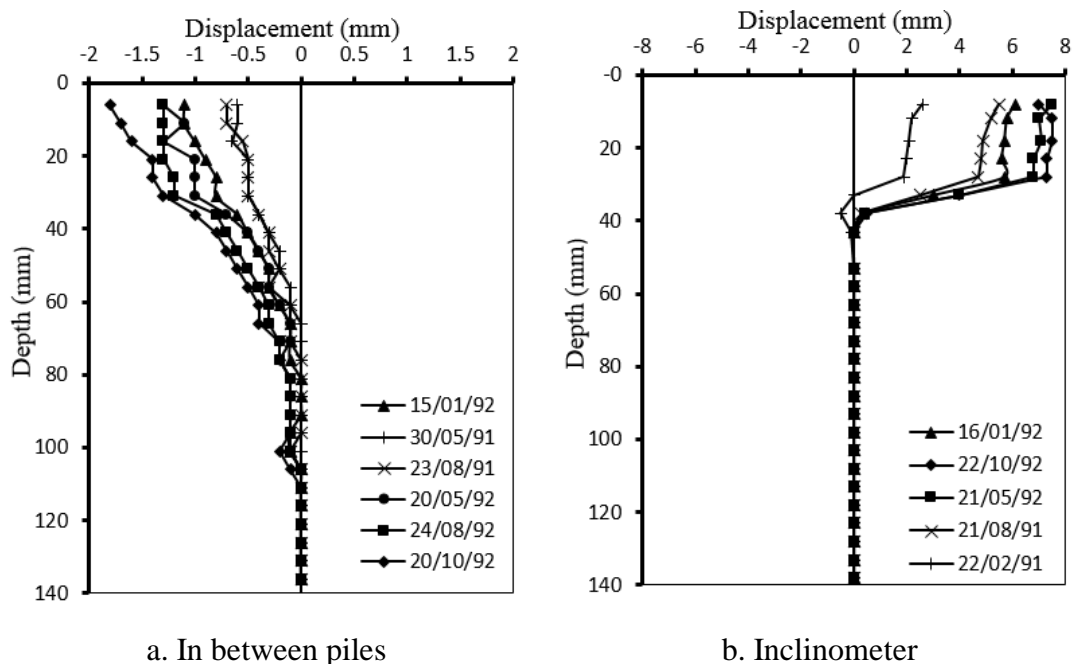


Fig. 2.17 Measured lateral displacement versus depth (adopted from Kalteziotis et al., 1993)

Ong et al. (2003) investigated the pile responses due to excavation-induced soil movement in clay. The free-field lateral soil movement has been measured and plotted for different stages of excavation construction as shown in Fig. 2.18. It can be noticed that the profile of soil movement is approximately a triangle, starting with maximum value at ground surface to zero movement at a certain depth of the soil. It is also obvious that the angle of inclination of those semi-triangular shapes is changed during excavation progress.

Smethurst and Powrie (2007) reported the monitoring and analysis of the bending behaviour of discrete concrete piles used to stabilise a railway embankment. The piles were instrumented with strain gauges to measure the bending moments induced in the pile by slope movements. Inclinator tubes were installed both inside the strain-gauged piles and in the slope midway between each pair of instrumented piles to measure the relative movement between the piles and soil midway between the piles. The shape of the pile and soil displacements measured by inclinometers over a period of 4 years is plotted in Fig. 2.19. The profile of soil movement can be described as semi-triangular.

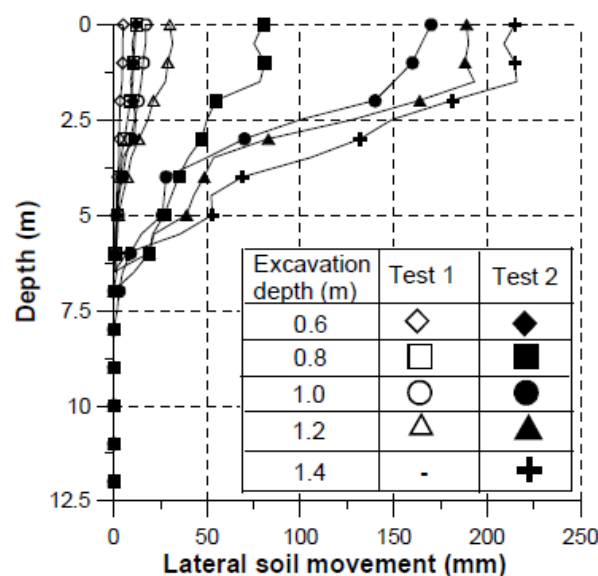


Fig. 2.18 Measured lateral soil movement profiles (Ong et al., 2003)

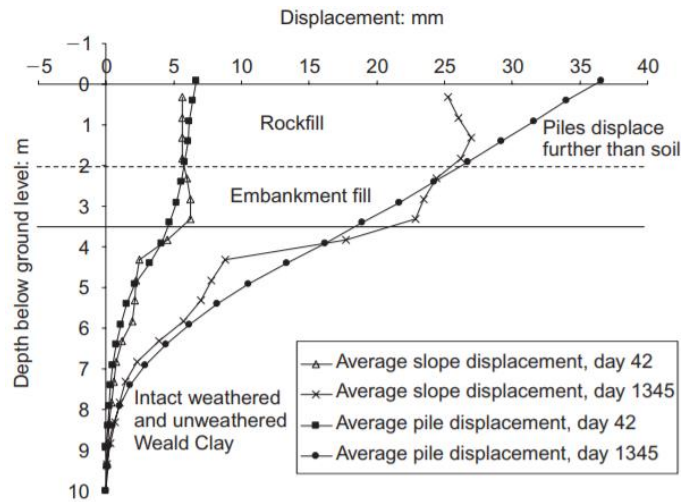


Fig. 2.19 Averaged measured pile and soil displacements with time (Smethurst and Powrie, 2007)

2.2.2 Theoretical studies

Available studies to evaluate the lateral response of vertical piles subjected to horizontal soil movement are summarised below.

De Beer and Wallays (1972) presented an empirical design method for embankment piles as shown in Fig. 2.20. When the factor of safety F_s of the whole soil mass was larger than 1.6, the soil around the piles was assumed to be in a state far from the rupture state and a uniform pressure was assumed to act on the piles over the full depth of the soft stratum. When the F_s was less than 1.6, the full ultimate soil pressure $10.5c_u$ was assumed to act on the pile in opposing directions above and below the point where the slip circle intersected the pile. This method can only predict the maximum bending moment and does not allow prediction of the distribution of the bending moments along the pile shaft.

Ito and Matsui (1975) presented a theoretical method to analyse the growth mechanism of the lateral force acting on stabilising piles in a row, due to the surrounding plastic deformation. They derived a formula to evaluate the limit soil pressure acting on a row of piles undergoing lateral soil movement. The derived formula is based on the assumption of rigid piles. As the piles were found in a relatively deep layer of soft soil, they were assumed to follow the deformation of the soil. As shown in Fig. 2.21, the

piles of same diameter (d) were placed in a row with a centre-to-centre spacing D_1 through plastically deforming ground (D_2 is the edge to edge spacing between the two piles). When a lateral deformation occurred within a soil layer of thickness H , in a direction perpendicular to that of the row of piles, the lateral forces are assumed to act on the piles as an interaction between the piles and soil layer. Although these assumptions do not represent the actual behaviour of piles practically, the proposed model appears in good agreement with some field results.

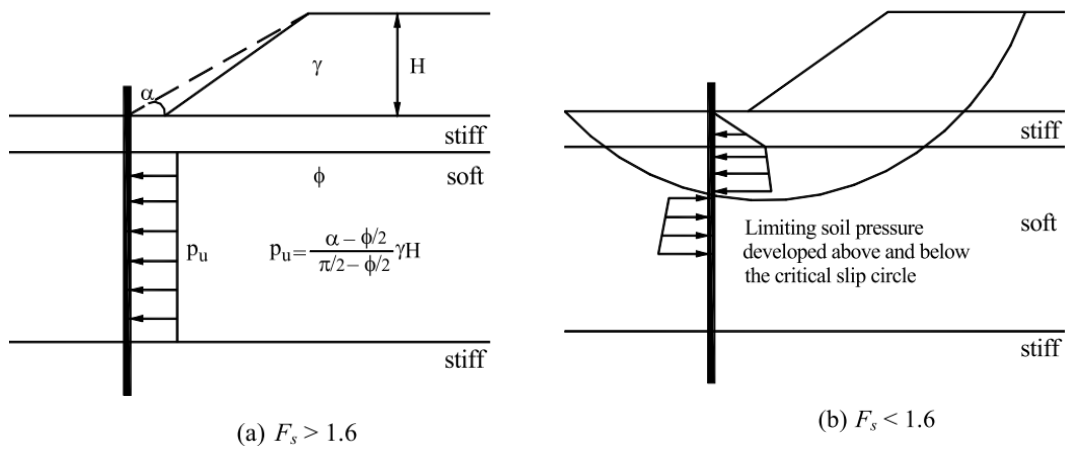


Fig. 2.20 Method of De Beer and Wallays (De Beer and Wallays, 1972)

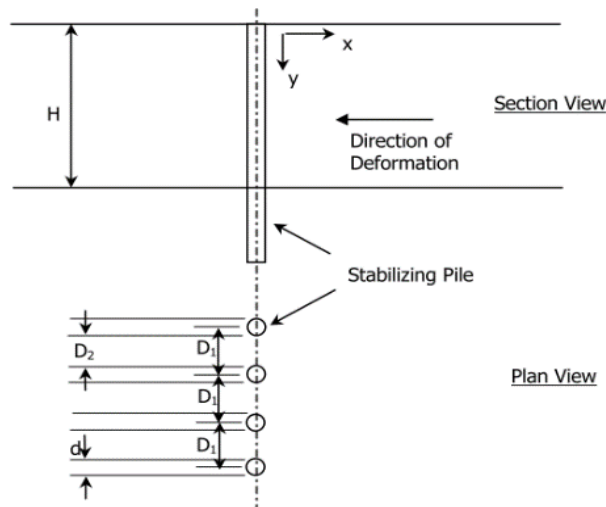


Fig. 2.21 Stabilising piles in a row through plastically deforming ground (Ito and Matsui, 1975)

Viggiani (1981) analysed the mechanism of interaction between a sliding soil mass and a pile crossing it, then penetrating the stable underlying soil, in which six possible failure modes were proposed. The piles, whose yield moment was greater than the bending moment acting upon them, were considered as rigid piles; and three possible soil failure modes were proposed. The failure modes of rigid piles are illustrated in Fig. 2.22. It is assumed that only the soil can fail into three different mechanisms labelled A to C. In mode A, the pile and the sliding soil translate together resulting in soil failure. This mode can occur when the pile penetrates a small distance below the sliding surface. Mechanism B represents failure of soil along the pile length. In this case the pile undergoes a rigid body rotation. The pile in mode C is under a small depth of the sliding layer in which only a small portion of the pile is subjected to lateral soil movements. In this mode, the pile is assumed to be fixed and the soil flows around the upper portion of the pile. For flexible piles, passive piles are assumed to fail by forming one or two plastic hinges at a certain depth where the induced bending moment reaches the yield moment of the pile (see Fig. 2.23). The occurrence of one of the six failure modes was perceived to be governed by the geometry of the problem (length and diameter of the pile, thickness of the sliding soil mass) on the yield moment of the pile section and on the undrained shear strength of the stable and sliding soil. The pressure distribution was assumed for each failure mode and, accordingly, shear force and bending moment in the piles were computed by the limit equilibrium method. The ultimate soil pressure (P_u), can be computed from the expression:

$$P_u = N_p c_u \quad (2.1)$$

Where:

N_p : the lateral capacity factor,

c_u : the undrained shear strength of the soil.

By examining the case of the lateral loads acting on the piles used to stabilise the landslides, Viggiani proposed that p_u would vary, depending on whether the pile was actively ($6.26 - 12.56c_u$) or passively ($2.8 - 4.0c_u$) loaded.

Chow (1996) described a displacement-based procedure for predicting the behaviour of clay soil stabilised piles. The method requires an input of the free-field soil movement

at each depth. Finite beam elements were used to model piles. A subgrade reaction method was used to simulate the soil, whereas the pile-soil-pile interaction was simulated using the theory of elasticity. Expressions for determining soil's Young's modulus, lateral soil stiffness, and limiting soil pressures were presented. Comparisons the predicted response with two case histories of single pile and pile group showed good agreement.

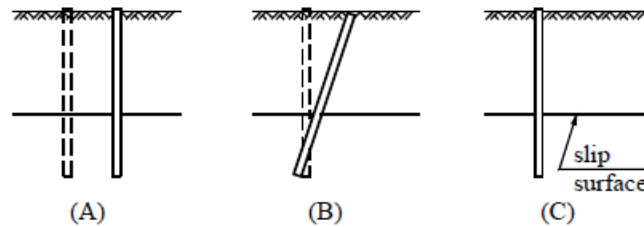


Fig. 2.22 Failure modes of rigid piles (Viggiani, 1981)

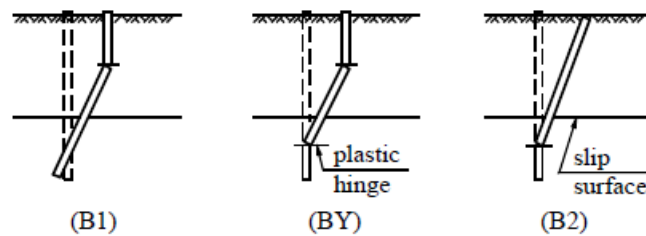


Fig. 2.23 Failure modes of flexible piles (Viggiani, 1981)

Bransby and Springman (1996) also conducted a series of finite element analyses through the program CRISP94 (Britto and Gunn 1987; 1990) on a single pile as well as on pile rows in clay. The piles translating through elastic-plastic soil were modelled as rigid circular adherent discs. A very fine mesh of 760 cubic strain triangles and 400 increments were used. Interface elements were not used to model slip between the soil and the pile. It was found that the ultimate soil pressure for a single isolated pile was 11.75cu. For two infinitely long rows of piles with different spacings, it was found that the leading and trailing pile p-y curves were almost identical with a maximum difference between rows of 0.8%.

Chen and Poulos (1997) presented a theoretical solution to analyse the lateral behaviour of passive single piles and piles group undergo to horizontal soil movements. A

boundary element program (PALLAS) has been developed in which the pile was modelled as elastic beam and the soil was considered as elastic continuum. The proposed procedure requires an appropriate assessment of lateral soil movements, soil elastic modulus with depth and maximum pile-soil pressure as input data. The findings from the theoretical analysis were compared with some published case histories and laboratory tests, and good agreement was achieved. Based on the analysis, design charts were derived giving the maximum bending moment and pile top deflection.

Cai and Ugai (2003) presented a subgrade reaction solution of flexible piles in landslide taking into consideration the laterally linear movement of the sliding layer. A study of case histories has been conducted to check the accuracy of the proposed solution. As a result of the comparison, it can be concluded that the calculated and measured lateral response of flexible passive piles agreed well with each other. Based on the subgrade reaction approach, design charts are proposed.

Chen and Martin (2002) studied the mechanism of load and stress transfer from the sand soil to passive pile group by linking pile load-displacement curves and the arching effects using the finite difference code FLAC^{3D}. The results showed that the formation of arching and the shape of arching zone depend on several factors i.e. pile configuration in the group, pile cross section, relative pile-soil displacements, interface properties and dilation angle of the soil. It was also found that the group effects can be eliminated if the pile spacing is over 4D (D is the pile diameter).

Pan et al. (2002) presented a 3D finite element analysis of rigid and flexible passive piles under lateral movements of soft clay layer. The analysis was carried out using ABAQUS software. The non-linear behaviour of soil was modelled using Von Mises model, while linear elastic behaviour was assumed for the pile. The study focused on the ultimate soil pressure acting along pile shaft due to soil movements. The results indicated that the maximum ultimate soil pressure for piles agreed with the measured results, and the magnitude of soil movement at the boundary to achieve this soil pressure was found to be 0.2 of pile width.

Miao et al. (2006) carried out a 3D finite element analysis to investigate the behaviour of single piles subjected to lateral ground displacements in cohesive soil using ABAQUS software. The pile and soil were modelled using 20-node quadrilateral brick element with reduced integration. A Mohr-Coulomb constitutive model was chosen for

the soil, while a linear elastic behaviour was used to model the pile. Uniform and trapezoidal profiles up to $0.6D$ (D is the pile diameter) were applied $9D$ away from the pile centre to the left and right boundaries. It was found that soil pressure acting on the pile did not change for values of soil movements larger than $0.45D$. A number of factors namely, (1) pile flexibility, (2) the magnitude, (3) the depth, (4) the shape of soil movement (5) and the pile head fixity conditions were tested. The analysis indicated that the response of piles in moving soil is significantly influenced by the above parameters.

Kahyaoglu et al (2009) carried out a 3D finite element analysis to study the response of single pile and pile group under moving cohesionless soil using PLAXIS software. The influences of pile spacing, interface properties and pile-soil relative displacement on lateral earth pressure against piles were investigated. The analytical solution has been validated against some small-scale test results. It is observed that the analytical and experimental results were in a good agreement. It is also revealed that a pile spacing of more than $8 \times$ pile diameter makes piles in a group behave like single piles without arching effect. The influence of variation of soil friction angle is also limited for this pile spacing.

Zhang and Li (2010) adopted the 3D finite element software ANSYS to study the bending response of axially loaded pile group under lateral ground movements taking into account the effect of pile cap. The soil and pile were modelled as a Drucker-Prager and linear materials respectively, with 8-node hexahedron elements. As a result of this analysis, it is concluded that axial load produces additional moments when the pile top is free. Likewise, the existing of pile cap affected the bending response obviously.

Ghee and Guo (2011) used the finite difference code FLAC^{3D} to investigate the behaviour of single passive pile with and without axial loads. The soil was modelled using eight-noded brick elements with Mohr-Coulomb model and a constant value of Young's modulus. Laboratory tests which have already carried out by the authors were re-examined in order to check the accuracy of the analytical solution. The comparison was presented in terms of bending moment, shear force and pile deflection profiles. A parametric study has been conducted to study the effect of moving/stable soil depth ratio on the pile response. The results showed some difficulty in predicting the pile behaviour.

Liang et al. (2013) solved the flexural differential equations of axially loaded single piles and pile group in moving sand soil by the finite difference method. A Winkler's spring model was used for soil-pile interaction. The analysis of pile group was performed by adding deflections and stresses of single piles. A parametric study was carried out to investigate the effect of pile spacing, number of piles and axial load. The results showed that pile spacing and axial load level effected the pile-pile interaction.

Liyanapathirana and Nishanthan (2016) used ABACUS to study the response of single piles subjected to lateral soil movement from nearby excavation. The proposed numerical model was verified using experimental results from the literature. A parametric study was carried out aimed to investigate the influence of excavation depth, soil properties including over consolidation ratio, wall support condition and stiffness and pile head fixity condition. Results showed that pile response in terms of bending moment and deflection increases as the depth of excavation increases and decreases with the increase in over consolidation ratio of the soil. Utilising parametric study results, a set of design charts were derived to estimate pile response embedded in clayey soils.

2.3 Research review on batter pile

During the last few decades, several researchers have studied the behaviour of batter piles subjected to lateral or vertical loads using both experimental tests and theoretical studies.

2.3.1 Experimental tests

Murthy (1965) developed a relationship between vertical and batter piles using an instrumented model batter pile installed in the sand, the batter angles varied within 0 to $\pm 45^\circ$ range. In these relationships, Murthy (1965) introduced important factors as pile material modulus of elasticity, second moment of area, pile length, pile diameter, free head of the pile, soil internal friction angle, soil density, and batter angle. The results reported that lateral resistance of a negative batter pile is higher than a positive batter pile.

Meyerhof and Ranjan (1972a) conducted a series of experimental model tests on rigid batter piles under inclined load in sand. The bearing capacity of axially loaded batter

piles is discussed by comparing experimental results and theoretical estimates. The theory for ultimate resistance of rigid vertical piles under horizontal loads is extended to that of laterally loaded batter piles. Experiments indicated that the ultimate loads for batter piles decrease with greater inclinations of the load. For small inclinations of load with the vertical, positive batter piles have greater ultimate loads compared with corresponding negative batter piles. However, at larger inclinations of load with the vertical, the trend changes and under horizontal load negative batter piles have greater ultimate loads than corresponding positive batter piles. Model test results were compared with those of theoretical estimates and good agreement was found.

Meyerhof and Ranjan (1972b) carried out a series of experimental tests to estimate the ultimate capacity of a pile bent in sand soil (1 by 2 pile group) under inclined load. The results of loading tests on two model pile bents with depth/diameter ratios of 13 and 23 for free standing bents and 15 and 25 for pile bents are presented. The experimental results indicated that the ultimate vertical load for the pile bent with vertical piles was not very much different than that for the pile bent with vertical and batter piles. However, as the inclination of load with the vertical increased a bent with one vertical and one batter pile had higher ultimate load than that of a bent with only vertical piles.

Ranjan et al. (1980) carried out Laboratory tests on single and group batter piles in sand. The results revealed that, the negative batter piles offer more resistance than positive batter piles, and a group of one vertical pile and one batter pile (positive or negative) has more resistance to lateral deflection compared to a similar pile group consisting two vertical piles.

Hanna and Afram (1986) presented an experimental study to investigate the pull-out capacity of single rigid vertical and batter piles in sand and subjected to axial loading. An experimental investigation was presented concerning the pull-out capacity of single vertical and batter piles in sand. From the experimental results, it was found that the pull-out capacity of batter piles decreases slightly when the pile inclination is increased. This investigation provides good agreement with the theoretical estimates.

Meyerhof and Yalcin (1993) conducted a series of extensive laboratory tests to determine the bearing capacity and displacements of single model flexible vertical and batter piles under inclined loads in two-layered soil consisting of soft clay over loose sand. Based on the experimental results, it was found that the bearing capacity of the

piles is found to depend on the layered structure, load inclination, and pile batter. Where, the ultimate loads of vertical and batter piles decrease rapidly with increasing load inclination and decreasing clay-layer thickness. The maximum capacity is developed under axial loads regardless of the clay-layer thickness, and this capacity is somewhat smaller for batter piles than for the corresponding vertical piles. The minimum capacity is obtained under lateral loads, with values for the piles with negative batter exceeding those with positive batter. Practical equations for horizontal and vertical displacements of flexible batter piles are presented on the basis of resultant influence factors that are related to the batter angle, load inclination, and distribution of soil modulus with depth. The observed horizontal and vertical displacements of the piles are in reasonable agreement with the theoretical estimates.

Meyerhof and Yalcin (1994) extended the previous study to investigate the behaviour of single free-head model flexible vertical and batter piles under the general case of eccentric and inclined loads in two-layered soil. The bearing capacity of the piles is found to depend on the layered structure, the eccentricity and inclination of the load, and the pile batter. Where the test results indicate that the ultimate loads of vertical and batter piles decrease rapidly with increasing angle of inclination and load eccentricity. In all cases the maximum bearing capacity develops under axial load, regardless of the angle of inclination and eccentricity of loading, and it is independent of the thickness of clay layer. The maximum capacity is found to be somewhat smaller for batter piles than for the corresponding vertical piles. The minimum pile capacity is obtained under lateral loads, and it is greater for piles with negative batter than for those with positive batter. The theoretical estimates of ultimate loads obtained from semi empirical relationships agree fairly well with the test results.

Rao et al. (1994) carried out an experimental study on model batter piles in clay under lateral loads. It is found that negative batter angle gives more resistance compared to vertical and positive batter angles. It was also verified in this study that this trend holds true for different embedment ratios (L/D) and the lateral resistance increased with more embedment.

Zhang et al. (1999) performed a centrifuge lateral load tests on single batter piles in sand with different relative density sands, see Fig. 2.24. Five pile inclinations were modelled: 7° and 14° at a negative pile batter, vertical, and 7° and 14° at positive pile batter. The effects of pile batter and soil density on lateral resistance were studied. Pile

batter had significant effects in dense sands, but minor effects in loose sands. The lateral pile resistance was influenced by pile batter and soil density. Based on the centrifuge test results, the resistance increases over vertical piles were 4, 14, 24, and up to 50% in very loose, loose, medium-dense, and dense sands, respectively, at positive 14° batter. In contrast, the resistance decreases over vertical piles were 4, 5, 15, and up to 35%, respectively, at negative 14° batter. The effects of pile batter were significant in medium- dense and dense sands, but minor in loose and very loose sands, see Fig. 2.25.

Zhang et al. (2002) presented a centrifuge model test programme for studying the effects of vertical dead loads on the lateral response of 3×3 and 4×4 batter pile groups in sand. Vertical dead loads ranging from approximately 20 to 80% of the vertical ultimate group capacity (P_{uv}) were applied. Based on these tests, the effects of vertical dead load on the lateral resistance of the batter pile groups are found to depend on pile arrangement, pile inclination, and soil density. The lateral resistances of the 3×3 pile groups do not appear to vary considerably with the vertical dead loads in the range of the vertical loads studied. However, the lateral resistances for the 4×4 pile groups at vertical loads of approximately 50 and 80% P_{uv} may be 26–29% and even 40% higher than that at the 20% P_{uv} dead load. Also, numerical analyses are performed to simulate the responses of some of the batter pile groups.

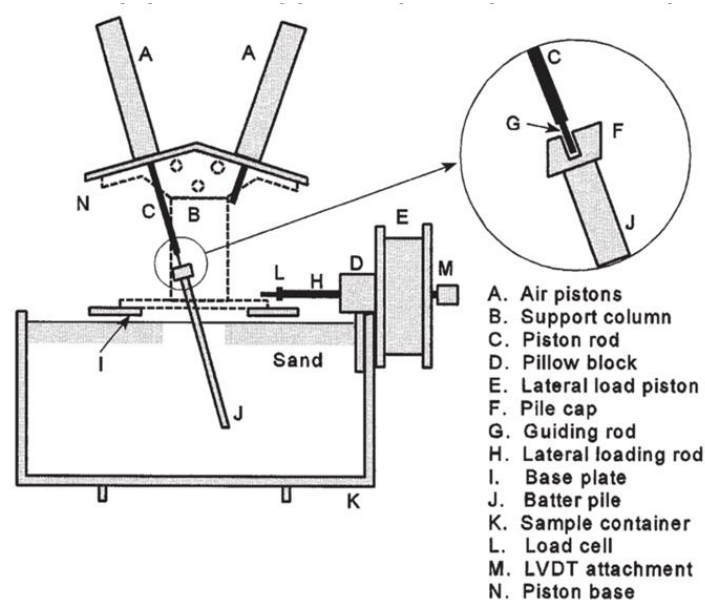


Fig. 2.24 Schematic view of the in-flight pile installation equipment for single batter pile tests in the centrifuge (Zhang et al., 1999)

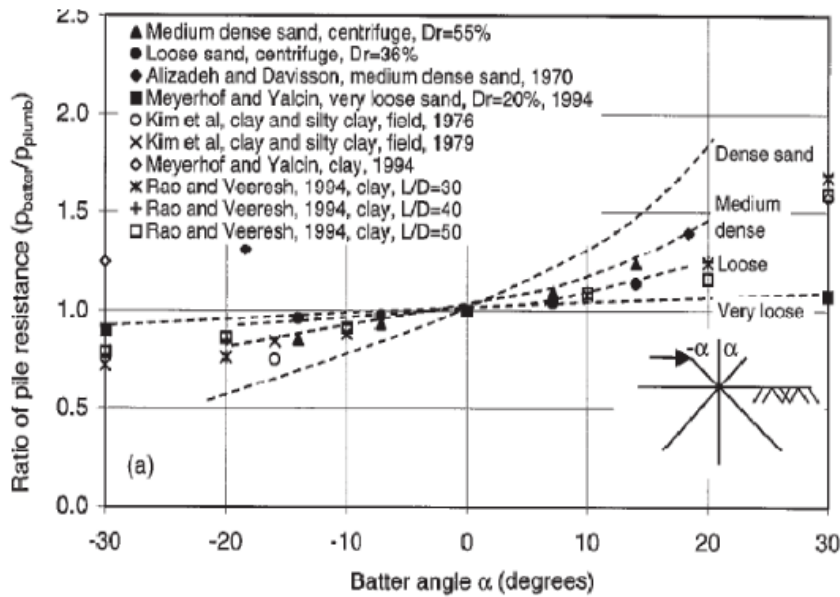


Fig. 2.25 Influence of pile batter on pile resistance (Zhang et al., 1999)

Manoppo (2010) carried out a series of experimental tests to investigate the behaviour of the ultimate bearing capacity of single flexible batter piles in homogeneous sand under horizontal load, see Fig. 2.26. Model tests were conducted using instrumented flexible piles. The piles were buried in loose, medium and dense homogeneous sand at batter angles $\beta=0^\circ, \pm 15^\circ$ and $\pm 30^\circ$ were subjected to incrementally increasing horizontal loads. The results of model tests on single vertical and batter piles under horizontal loads in homogeneous sand show that the batter angle (β) and the unit weight of soil (γ) significantly influenced the ultimate bearing capacity of the piles. Batter angles $\beta= -15^\circ$ or negative batter piles were higher compared then vertical piles and positive batter piles.

Prabha and Boominathan (2010) carried out small scale model tests on batter pile groups embedded in soft clay in a specially designed large test-chamber (Fig. 2.27). The static and cyclic lateral responses were investigated for 1×2 batter pile groups with different configurations: Batter-Vertical (BV), Vertical-Batter (VB) and Both-Batter (BB). The effect of centre to centre pile spacing, number of cycles of loading on the load-deflection and bending moment behaviour of the pile groups were studied. It was observed that under static loading VB configuration has a higher lateral capacity

of smaller pile spacing, whereas BV configuration has higher capacity at larger spacing. Under cyclic loading, VB configuration showed smaller percentage reduction in the ultimate capacity in comparison to other configurations. 3D Finite Element analysis was carried out using ANSYS and the estimated static ultimate resistance was found to match well with the experimental findings for BV and VB pile.



Fig. 2.26 Experimental box (Manoppo, 2010)

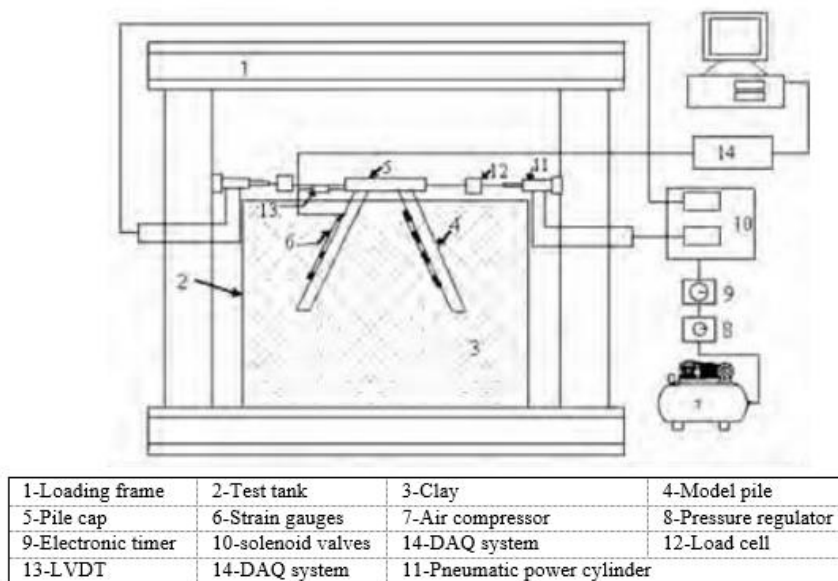


Fig. 2.27 Schematic sketch of experimental set up for cyclic lateral load tests (Prabha and Boominathan, 2010)

Lv et al. (2011) carried out experimental work to study the lateral bearing capacity of negative batter pile under different batter and different constraints at pile head. These piles were embedded in sand. The pile batter angle to vertical, β , is 0° , 10° or 20° . The analysis indicates that (1) the lateral capacity of the negative batter pile decreases as the batter angle decreases when the pile head is only horizontal movement (translational), (2) the lateral capacity of the negative batter translational pile is more than that of the positive batter.

Pathak et al. (2011) conducted a full-scale lateral load test on batter pile group foundation that supports the M19 eastbound pier of the I- 10 Twin Span Bridge over Lake Pontchartrain, Louisiana. The test was conducted by pulling the M19 eastbound and westbound piers toward each other using high strength steel tendons. A maximum of 8318 kN static lateral load was applied in increments. The tested pile group consists of 24 driven square precast prestressed concrete (PPC), 33.5 m long and 0.91 m wide batter piles; among which 8 piles were instrumented with In-Place In- clinometers (IPIs) and 12 piles were instrumented with strain gauges. The batter piles were spaced 4.3 pile width in the direction of lateral loading. A seventh-order polynomial curve fitting method was applied, for each load increment, to fit the measured rotation profiles from the inclinometers. The fitted rotation curves were then used to deduce the bending moment, shear force, and soil reaction profiles based on specific mathematical derivations. The calculated moments from curve fitting were compared with the moments calculated from strain gauges, and the results showed good agreements. The soils' p-y curves at different depths were also back-calculated from the derived soil reaction profiles. The resulted p-y curves showed no evidence of a group effect.

Singh and Arora (2017) conducted a series of laboratory tests to study the effect of pile inclination on load bearing capacity of batter pile group in sand under cyclic lateral load test (Fig. 2.28). Piles used in the tests were aluminium pipes with outer diameter 20mm and wall thickness of 1mm. Total length of pile was kept 0.90m with embedded length of 0.80m. Results indicate that negative batter pile individually as well as in a pile group show less amount of deflection. Further as batter angle increases from 20° to 25° pile capacity increases and decreases beyond 25° .

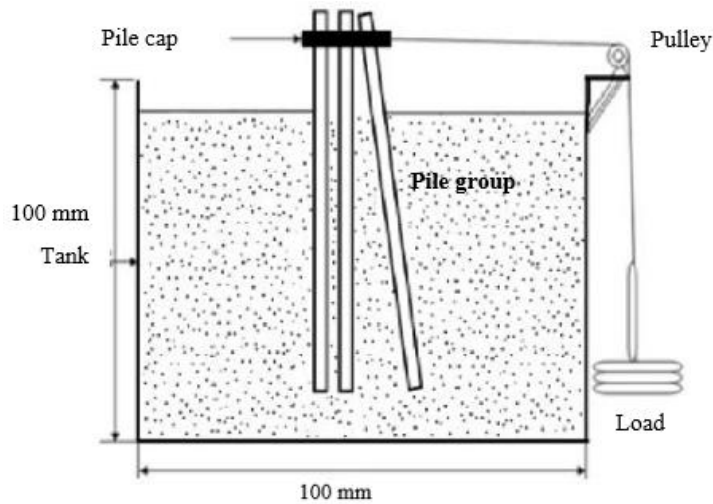


Fig. 2.28 Experimental setup (Singh and Arora, 2017)

2.3.2 Analytical studies

Rajashree and Sitharam (2001) developed a nonlinear finite element model to study the behaviour of batter piles under static and cyclic lateral loads in soft clay. The static and cyclic lateral responses of vertical and batter piles were studied based on developed nonlinear finite element code using hyperbolic and modified hyperbolic relationships to represent the nonlinear behaviour of soil. The results of the analysis revealed that the static lateral capacity of a negative batter pile is more than for a positive batter pile and a vertical pile, see Fig. 2.29. Also, the cyclic lateral capacity of a negative batter pile is more than that for a positive batter pile, see Fig. 2.30.

Poulos (2006) used computer program EMPIG to study the response of a 3×2 pile group containing batter piles in clay soil. Three cases are examined: 1) a group subjected to vertical and lateral loadings, with no ground movements; 2) a group subjected to vertical and lateral loadings, but with vertical ground movements also acting on the group; and 3) a group subjected to vertical and lateral loadings, but with horizontal ground movements acting on the group. In each case, the effect of pile incline on typical behaviour (group settlement, lateral deflection and rotation, and pile loads and moments) are examined. It is found that, while the presence of batter piles can provide some advantages when the group is subjected to applied vertical and lateral loadings, especially in relationship to a reduction in lateral deflection, and also in pile vertical load and pile head moment. However, in the presence of ground movements, the performance of a pile group with batter piles affected adversely as compared to a

group with only vertical piles. The rotation and vertical movement of the group increase significantly in magnitude, while all the loads on the batter piles increase.

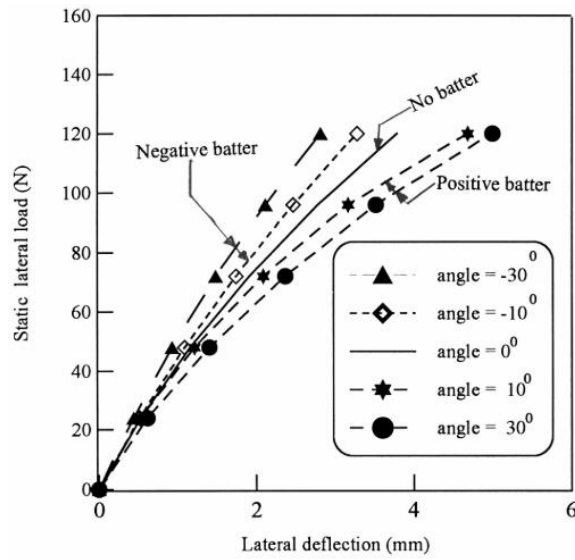


Fig. 2.29 Comparison of lateral load-deflection curves of batter pile at different batter angles (Rajashree and Sitharam, 2001)

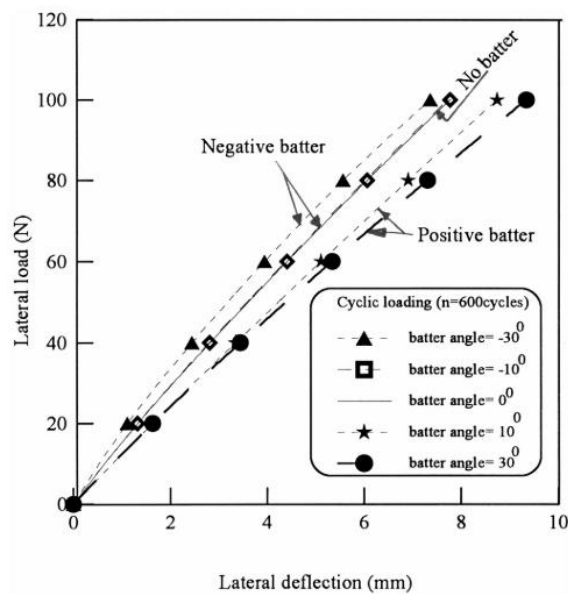


Fig. 2.30 Comparison of lateral load-deflection curve for different batter angles at $n = 600$ cycles (Rajashree and Sitharam, 2001)

Rahimi and Bargi (2010) used finite element framework by using ABAQUS software to simulate the response of batter piles in a pile supported wharf founded in dense sands with 21 vertical and 4 batter piles. Several numerical static tests were conducted using load control at the pile head with the lateral loading in X direction. A number of different pile-supported wharf with different batter pile positions and inclination angles were analysed in term of displacement, bending moment and load distribution among individual piles. From the numerical results, it was observed that the change in pile inclination as well as change in batter piles position in a pile-supported wharf can significantly influence the distribution of pile forces and moments.

Chen and Tsai (2014) used 3D finite difference programme (FLAC^{3D}) to analyse the mechanical response of a batter pile subjected to lateral soil movement. In order to verify the correction of the numerical simulation, its validation was compared with a published case study. The analysis of a single pile in different incline angles subjected to lateral soil movement was modelled. The results of the analysis show that batter pile under the conditions of lateral soil movement will cause pile larger lateral displacement and increasing bending moment on the pile shaft. The pile displacement reduced with the increasing pile incline angle. Vertical pile shaft subjected to negative and positive moment during soil movement, while only positive moment distributed in the batter pile shaft. The moment is higher in batter pile shaft in a weak layer than in non-weak layer. The pile shaft maximum moment occurred nearby the interface of weak layer and stable layer. The moment increased with the incline angle of batter pile, while the moment increasing rate reduced with the increased incline angle.

Wang et al (2014) presented a numerical model using a finite element method (ABAQUS) to discuss the couple effect of soil displacement and axial load on the single inclined pile in cases of surcharge load and uniform soil movement in detail. Parametric analyses are carried out including the degree of inclination and the distance between the clay soil and pile. When the displacement of soil on the left side and right side of a pile is identical, deformation of a vertical pile and an inclined pile is highly close in both cases of surcharge load and uniform soil movement. When the couple effect of soil displacement and axial load occurs, the settlement of an inclined pile is greater than that of a vertical pile under the same axial load and bearing capacity of an inclined pile is smaller than that of a vertical pile. This is quite different from the case when the inclined pile is not affected by soil displacement. When the thickness of the soil is less

than the pile length, the maximum bending moment at the lower part of the inclined pile. Whereas, when the thickness of soil is larger than the pile length, bending moment at the lower part of the inclined pile is zero.

Hazzar et al. (2015) presented numerical models to investigate the effect of the batter angle on the behaviour of laterally loaded batter piles in sand soil. The numerical models were conducted using the computer programme FLAC^{3D} and the model were verified using centrifuge model testing data. The verified numerical model was used to perform a parametric study considering different variations of batter angle and soil density to evaluate the lateral capacity of steel batter piles subjected to lateral loads. Based on the results of this parametric study, the lateral capacities of the batter piles in sandy soils under lateral loads are influenced by the both pile batter angle and sand density.

2.4 Summary

This chapter has given an extensive review of a wide range of literature concerned with the behaviour of piles under both active and passive lateral loads. Some significant aspects have been covered and conclusions are drawn. It is found that, many studies (experimental and theoretical) have been conducted to investigate the behaviour of vertical piles and pile groups under lateral soil movement. A special focus has been given to the experimental investigations that were conducted before. Numerous experimental studies were made through small-scale experiments and centrifuge modelling. These studies were conducted to investigate the response of single vertical piles and pile groups under lateral soil movement taking into account a wide range of influencing factors such as pile diameter, depth of moving layer, pile spacing, number of piles and head fixity condition (e.g. Poulos et al., 1995; Pan et al., 2000a; White et al., 2008; Guo and Qin, 2010; Al-abboodi and Sabbagh, 2017).

Similarly, studies on ‘active’ batter piles subjected to combined lateral and vertical loads have significantly attracted research efforts for the last four decades (Meyerhof and Ranjan, 1972; Meyerhof and Yalcin, 1993; Zhang et al., 1999; Zhang et al., 2002; Prabha & Boominathan, 2010; Wang et al., 2014; Singh and Arora, 2017). In these studies, both experimental and theoretical, researchers focused on the effect of a number of parameters such as batter angle, soil density, pile diameter, pile spacing,

number of piles and direction of the active load on the lateral response of single batter pile and pile group. Additionally, there are some theoretical investigations to evaluate the behaviour of batter piles and batter pile groups under 'passive' loads (Poulos, 2006; Chen and Tsai, 2014). Nevertheless, previous studies did not address the behaviour of batter pile and pile groups subjected to lateral soil movement (inducing 'passive' type of load) in the laboratory. Therefore, little experimental information is available assessing the impact of batter angle, soil density and the depth of moving layer on the response of single batter pile and pile groups. Consequently, further studies on single batter piles and batter pile groups subjected to lateral soil movement using experimental methods are necessary.

Analytically, researchers developed theoretical and numerical methods to study passive and active piles. Complex problems including multi-layer soil, pile groups and soil-pile-cap interaction were investigated using numerical methods such as finite elements and finite difference methods (e.g. Bransby, 1995; Chen and Martin, 2002; Miao et al., 2006; Kahyaoglu et al., 2009; Liyanapathirana and Nishanthan, 2016). On the other hand, theoretical and empirical methods were developed mainly to estimate the lateral pressure on single piles (e.g. De Beer and Wallays, 1972; Ito and Matsui, 1975; Viggiani, 1981). A wide variety of parameters have been studied using various computer softwares such as PLAXIS, FLAC^{3D}, ANSYS and ABAQUS. Although PLAXIS 2D and 3D have been widely used to investigate the response of pile foundations under various loading conditions, a limited information is available concerning the ability of "embedded pile" feature, in which the pile is represented by beam elements surrounded by special interface elements, to simulate the response of single batter pile and batter pile groups under progressively moving sand.

Table 2.1 Summary of previous studies on Piles subjected to horizontal soil movement and batter piles under lateral loading

Authors	Type of study			Type of pile					Type of load		Type of soil	
	Theoretical	Experimental		Vertical	Batter	Only vertical	Only batter	Vertical & Batter	Passive	Active	Sand	Clay
		Field	Lab.									
Murthy (1965)			*	*	*					*	*	
De Beer and Wallays (1972)	*			*		*			*			*
Meyerhof and Ranjan (1972a)	*		*	*	*					*	*	
Meyerhof and Ranjan (1972b)			*			*		*		*	*	
Ito and Matsui (1975)	*					*			*			*
Ranjan et al. (1980)			*	*	*			*		*	*	
Viggiani (1981)	*			*					*			*
Matsui et al. (1982)	*					*			*		*	*
Hanna and Afram (1986)			*	*	*					*	*	
Kalteziotis et al. (1993)		*				*			*			*
Meyerhof and Yalcin (1993)	*		*	*	*					*	*	*
Meyerhof and Yalcin (1994)	*		*		*					*	*	*
Rao et al. (1994)			*		*					*		*
Poulos et al (1995)	*		*	*					*		*	
Bransby and Springman (1996)	*					*			*			*
Chow (1996)	*					*			*			*
Chen and Poulos (1997)	*		*			*			*		*	
Zhang et al. (1999)	*		*		*					*	*	
Tsuchiya et al. (2001)			*	*					*		*	
Rajashree and Sitharam (2001)	*				*					*		*
Chen and Martin (2002)	*					*			*		*	
Pan et al. (2002)	*			*					*			*
Pan et al. (2002a)			*			*			*			*
Zhang et al (2002)			*				*			*	*	
Ong et al. (2003)		*			*				*			*
Cai and Ugai (2003)	*			*					*		*	*

Table 2.1 Summary of previous studies on Piles subjected to horizontal soil movement and batter piles under lateral loading (Continued)

Authors	Type of study			Type of pile					Type of load		Type of soil	
	Theoretical	Experimental		Vertical	Batter	Only vertical	Only batter	Vertical & Batter	Passive	Active	Sand	Clay
		Field	Lab.									
Leung et al (2003)			*			*			*		*	
Poulos (2006)	*							*	*		*	
Miao (2005)	*		*	*		*			*		*	
Miao et al. (2006)	*			*					*		*	
Guo and Ghee (2006)			*			*			*			*
Lee and Chiang (2007)			*	*					*			*
Smethurst and Powrie (2007)	*					*			*		*	
White et al. (2008)		*		*					*		*	
Kahyaoglu et al (2009)	*			*		*			*		*	
Rahimi and Bargi (2010)	*							*		*		*
Prabha and Boominathan (2010)	*		*				*	*		*		*
Zhang and Li (2010)	*					*			*		*	
Qin, (2010)			*	*		*			*		*	
Manoppo (2010)			*		*					*	*	
Lv et al. (2011)			*		*					*	*	
Ghee and Guo (2011)	*			*					*		*	
Pathak et al. (2011)		*						*		*	*	
Liang et al. (2013)	*					*			*		*	
Wang et al (2014)	*				*					*		*
Chen and Tsai (2014)	*				*				*		*	
Ersoy and Yildirim (2014)			*			*			*		*	
Hazzar et al. (2015)	*				*					*	*	
Liyanapathirana and Nishanthan (2016)	*				*				*			*
Singh and Arora (2017)	*							*	*		*	
Al-abboodi and Sabbagh (2017)			*			*			*		*	

Chapter 3

Experimental Apparatus and Test Procedures

3.1 Introduction

As mentioned in Chapter 2, extensive studies have been conducted by a number of researchers on laterally loaded piles. The majority of these studies focused on the vertical pile and pile group subjected to lateral soil movements. Likewise, there were many experimental and theoretical studies reported about the batter pile subjected to active load. On the other hand, limited laboratory work has been conducted to investigate the behaviour of batter pile under progressively moving soil. To this end, a new experimental apparatus has been designed and manufactured by Al-Albboodi and Toma-Sabbagh (2017) was modified and used to carry out a series of laboratory model tests. These tests were performed on instrumented model piles embedded in sandy soil subjected to lateral soil movements to evaluate the effect of different parameters on the behaviour of batter pile and batter pile group. The testing programme involved two main parts; namely single batter pile tests and pile group tests.

The main objectives of this experimental study are:

- To investigate the effects of different parameters on the behaviour of single batter piles subjected to lateral soil movement, i.e., batter pile angle, sand density, pattern of soil movement, thickness of the moving soil mass, pile head boundary conditions and batter pile diameter.
- To investigate the lateral responses of a batter pile group due to lateral soil movement, with a number of parameters, including the pile spacing, pile cap and the arrangement of piles within a group.

In this chapter, firstly, the experimental apparatus and loading system for generating soil movement are described. Secondly, the model ground preparation, properties of sand used, instrumentation of the model piles and the data acquisition system are presented. Thirdly, experimental procedures for conducting the passive pile tests are elaborated. Fourthly, test programme and test details for single piles and pile groups undergoing lateral soil movement are described. Finally, processes and preliminary analysis of the collected data via the data acquisition system are discussed. The experimental results are presented in chapters 4 and 5.

3.2 Experimental apparatus

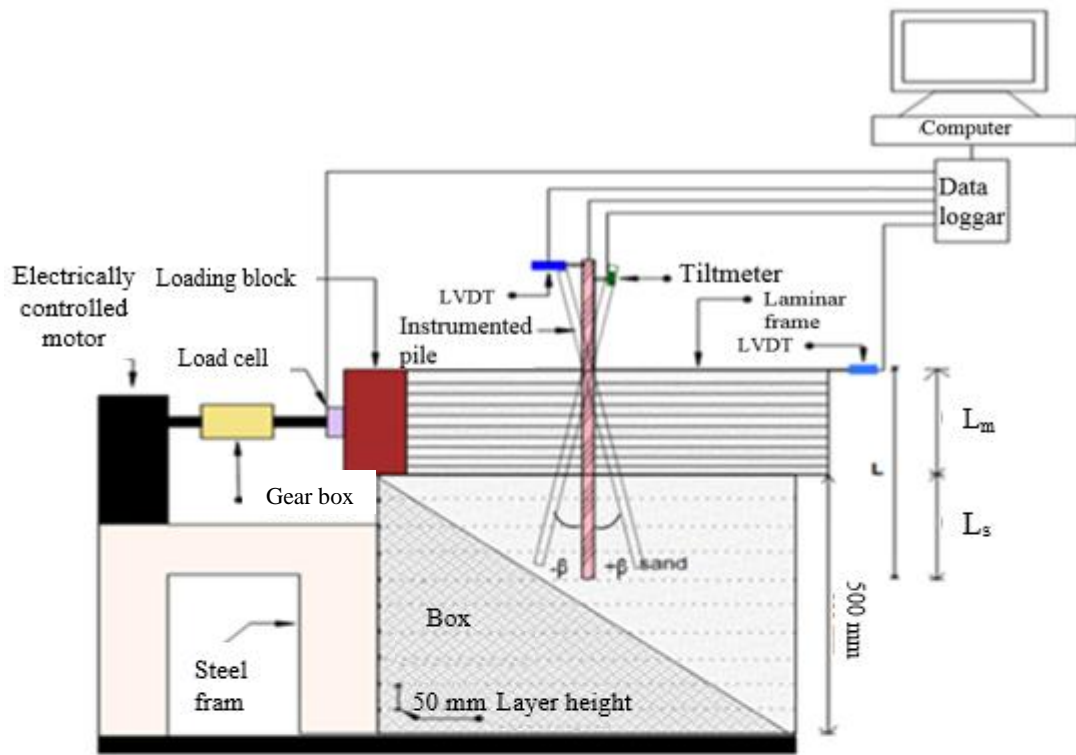
The experimental apparatus primarily consists of a specially designed wooden box, a loading system and a measurement system. The model soil is primarily a sandy soil, in which a single pile or pile group was installed. The loading system allows lateral soil movement to be applied to the single pile or pile group embedded in the sand. The measurement system consists of a data acquisition system, pile instrumentation, LVDTs and a Tiltmeter. The experimental data obtained from the measurement system will provide information that assists to investigate the effect of lateral soil movement on single piles and pile group. The experimental apparatus, sand properties, preparation of model ground and model piles instrumentation are presented in the following sections.

3.3 Experimental testing box

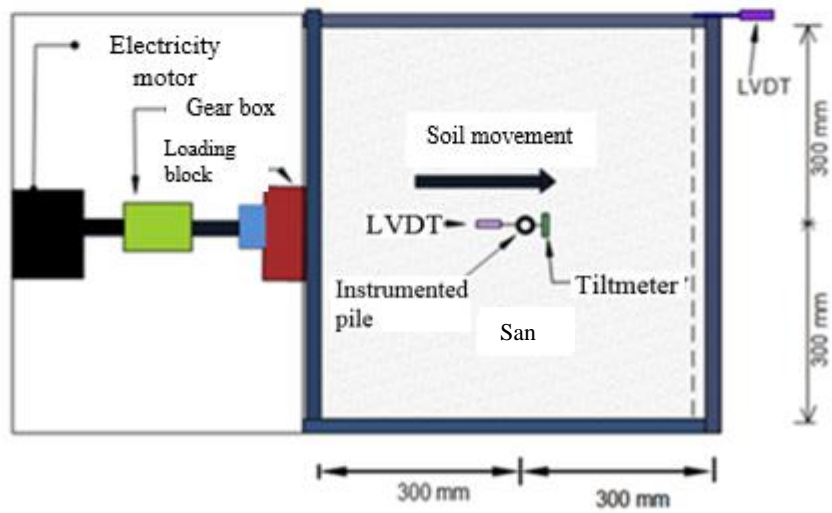
A schematic cross section and an overview of the wooden box and the loading system, which used in this study, is shown in Fig. 3.1 and Fig. 3.2. The internal dimensions of the box are 600 mm by 600 mm, and 700 mm in height. The upper part of the box is made of a series of 20mm thick square laminar timber frames. These frames have smooth upper and lower surfaces to facilitate sliding of the frames in the horizontal direction. The frames, which are allowed to slide horizontally, contain the “moving layer of soil” of thickness L_m ($L_m \leq 200$ mm). The lower section of the box comprises a 500 mm high fixed timber (plywood) box. Moreover, changing the number of movable frames in the upper section, the thicknesses of the stable (L_s) and moving layers (L_m) are varied accordingly. The inner face of the testing box was marked at 50 mm intervals to assist accurate formation of sand stacking inside the testing box during the tests.

3.4 Design of the testing box

The dimensions of the testing box have been chosen according to previous researches taking into consideration the boundary conditions influence of the testing box. In other words, there was minimum or no interference between the walls of the soil tank and the effected zone around the piles. Therefore, for piled raft foundation under lateral loading, the size of soil tank should be extended up to 8–12D and 3-4D in the direction and perpendicular to lateral load, respectively, also, the soil thickness must be kept below pile tip at least 6D (Khari, 2013), where D is the pile diameter.



(a) Elevation view



(b) Top view

Fig. 3.1 Schematic diagram of testing box (a) Elevation view and (b) Top view

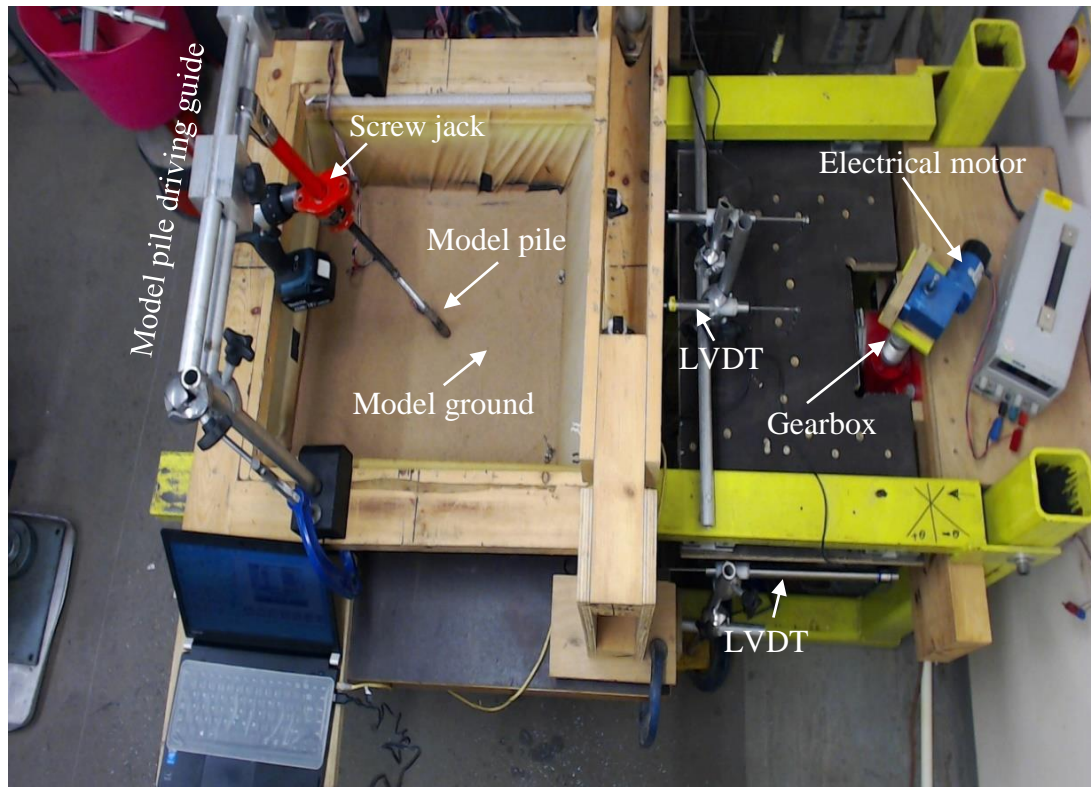


Fig. 3.2 Testing box

3.5 Lateral loading system

The lateral loading system consists of a loading block (Fig. 3.3) and a screw jack connected to electronically controlled motor with maximum capacity of 25 kN as shown in Fig. 3.4. Although in reality piles may be subjected to different types of profiles of lateral soil movement such as trapezoidal, triangular or rectangular, the loading block has been designed to apply a triangular and rectangular profile of lateral soil movement on the laminar frames. The application of such soil movement profile is justified by some real cases (see Chapter 2, Subsection 2.2.1.2). Throughout all the test programmes, the rate of movement of the upper box (the laminar frames) is controlled by the motor screw jack loading system. Loading rate was chosen in this study according to the model tests adopted by (Poulos et al., 1995), in which the rate of 3 mm/min.



Fig. 3.3 Triangular and rectangular loading blocks



Fig. 3.4 Motor and screw jack

3.6 Sand properties

The model piles were embedded in sand of medium to fine particles size. The sand properties as shown in Fig. 3.5, Fig. 3.6 and Table 3.1 which were obtained from various laboratory tests were conducted on sand in accordance to BS-1377 specifications. To minimise scaling effects, the ratio between pile diameter and mean particle size of sand (D_{50}) should be greater than 50 (D'Arezzo et al., 2014). Also, pile diameter should be kept (15-30) times greater than the maximum particle size (Khari et al., 2014). However, the model pile diameter was 60 times greater than the mean grain size and 16 times greater than the maximum particle size. Thus, there is no important impact of the model sand on the pile behaviour regarding scaling effect.

3.7 Model piles

Fig. 3.7 shows a schematic diagram of the instrumented pile subject to testing loads. Three types of model piles were fabricated from a hollow circle aluminium tube with outer diameter of 16, 20 and 25 mm and a wall thickness of 1.2 mm, respectively. The total length of the model pile is 350 mm with variable embedded pile length depending on the test type.

Table 3.2 shows the dimensions and the material properties of the piles used. The piles were instrumented with six strain gauges to measure the bending moment along the

embedded lengths numbered from SG1 to SG6. Each strain gauge was glued on the model pile surface at a vertical interval of 50 mm. After that, to protect them from damage, the gauges were covered with clear heat shrink tube to the entire length of the pile. The model pile surface has been made rough by gluing dry sand particles to simulate concrete piles (see Fig. 3.7). A conical head was installed at the tip of piles to facilitate pile jacking.

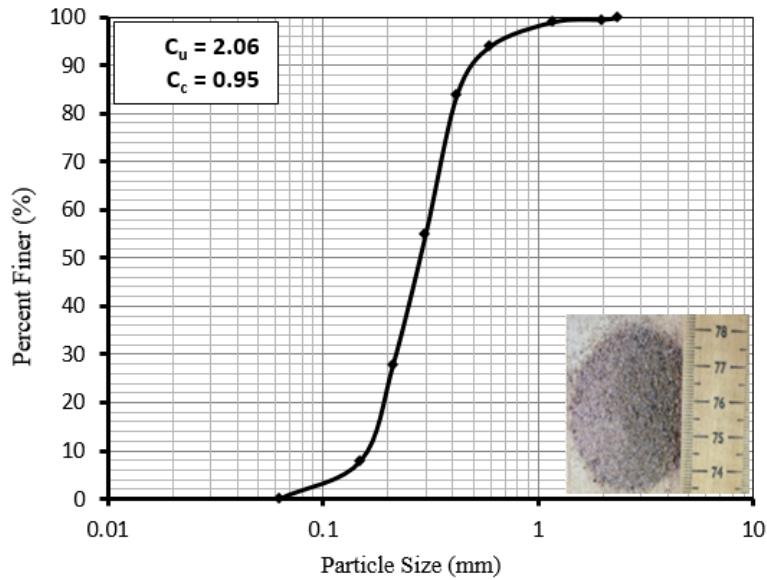


Fig. 3.5 Gradation curve of the sand

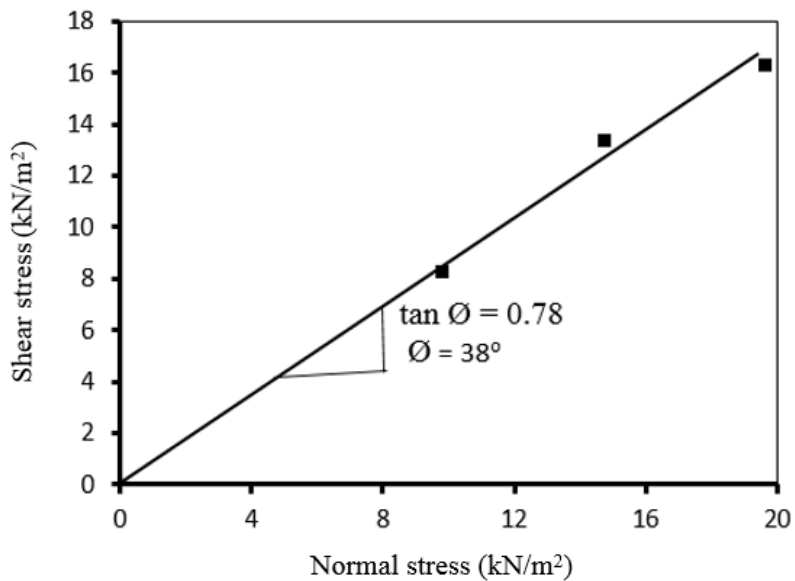


Fig. 3.6 Direct shear box test

Table 3.1 Properties of the model sand

Property	Value
Specify gravity G_s	2.7
Effective size D_{10} (mm)	0.15
D_{30} mm	0.21
Mean grain size D_{50} (mm)	0.29
D_{60} mm	0.31
Particle size range (mm)	0.063 – 1.18
Coefficient of uniformity C_u	2.06
Coefficient of curvature C_c	0.95
Soil classification	SP
Soil description	Poorly graded sand
Max. dry unit weight (kN/m^3)	16.63
Min. dry unit weight (kN/m^3)	14.0
Max. void ratio	0.9
Min void ratio	0.6
Dry unit weight (kN/m^3)	15.2
Angle of internal friction (ϕ)	38°

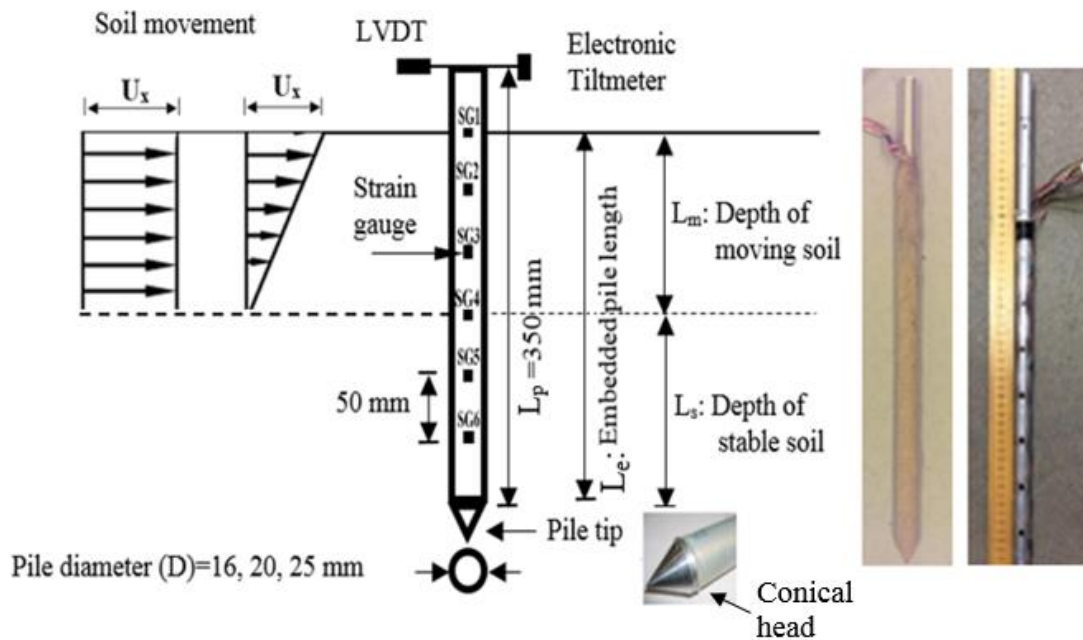


Fig. 3.7 Schematic diagram of a pile subjected to rectangular and triangular loading block

Table 3.2 Pile dimensions and material properties

Pile details	Value
Outside diameter (D) (mm)	16, 20 and 25
Wall thickness (t) (mm)	1.2
Type of pile	Aluminium
Modulus of Elasticity (E_p) (MPa)	65000
Unit weight (γ_p) (kN/m^3)	27
Yield bending moment (M_y) (N.mm)	46200

3.8 Data acquisition system

The data acquisition system consists mainly of a data logger and a desktop computer, these were utilised to monitor the test and allow readings to be taken and stored automatically. A computer software "Catman" version 3.5 was used to measure and record the outputs from LVDTs, load cell, strain gauges and electronic tiltmeter.

3.8.1 Strain gauges:

Strain gauges of MMF307381 type were used. Each strain gauge has a resistance of 120Ω with 5 mm gauge length and a gauge factor of 1.2. The strain gauges were glued to the surface of the model pile using an adhesive after the pile surface had been smoothed.

3.8.2 LVDT (Linear variable differential transformer)

Solartron DC LVDT (Linear variable differential transformer) with 50 mm measurement range and 0.00001 mm accuracy has been adopted. Two LVDTs have been used in order to measure the horizontal displacements of the pile head and laminar frames. These LVDT have been connected to the pile using thin wires to avoid any interfering with loading system (see Fig. 3.8).

3.8.3 Electronic tiltmeter

Tiltmeter, Seika.de NB3 sensor type was installed along the length of pile to measure rotation during lateral loading (see Fig. 3.9).

3.8.4 Load cell

A load cell of 10 kN capacity was used to measure the load applied by the motor gear loading system. See Fig. 3.10.

3.8.5 Data logger

HBM (MX440A) data logger as shown in Fig. 3.11 was used to automatically record the data from the strain gauges, LVDTs and the load cell during tests, and then transfer data to a computer.

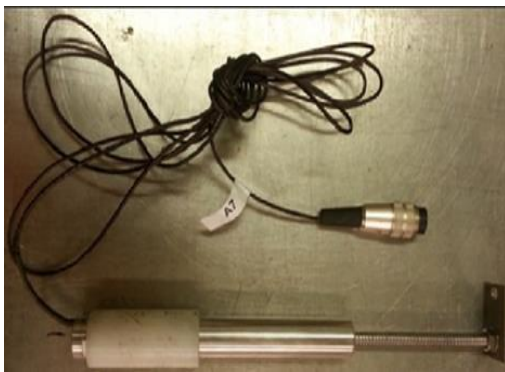


Fig. 3.8 LVDT



Fig. 3.9 Electronic tiltmeter



Fig. 3.10 Load cell



Fig. 3.11 Data logger

3.9 Calibration of piles

In order to ensure an appropriate relationship between the strain gauge output and bending moment, all the piles have been calibrated in bending by testing the pile as a

cantilever beam in which one end of the pile was fully fixed against rotation and displacement while the other end was free and under a point load. The piles were carefully orientated so that the loads were applied in the plane of the strain gauges. Fig. 3.12 shows the test setup for the calibration of a model pile. Two levels of loads (1 kg and 2 kg) were applied at the free end of the pile, which have then been removed sequentially to represent the loading and the unloading process. Strain gauges were tested in both tension and compression states of loading. The recorded strain at each strain gauge location has been compared with the calculated bending moment (see Fig. 3.13). Thus, each strain gauge had a conversion factor in which it is multiplied by a gauge reading to obtain the bending moment directly at the strain gauge locations by applying the elastic flexure formula (equation (3.1)).

Where:

$$M = \sigma \cdot Z_p = \varepsilon E_p Z_p \quad (3.1)$$

$$Z_p = \frac{\pi(D^4 - D_i^4)/64}{D/2} \quad (3.2)$$

Where:

M: the bending moment of the pile at the strain gauge locations,

σ : flexural stress, ε : the measured strain,

$E_p Z$: conversion factor,

E_p : Young's Modulus of the pile

Z_p : elastic section modulus of the pile cross section,

D: outer diameter of the pile cross section,

D_i : inner diameter of the pile cross section.

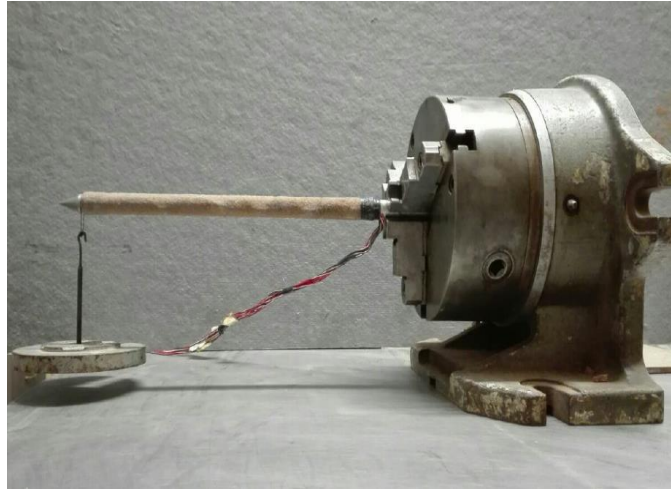


Fig. 3.12 Strain gauges calibration

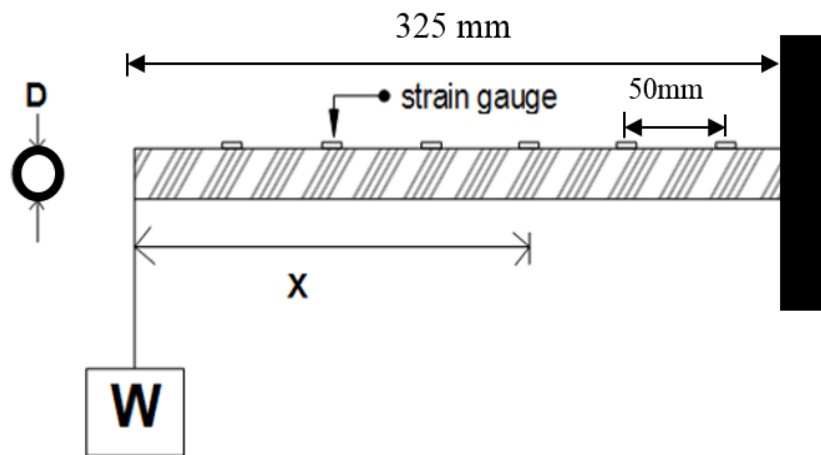
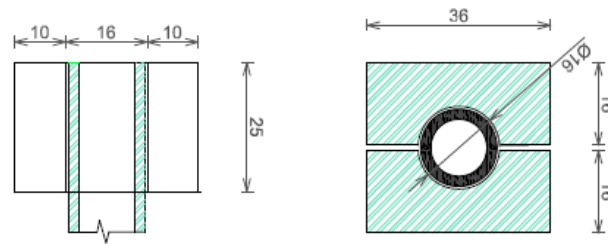
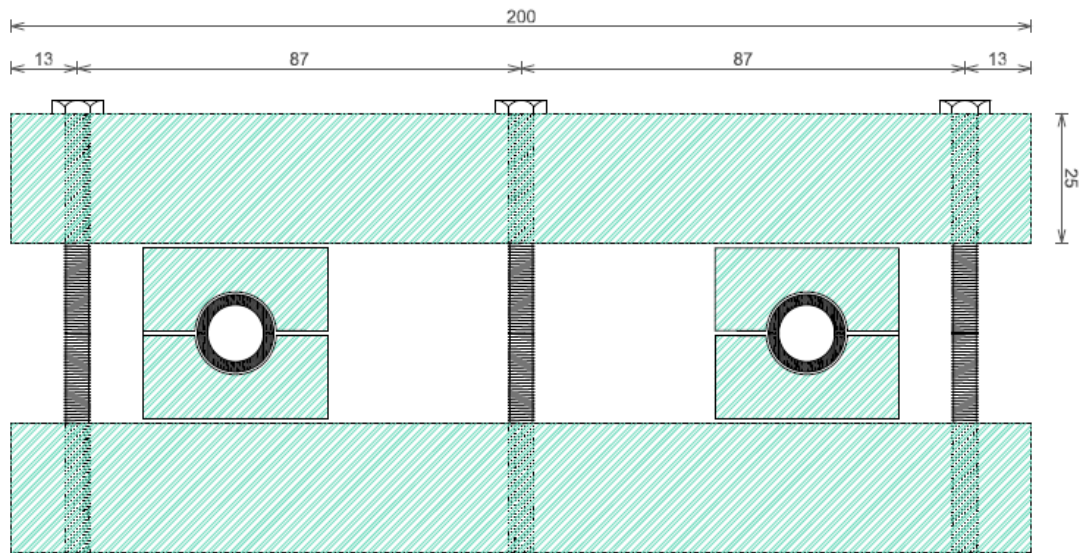


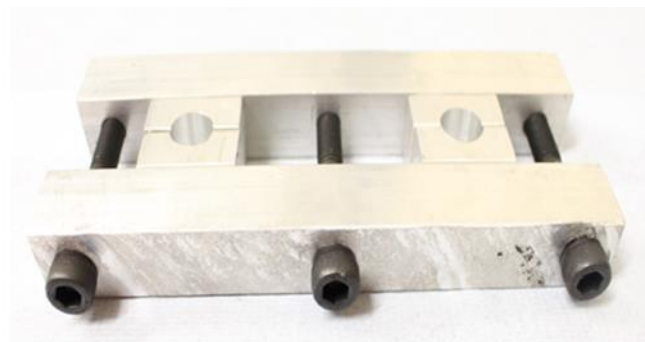
Fig. 3.13 Setup for Strain gauges calibration

3.10 Model pile cap

The pile cap for both vertical and batter piles group was made of two aluminium alloy pieces in order to ensure an easy assembly after piles installation into sand was completed. The details and dimensions of the pile cap and relevant settings used in the tests are described in Fig. 3.14. The pile cap was specifically designed to enable each pile in the group to be installed in required batter angle. To ensure rigidly connection between the piles and the cap (the head of each pile was completely secured against movement and rotation to the cap), the bolts tightening was performed strongly.



(a) Schematic diagram of pile cap (all dimensions are in mm)



(b) Side view



(c) Top view



(d) Assembly of batter piles and pile cap piece.

Fig. 3.14 The details and dimensions of the pile cap

3.11 Soil preparation

The sand was first placed in layers using tamping technique to maintain a uniform density throughout (Gaaver, 2013). Accordingly, the testing box is divided into 14 layers (each layer with 50 mm in height) by marking the interior sides of the box. The quantity of sand for each layer is weighed via an electronic scale. Then, the sand is spread inside the testing box and compacted with wooden tamping hammer, as shown

in Fig. 3.15, until the required density is achieved by levelling the soil surface with the marked line. The compaction process was carefully chosen to produce a homogeneous sample that is used in a parametric study. This operation is repeated until the box is full.

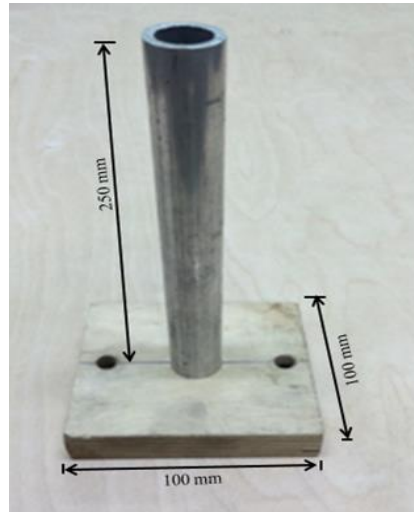


Fig. 3.15 Wooden tamping hammer

3.12 Pile installation

After the sand is prepared inside the testing box, an installation guide was installed onto the top of the testing box as shown in Fig. 3.16a. The main parts of the installation guide are a rotational screw jack and an aluminium frame as shown in Fig. 3.16b. The installation guide was used to place the batter pile into the sand to a desired embedded length and batter angle. Prior to the installation of the batter pile at the exact location into the sand surface, the angle of the pile inclination was adjusted by an angle meter (see Fig. 3.17). Subsequently, tightening an installed bolt at the head of a screw jack to prevent it from rotation. Then the pile was slowly driven into the sand by means of rotating screw jack by rechargeable drill. After the installation was finished, the driving guide was removed. The final view of the instrumented pile prior to testing (free pile head test) is shown in Fig. 3.18. For a fixed-head pile test, another type of aluminium frame was installed by two clamps onto the top of testing box as shown in Fig. 3.19. To restrain the pile head from moving (horizontally and/ or vertically) or rotating, parallel clamp was used to secure pile head onto the frame tightly (see Fig. 3.20).

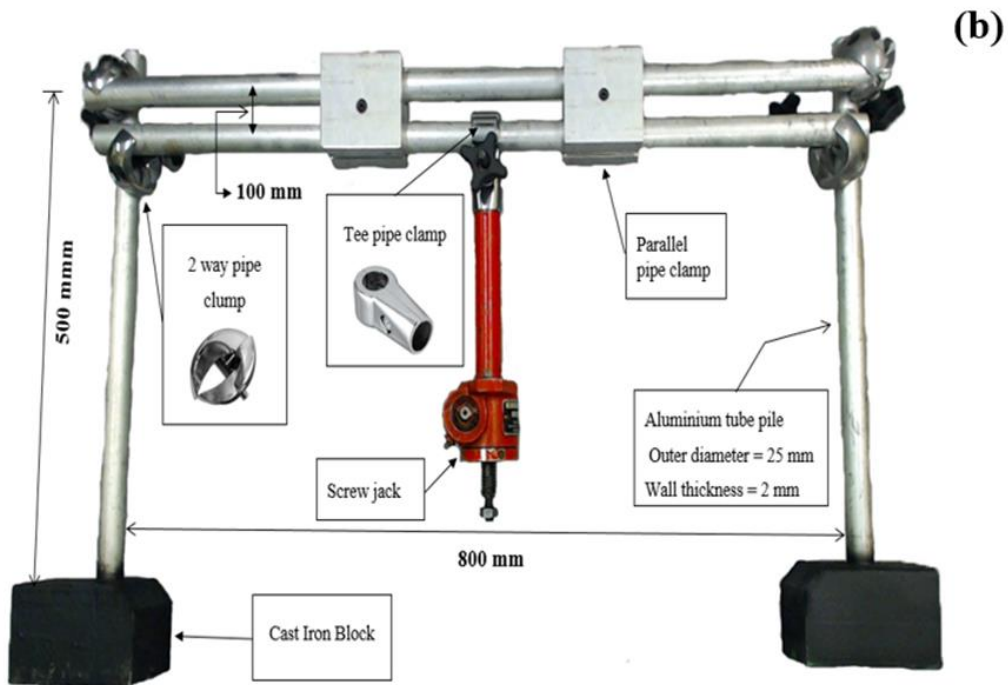


Fig. 3.16 The installation guide of batter pile



Fig. 3.17 Angle meter

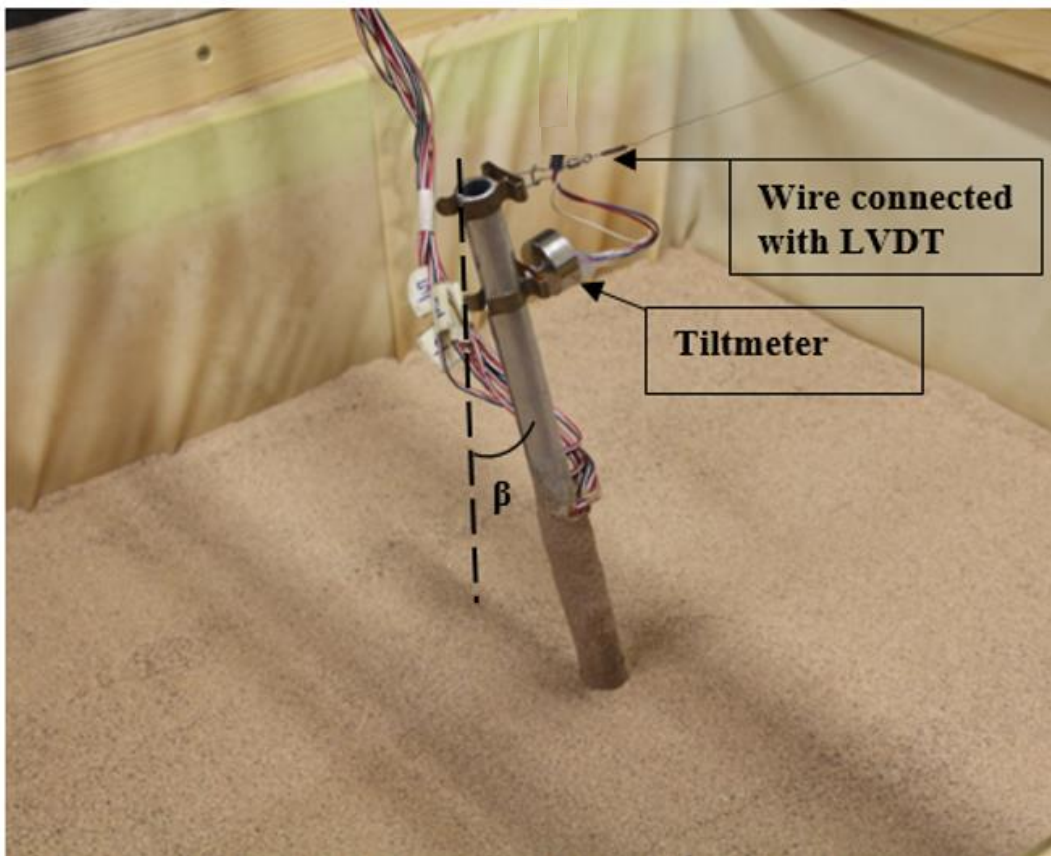


Fig. 3.18 Final view of the instrumented batter pile to testing (free-head pile test)

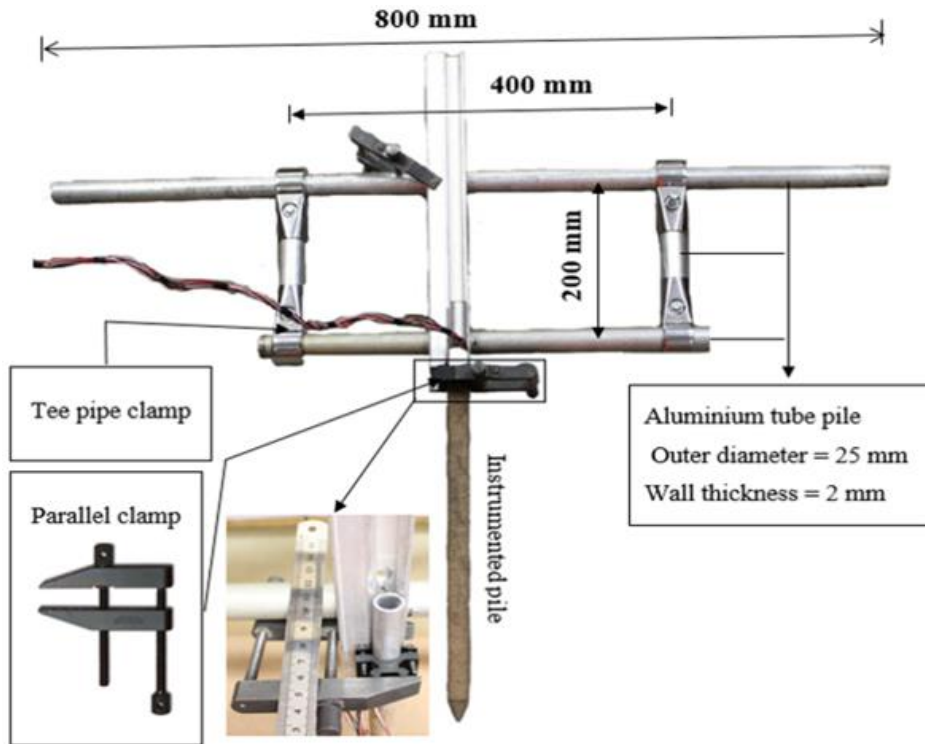


Fig. 3.19 Details of aluminium frame used for a fixed-head pile test

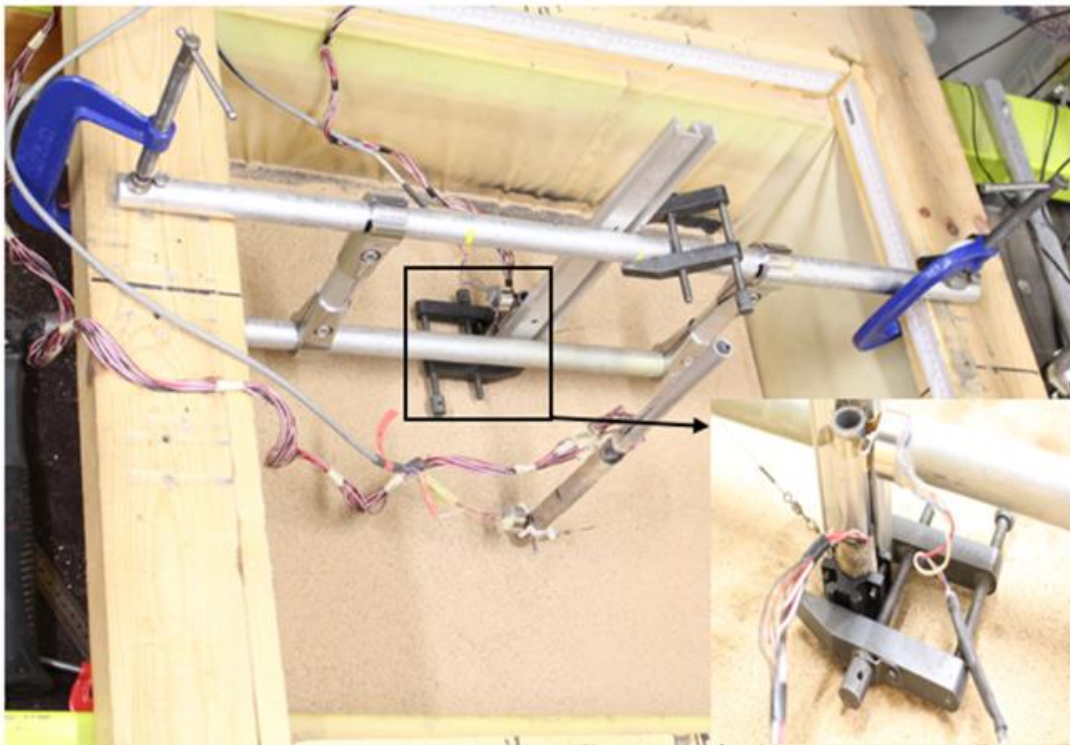


Fig. 3.20 Final view of the instrumented pile prior to testing (fixed-head pile test)

3.13 Experiment procedure

For each test, these procedures are following:

1. Prepare the soil sample in a way described previously in section 3.11 to a required depth.
2. Install the guiding frame.
3. Place the instrumented pile in the centre of the testing box using the guide frame with a pre-set embedded depth below the sand surface and required pile inclination.
4. Connect the load cell, LVDT and Tiltmeter to the data logger.
5. For free pile-head test, the guiding frame has to be removed.
6. Apply Lateral force via the loading blocks (rectangular or triangular) on the movable frames with a specified loading rate to the horizontal movement of the soil towards the pile.
7. Empty the sand from the testing box after the end of each test.

Fig. 3.21 shows the procedure of a single pile test. During the passive loading, the strain gauge, LVDTs, Tiltmeter readings and the lateral force on the frames were taken for every 5 mm movement of the top laminar frame.

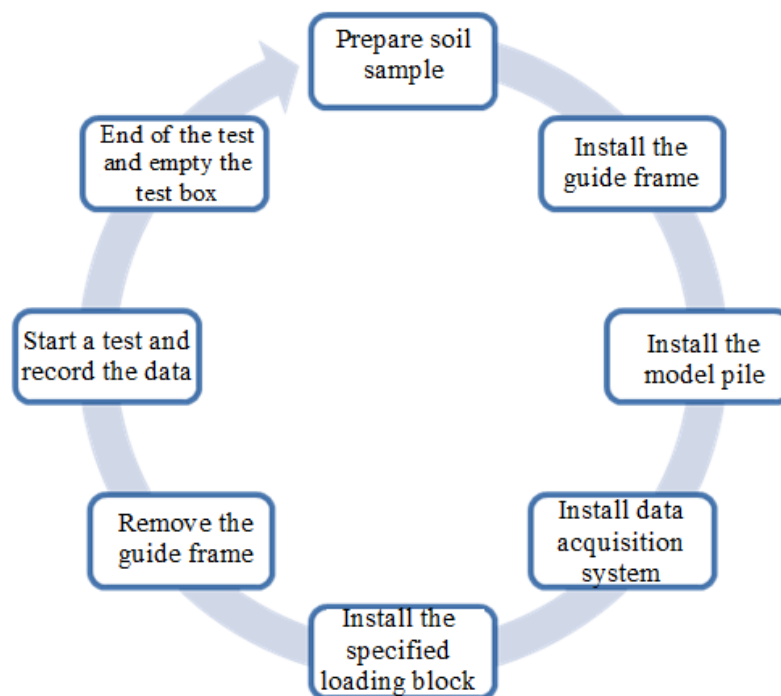


Fig. 3.21 Testing procedure of single pile test

3.14 Sign convention

Before presenting a method for determining the pile rotation, displacement, shear force, and soil reaction, it is necessary to establish a sign convention so as to define “positive” and “negative” pile responses in the interpretation of test results. Fig. 3.22 illustrates the positive directions of the pile responses. They are explained below.

Frame (soil) movement

The hydraulic jack and loading block system generate positive frame movement thus soil movement in the loading direction across the testing box.

Pile displacement

The pile displacement away from the loading side is considered positive.

Pile rotation

The pile rotation in clockwise direction is deemed positive.

Bending moment

The internal moment which causes tension in the front side (closer to the loading direction) of the pile is taken as positive.

Shear force

The internal shear force which causes a counter-clockwise rotation of the pile segment on which it acts is regarded positive.

Soil pressure

The soil pressure which acts in the direction away from the loading side, i.e. causing positive pile displacement, is deemed positive.

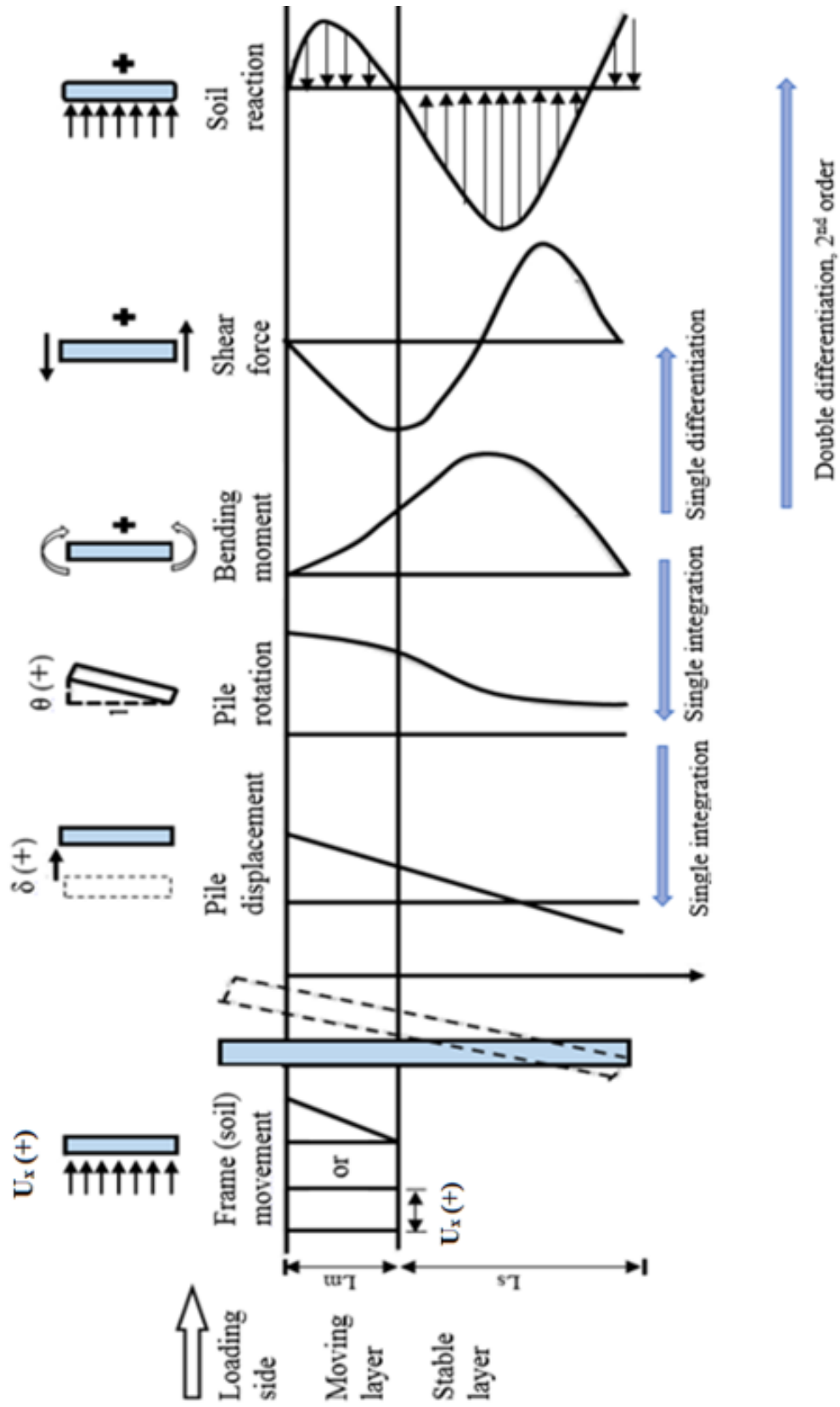


Fig. 3.22 Pile behaviour based on beam theory (Qin, 2010)

3.15 Data analysis and processing

The data obtained from the strain gauges were converted to bending moments and plotted to a series of bending moment profiles at different magnitudes of the lateral soil movements. In order to derive the other pile responses, the bending moments and the displacement measurements were then subjected to extensive analysis and data processing. For this purpose, the finite difference method was used.

3.15.1 Numerical differentiation

In order to the finite difference method to be applied easily to the pile, the strain gauges were spaced at equal lengths, Δz , as shown in Fig. 3.23. The strain gauge measurement, in terms of the bending strain of the beam, was measured at each point of the pile. A series of bending strain, against depth, z , were plotted for each loading increment, in this case the applied soil movement (U_x). Consequently, the shear force (f_i) could be obtained by differentiating the bending moment (m_i). This differentiation was achieved by using the 1st order finite differentiation relationship from Equation 3.3 (Ghee, 2009).

$$f_i = \frac{1}{2} \frac{m_{i+1} - m_{i-1}}{\Delta z} \quad (3.3)$$

Where:

Δz : the subinterval for dividing the pile length, equalling to 50 mm, or the spacing of the strain gauges.

m_i : the bending moment at a section on the pile.

The soil reaction could be obtained by the 2nd order finite differentiation relationship from Equation 3.4 (Ghee, 2009).

$$p_i = \frac{1}{7} \frac{2m_{i-2} - m_{i-1} - 2m_i - m_{i+1} + 2m_{i+2}}{\Delta z^2} \quad (3.4)$$

3.15.2 Numerical integration

Numerical integration using the trapezoidal rule was used to compute the pile rotation profile with the pile rotation at the ground surface as the input boundary condition. Referring to Fig. 3.23, the pile rotation at a specific point was calculated by the following generalised equations (Qin, 2010) based on five sections (i.e. k=1 to 5):

$$\theta_i \text{ (i=5)} \quad \theta_i = \theta_0 - \frac{\Delta z}{2I_p E_p} (m_0 + m_5) \quad (3.5a)$$

$$\theta_i \text{ (i=1, 2, 3, 4)} \quad \theta_i = \theta_0 - \frac{\Delta z}{2I_p E_p} \left(m_0 + 2 \sum_{k=i+1}^5 m_k + m_i \right) \quad (3.5b)$$

$$\text{Pile tip} \quad \theta_{tip} = \theta_0 - \frac{\Delta z}{2I_p E_p} \left(m_0 + 2 \sum_{k=1}^5 m_k \right) \quad (3.5c)$$

Where:

θ_0 : rotation of the pile at soil surface (was measured by electronic tiltmeter),

$I_p E_p$: bending rigidity of pile.

Once the pile rotation profile was obtained, it was further integrated to derive the pile deflection with Equations 3.6 (Qin, 2010) as:

$$\delta_i \text{ (i=5)} \quad \delta_i = \delta_0 + (\theta_0 + \theta_7) \frac{\Delta z}{2} \quad (3.6a)$$

$$\delta_i \text{ (i=1, 2, 3, 4)} \quad \delta_i = \delta_0 - \left(\theta_0 + 2 \sum_{k=i+1}^5 \theta_k + \theta_i \right) \frac{\Delta z}{2} \quad (3.6b)$$

$$\text{Pile tip} \quad \delta_{tip} = \delta_0 - \left(\theta_0 + 2 \sum_{k=1}^5 \theta_k + \theta_{tip} \right) \frac{\Delta z}{2} \quad (3.6c)$$

Where:

δ_0 : pile displacement at soil surface (was measured by LVDT).

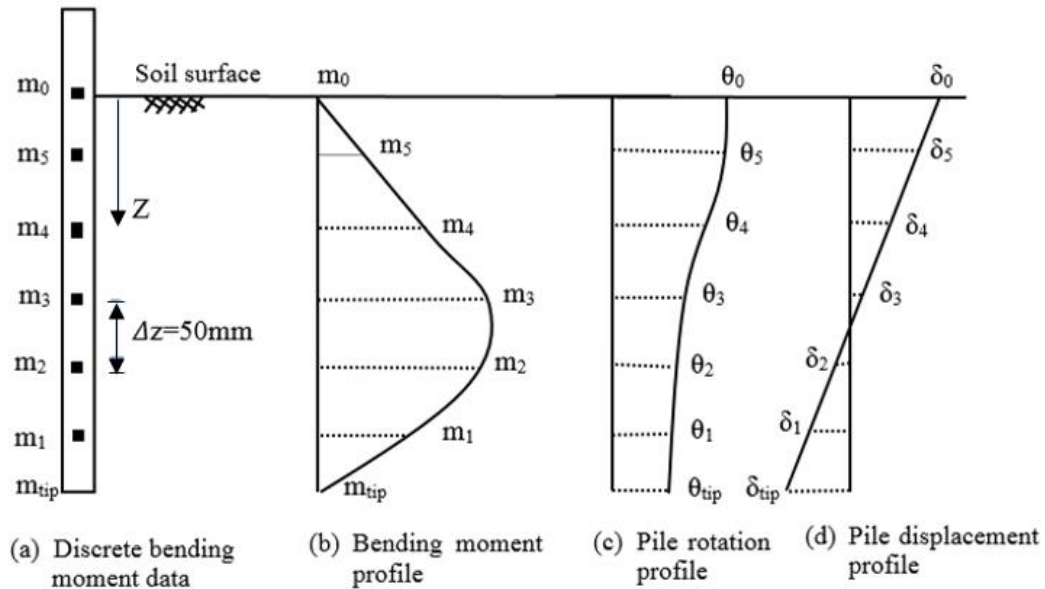


Fig. 3.23 Numerical integration for calculating pile rotation and displacement

3.16 Spreadsheet program for data processing

A spreadsheet program using Microsoft Excel 2013 was prepared to process and analyse the measured data based on the methods mentioned above. Pile response profiles of bending moment, shear force, soil reaction, rotation and displacement can be deduced and plotted automatically for a single pile or a pile within a group at each frame movement. This program has greatly facilitated the analysis of all tests.

3.17 Testing programme

A series of tests were conducted on piles with different batter angles under both rectangular and triangular loading blocks, as shown in Fig. 3.24; total of 54 tests (44 tests on single pile and 10 tests on pile groups). Sample results for individual tests were presented in Appendices A & B (see Figs. A.1 to A.44 and Figs. B.1 to B.10). The tests intended to explore effects of the following parameters on pile response subject to lateral soil movement:

- Density: three different soil densities and five batter angles; -20° , -10° , 0° , $+10^\circ$, $+20^\circ$, (a total number of 15 tests) were tested under triangular loading profile.
- Pile diameter: three pile diameters and five batter angles; -20° , -10° , 0° , $+10^\circ$,

- +20°, (a total number of 15 tests) were tested under rectangular loading profile.
- Moving and stable soil depth (L_m and L_s): five values of moving and stable layer depths were applied and batter angle of zero value (vertical piles) were tested under rectangular loading profile (a total number of 5 tests).
 - Effect of distance from soil movement source to the pile location under rectangular loading profile: two distances and two batter angles; 0°, +10°, (a total number of 4 tests).
 - Pile head fixity: five batter angles; -20°, -10°, 0°, +10°, +20° tests with fixed head condition, (a total number of 5 tests) were tested under rectangular loading profile.
 - Batter angle: this parameter is included in the experiments of the density, the pile diameter, pile head fixity and the effect of the distance from soil movement source.
 - Group configuration: seven different pile group configurations were studied. The details are shown in Fig. 3.25. The configurations of the pile group involved in this series of tests had a pile spacing value (s) of 3D. One test for VVL, two tests for BBL, two tests for BVL and two tests for VBL (a total number of 7 tests) were performed under rectangular loading profile.
 - Pile spacing: two additional tests were conducted for BVL configuration with pile spacing values of 5D and 7D (a total number of 2 tests).
 - Effect of piles cap: one test was carried out on a pile group without cap to compare its behaviour with that of the pile group with cap.

More details on all series of tests conducted in this study are given in Table 4.1 in chapter 4 and Table 5.1 in chapter 5.

Each test on single pile was denoted by a combination of letters and numbers to express shape of loading block, pile head fixity, pile diameter, and batter pile angle. For example, tests (RSF25, 0°), (TSL16, 0°), and (RSF25, +10°):

- T, R denoted the triangular or rectangular loading block.
- S denoted to single pile.
- F, L denoted to free and fixed pile head condition.
- 16, 25 indicate outer diameter of the pile, 16 mm or 25 mm.
- 0°, +10° represent pile inclination (0, ±10, and ±20) degree.

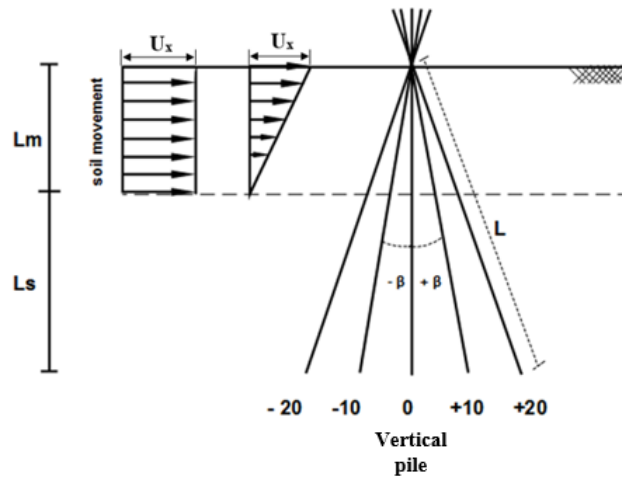


Fig. 3.24 Batter pile setup for lateral soil movements

While, every test in the case of group pile 2×1 was indicated by three letters (see Fig. 3.25);

- BVL: Front pile is battered (B), rear pile is vertical (V).
- VBL: Front pile is vertical (V), rear pile is battered (B).
- BBL: Both piles are battered (BB).
- VVL: Both piles are vertical (VV).
- VVF: Both piles are vertical (VV).
- L, F: Limited piles (with pile cap) and free piles (without pile cap), respectively.

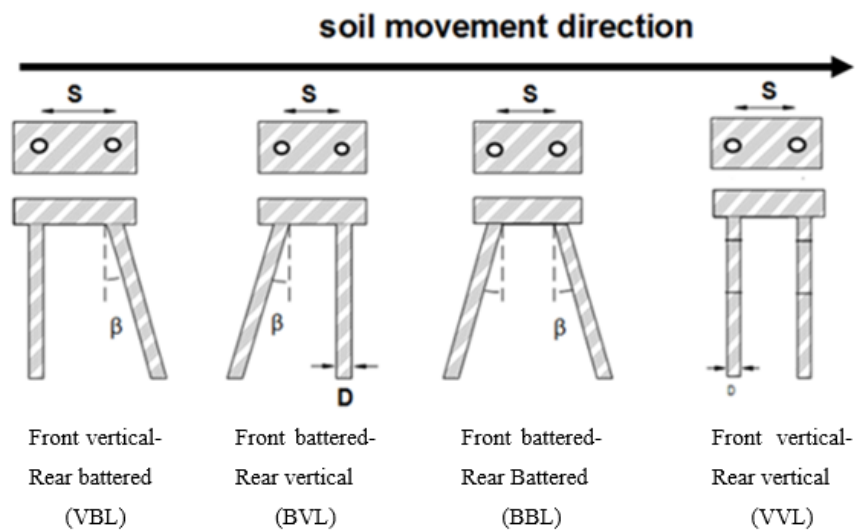


Fig. 3.25 Types of 2×1 pile group configurations

3.18 Summary

The experimental apparatus and the procedure adopted for conducting the model tests on batter piles, subjected to lateral soil movement, have been described in this chapter. Three new aluminium model piles having the same length, but different diameters were designed and manufactured. The piles were instrumented with strain gauges along the shaft for the measurement of bending moments, and LVDT and Tiltmeter were used to record the pile head deflection and head rotation. From these measurements, the finite difference method was used to derive the shear force and the soil reaction, also to derive the pile rotation and the pile deflection. The results from the model tests are presented and discussed in chapters 4 and 5.

Chapter 4

Experimental Results of Single Batter Pile Tests

4.1 Introduction

This chapter presents an overview of the investigation into the behaviour of single batter piles subjected to lateral soil movement. A series of model tests were conducted with a set of piles at different inclinations and diameters. The experimental results obtained from laboratory tests are presented and discussed in this chapter. The tests are carried out with rectangular and triangular soil movement profiles. The test results are presented in the form of the profiles of bending moment, shear force, soil reaction, displacement and rotation measured along the pile length; and the development of maximum bending moment against soil movement. The test results are analysed to:

- show the behaviour of batter piles in progressively moving sand;
- examine the effect of the distance between the batter piles location and soil movement source, moving and stable soil depth, batter angle, pile diameter, pile head fixity, sand density and soil movement profile on the response of the piles;
- examine the development of the moment and soil pressure with progressively moving soil; and
- establish the relationship between maximum bending moment and maximum shear force.

Table 4.1 shows the tests conducted on single batter and vertical piles. The results obtained from each test are tabulated in Appendix A (Figs. A.1 to A.44). The pile response is presented in terms of bending moment, shear force, soil reaction, pile rotation and pile deflection.

Table 4.1 Tests conducted on single batter and vertical piles

No.	Test description	L_m (mm)	L_s (mm)	L_e (mm)	Purpose of tests	Section	Appendix
1	RSF16, 0°	150	150	300	standard test	4.3.1	Fig. A.1
2	RSF16, 0°	150	50	200	effect of L_s & L_m $\gamma_s=15.2$ kN/m ³	4.3.2	Fig. A.2
3			75	225			Fig. A.3
4			100	250			Fig. A.4
5			125	250			Fig. A.5
6			125	150			275
7	RSF16, +10°	150	150	300	effect of β $\gamma_s=15.2$ kN/m ³	4.3.3	Fig. A.7
8	RSF16, +20°						Fig. A.8
9	RSF16, -10°						Fig. A.9
10	RSF16, -20°						Fig. A.10
11	RSF6, 0° ds=200 mm	150	150	150	effect of pile distance, $\gamma_s=15.2$ kN/m ³	4.3.5	Fig. A.11
12	RSF6, 0° ds=400 mm						Fig. A.12
13	RSF16, +10° ds=200mm						Fig. A.13
14	RSF16, +10° ds=400mm						Fig. A.14
15	RSL16, 0°	150	150	150	effect of pile head fixity, $\gamma_s=15.2$ kN/m ³	4.3.6	Fig. A.15
16	RSL16, +10°						Fig. A.16
17	RSL16, +20°						Fig. A.17
18	RSL16, -10°						Fig. A.18
19	RSL16, -20°						Fig. A.19
20	RSF20, 0°	150	150	150	effect of pile diameter, $\gamma_s=15.2$ kN/m ³	4.3.7	Fig. A.20
21	RSF20, +10°						Fig. A.21
22	RSF20, +20°						Fig. A.22
23	RSF20, -10°						Fig. A.23
24	RSF20, -20°						Fig. A.24
25	RSF25, 0°	150	150	150			Fig. A.25
26	RSF25, +10°						Fig. A.26
27	RSF25, +20°						Fig. A.27
28	RSF25, -10°						Fig. A.28
29	RSF25, -20°						Fig. A.29
30	TSF16, 0°	150	150	300	effect of soil density $\gamma_s=14.7$ kN/m ³	4.4.1	Fig. A.30
31	TSF16, +10°						Fig. A.31
32	TSF16, +20°						Fig. A.32
33	TSF16, -10°						Fig. A.33
34	TSF16, -20°						Fig. A.34
35	TSF16, 0°	150	150	300	effect of soil density $\gamma_s=15.2$ kN/m ³	4.4.2	Fig. A.35
36	TSF16, +10°						Fig. A.36
37	TSF16, +20°						Fig. A.37
38	TSF16, -10°						Fig. A.38
39	TSF16, -20°						Fig. A.39
40	TSF16, 0°	150	150	300	effect of soil density $\gamma_s=15.7$ kN/m ³	4.4.3	Fig. A.40
41	TSF16, +10°						Fig. A.41
42	TSF16, +20°						Fig. A.42
43	TSF16, -10°						Fig. A.43
44	TSF16, -20°						Fig. A.44

4.2 Repeatability

Repeatability is the variation in results caused by repetition of the original test in the same conditions more than once. In order to assess the repeatability and confirm the reliability of the small-scale laboratory test results, a number of influencing factors should be overcome. These factors include:

1. Variation in soil density.
2. Horizontality of pile cap and soil surface.
3. Orientation of single pile and piles within the group.
4. Rotation of the sliding box during movement.

Therefore, great efforts have been made to overcome these issues, i.e. conducting a series of "check tests" before starting to accept the test results. Moreover, each test has been repeated at least twice to achieve its repeatability checks. An example for results of repeated tests and the effects of the above variation on the maximum bending moment for test RSF16, 0° at soil displacement (U_x) of 30 mm are given in Table 4.2. The table shows that when the relative variations was around 4 % in load cell readings, 9 % in LVDT, 11 % in tilting recordings and 7 % in strain gauge measurements, the variation between measured maximum bending moment (M_{max}) of both repeated tests was around 6%. The final adopted M_{max} was determined from an average value of two tests. These figures clearly confirm the reliability of the repeated tests under the same procedure and conditions.

Table 4.2 Effect of error in test data on M_{max}

Test Description	Load cell	LVDT	Tilting recordings	Strain gauge	M_{max}
	[kN]	[mm]	[Rad.]	[$\mu\text{m/m}$]	[N.mm]
RSF16,0° (r_1)	1.330	10.188	0.063	281.159	3833
RSF16,0° (r_2)	1.386	11.095	0.070	300.278	4067
relative variation (%) $rv = (r_2 - r_1) / r_1 * 100$	4.2	8.9	10.6	6.8	6.1

4.3 Tests for single piles subjected to rectangular soil movement profiles

In the following subsections 4.3.1 to 4.3.7, the effect of embedded length, batter angle, and pile location in the testing box, pile head fixity, and pile diameter on the lateral response of batter pile are investigated.

4.3.1 Free-head tests on a 16 mm diameter pile (RSF16, 0°)

A number of tests were performed on a free-head vertical pile ($\beta = 0^\circ$) of 16 mm diameter pile (D) and subjected to rectangular loading block at sand density (γ_s) of 15.2 kN/m³. For the first test (referred to hereafter as the "standard" test), the box was filled with sand to the top. The pile length in the upper "moving" sand layer (L_m) was 150 mm, while that in the lower "stable" sand layer (L_s) was 150 mm.

Fig. 4.1a shows the distribution of bending moment along the pile shaft at six different values of soil surface displacement (U_x). The figure shows that the bending moment profiles are similar to a parabolic shape at $U_x \geq 10$ mm. The measured maximum moment, M_{max} , occurs at the vicinity of the interface between the moving and stable sand layers at a depth of 200 mm below the ground surface. This behaviour agreed well with the general trend observed by Qin (2010).

Bending moments at different positions (corresponding to the locations of strain gauged load cells) along the pile shaft are plotted against the soil surface displacement (U_x) in Fig. 4.1b and it is found that the relationship is non-linear. The bending moment increases with increasing soil displacement, but the rate of increase reduces, especially when the soil surface displacement U_x is greater than about 20 mm. Since the pile did not reach its yield moment (46200 N.mm given in Table 3.2), the measured non-linear response is due to the plastic flow of the sand.

The finite difference method was used to obtain the pile response in terms of shear force, soil reaction, deflection and rotation along the pile length. The shear force and the soil reaction are derived from differentiation of the bending moment distributions shown in Fig. 4.2. On the other hand, the pile inclination and pile deflection are derived from integration of the bending moment distributions (see Chapter 3, section 3.15).

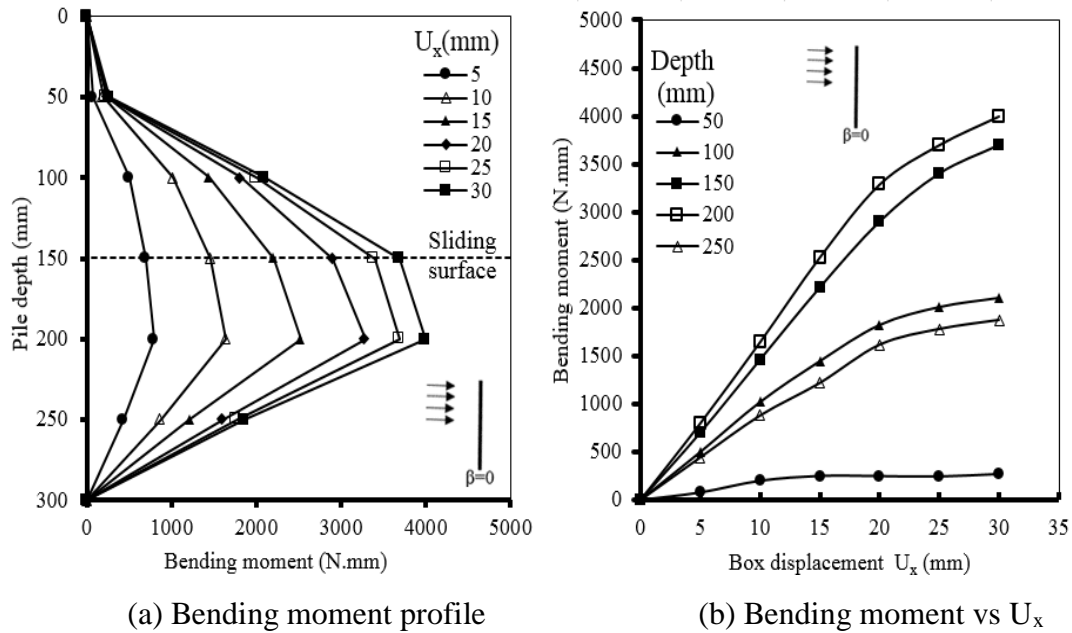


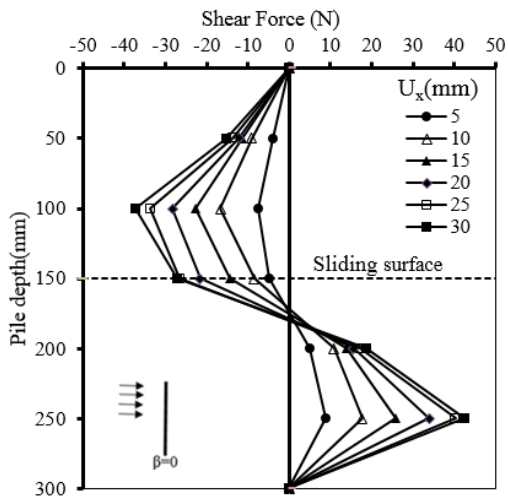
Fig. 4.1 Bending moment distributions from the "standard" test, $\beta = 0^\circ$

Fig. 4.2 presents the pile response in terms of shear force, soil reaction, pile rotation and pile deflection, subjected to soil movements from 5 mm to 30 mm.

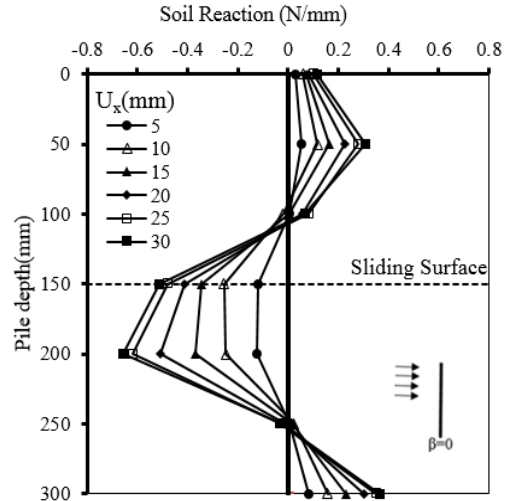
The following characteristics are identified from the pile response:

- Shear force and soil reaction attain their maximum value after which remain approximately constant when $(U_x) \geq 15$ mm ($U_x/D=0.94$), see Fig. 4.2a and b.
- The two largest local shear forces were obtained at depths of 100 mm and 250 mm, see Fig. 4.2a.
- Soil reaction within the moving soil layer (L_m) showed an arch shape and reaches its maximum (p_{max}) at a depth of approximately 50 mm ($L_m/3$), as shown in Fig. 4.2b.
- Rotation angle remains positive for the entire pile length, with small differences between the top and bottom section of the pile (see Fig. 4.2c).

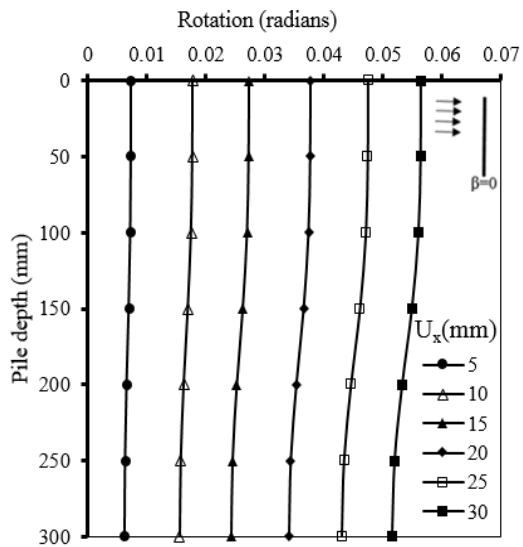
Fig. 4.2d shows that the pile deflection increases with increasing soil displacement. Also, the pile deflection at the soil surface is about 33 % (10 mm) of the total soil displacement ($U_x = 30$ mm). This refers to the fact that the moving sand is flowing around the pile.



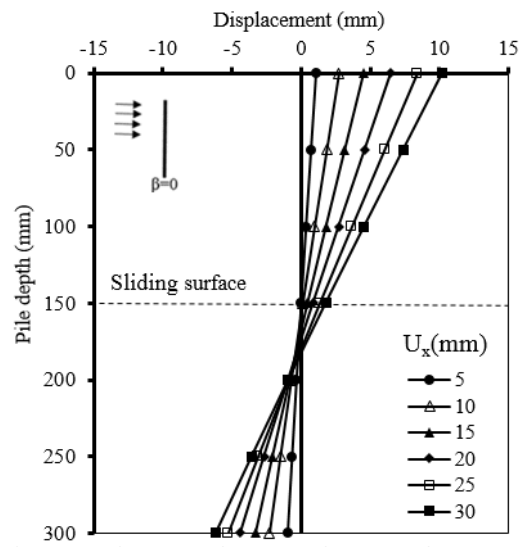
(a) Shear force profile (N)



(b) Soil reaction profile (N/mm)



(c) Pile rotation (radian)



(d) Pile deflection (mm)

Fig. 4.2 Response of the 16 mm diameter pile in terms of shear force, soil reaction, pile rotation and pile deflection at $L_m/L_s = 150/150$

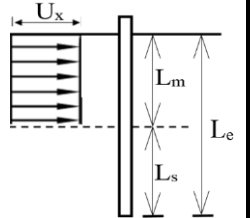
4.3.2 Influence of embedded length

To investigate the effect on the pile response of the pile embedded lengths L_e in the upper "moving" sand layer (L_m) and in the lower "stable" sand layer (L_s), two more series of tests were conducted on the same pile. The effect of L_s and L_m on the pile response was investigated in the first and second series of tests, respectively, as detailed in Table 4.3.

In all these cases, the distributions of bending moments along the pile shaft and the variations of bending moments with increasing soil displacements are quite similar in shape but different in magnitude to those of the "standard" test. Summarized results are shown in Fig. 4.3 - Fig. 4.6.

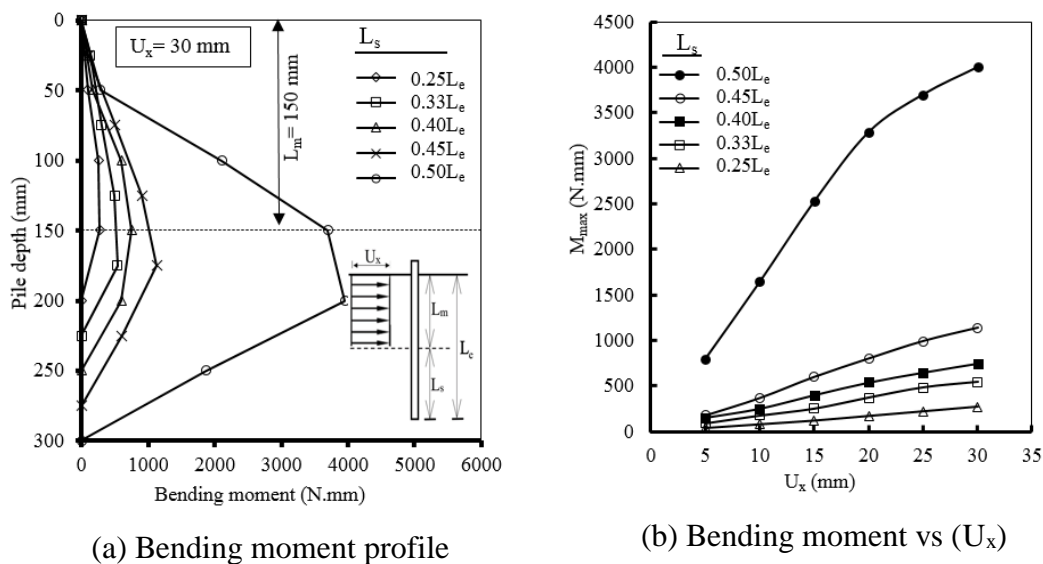
Table 4.3 Details of each test on a single free-head pile of 16 mm diameter

Test No.	L_m (mm)	L_s (mm)	L_e (mm)	Remark
1	150	150	300	Standard test
2	150	50	200	Investigation of the effect of L_s
3		75	225	
4		100	250	
5		125	275	
6	125	150	275	Investigation of the effect of L_m



For series 1, L_m was kept constant at 150 mm while L_s was varied in increments of 25 mm. The bending moment distribution corresponding to a soil surface displacement U_x of 30 mm for each L_s is plotted against depth in Fig. 4.3a, while the bending moment corresponding to the location of the maximum bending moment for each L_e , is plotted against the soil surface displacement U_x in Fig. 4.3b. It is found that the bending moment increases with increasing L_s , but the rate of increase is not the same although each increment of L_s is same. The initial increasing rate is followed by a larger rate of increase when the value of L_s approaches L_m . However, the location of the maximum bending moment in each case is found to be generally near the vicinity of the interface between the two layers.

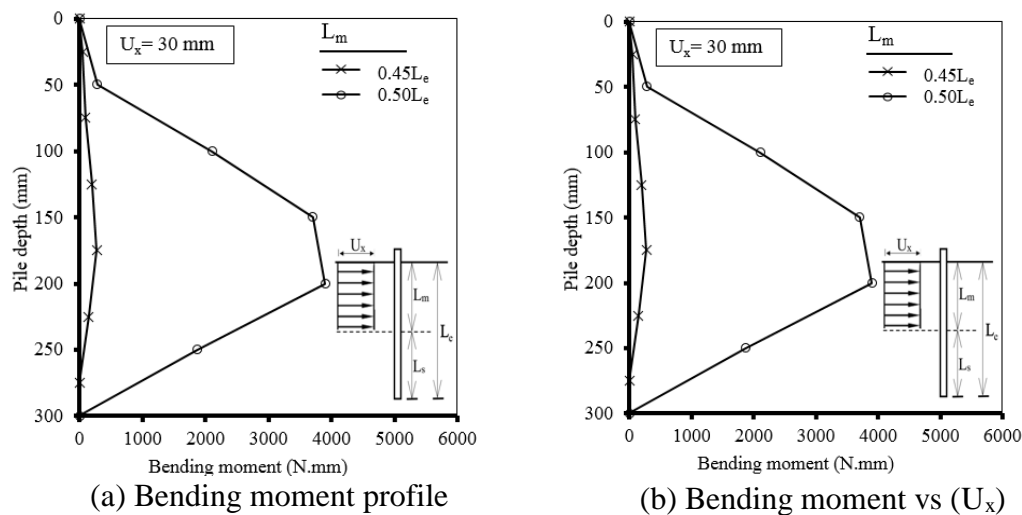
For series 2, L_s was kept constant at 150 mm while L_m was varied in increment of 25 mm. Fig. 4.4a shows the distribution of bending moment corresponding to a soil surface displacement U_x of 30 mm, and Fig. 4.4b shows the relationship between the bending moment at the location of the maximum bending moment and the applied soil surface displacement U_x for each L_m value. It is found that the bending moment increases sharply with increasing L_m (from $0.45L_e$ to $0.5L_e$) and the location of the maximum bending moment for both cases again was found to be close to the interface between the two layers. The maximum bending moment corresponding to (U_x) is presented for each case in Table 4.4.



(a) Bending moment profile

(b) Bending moment vs (U_x)

Fig. 4.3 The effect of L_s on bending moment for a fixed L_m (150 mm)



(a) Bending moment profile

(b) Bending moment vs (U_x)

Fig. 4.4 The effect of L_m on bending moment for a fixed L_s (150 mm)

Table 4.4 Maximum bending moments from test series 1 and 2

Test No.	L_m (mm)	L_s (mm)	L_e (mm)	L_m/L_e	M_{max} (N.mm) for different values of U_x (mm)						
					5	10	15	20	25	30	
1	Series 1	150	50	200	0.75	44	83	122	171	243	275
2			75	225	0.66	71	125	253	374	482	541
3			100	250	0.60	105	223	406	541	653	752
4			125	275	0.54	150	370	602	804	990	1135
5	Standard test	150	150	300	0.50	798	1644	2527	3288	3700	3950
6	Series 2	125	150	275	0.45	51	75	115	153	204	273

In order to examine the combined effects of L_m and L_s on the pile response, the maximum bending moments from all cases are plotted against the dimensionless embedded lengths L_s/L_e and L_m/L_e in Fig. 4.5. This figure shows that for a constant L_m , there exists a threshold value for L_s . When L_s is less than this threshold value, the bending moment increases with increasing L_s whereas when L_s is greater than the threshold value, the bending moment decreases with increasing L_s . On the other hand, for a constant L_s value, there also exists a threshold value for L_m . When L_m is less than the threshold value, the bending moment increases with increasing L_m , whereas when L_m is greater than the threshold value, the bending moment decreases with increasing L_m value.

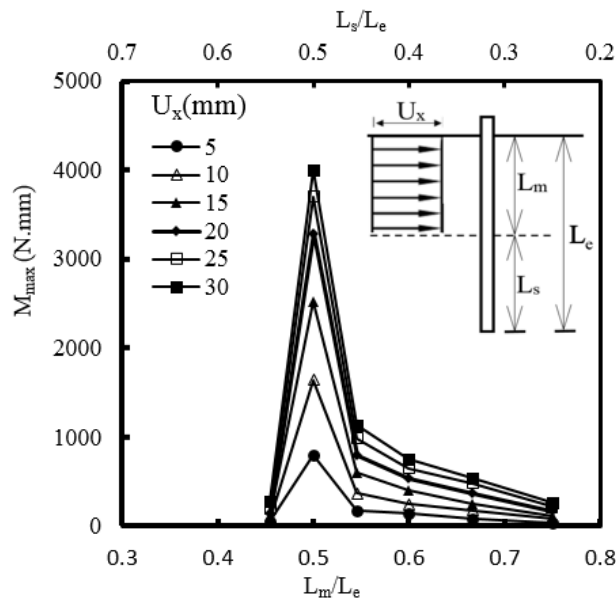


Fig. 4.5 The relationship between maximum bending moment and dimensionless embedded length (L_e)

These two results seem to suggest that when L_s is very small as compared to L_m , the moving soil tends to carry the pile, without causing substantial bending moments in the pile, thus producing a "short pile" mode of pile response. When L_m is very small as compared to L_s the moving soil tends to move past the pile without causing substantial bending moments in the pile, and thus produces a "flow" mode of soil movement around the pile. In between these two modes, there is an "intermediate" mode, when both L_s and L_m are equal, and the bending moment in the pile in this case is larger than that in the other two cases. Hence, it appears that the bending moment in the pile induced by moving soils may reach its peak value when the values of L_s and L_m are equal.

An attempt has been made to normalise the maximum bending moment caused by different amounts of soil displacement by the value of the soil surface displacement (U_x), to give a unified relationship with pile embedded length, as shown in Fig. 4.6. Algebraic expressions may be obtained from Fig. 4.6 and can be expressed as follows:

$$\frac{M_{\max} \times D^2}{E_p I_p U_x} \times 10^4 = 76 \frac{L_m}{L_e} - 34 \quad 0.4 \leq L_m/L_e \leq 0.5 \quad (4.1)$$

$$\frac{M_{\max} \times D^2}{E_p I_p U_x} \times 10^4 = -61 \frac{L_m}{L_e} + 34.4 \quad 0.5 \leq L_m/L_e \leq 0.55 \quad (4.2)$$

$$\frac{M_{\max} \times D^2}{E_p I_p U_x} \times 10^4 = -3.6 \frac{L_m}{L_e} + 2.9 \quad 0.55 \leq L_m/L_e \leq 0.75 \quad (4.3)$$

Where E_p and I_p are the modulus of elasticity and moment of inertia of the pile, respectively. It should be noted that the above expressions are derived based on model tests and may not be applicable to full scale situations because of scale effects. However, if these could be calibrated against some field tests, then they might be of some practical use.

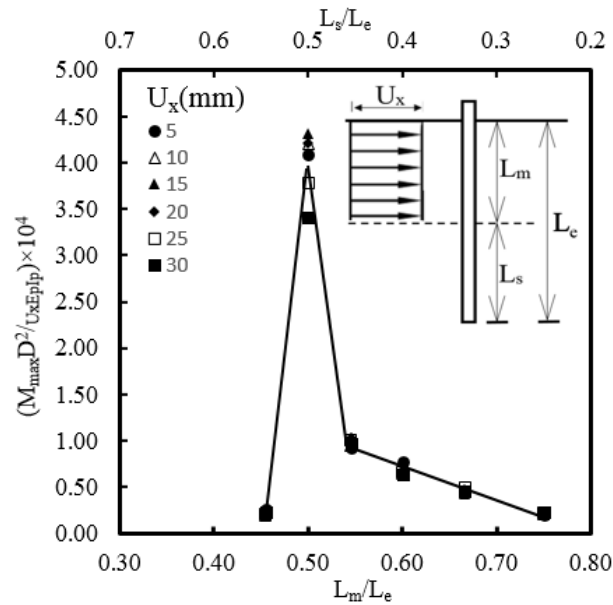


Fig. 4.6 The relationship between normalised maximum bending moment and dimensionless embedded length (L_c)

4.3.3 Effect of batter angle (RSF16, β)

In order to investigate the influence of batter angle (β) on the batter pile response, four tests were conducted on the 16 mm diameter pile under the same conditions as those of the "standard" test with different angles of inclination ($\beta = \pm 10^\circ$ and $\pm 20^\circ$), see Table 4.1. The results have indicated that all graphs had almost the same general trends of the corresponding graphs plotted for the 'standard' test.

Fig. 4.7 shows the response of the batter pile in terms of bending moment measured at 25 mm of soil displacement (U_x) for the four tests plus the standard test. According to the figure Fig. 4.7, the following observations can be drawn:

- The shape of bending moment profile for all tests are almost similar (parabolic shape).
- Maximum bending moment, M_{max} occurs at a depth of 200 mm ($0.67 L$), (at this depth).
- Bending moments developed along the embedded length of the pile were all positive.

The relationship between the M_{max} and lateral soil displacement (U_x) for various batter angles (β) is shown in Fig. 4.8a which indicated the following:

- The M_{\max} increases linearly as the U_x increases at about $U_x \leq 20$ mm (1.25D), but afterwards they are nonlinear. The rate of an increase in the M_{\max} increases from $\beta = +20^\circ$ to $\beta = -20^\circ$.
- Regardless of batter angle, the M_{\max} reaches its peak and approximately remains constant (at $U_x > 20$ mm).

The variation of M_{\max} with batter angles (β), at $d_{\max} = 200$ mm, with different value of soil displacements (U_x) are shown in Fig. 4.8b. It can be seen that the M_{\max} measured at $\beta = -20^\circ$ (negative batter pile) was the greatest for different stages of (U_x). Conversely, M_{\max} measured at $\beta = +20^\circ$ (positive batter pile) was the smallest. It is interesting to note that the above findings agree well with those presented by Poulos (2006). He found that the forces imposed on the piles due to lateral soil movement are highly affected by their inclination direction relative to the direction of soil movement. The forces imposed on the piles which are inclined against the lateral soil movement (or negative batter piles) were the highest compared to the vertical and positive batter piles (where the pile is battered toward the direction of soil movement). Also, he showed that reason may be attributed to the additional loads due to drop the soil above the negative batter pile.

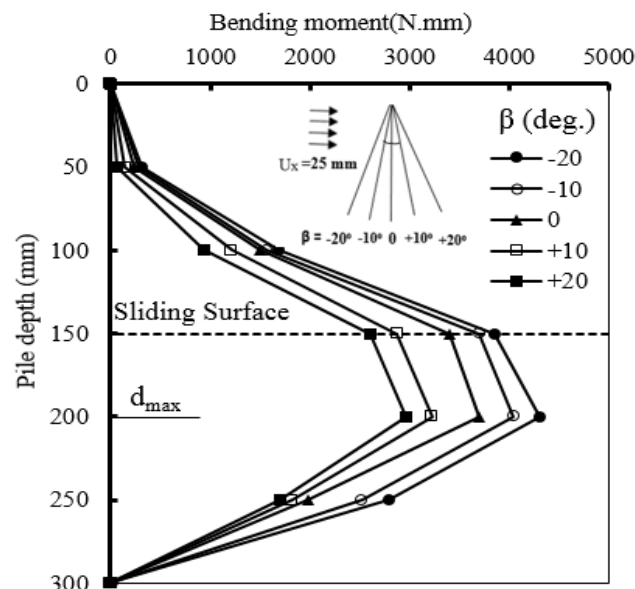


Fig. 4.7 Bending moment profiles for different batter angles (β)

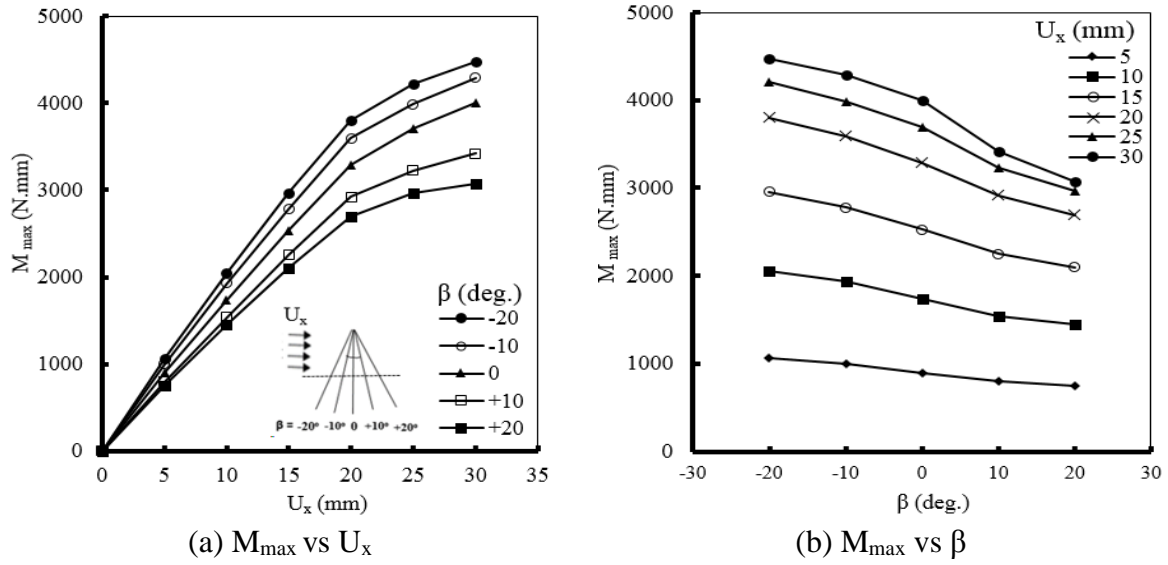


Fig. 4.8 Bending moment of batter pile for different values of (β) and (U_x), $d_{\max} = 200$ mm

Fig. 4.9 illustrates the variation of the ratio ($M_{B,\max}/M_{V,\max}$) with the batter angle (β) for different values of soil displacements (U_x).

Where:

$M_{B,\max}$: maximum bending moment of batter piles with different values of β ,

$M_{V,\max}$: maximum bending moment of vertical pile ($\beta=0$).

The general trends indicate that the maximum bending moment on batter piles depends on the batter angle and the soil displacement. For “positive” batter angle ($\beta = +10^\circ$ and $+20^\circ$), the M_{\max} of the positive batter pile decreases with increasing β for different values of soil displacements U_x . When U_x increases from 5 to 30 mm, the ratio ($M_{B,\max}/M_{V,\max}$) decreases from 0.85 to 0.89 at $\beta = +10^\circ$ and from 0.77 to 0.84 at $\beta = +20^\circ$. In contrast, for “negative batter angle ($\beta = -10^\circ$ and -20°), the M_{\max} increases with increasing β values. Again, when U_x increase from 5 to 30 mm, the ratio ($M_{B,\max}/M_{V,\max}$) increases from 1.07 to 1.11 at $\beta = +10^\circ$ and from 1.12 to 1.18 at $\beta = +20^\circ$ (see Table 4.5).

Table 4.5 Comparisons of different behaviours of single vertical and batter piles

		$(M_{B,max}/M_{V,max})$				
		-20	-10	0	+10	+20
U_x (mm)	β (deg.)	Negative batter angle		Vertical pile	Positive batter angle	
	5		1.18	1.11	1.00	0.89
10		1.18	1.11	1.00	0.88	0.83
15		1.17	1.10	1.00	0.89	0.83
20		1.16	1.09	1.00	0.89	0.82
25		1.14	1.08	1.00	0.87	0.80
30		1.12	1.07	1.00	0.85	0.77

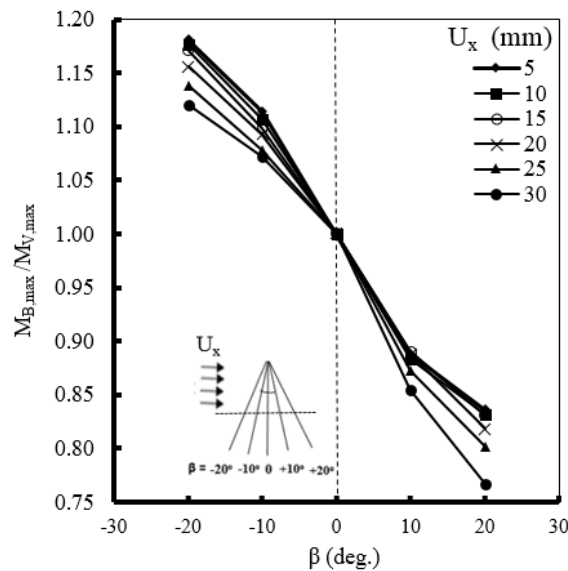


Fig. 4.9 Influence of pile batter angle on M_{max} of piles with different U_x

Fig. 4.10 demonstrates the response of the batter piles in terms of shear force measured at 25 mm of box displacement (U_x) for all tests. According to Fig. 4.10, the following observations can be drawn:

- Shear force profiles for batter pile, with different values of β , are similar in shape to the corresponding profiles measured in the vertical pile test ('standard' test)
- The largest negative shear force developed at a depth of 100 mm (0.33L), while the maximum positive shear force occurred at a depth of 250 mm (0.83L).

Fig. 4.11 presents the soil reaction profiles of the five different batter angles ($\beta = 0^\circ$, $\pm 10^\circ$ and $\pm 20^\circ$) when subjected to soil movement of $U_x = 25$ mm. were:

- The maximum soil resistance (p_{max}) occurred at the depth of 200 mm ($0.67L$).
- The soil reaction within the moving soil layer (L_m) has an arc shape and reaches its maximum at a depth of approximately 50 mm ($L_m/3$).
- In the vicinity of the sliding surface (115 mm below soil surface), there was a remarkable change in the reaction distribution (sign change). This change is expected as both moving and stationary soil layers have opposite actions on the pile shaft.
- The batter pile with $\beta = -20^\circ$ exhibited largest soil reaction compared to the others.

As can be seen in Fig. 4.12, the pile rotation profile indicates the pile behaving as a rigid element (rotation angle remains positive for the entire pile length, with small differences between the top and bottom section of the pile). The shapes of the pile rotation profiles are similar for all the tests. It is evident that the rotation at the soil surface, for the test with $\beta = 0^\circ$ is about 200 % higher than that with $\beta = -20^\circ$.

Fig. 4.13 shows that the pile deflection at the soil surface for various batter angles was generally less than the corresponding lateral soil displacement (U_x). This refers to the fact that the moving sand is flowing around the pile. For instance, in test with $\beta = 0^\circ$ the pile displacement at the ground surface was about 8.0 mm ($0.25D$) at $U_x = 25$ mm ($1.56D$). In addition, it can be seen that the pile head deflection for positive batter piles ($\beta = +10^\circ$ and $+20^\circ$) was lower than that at negative batter piles ($\beta = -10^\circ$ and -20°) and vertical pile, respectively. For example, the pile head deflection at $\beta = -10^\circ$ was 75% lower than that of the vertical pile.

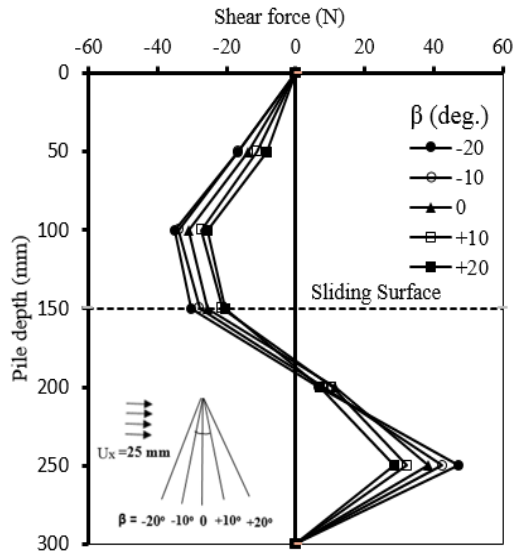


Fig. 4.10 Shear force profiles with different values of β , $U_x = 25$ mm

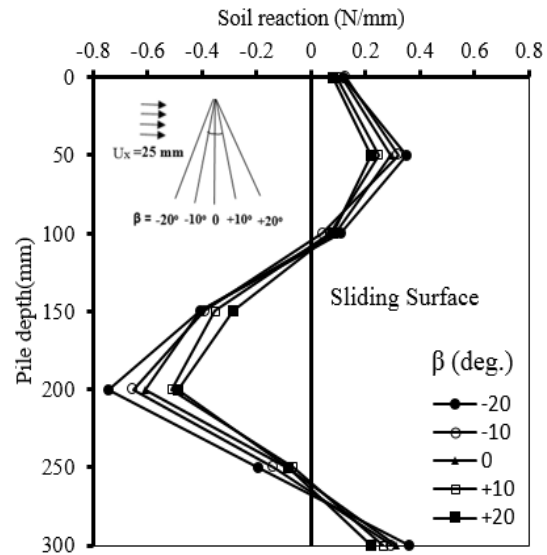


Fig. 4.11 Soil reaction profiles with different values of β , $U_x = 25$ mm

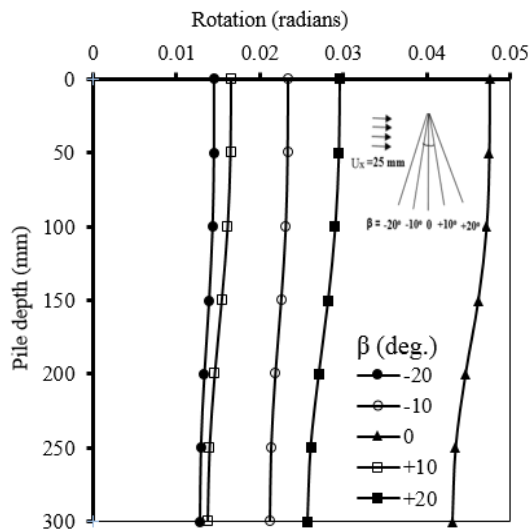


Fig. 4.12 Pile rotation profile with different values of β , $U_x = 25$ mm

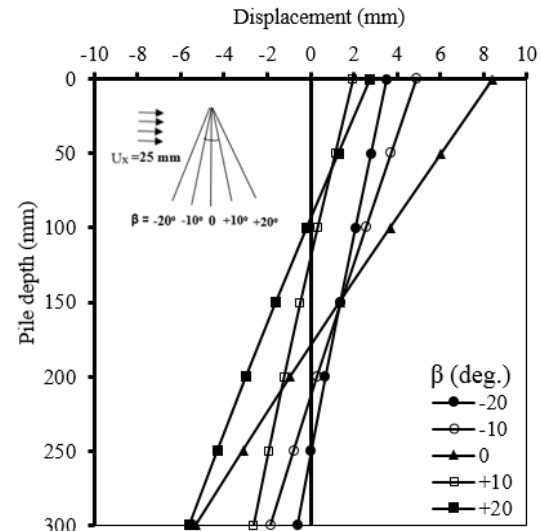


Fig. 4.13 Pile deflection profile with different β , $U_x = 25$ mm

The relationship between the maximum bending moments (M_{\max}) and the corresponding absolute maximum shear forces (F_{\max}) obtained from the tests with $\beta = 0^\circ, \pm 10^\circ$ and $\pm 20^\circ$ is illustrated in Fig. 4.14. It can be seen that M_{\max} increases linearly with F_{\max} ; and that M_{\max} and F_{\max} can be fitted in the relationship $M_{\max} = \alpha F_{\max}$, with $\alpha = 99.25$, where α is the coefficient of the linear fit, with a high value of the coefficient

of determination (R^2) of 0.9944. This form can be expressed in terms of pile length ($L_p = 300$ mm) as:

$$M_{\max} = 0.33L_p F_{\max} \quad (4.4)$$

The above equation was in a very good agreement with the equation proposed by Qin (2010) of $M_{\max} = 0.357 L_p F_{\max}$ for tests conducted on single vertical pile embedded in sand.

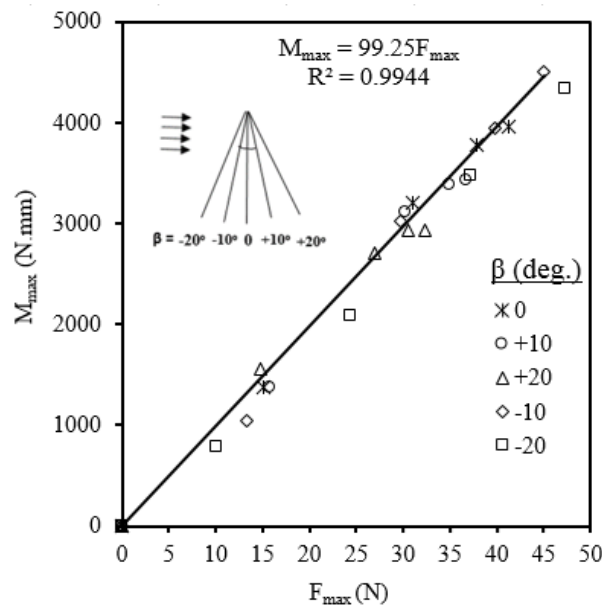


Fig. 4.14 Maximum bending moment (M_{\max}) against maximum shear force (F_{\max}) relationship for single batter piles tests conducted at ratios of $L_m/L_s=150/150$

4.3.4 Limiting soil pressure profile

The soil reaction profiles for all the batter pile tests were presented in the earlier sections. These profiles are summarised to identify the maximum soil reaction (p_{\max}) on the batter piles. The soil reaction on the batter piles was investigated separately in the moving layer (L_m) and in the stable layer (L_s). In L_s , the stable soil provided resistance to the whole batter pile. Thus, in L_s , the pile is similar to that of the laterally loaded piles (active pile).

The maximum soil reaction, p_{\max} in both the L_m and L_s layers were obtained from the soil reaction profile of the batter pile tests, as shown in Fig. 4.15.

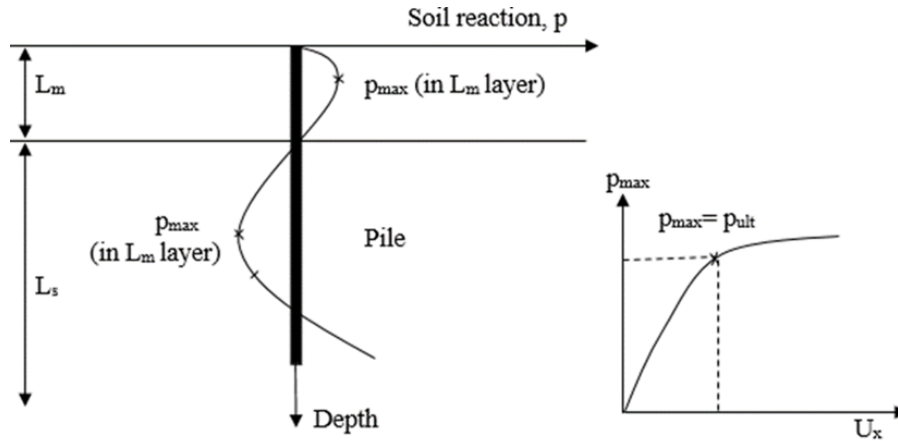


Fig. 4.15 Typical soil reaction profiles showing the p_{\max} in moving (L_m) and stable (L_s) layer

The maximum soil reaction was converted to its maximum soil pressure, P_{\max} ($P_{\max} = p_{\max}/D$), for comparison purposes. The P_{\max} acting on batter piles at $U_x = 30$ mm are plotted in Fig. 4.16 and Fig. 4.18. The Figures demonstrate a comparison between the measured soil pressure and the ultimate soil pressure which was first estimated by: 1) $K_p\gamma z$, (Rankine's passive earth pressure P_p); 2) $3K_p\gamma z$, (Broms 1964); and 3) $K_p^2\gamma z$, (Barton 1982), respectively. Where K_p is the coefficient of passive earth pressure ($K_p = \tan^2(45 + \phi/2)$), γ is the soil unit weight, and z is the depth below soil surface. For ease of comparison, the absolute value of P_{\max} is measured from the soil reaction profile, (p_{\max} is positive in L_m and is negative in L_s).

4.3.4.1 Maximum soil pressure in the moving layer L_m

Fig. 4.16 shows the maximum soil pressure (P_{\max}) recorded at moving layer (L_m) from the tests at different values of batter angles ($\beta = 0^\circ, \pm 10^\circ$ and $\pm 20^\circ$), $L_m/L_s = 150/150$, $U_x = 30$ mm and $D = 16$ mm. The locations of the P_{\max} found to be at depth of 50 mm for all the tests. Batter piles at $\beta = -20^\circ$ and $\beta = +20^\circ$ recorded higher and lower soil pressures, respectively. The magnitude of the soil pressure recorded at $\beta = +10^\circ$ and $+20$, falls between $3K_p\gamma z$ and $K_p^2\gamma z$. However, the maximum soil pressure (P_{\max}) recorded for batter piles with $\beta = 0^\circ, -10^\circ$ and -20° exceeds the limiting soil pressure described by Barton (1982); P_{\max} is higher than ($K_p^2\gamma z$) by 20% at $\beta = -20^\circ$.

Fig. 4.17 shows the relationship between normalised soil pressure (P/P_p) and normalised lateral soil movement (U_x/D) in moving layer at depth of 50 mm for different β values ($\beta = 0^\circ, \pm 10^\circ$ and $\pm 20^\circ$) at $L_m/L_s = 150/150$. It can be seen that (P/P_p) for all values of β increases linearly with (U_x/D), at almost the same rate, but the rate showed a decreased value after (U_x/D) of 1.5. The results also show that (P_u/P_p) are 5.2, 5.0, 4.7, 4.0 and 3.5 for β values of $-20^\circ, -10^\circ, 0^\circ, +10^\circ$ and $+20^\circ$, respectively. As a result, batter piles embedded with $\beta = -20^\circ$ need less soil displacement to reach the ultimate soil reaction compared to those embedded with $\beta = -10^\circ, 0^\circ, +10^\circ$ and $+20^\circ$. For comparative purposes, and when $\beta = 0^\circ$ (vertical pile), the ratio ($P_u/P_p=4.7$) showed close similarity to that found by Chen and Poulos (1994). In their study, the ultimate soil pressure (P_u) on single vertical piles embedded in sand and subjected to lateral soil movements, the soil is pushed towards the pile (like the case of piles in landslides), is found to be $4.6P_p$.

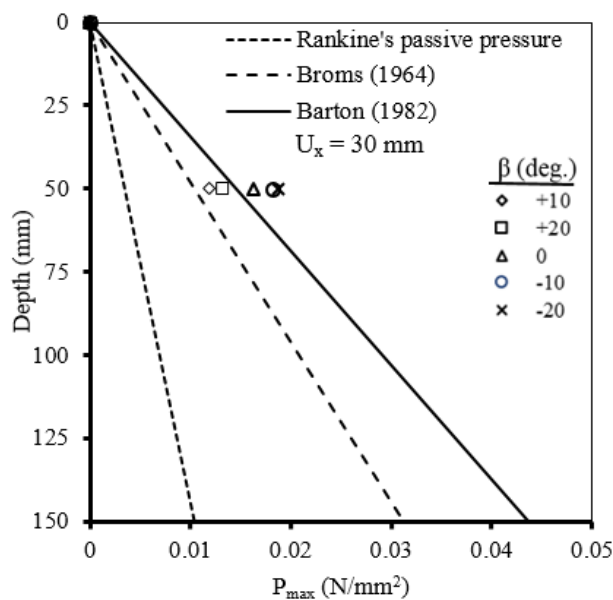


Fig. 4.16 Maximum soil pressure in L_m for tests with $L_m/L_s = 150/150$, $U_x = 30$ mm

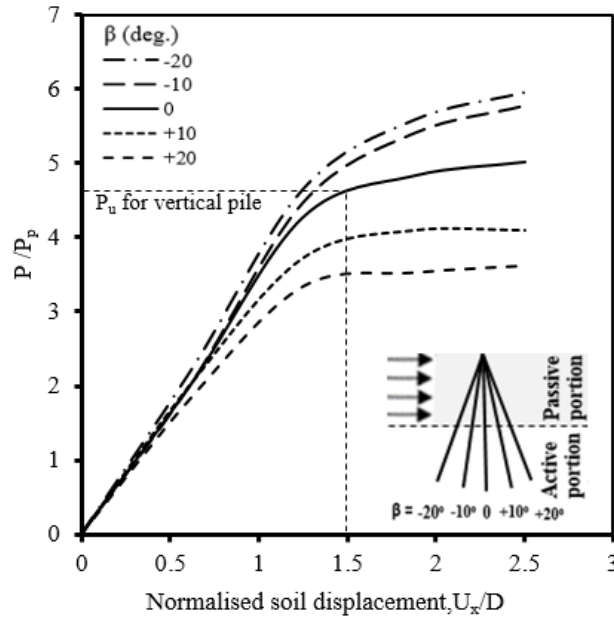


Fig. 4.17 Normalised ($P - U_x$) curve for a single batter piles embedded in sand (moving layer)

4.3.4.2 Maximum soil pressure in the stable layer L_s

As shown in Fig. 4.18, the p_{max} in the stable layer (L_s) is taken from the maximum value of the soil reaction profile (in L_s) of the batter piles. Fig. 4.18 shows the P_{max} obtained from all batter piles with $L_m/L_s = 150/150$ and $U_x = 30$ mm. The locations of the P_{max} are at a depth of 200 mm for all the tests (12.5D). Generally, P_{max} on all the tests are below $3K_p\gamma z$, except for one test where $\beta = -20^\circ$ shows the P_{max} higher than $3K_p\gamma z$ by 3%. The locations of the P_{max} on batter piles are generally at a depth of 200 mm. This depth is approximately 6.25D below the sliding depth.

Fig. 4.19 shows the relationship between the normalised soil pressure (P/P_p) and normalised lateral soil movement (U_x/D) in stable layer for different values of batter angles ($\beta = 0^\circ, \pm 10^\circ$ and $\pm 20^\circ$) with $L_m/L_s = 150/150$. The ($P-U_x$) curves of the batter piles in the stable layer (L_s) had an upward trend with increased soil displacement, similar to that in the moving layer (L_m). Where, the normalised soil pressure P/P_p almost linearly increases with the normalised soil displacement (U_x/D) until the (U_x/D) of about 1.5 for all values of β , but afterwards they are nonlinear. The normalised ultimate soil pressure P_u/P_p varies in range of 2.4 ~ 3.4, depending on the batter pile angle (β).

Where the $P_u/P_p = 3.4, 3.1, 2.7, 2.6$ and 2.4 for $\beta = -20^\circ, -10^\circ, 0^\circ, +10^\circ$ and $+20^\circ$. For comparison, the P_u/P_p for vertical pile ($\beta = 0^\circ$) was 2.7 , which was very close to value of 3 suggested by Broms (1964) for a pile loaded laterally (active pile) in sand soils. This may imply that the ultimate soil pressure P_u in the stable layer is essentially the same for a single isolated pile subjected to either lateral soil movement or lateral loading (active load).

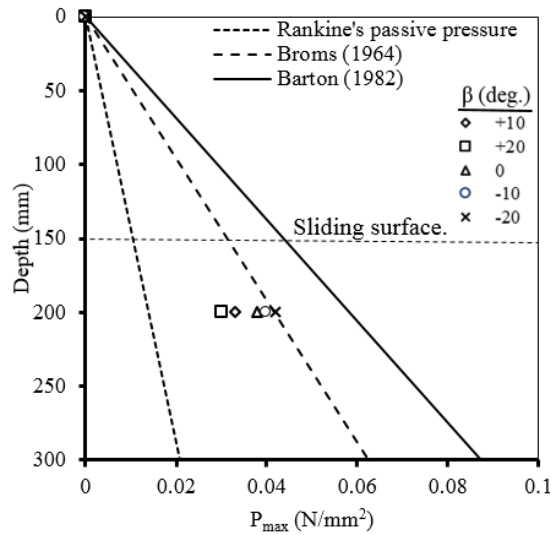


Fig. 4.18 Maximum soil pressure in L_s for tests with $L_m/L_s = 150/150, U_x = 30$ mm

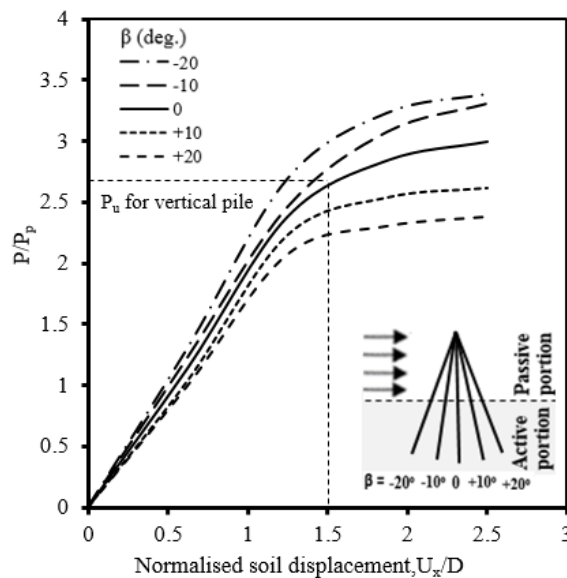


Fig. 4.19 Normalised "P – U_x " curve for a single batter piles embedded in sand (stable layer)

4.3.5 Effect of pile location in the testing box (boundary effect)

Six tests were conducted to study the boundary effect of the box on the batter pile response. The tests are carried out using a rectangular loading block and 16 mm diameter pile. Table 4.6 shows the parameters of six tests conducted on 16 mm diameter pile installed at distance (d_s) of 200, 300, and 400 mm, which is measured between the centre of the pile to the inner face of the testing box wall with $L_m/L_s=1$. Fig. 4.20 shows the plan view of the testing box, and the three pile locations.

Table 4.6 Tests conducted to study the boundary effect of the testing box

Pile-head condition	Soil movement profile	Distance from boundary, d_s (mm)	L_m/L_s	Test number
Free-head	Rectangular	200	1	RSF16, 0°
		300		
		400		
		200		RSF16, $+10^\circ$
		300		
		400		

The first three tests described in Table 4.6 were conducted to investigate the boundary effect on vertical piles ($\beta = 0^\circ$). Fig. 4.21 shows the pile response in term of the bending moment and the soil reaction at $U_x = 25$ mm. The last three tests described in Table 4.6 were conducted to investigate the batter pile response at ($\beta = +10^\circ$) with (d_s) of 200, 300 and 400 mm, respectively. Fig. 4.22 shows the batter pile response of these tests in term of bending moment and the soil reaction. Summary of pile behaviour on both tests are given below:

- M_{+max} at $d_s = 200$ mm is higher than that at $d_s = 300$ and 400 mm, respectively.
- The shape of bending moment profile for the all tests are almost similar (analogous parabolic shape).
- above the sliding surface, the soil pressure developed on the pile is positive, as a result of the soil movement
- The maximum soil pressure in the moving layer decreases about 46% from approximately 0.34 N/mm to 0.18 N/mm for vertical pile and around 62% from almost 0.31 N/mm to 0.12 N/mm for batter pile at $\beta = +10^\circ$, as (d_s) increases

from 200 mm to 400 mm. This reduction indicates that the location where the pile is placed has a significant effect on the pile response, even at $ds = 400$ mm (or 25 D).

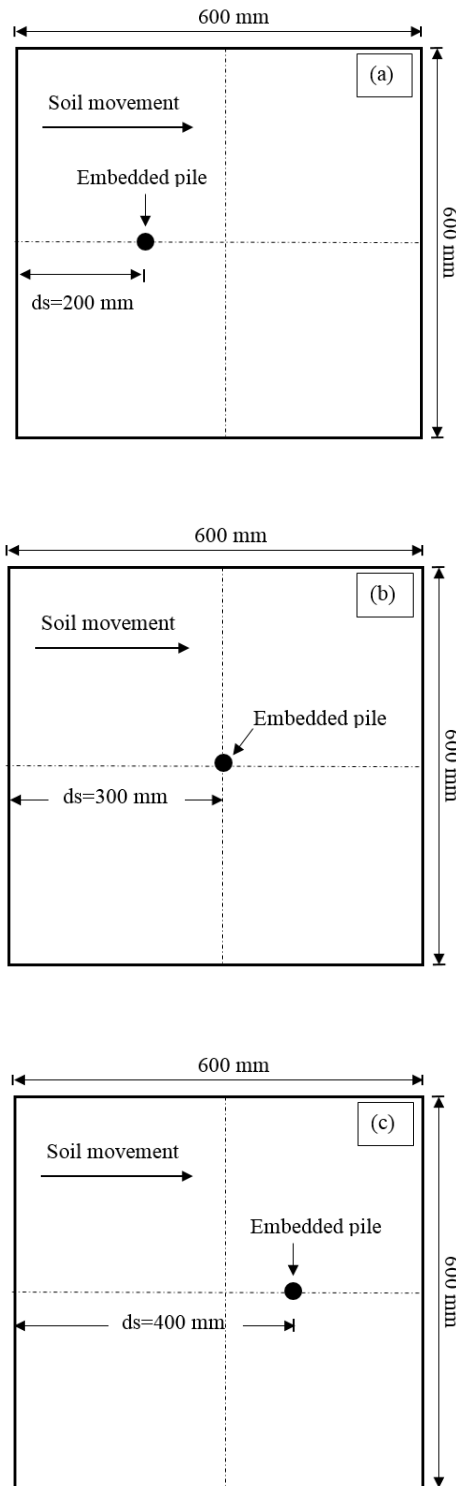


Fig. 4.20 Location of a model batter pile in the testing box

To conclude, as the distance (ds) increases the soil pressure, acting on the pile, reduces. This decrease in soil pressure causes the bending moment to be reduced.

From Fig. 4.23(a, b), for vertical ($\beta = 0^\circ$) and batter ($\beta = +10^\circ$) piles, shows that the M_{max} increases as (U_x) increase for all (ds) and gradient of the linear segment of the M_{max} and U_x curves ($U_x = 0 \sim 15$ for vertical pile and $U_x = 0 \sim 10$ mm for batter pile) decreased with the distance (ds) increased.

The values of M_{max} are plotted in Fig. 4.24 against the distance (ds) at $U_x = 25$ mm. Initially, the relationship between M_{max} and the distance (ds) is seen to have approximately linear shape. Where, at vertical pile ($\beta = 0^\circ$), a reduction of about 2900 N.mm in M_{max} is obtained as the pile was relocated from $ds = 200$ mm to 400 mm, while, at batter pile ($\beta = +10^\circ$), a reduction of about 2230 N.mm from $ds = 200$ mm to 400 mm.

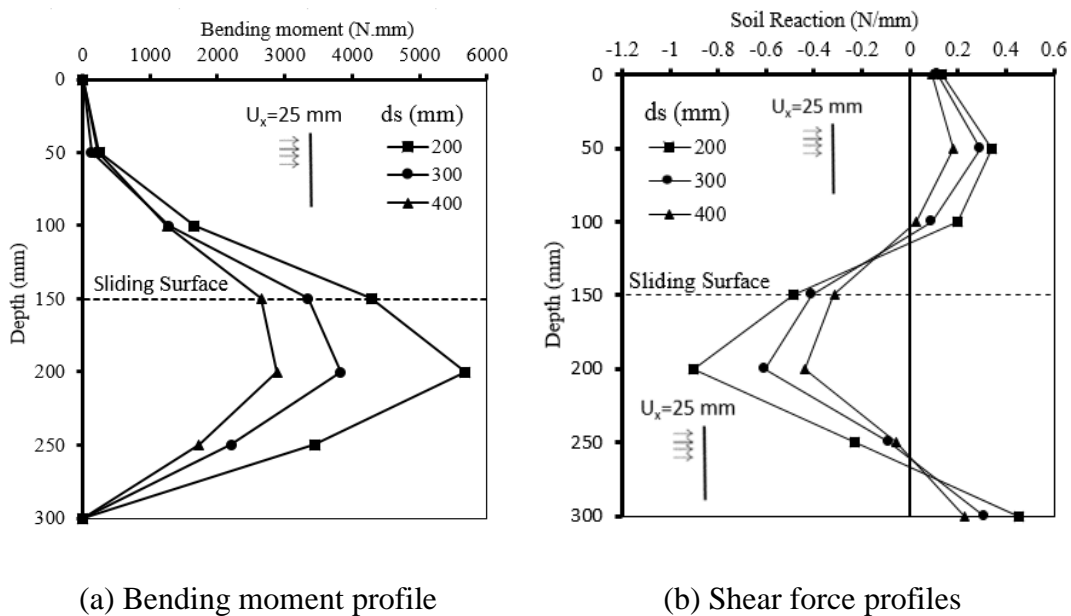
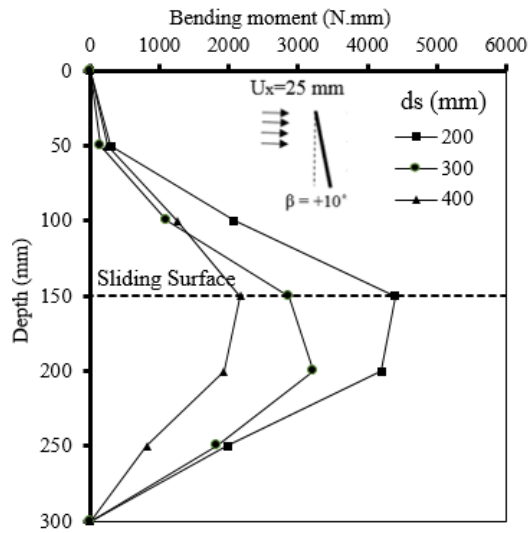
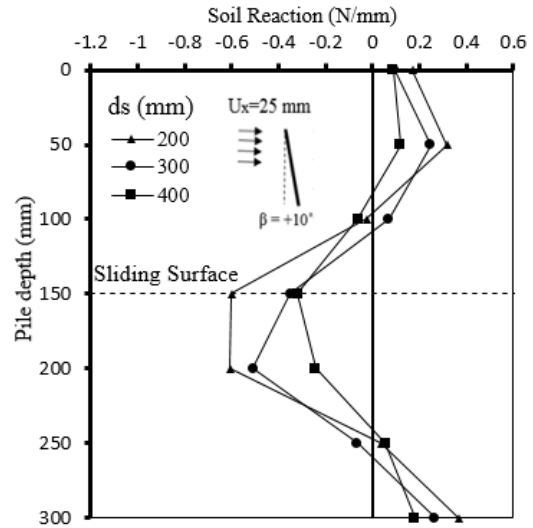


Fig. 4.21 Responses of the piles tested at different locations in the testing box, $\beta = 0^\circ$



(a) Bending moment profile



(b) Shear force profiles

Fig. 4.22 Responses of the piles tested at different locations in the testing box, ($\beta = +10^\circ$)

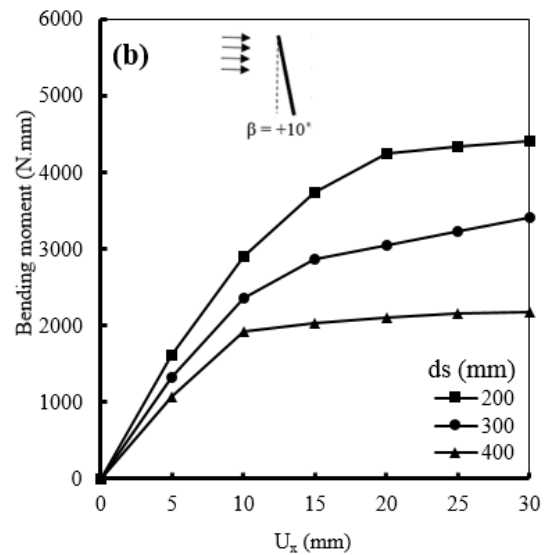
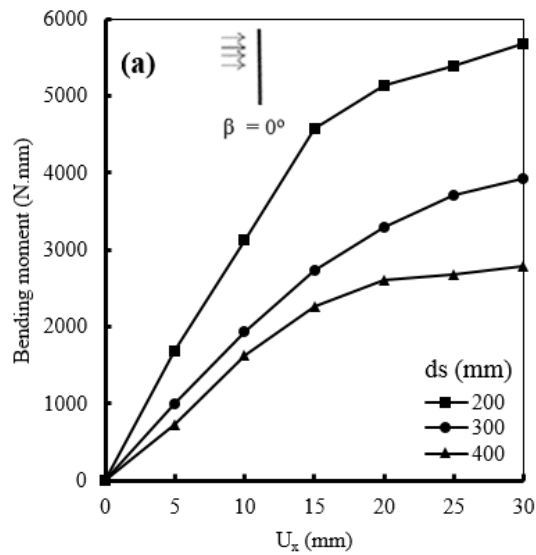


Fig. 4.23 M_{\max} vs (U_x) with different values of (ds) at $\beta = 0^\circ$ and $+10^\circ$

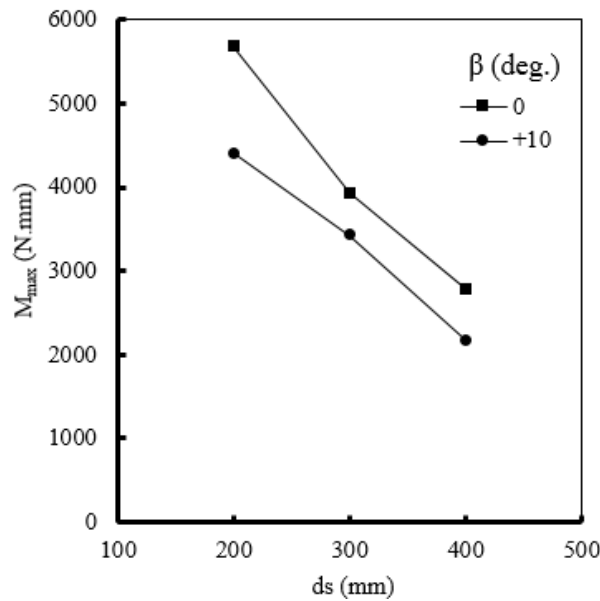


Fig. 4.24 M_{\max} vs d_s with two values of β

4.3.6 Influence of pile head fixity (RSL16, β)

A number of tests were performed on the same pile (16 mm in diameter) with different angle of inclination (β) under the same conditions as that of the "standard" test, except that the pile head was fixed against both rotation and displacement. Fig. 4.25 shows the bending moment distribution along the vertical pile shaft, and it can be seen that the bending moment profile is completely different from that of the free-head pile (standard test), see Fig. 4.1a. Due to the provision of head fixity, negative bending moment induced along the pile except small positive bending moment was obtained at pile head. The position of the maximum negative bending moment is also shifted upward to be above the interface between the stable and moving soil layers. Fig. 4.26 shows that the magnitude of the M_{\max} (for free and fixed head-pile condition), for different values of (β), are approximately equal with different sign and position, i.e. the maximum positive bending moment in test of free-head pile, $\beta = 0^\circ$, was measured as +3748 N.mm at $U_x = 25$ mm, occurring at a depth of 200 mm. This value is almost equal to the maximum negative bending moment of -3824 N.mm that occurred at 100 mm down the pile head in case of free-head pile test, $\beta = 0^\circ$. Similarly, a small magnitude of positive maximum bending moment was measured in tests of fixed-head pile at pile head. In contrast, only positive bending moment was measured along the embedded batter piles in cases of free-head pile test.

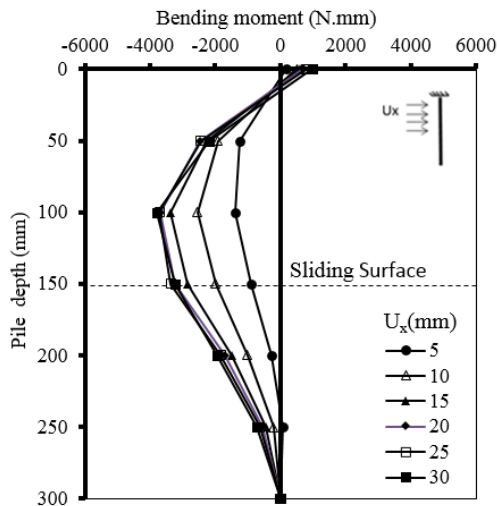


Fig. 4.25 Bending moment profile for a fixed-head pile along the pile shaft, $\beta = 0^\circ$

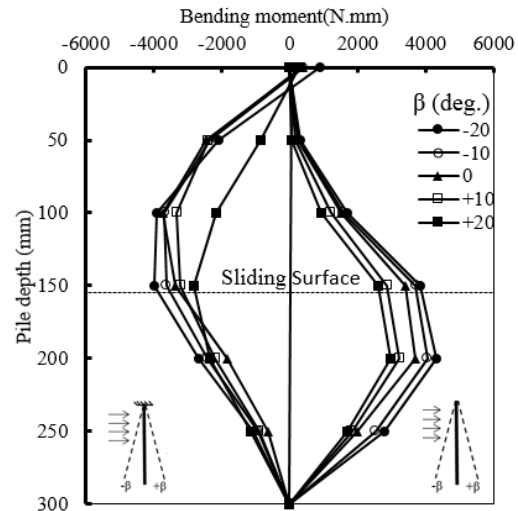


Fig. 4.26 Bending moment profile for a fixed and free head batter pile with different values of β , $U_x = 25$ mm

4.3.7 Influence of pile diameter (RSF20, β) & (RSF25, β)

In order to investigate the influence of pile diameter on the batter pile response, a series of tests were conducted on the 20 and 25 mm diameter pile (D), respectively, under the same conditions as those of the "standard" test (16 mm pile diameter) with different values of diameter (D), see Table 4.1. It was found that the bending moment profile is essentially the same for the three cases, but the magnitude increases with increasing diameter as shown in Fig. 4.27. This response can be attributed to the fact that piles with larger diameters offering more resistance to the soil movements, resulting in a higher load carried by piles which leads, in turn, to increase moments on the piles. Maximum bending moments at different values of soil surface displacement (U_x) are plotted against pile diameter with different values of (β) in Fig. 4.28 (a, b, c, d and e), which clearly shows the increasing trend of M_{max} with increasing diameter for a various value of batter angle (β). (Results of BM, SF, soil section, pile rotation and pile deflection for 20, 25 mm pile diameter are shown in Appendix A (Fig. A.20 to A.29).

The maximum bending moments shown in Fig. 4.28c ($\beta = 0^\circ$) have been normalised and are plotted against pile diameter in Fig. 4.29. It can be seen that the normalised

maximum moment $M_{\max} d^2 / U_x E_p I_p$ is approximately the same for different diameters but varies within a small range for different values of soil displacement (U_x). This variation is since the bending moment does not increase with increasing value of U_x in a perfect linear way, especially when U_x is greater than about 20 mm. Thus, the results provide an upper and lower bounds for estimating $M_{\max} d^2 / U_x E_p I_p$, being 7×10^{-4} and 3×10^{-4} , respectively.

Fig. 4.30 illustrates the combined effect of pile diameter and the value of batter angle (β) on the M_{\max} . In summary, the M_{\max} increases as the pile diameter (d) increases, regardless of batter angle values (β). It can also be seen that at the M_{\max} was largest at $\beta = -20^\circ$ followed by $-10^\circ, 0^\circ, +10^\circ$ and $+20^\circ$.

Fig. 4.31 shows the pile head deflection as functions of soil displacement U_x . For the same amount of soil movement, the head deflection decreases with increasing diameter.

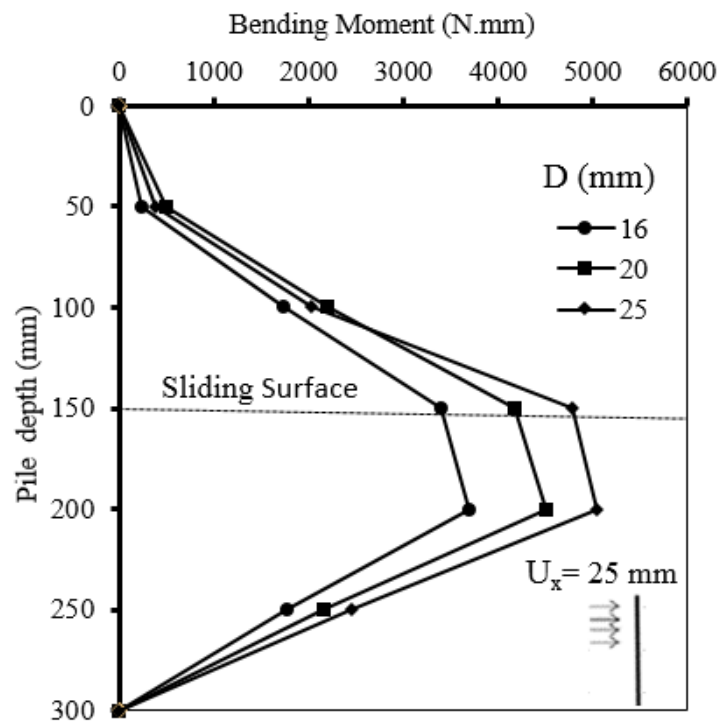


Fig. 4.27 Bending moment profiles of 16, 20 and 25 mm diameter piles

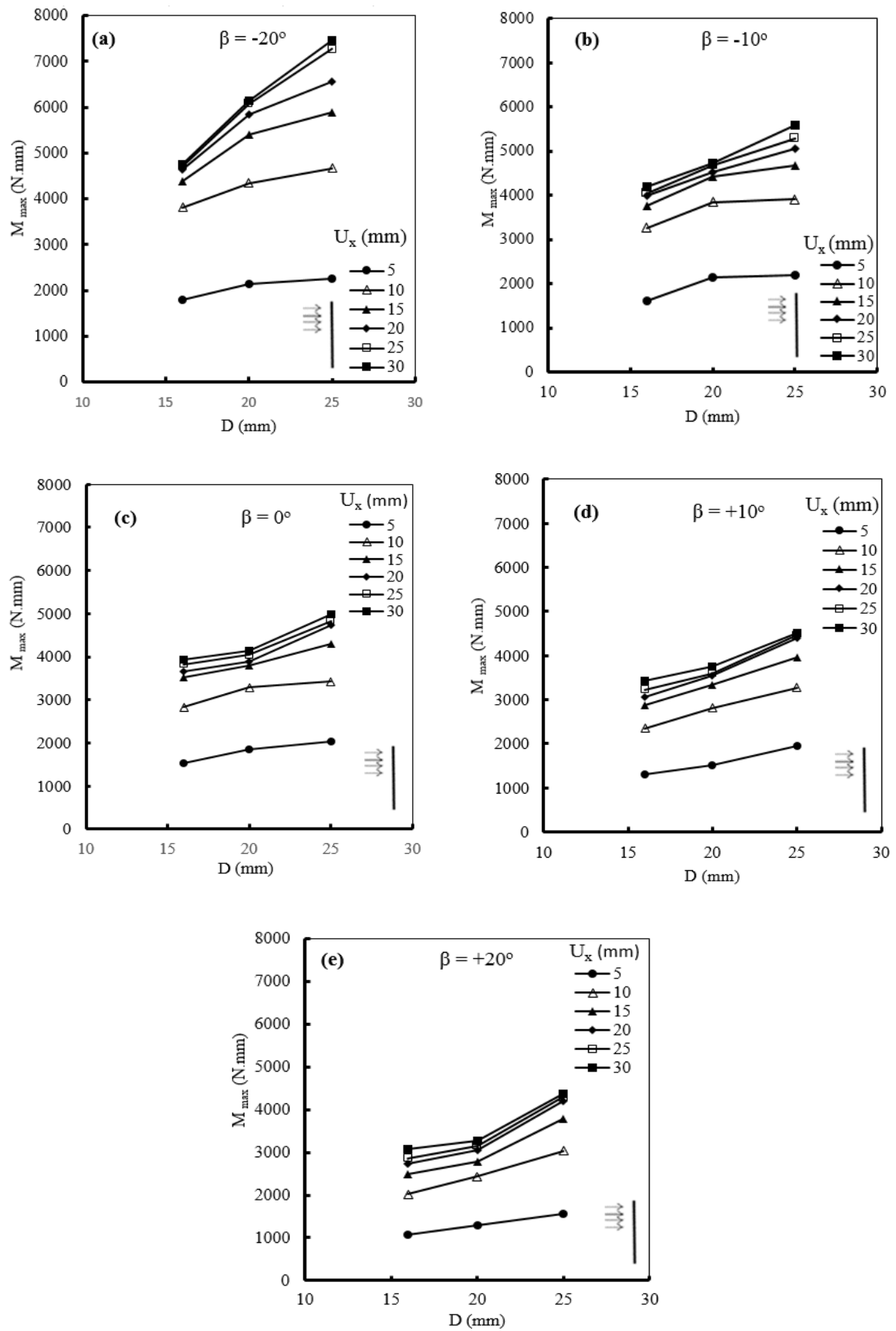


Fig. 4.28 M_{max} against pile diameter at different values of (β)

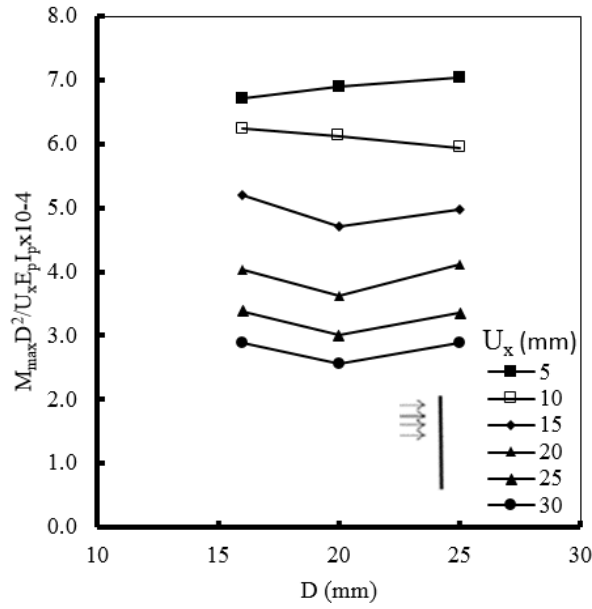


Fig. 4.29 Normalised M_{max} vs pile diameter, $\beta = 0^\circ$

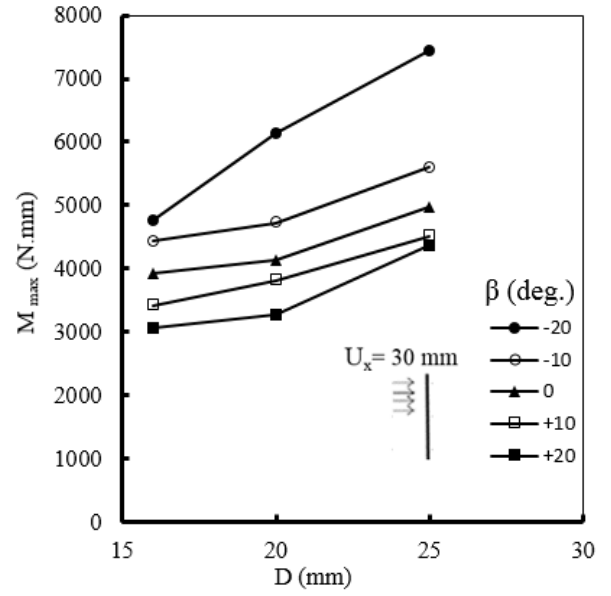


Fig. 4.30 M_{max} vs pile diameter with different values of β

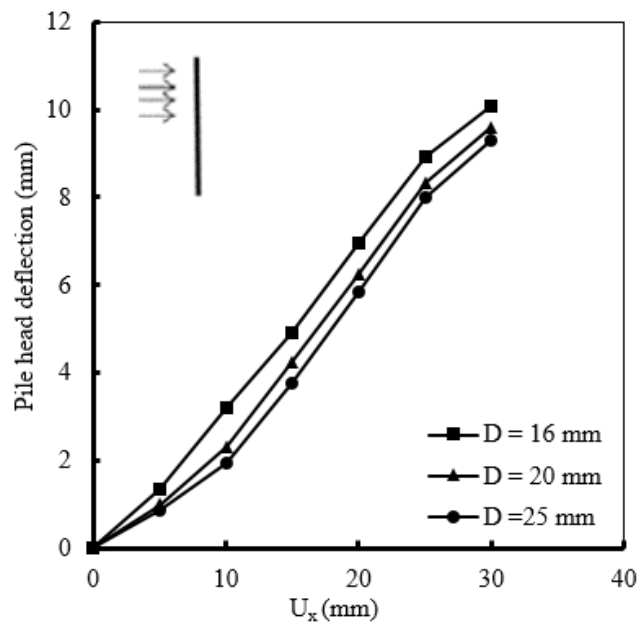


Fig. 4.31 Pile head deflection vs soil displacement (U_x)

4.4 Tests for single batter piles subjected to triangular soil movement profile (TSF16, β)

A series of tests was conducted by using the triangular soil movement profile to study the effect of soil density on the batter pile response. These tests were conducted with three sand densities (14.7, 15.2 and 15.7) kN/m³ with pile diameter of 16 mm, see Table 4.1. The results for the measured displacements are not presented here but can be found in Appendix A (Fig. A.30 to A.44). Instead, attention is focused in this stage on the measured bending moments in the pile, in particular, the maximum bending moments.

The following subsections 4.3.1 to 4.3.3 outline the effect of the batter pile angle ($\beta = 0^\circ, \pm 10^\circ$ and $\pm 20^\circ$) on pile response with L_m and L_s of 150 mm.

4.4.1 Experimental results with density (γ_s) = 14.7 kN/m³

Five tests were conducted under this density (loose - relative density of 30 %) to study the influence of the different batter pile angles (β) on the behaviour of batter pile under triangular soil movement profile. Fig. 4.32a present the pile response in the form of bending moment at a soil movement of $U_x = 25$ mm. The bending moment obtained for all the batter pile angles ($\beta = 0^\circ, \pm 10^\circ$ and $\pm 20^\circ$) were similar in shape (analogous to a parabolic shape), but different in magnitude. The difference in the M_{max} for the (-20°) batter angle, when compared to the ($+20^\circ$) batter angle is about 3-fold. The location of the M_{max} for all tests is 200 mm, at stable layer. The test result on vertical pile is consistent with the experimental results reported by Chen et al. (1995) and Guo and Qin (2009).

As shown in Fig. 4.32b, in all the tests ($\beta = 0^\circ, \pm 10^\circ$ and $\pm 20^\circ$), the M_{max} increases with (U_x). The rate of the M_{max} increment obtained from the test with $\beta = -20^\circ$ is the highest among all the tests.

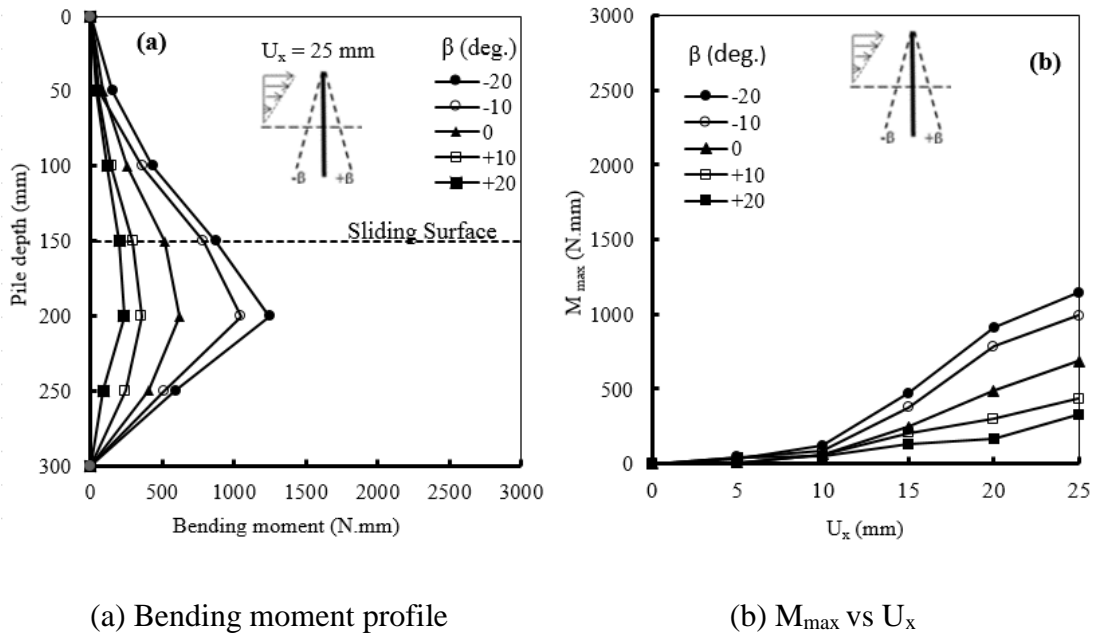


Fig. 4.32 Responses of batter piles subjected to triangular soil movement profile with different values of β , $\gamma_s = 14.7 \text{ kN/m}^3$

4.4.2 Experimental results with density (γ_s) = 15.2 kN/m³

Another five tests were conducted with 15.2 kN/m^3 sand density (medium- relative density of 50 %) with ($\beta = 0^\circ, \pm 10$ and $\pm 20^\circ$). Fig. 4.33a presents the bending moment profiles at the soil movement, $U_x = 25 \text{ mm}$. The shapes of the bending moment profiles are of a single curvature, with the M_{\max} , occurs at the vicinity of the interface between the moving and stable sand layers at a depth between 150 ~ 200 mm below the ground surface. The highest value of bending moment is obtained when $\beta = -20^\circ$.

Fig. 4.33b shows that M_{\max} has a slower trend at the start (up to $U_x = 10 \text{ mm}$), followed by a sharp increase up to $U_x = 20 \text{ mm}$ beyond which the rate of M_{\max} shows slower rate for all the tests.

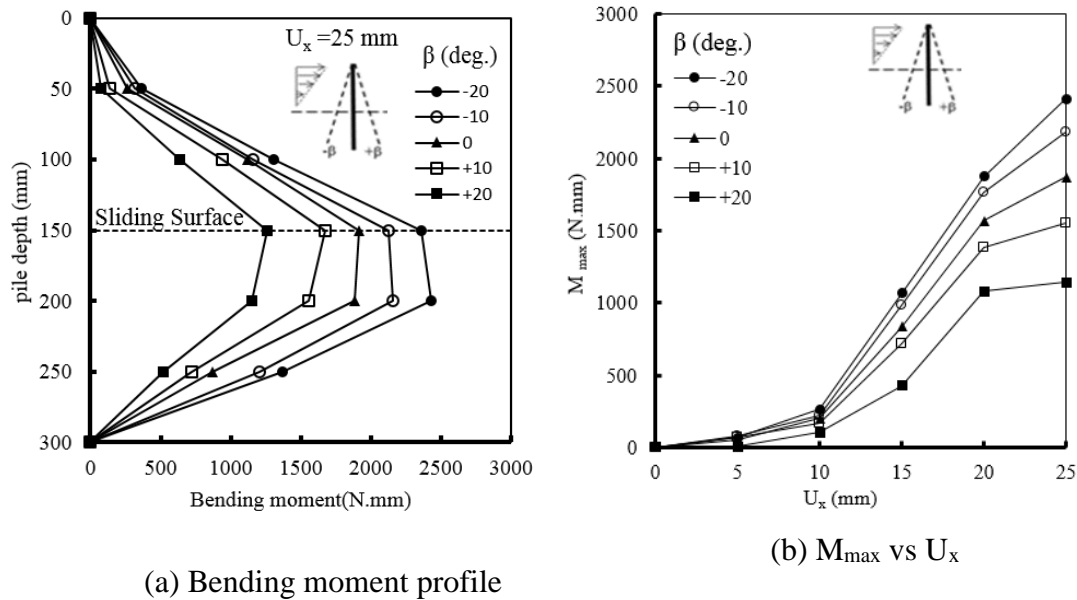


Fig. 4.33 Responses of batter piles subjected to triangular soil movement profile with different values of β , $\gamma_s = 15.2 \text{ kN/m}^3$

4.4.3 Experimental results with density (γ_s) = 15.7 kN/m³

Fig. 4.34a present the pile responses of the five tests with sand soil of 15.7 kN/m^3 (dense-the relative density of 70 %). The shape of the bending moment profiles on all tests are similar (parabolic shape), while the M_{\max} (2670 N.mm) obtained from the $\beta = -20^\circ$ is approximately 71% higher than the M_{\max} (1560 N.mm) obtained from the $\beta = +20^\circ$.

Fig. 4.34b shows the relationship between the M_{\max} with different (U_x) values. The M_{\max} increases when (U_x) values increase and show its the highest in the test with $\beta = -20^\circ$ followed by -10° , 0° , $+10^\circ$ and $+20^\circ$ for the whole range of (U_x).

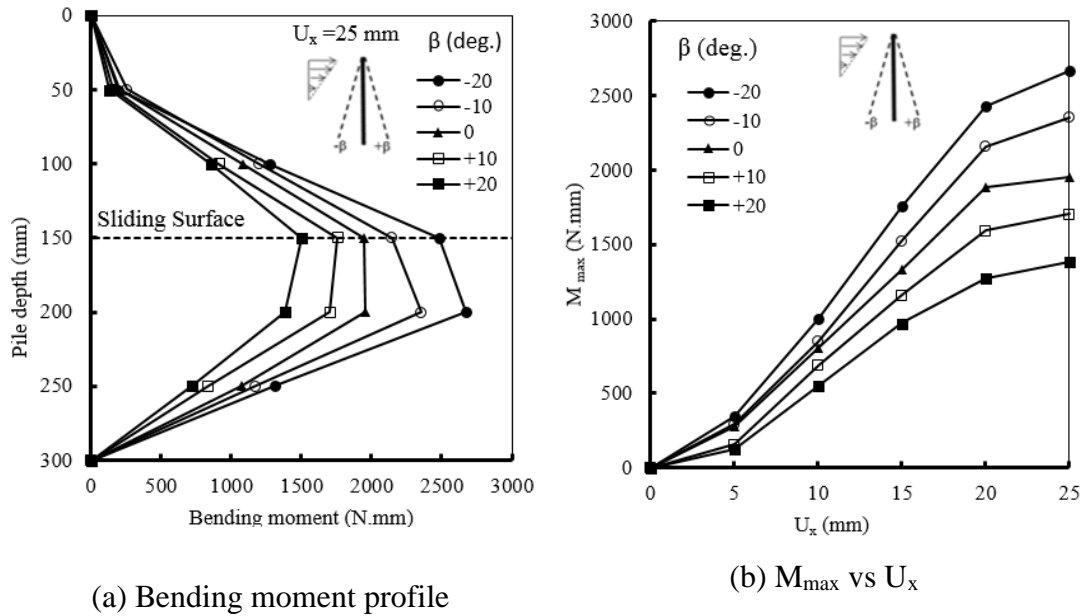


Fig. 4.34 Responses of batter piles subjected to triangular soil movement profile with different values of β , $\gamma_s = 15.7 \text{ kN/m}^3$

4.5 Summary of single piles subjected to triangular soil movement

Fig. 4.35 shows the relationship between the M_{max} against the three sand densities with different values of pile batter angle (β). The M_{max} values were recorded at $U_x = 25 \text{ mm}$.

The findings revealed that for all values of batter angle (β), the M_{max} increases as the sand density increases. However, the rate of the increment is different. For instance, at $\beta = -20^\circ$, as the sand density increases from 14.7 kN/m^3 to 15.2 kN/m^3 , the M_{max} increases by 90 %. Whereas a variation of sand density from 15.2 kN/m^3 to 15.7 kN/m^3 leads to a smaller increase in the M_{max} (12 %).

The effect of batter angle was studied through the selection of five angles ($0^\circ, \pm 10^\circ, \pm 20^\circ$) with different densities ($14.7, 15.2$ and 15.7 kN/m^3), see Fig. 4.36. The results have indicated that all graphs had almost the same general trends. The M_{max} increases with the increase in sand density for all values of batter angles β , but the rate of increase reduces, when the soil density is greater than 15.2 kN/m^3 . The value of M_{max} was higher at $\beta = -20^\circ$ compared to the other values of batter angles. However, $\beta = +20^\circ$ was lower value of M_{max} than the others β .

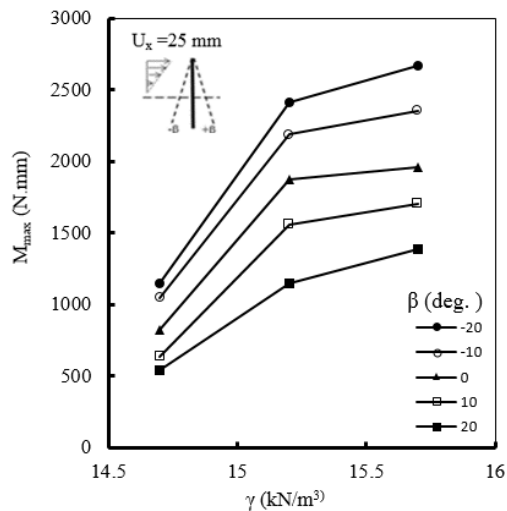


Fig. 4.35 M_{\max} vs γ (kN/m^3) with different values of β , $U_x = 25$ mm

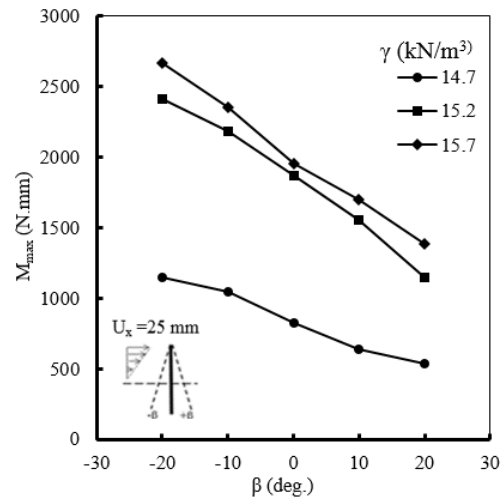


Fig. 4.36 M_{\max} vs β with different values of sand densities, $U_x = 25$ mm

4.6 Comparison of pile responses obtained from different soil movement profiles (RSF16, 0°) & (TSF16, 0°)

Tests were undertaken to compare the pile responses obtained from two types of soil movement profiles. Results at $\beta = 0^\circ$ are presented in the following sections.

4.6.1 Tests with $\beta = 0^\circ$

The tests carried out on two types of soil movement profiles (rectangular and triangular) are shown in Fig. 4.37. These tests were conducted with the 16 mm diameter pile, $U_x = 25$ mm, the $L_m = L_s = 150$ mm) and sand density of (15.2 kN/m^3). The pile response is discussed below:

- Both bending moment profiles show the shape of a single curvature shape (see Fig. 4.37a).
- The M_{\max} for the test with the rectangular soil movement profile is the higher than triangular profile.
- The M_{\max} values of 3825 N.mm with rectangular profile and 1925 N.mm with triangular profile occur at a depth of 200 mm and 150 mm, respectively.
- Soil pressure measured on Pile indicates that its magnitude is highly dependent on the type of soil movement profile. Pile subjected to rectangular profile was under a higher soil pressure compared to this undergoing triangular profile. The

position of maximum passive and active soil pressures, in general, were recorded at depth of 50 and 200 mm, respectively (see Fig. 4.37b).

- Fig. 4.37c investigates deflection profiles of the pile. It can be seen that maximum deformations occurred when the soil movement profile was rectangular, in which the pile deflection at the surface is about 2-fold compared to the triangular profile.
- The difference in M_{max} at any given (U_x) is significant for the soil movement profiles in which the magnitude of the M_{max} in the case the rectangular was higher than that of the triangular profiles for the entire range of (U_x) values (see Fig. 4.37d).

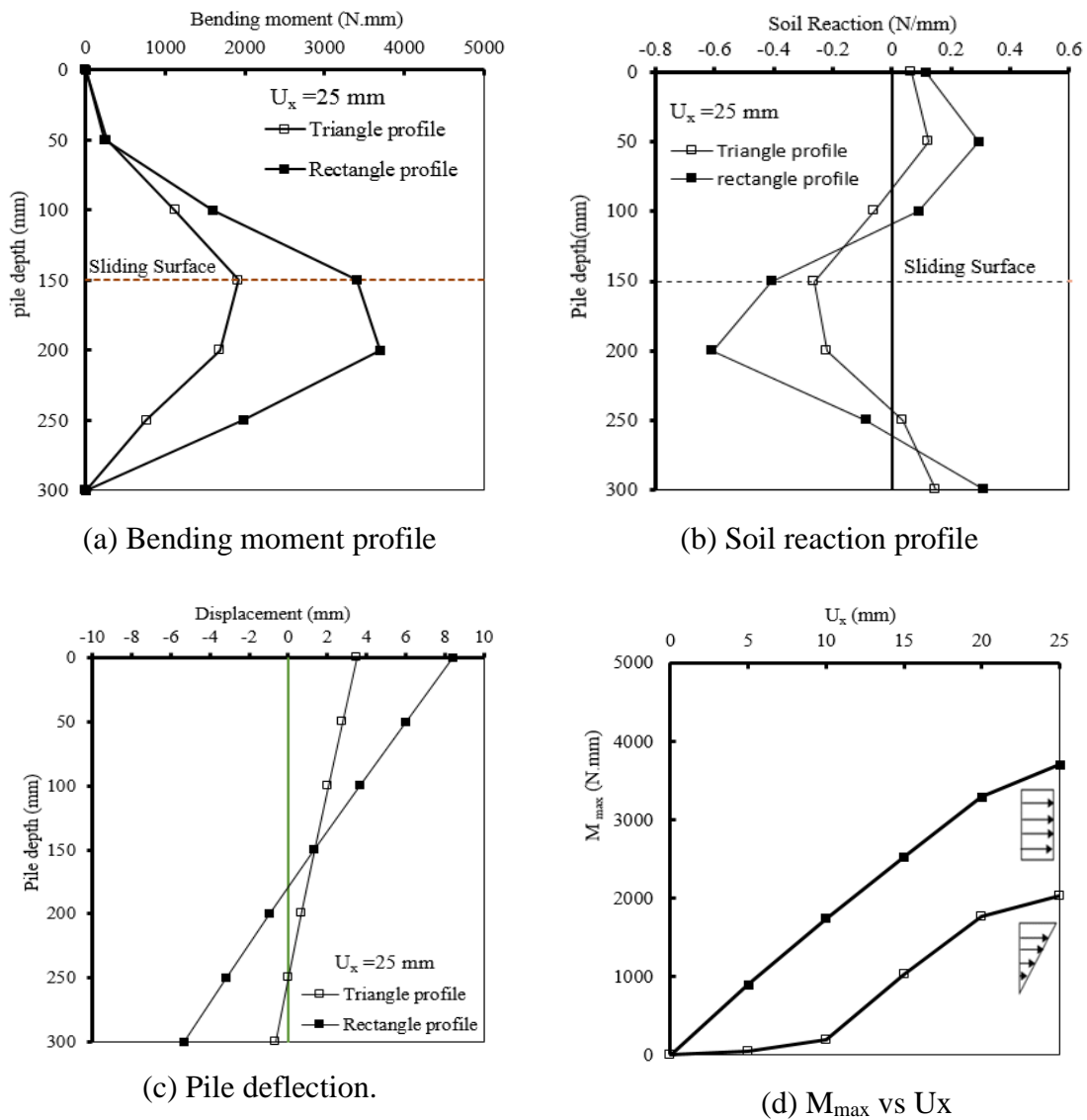


Fig. 4.37 Responses batter pile subjected to two types soil movement profiles (L_m and $L_s = 150$ mm), $U_x = 25$ mm

4.7 Summary

A number of model tests had been conducted on single batter piles. From these tests, the following conclusions of batter pile behaviour were observed for the two soil movement profiles (rectangular and triangular) under the effect of the following parameters: 1) pile diameter; 2) density of sand; 3) batter angle; 4) pile head fixity; and 5) the ratio of the pile embedded length in the upper moving soil layer to the length in the lower stable soil layer (L_m/L_s).

4.7.1 Rectangular soil movement profile

In relationship to the rectangular soil movement profile, it was noted that the pile responded as follows:

- The bending moment profile for a free-headed pile is a parabolic curve for all values of (β), with zero value at both pile head and pile tip and maximum value at the proximity of the interface between the upper moving layer and the lower stable layer. The bending moment increases with increasing soil movement in a non-linear manner.
- The value of the maximum bending moment induced in the pile is dependent on the ratio of the pile embedded length in the upper moving soil layer (L_m) and the lower stable soil layer (L_s). It has been found that the bending moment in the pile induced by moving soils may reach its peak value when the values of L_m and L_s are equal.
- Batter angle has shown a substantial effect on the behaviour of pile. The bending moment of the “negative” batter pile ($\beta = -10^\circ$ and -20°) increases as the batter angle increases. In contrast, the bending moment of the positive batter pile ($\beta = +10^\circ$ and $+20^\circ$) decreases as the batter angle increases.
- The shape of the bending moment profile was a single curvature for all values of (β).
- Regardless of the magnitude of soil movement and batter pile inclination (β), a unique linear relationship $M_{\max} = \alpha F_{\max} L_p$, with α of 0.33, was found by fitting all the single pile tests results in a regression analysis. This relationship was consistent with that proposed by Qin (2010).
- The maximum soil reactions for all tests did not exceed the limiting pressure

proposed by Barton (1982).

- The P_u value for a single vertical pile in a sand soil obtained by the present study agrees well with that obtained by Chen & Poulos (1994) and Broms (1964).
- Depending on the value of batter angle β , the ultimate soil pressure P_u for single batter piles ranged from 3.5 to 5.2 Rankine passive pressure P_p at moving layer L_m and (2.4 to 3.4) P_p at stable layer L_s .
- The bending moment and soil reaction reduce with the increase of distance (ds) from loading source.
- For a fixed-headed pile, the bending moment profile is totally different from that of the free-headed pile, with positive bending moment developed at pile head, and negative bending moment along the middle portion of the pile. The negative maximum bending moment is larger than the positive moment but is smaller than that for the free-headed case.
- The bending moment increases with the increase in the diameter of the pile, but the maximum pile deflection (at the sand surface) reduced as the pile diameter increased.

4.7.2 Triangular soil movement profile

The batter pile behaviour is described as follows:

- Regardless of the value of batter angle, the bending moment and soil reaction increased with the increase in sand density.
- Regardless of the value of soil density, the bending moment of the “negative” batter pile ($\beta = -10^\circ$ and -20°) increases as the batter angle increases. In contrast, the bending moment of the “positive” batter pile ($\beta = +10^\circ$ and $+20^\circ$) decreases as the batter angle increases.
- As in the case of rectangular soil movement profile, it is found that the shape of the bending moment profile was a single curvature and remained same for all values of (β).
- The bending moment and deflection developed along the pile length due to rectangular soil movement were higher compared to those in triangular profile.

Chapter 5

Experimental Results of Pile Group Tests

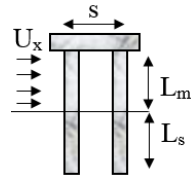
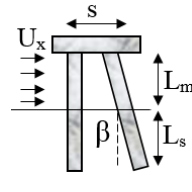
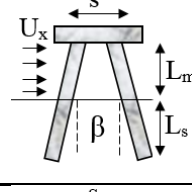
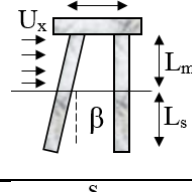
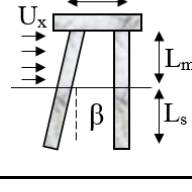
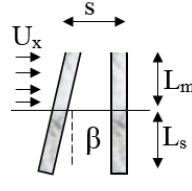
5.1 Introduction

In practice, batter piles are generally used in combination with vertical piles in a group where the pile foundations are subjected to significant amount of lateral load (Hirani & Verma, 2011). The behaviour of piles in a group may be influenced by several factors, including pile spacing, pile inclination angle and pile head/cap connection conditions. To understand the group effect on the response of an individual pile within a group, it is desirable to carry out pile group tests and to compare the result of a group test with that of a single batter pile test. To this end, a series of laboratory tests has been carried out on some model pile groups subjected to lateral soil movement and their results are discussed in this chapter. The lateral responses were investigated for 2×1 batter pile group with different configurations. These groups of batter piles were driven into the sand was either free (free displacement and free rotation) or else connected with a rigid cap located 25 mm above the sand surface. The effects of the pile group arrangement, batter angle and the pile group spacing (S) on the lateral response of the individual piles (batter and vertical) within a pile group were also investigated experimentally; the piles were subjected to a rectangular profile of soil movements. All tests are conducted in medium sand density of 15.2 kN/m^3 (corresponding to relative density of 70%), $L_m = L_s = 150 \text{ mm}$ and piles diameter of 16 mm (the geometry of each model pile was the same as that of the "standard" test model pile, as described in chapter three). The results of the batter pile group tests were compared with those of the "standard" single pile test to examine the difference in behaviour between a single pile and a pile group.

The main purpose of this chapter is to investigate the effect of a number of parameters, including the pile spacing, the pile group arrangements and the piles head fixity condition (with and without cap), on the lateral response of a batter pile within a group. It is hoped that a better understanding of the mechanism of the pile-soil-pile interaction when subjected to lateral soil movements may be achieved through this investigation. Table 5.1 shows the tests conducted on batter and vertical piles in a group. The results obtained from each test are tabulated in Appendix B (Figs. B.1 to B.10). The pile group response is presented in terms of bending moment, shear force, soil reaction, pile

rotation and pile deflection for both piles (front and back pile).

Table 5.1 Tests conducted on piles in a group

Test NO.	Test description	s/D	β	Purpose of test	Section	Appendix
1	VVL 	3	$0^\circ, 0^\circ$	Effect of pile groups arrangements (inclined configurations)	5.3.1	Fig. B.1
2	VBL 	3	$0, +10^\circ$		5.3.2	Fig. B.2
3			$0, +20^\circ$		Fig. B.3	
4	BBL 	3	$\pm 10^\circ$		Fig. B.4	
5			$\pm 20^\circ$		Fig. B.5	
6	BVL 	3	$-10^\circ, 0^\circ$		Fig. B.6	
7			$-20^\circ, 0^\circ$		Fig. B.7	
8	BVL 	5	$-10^\circ, 0^\circ$	5.4	Fig. B.8	
9		7			Fig. B.9	
10	BVF 	7	$-10^\circ, 0^\circ$	Effect of pile cap (Free head)	5.5	Fig. B.10

5.2 Setup of pile group testing programme

For each group test, the response of two instrumented piles in the group was recorded. Fig. 5.1 shows the arrangement and details of the pile group used in the testing programme. The instrumented piles (front and back) arrangements used are as follows:

- Batter-Vertical with cap (BVL), $(-\beta, 0^\circ)$;
- Vertical-Batter with cap (VBL), $(0^\circ, +\beta)$;
- Batter- Batter with cap (BBL), $(-\beta, +\beta)$;
- Vertical-Vertical with cap (VVL), $(0^\circ, 0^\circ)$ and
- Batter -Vertical without cap (BVF), $(-\beta, 0^\circ)$.

Both front and back pile had six strain gauges on their front side. Linear Variable Displacement Transducers (LVDT) and electronic tiltmeter were used to measure the displacement and rotation of the pile cap, respectively (piles at pile cap level have the same rotation and displacement values). The final view of the pile group prior to testing with different configurations is shown in Fig. 5.2

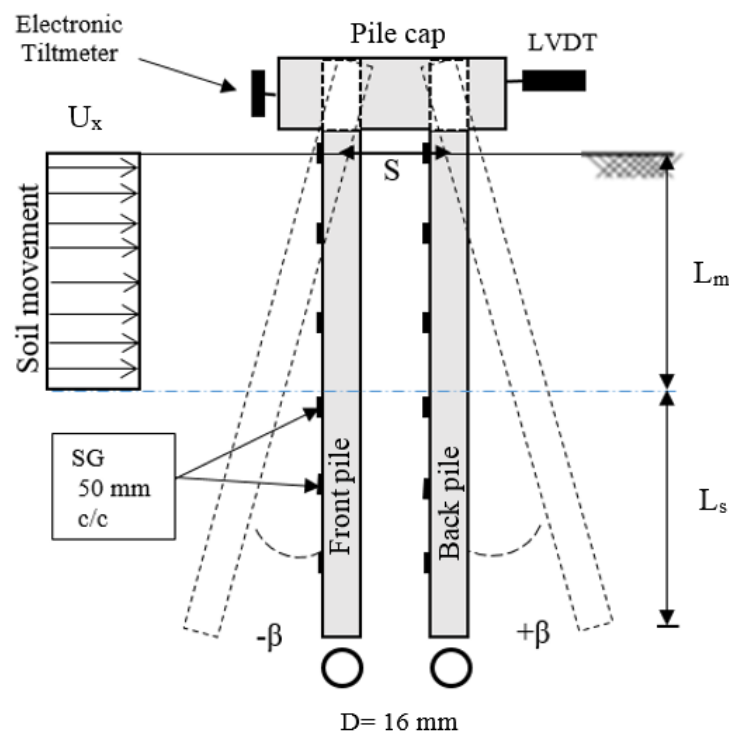
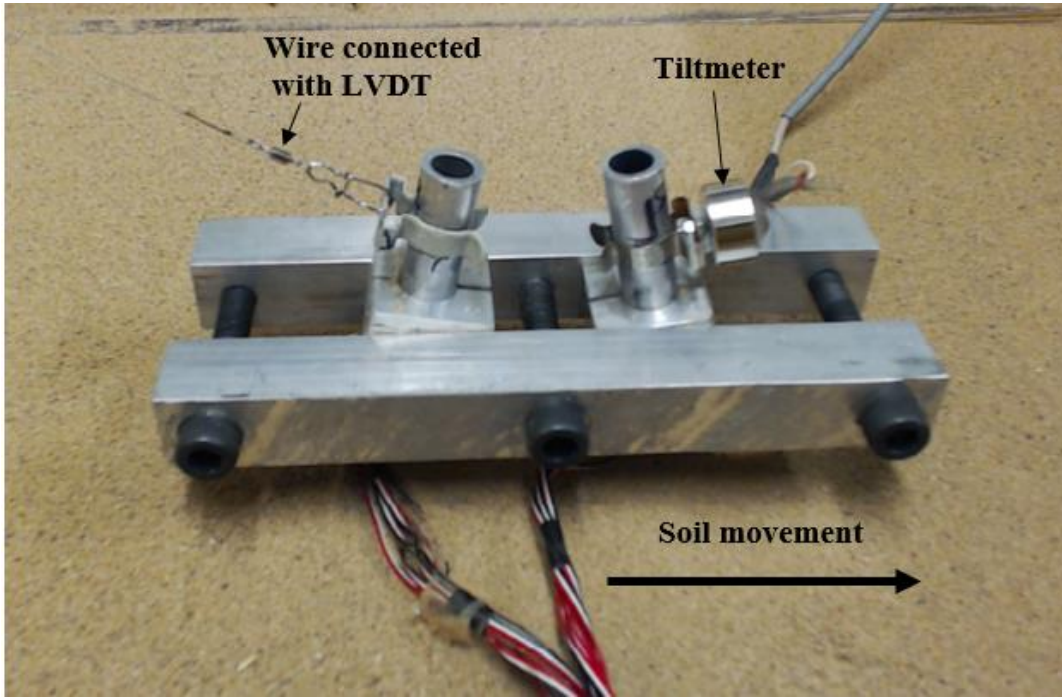
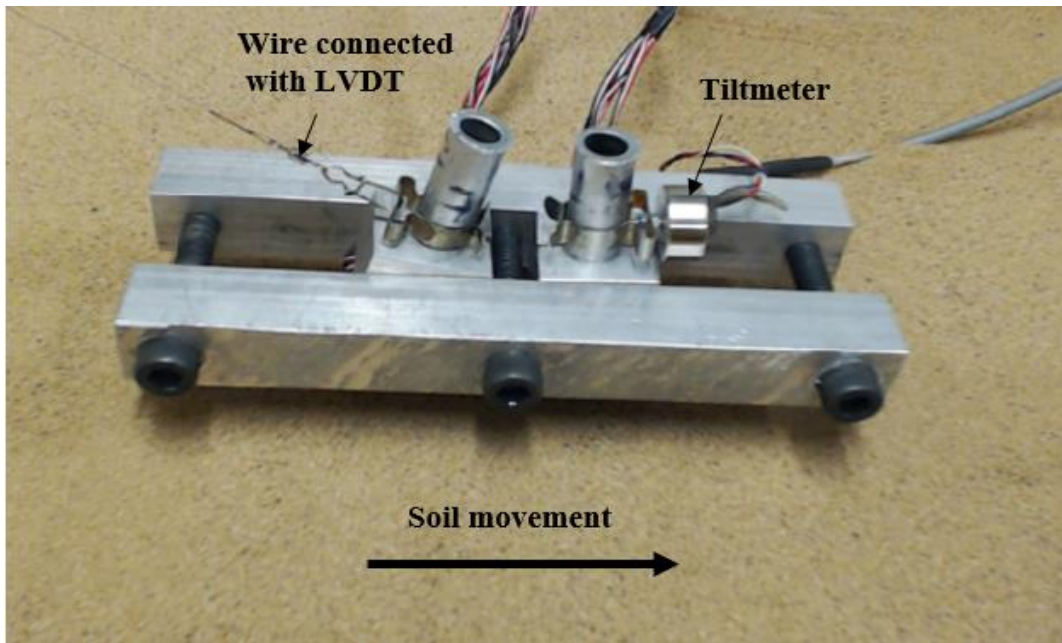


Fig. 5.1 Schematic diagram showing group test setting up



(a) BBL configuration



(b) BVL configuration

Fig. 5.2 The final view of the pile group prior to testing with different configurations

5.3 Effect of pile groups arrangement

The following subsections 5.3.1 to 5.3.2 highlight the effect of batter pile groups configuration and batter angle (β) on the lateral response of the pile group. All the tests were conducted at $s=3D$ (s : centre to centre spacing between piles in pile group at soil surface level).

5.3.1 Results for (VVL) batter pile group configuration test

Bending moment results at each strain gauge measured along both piles measured during the test is illustrated in Fig. 5.3. It can be noticed that the bending moment recorded at both front and back piles were gradually increased with increasing soil movement (box displacement). At depth of 50 mm ($0.16L_e$, where L_e is embedded length of pile), both front and back pile recorded negative moments, while at the depth ≥ 100 mm the bending moment showed positive values at both piles. It is to note that measured moments (negative and positive) at the front and back pile reached their peak values after 15-20 mm of box displacement, after which they remain almost constant.

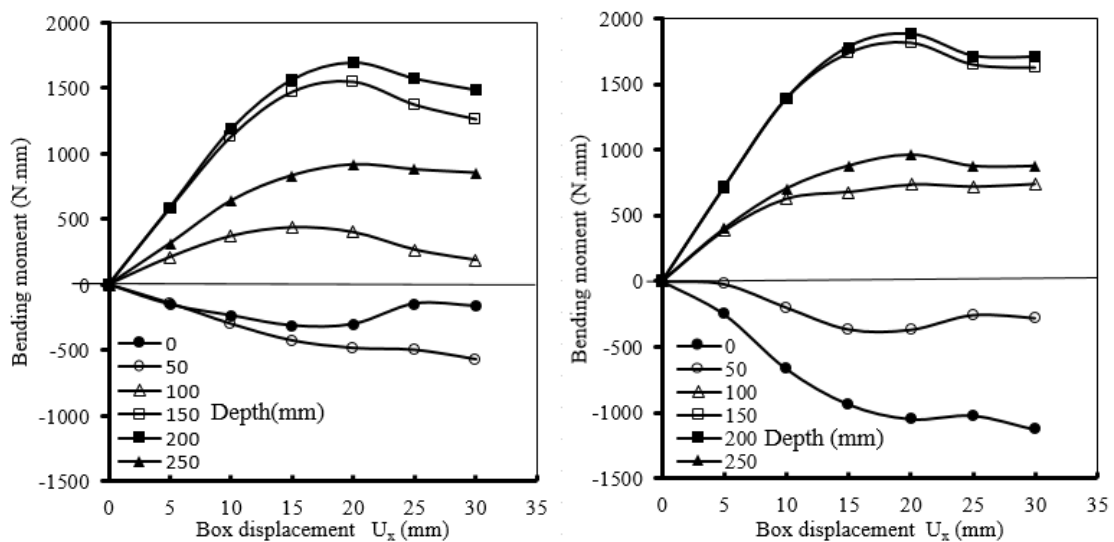


Fig. 5.3 Measured moments at each strain gauge during test

The moment distribution measured along the pile length recorded every 5 mm and up to 30 mm of box displacement is illustrated in Fig. 5.4 for front and back pile. A number of conclusions can be drawn:

- Bending moment distributions for the front and back piles were different in shape, especially in the upper pile portion, and both are different from that for the single vertical pile (standard test), see section of 4.3.1. It is noted that negative bending moments are developed along the upper portion of both piles and this is believed to be attributed to the restraint provided by the cap. This behaviour agreed well with the general trend observed by Chen et al. (1997) and Leung et al. (2000).
- The value and position of the maximum positive bending moment M_{+max} for both front and back piles are recorded the same values, and despite the developed negative bending moment, the position of the maximum bending moment remains essentially the same as that for the single vertical pile in standard test (at depth of 200 mm below the pile cap or $0.67 L$), but its value was smaller than that of the single vertical pile (by about 52.8 %) at $U_x = 30$ mm, see Fig. 4.1.
- The variation of bending moment values measured along the back pile is almost linear up to the maximum value, while it tends to have an arc shape with double curvature along the front pile. It is worth pointing out that both profile shapes remain almost constant during the test. Furthermore, the point of zero bending moment is located at the vicinity of the sliding surface for both piles, at depth of 70 mm below sand surface.

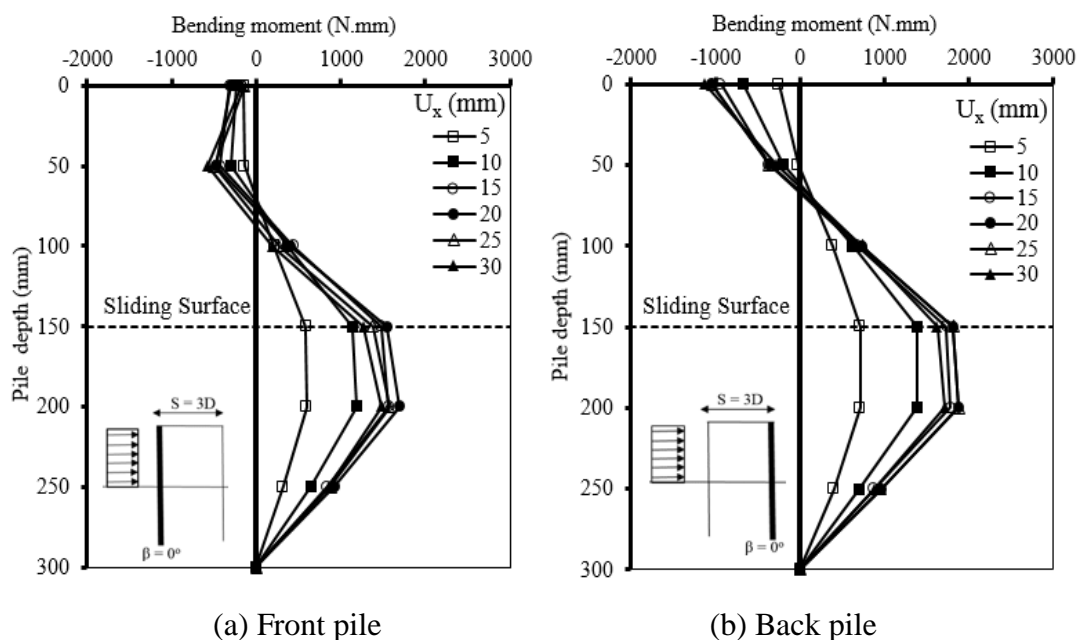


Fig. 5.4 Bending moment profiles, test (VVL configuration)

Fig. 5.5 shows the shear force profile along the pile length in the group. It can be seen that the maximum shear forces in both piles is (21N) which occurred at the moving soil layer (at depth of 100 mm or 0.33L). Owing to the fact that the bending moment has changed linearly in the upper part of the back pile, it can be seen that this pile showed a relatively constant values of shear forces.

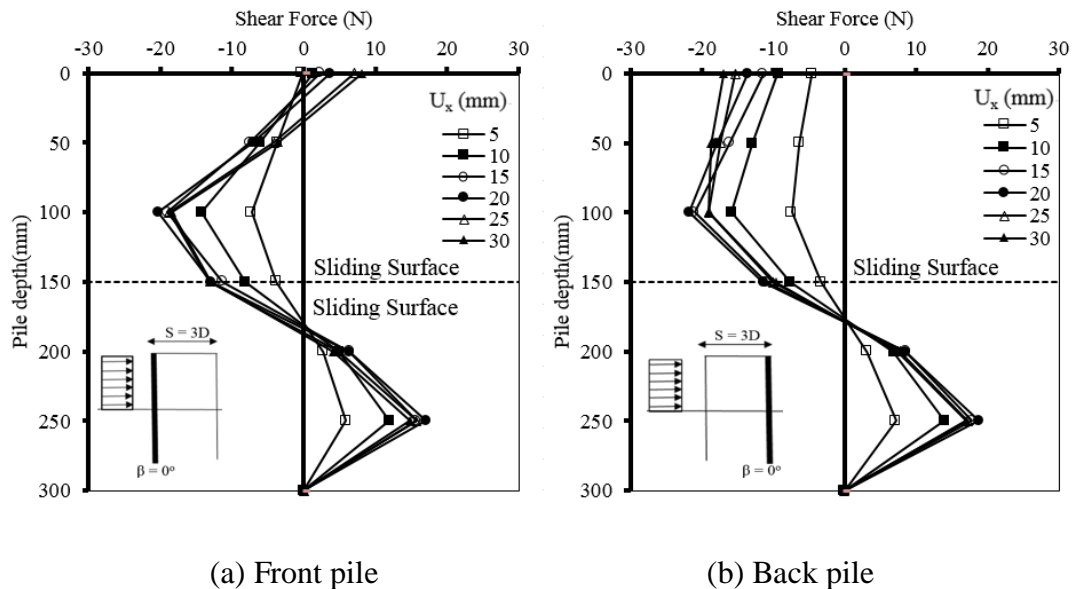


Fig. 5.5 Shear force profiles, test (VVL configuration)

Soil reaction profiles are illustrated in Fig. 5.6. The following observations can be concluded:

- The value and location of the maximum soil resistance for the front and back pile were almost the same (0.33N/mm and, at depth of 200 mm). This depth, also, showed a significant amount of soil resistance for the front pile.
- At (135 mm below soil surface), there was a noticeable change in the soil reaction distribution. This change is expected as both moving and stable soil layers have opposite actions on the pile shaft.
- Soil reaction recorded at the portion of back pile that exists in the moving layer is less than that measured on the front pile. This response suggests, for this pile spacing, that the front pile covers the back pile from a substantial part of the effects of direct soil movements, this is called the shadowing effects (Ilyas et al. 2004).

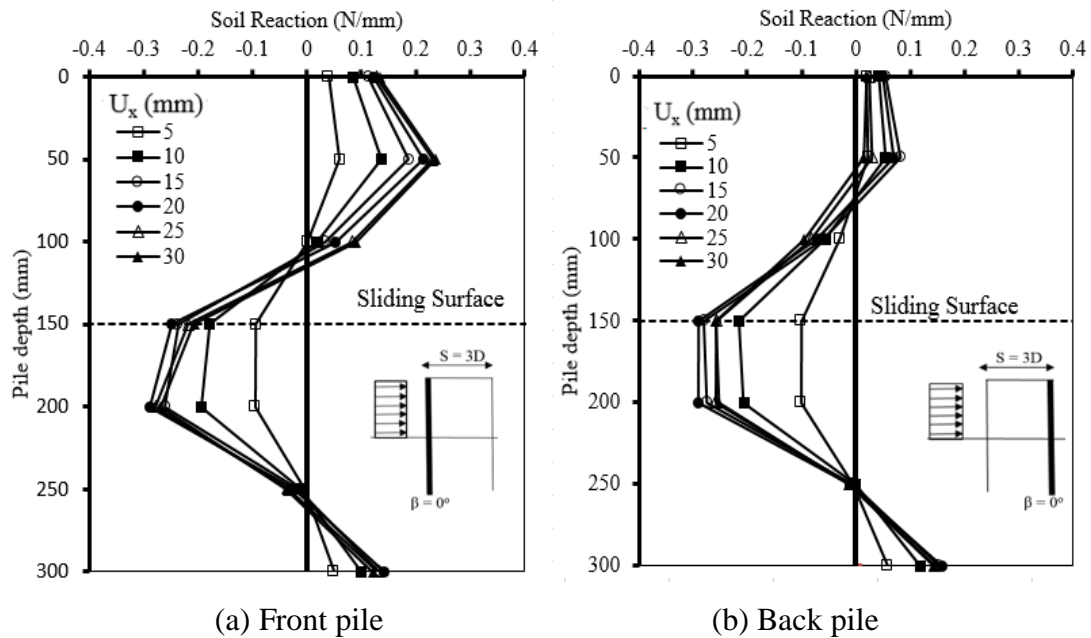


Fig. 5.6 Soil reaction profiles, test (VVL configuration)

Fig. 5.7 presents the response of both piles in terms of rotation. It can be seen that both piles develop a positive angle of rotation with a very small difference for the rotations measured along their lengths. Therefore, it can be concluded that both piles behaved as rigid piles.

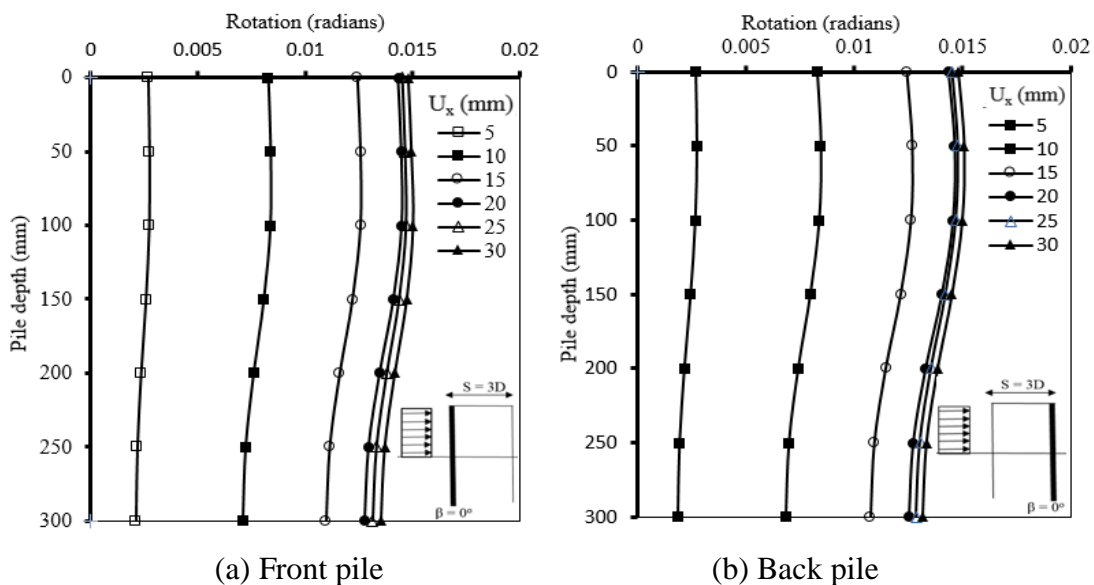


Fig. 5.7 Rotation profiles, test (VVL configuration)

Fig. 5.8 describes the deflection profiles for two piles in the group. Both piles recorded a maximum horizontal displacement of about 3.5 mm (at sand surface) corresponding to 30 mm of box movement. At each soil movement interval, it can be noticed that piles

move horizontally less than the corresponding lateral soil movement. This refers to the fact that the moving sand is flowing around the piles. Furthermore, both piles rotated approximately at depth of 200 - 250 mm below the sand surface.

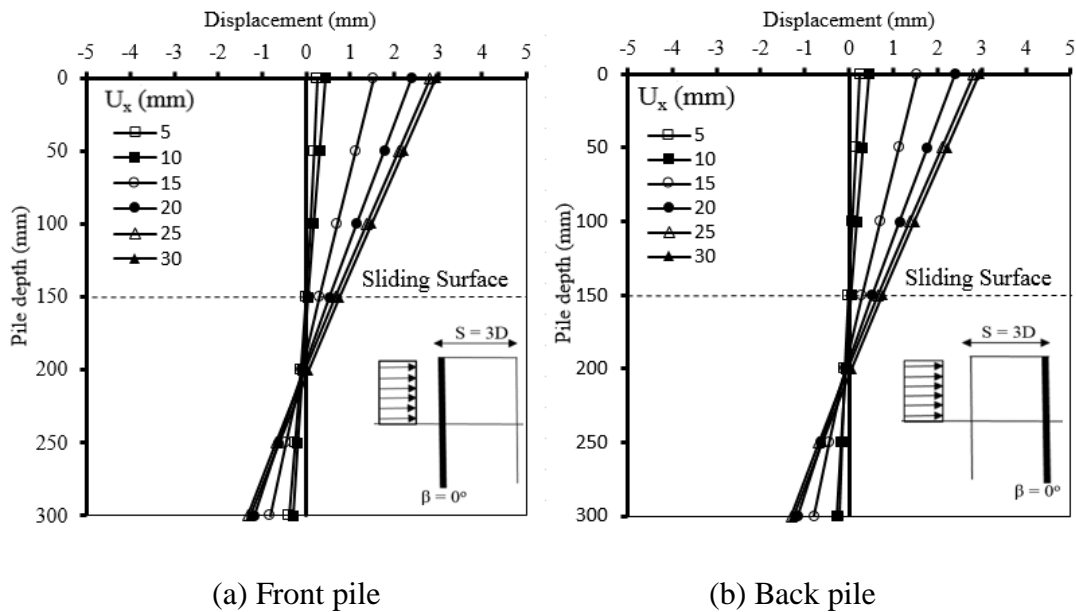


Fig. 5.8 Deflection profiles, test (VVL configuration)

5.3.2 Results for (VBL, BVL and BBL) configuration tests

In order to complete the series of tests related to investigation of the influence of the inclined piles on the lateral behaviour of passively loaded pile group, six more tests namely (VBL, $\beta = +10^\circ$ and $+20^\circ$), (BVL, $\beta = -10^\circ$ and -20°) and (BBL, $\beta = \pm 10^\circ$ and $\pm 20^\circ$) have been conducted. The results obtained from these tests were compared with the test result of the 2×1 vertical pile group (test VVL) of section 5.3.1. It is worth noting that all graphs of this test series had almost the same general trends with the corresponding graphs plotted for the first test (VVL). Due to the space limitation and the large amount of data involved in each test, the results of each individual test are presented in Appendix B (Figs. B.2 to B.7). However, the next section explains only the differences among the results of these tests.

Fig. 5.9 shows the response of the front and back pile in terms of bending moment measured at 30 mm of box displacement for the seven tests. According to this Figure, the following observations can be drawn:

- The positions of maximum negative and positive bending moments and the shape of moment profile for the all tests are almost similar. However, the negative bending moments developed along the front pile for all tests except that of vertical pile group (VVL) in which the moment showed positive values.
- The measured bending moments at the front pile heads are showing positive and negative values depending on the batter angle of the pile and pile group configurations.
- Owing to the pushing force (active load) by the front pile through the pile cap, a significant negative bending moment was observed to develop at the head of the back pile for all tests.
- The lateral loading on the front pile caused by soil movement was mainly resisted by the upper pile shaft.
- The recorded positive bending moment for back pile was at maximum values at depth of 200 mm in stable layer and was lower than that of the single vertical pile for all tests.

For the purpose of comparison, the variation of shear forces recorded with respect to pile depth at the end of all tests, ($U_x = 30$ mm), are plotted together in Fig. 5.10. The resulted shear force values reveal similar profiles for all tests. Front Pile showed maximum shear forces of about 25 N at pile head for two configurations, $(-20^\circ, +20^\circ)$ and $(-20^\circ, 0^\circ)$. Moreover, a new position of maximum shear force appeared at depth of (100-150) mm, that is to say nearly in the middle of the embedded pile depth. Fig. 5.10b showed that the shear force profile along the back pile for the all tests do not appear to be dependent on the batter pile group configurations, while the measured values of shear force were dependent on these arrangements. For instance, in the moving soil layer, the recorded value at the state of BBL $(-20^\circ, +20^\circ)$ is about twice as much as when compared to that obtained with VVL $(0^\circ, 0^\circ)$.

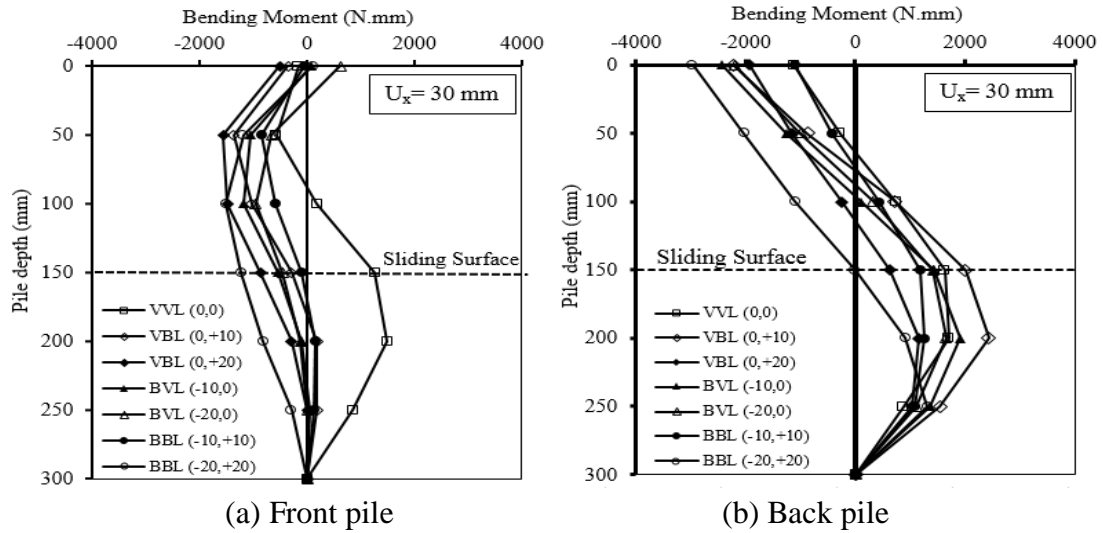


Fig. 5.9 Moment profiles for (2×1) batter pile groups with different configurations

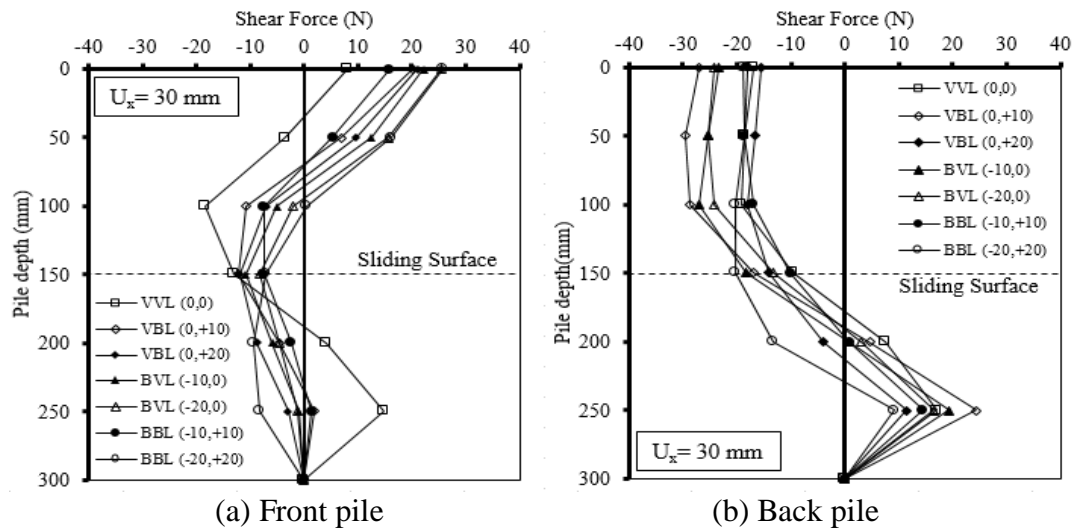


Fig. 5.10 Shear force profiles for (2×1) batter pile groups with different configurations

Fig. 5.11 reveals that the shape of soil reaction profile is independent on the batter pile group configurations, but the values are highly related to these arrangements. On the other hand, the upper portion of the back pile for all cases was not under a passive pressure although its location is within the moving layer. This could be due to the shadowing effect of the front pile.

Fig. 5.12 and Fig. 5.13 investigates the rotation and deflection profiles of the front and back piles. It can be seen that reveals that the shape of rotation and deflection profiles

of both piles are independent on the batter pile group configurations, but the values are highly related to these arrangements. The maximum deformations occurred when the batter pile group configuration in the case of (VVL), whereas minimum values recorded was at the state of BBL (-10°, +10°).

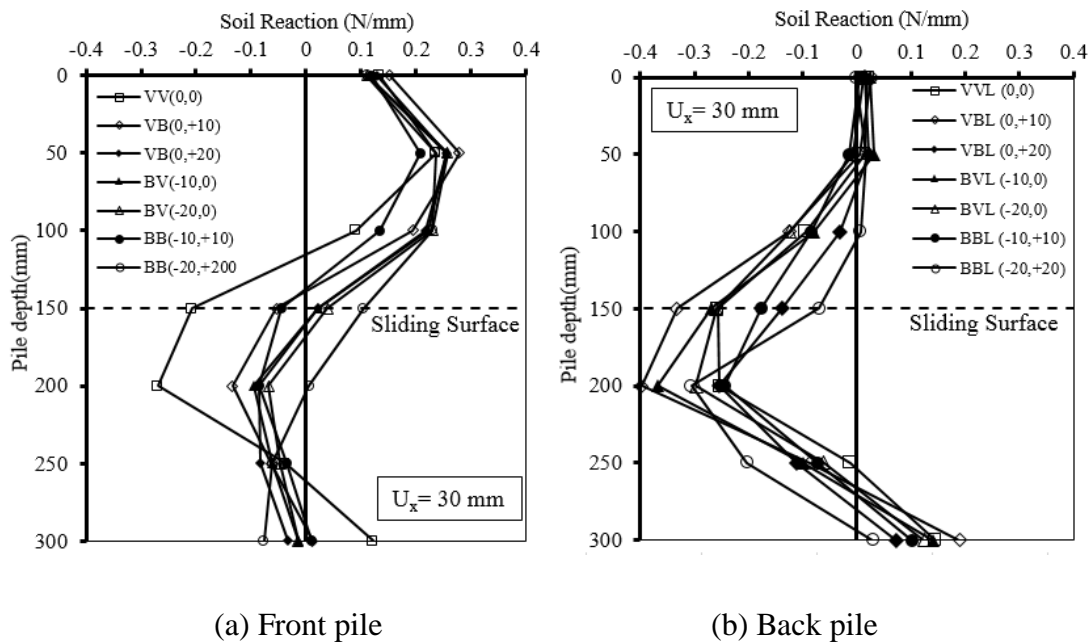


Fig. 5.11 Soil reaction profiles for (2 × 1) batter pile groups with different configurations

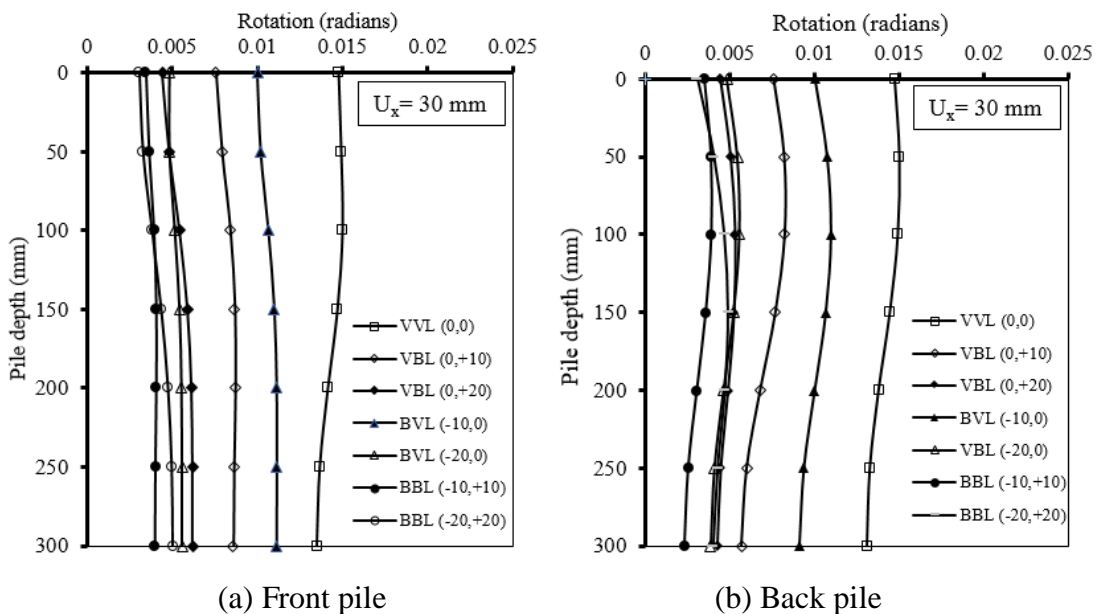


Fig. 5.12 Rotation profiles for (2 × 1) batter pile groups with different

configurations

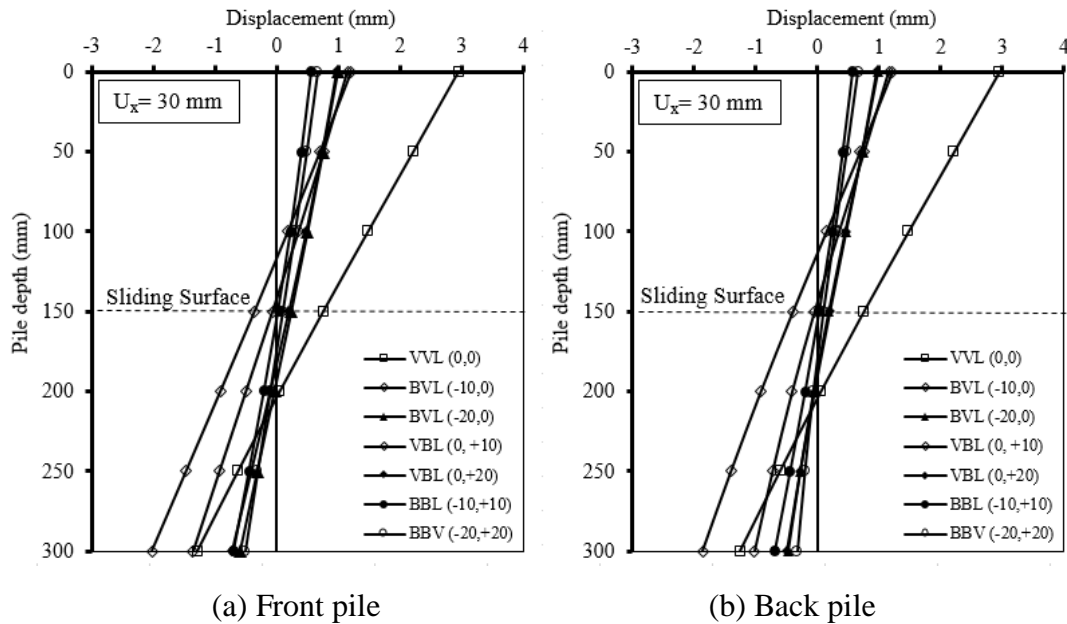


Fig. 5.13 Deflection profiles for (2×1) batter pile groups with different configurations

The maximum negative and positive bending moment (M_{-max} , M_{+max}) are plotted for both piles are shown in Fig. 5.14, for various pile group arrangements. It can be seen that the M_{+max} back pile of the VBL configuration with $(0^\circ, +10^\circ)$ attains the largest value. On the other hand, the greatest value for M_{-max} is at the back pile of BBL configuration with $(-20^\circ, +20^\circ)$. Moreover, it is noted that the M_{max} for both front and back piles was smaller than that of the single vertical pile for different pile group arrangements, and the back pile has a larger value than the front pile.

Fig. 5.15 shows the relationship between the normalised horizontal pile cap displacement and the normalised box displacement (U_x/D) for 2×1 pile groups with different configurations. It is found that the relationship is nonlinear, and the pile cap displacement increases with increasing box displacement. However, the rate of increase reduces, especially when the box displacement U_x is greater than pile diameter (D). In addition, it is observed that the BBL $(-10^\circ, +10^\circ)$ configuration offers more lateral resistance compared to other configurations. In contrast, vertical pile group (VVL) offers less lateral resistance, where, at the box displacement of 30 mm, cap displacement for the case of VVL configuration is about 7 times greater than this recorded for the BBL $(-10^\circ, +10^\circ)$ configuration. This result suggests that the BBL (-

10°, +10°) configuration helps the pile group in resisting the lateral force induced by soil movement more than other configurations while the bending moment decreases in both piles significantly (see Fig. 5.14). Accordingly, the section size of the piles, reinforcement ratio (concrete piles), can be reduced, and therefore the cost is reduced.

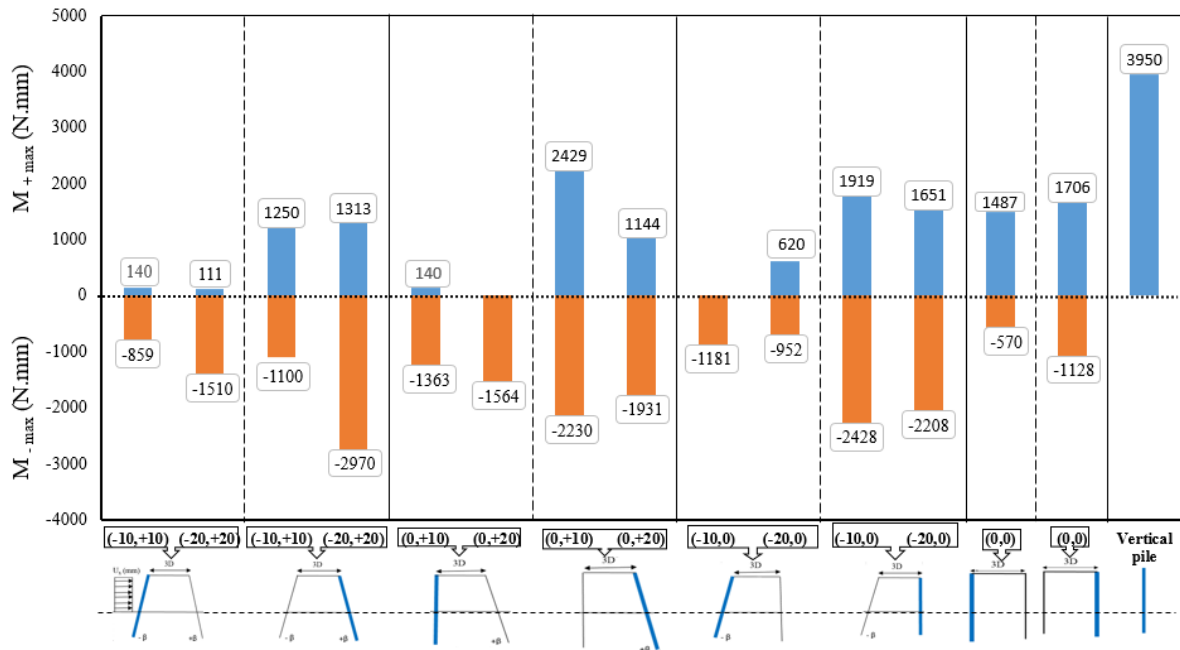


Fig. 5.14 M_{max} for capped-head two-piles with different configurations

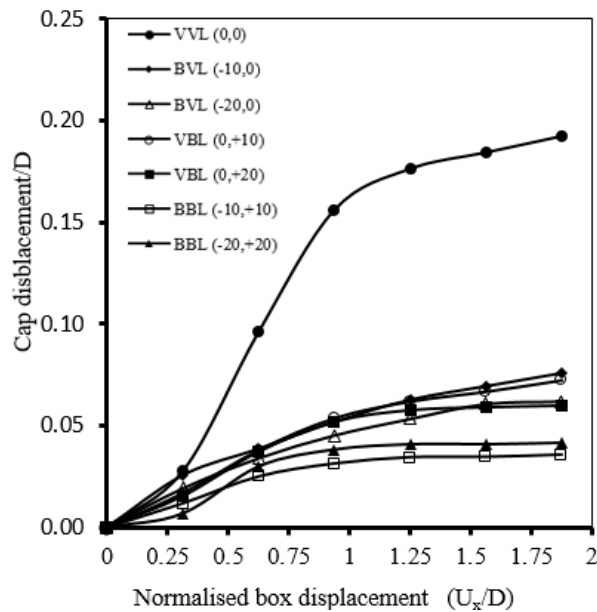


Fig. 5.15 Cap displacement versus box displacement for (2 × 1) batter pile groups with different configurations

5.4 Effects of pile spacing

The effects of pile spacing on the responses of two piles were also investigated by conducting tests on batter pile group (2×1) with (BVL) configuration, where $\beta = -10^\circ$, for three different spacing $s/D = 3, 5$ and 7 (D is the pile diameter), respectively, representing the practical range of pile spacing (Chen and Poulos, 1997). Only selected results ($U_x = 30$ mm) would be presented for comparison within this section at this stage of study. The results for each test are presented in Appendix B (Figs. B.8 and B.9). According to Fig. 5.16, the following observations can be drawn:

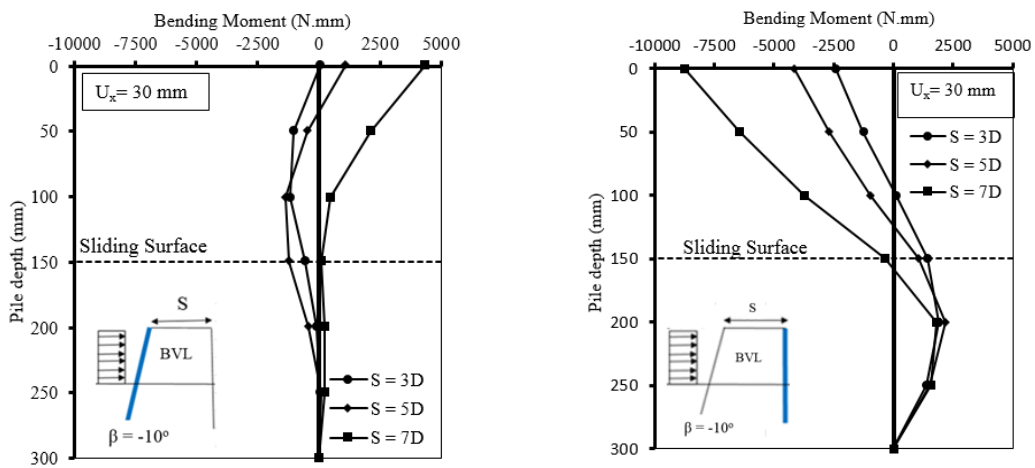
Relatively large negative bending moments are developed at the upper portion of the piles, which is due to the relatively large restraint provided by the cap,

- For front pile, the positive bending moment at the soil surface level increases with an increase in the pile spacing (s). As shown in Fig. 5.16a, $M_{+\max}$ increases from 65 N.mm to 1075 N.mm, as the (s) value changes from $3D$ to $5D$. Subsequently, as (s) increases further from $5D$ to $7D$, there is a significant increase of almost four-folds in the bending moment values. Beyond the depth of 200 mm, the pile bending moment was negligible.
- The profile of moment distribution is very similar in shape for each case, including the position of the maximum bending moment, but its magnitude is different.
- For back pile, although the moment profiles including the position of M_{\max} have a common deformation pattern in all the three tests, the difference in moment values was more than that observed in the front piles. Relatively large negative bending moments are developed at the upper portion of the piles, which is due to the relatively large restraint provided by the cap, and the negative moment may be smaller or larger than the positive moment depending on the pile spacing. An increase of about 75 % in the pile head moment has been observed when (s) increased from $3d$ to $5D$. Subsequently, a further increase in (s) to $7d$ caused a considerable increase in moment of about twice compared to that at $5d$ of pile spacing (s), (see Fig. 5.16b).
- For front Pile, the shear force at pile head was 22.0 N, 31.4 N and 43.8 N for spacings of $3d$, $5d$ and $7d$ pile spacing (s) respectively. In other words, shear force at (s) of $7d$ is twice as much as that measured when (s) had a value of $3d$

(see Fig. 5.16c). On the other hand, the shear force recorded at back pile showed, also, a tendency to increase with increasing (s), (see Fig. 5.16d).

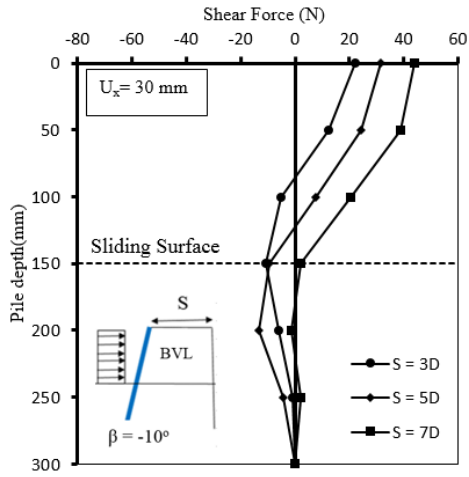
- Soil reaction/resistance values measured along the piles generally tend to increase as pile spacing increases. Based on the results, it is found that the trends of curves are generally consistent with each other including the position of maximum soil reaction (Fig. 5.16e & f).

Fig. 5.17 illustrates the relationship between the normalised pile cap displacements (cap displacement/D) and the normalised box displacements (U_x/D) for different values of pile spacing (s) with (BVL) configuration and $\beta = -10^\circ$. The result shows that the cap displacement increases with increasing box displacement for all values of (s). Also, it is observed that the pile spacing of $S=7D$ offers more lateral resistance compared to $s=3D$ and $s=5D$. Cap displacement was increased linearly with increasing box displacement in the case of $s=7d$. On the other hand, this relationship showed some nonlinearity in case of $s=3D$, and it was a clear nonlinear behaviour in the case of $s=3D$.

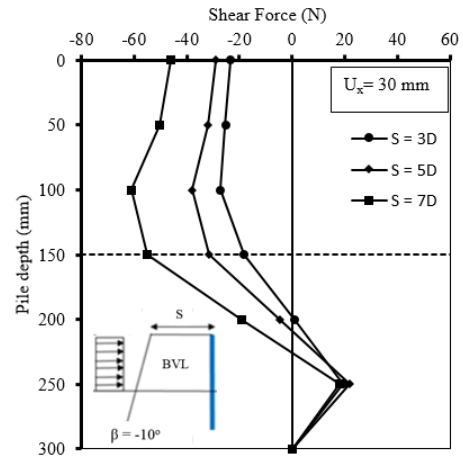


(a) Bending moment profile of front pile

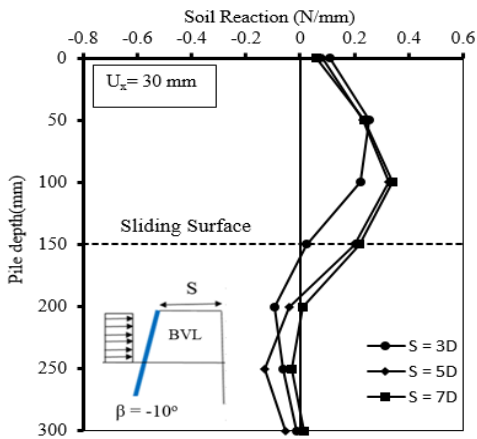
(b) Bending moment profile of back pile



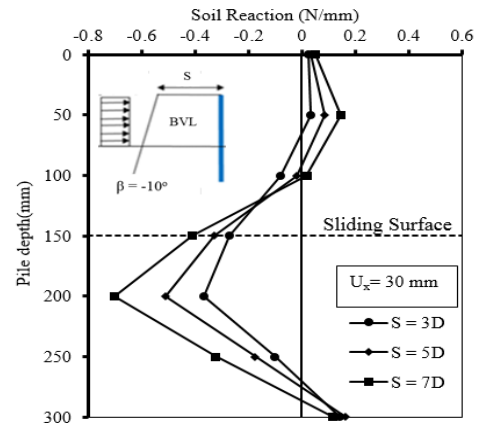
(c) Shear force profile of front pile



(d) Shear force profile of back pile



(e) Soil reaction profile of front pile



(f) Soil reaction profile of front pile

Fig. 5.16 The effect of pile spacing on the pile response of 2x1 pile group (BVL)

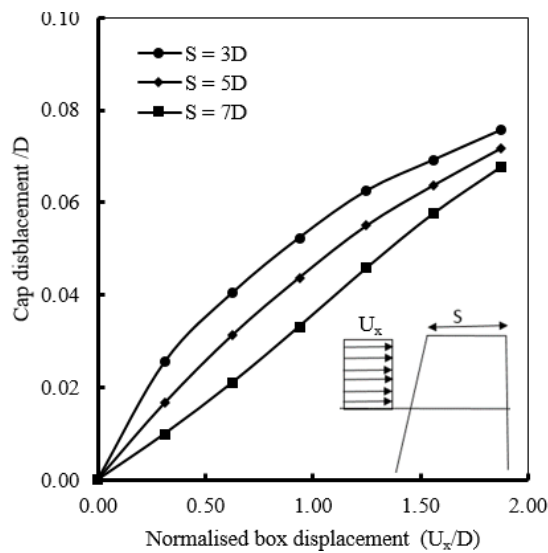


Fig. 5.17 Cap displacement versus box displacement at different values of (S), for BVL configuration and $\beta = -10^\circ$

5.5 Effect of pile cap

The effect of pile cap on the lateral pile group response of piles was investigated by conducting tests on free-head and capped 2-pile groups, with BVL and BVF configuration ($\beta = -10^\circ$) and pile spacing (s) of $7D$. Fig. 5.18 shows that the bending moment profiles for both pile head fixity were found to be totally differed in shape. On the other hand, the bending moment profiles for the front pile and the back pile for the free-head case is the same and similar to that of the single vertical pile, including the position of the maximum bending moment. However, the magnitude of the bending moment is seen to be quite different for the two piles (front and back). In contrast, the bending moment profile for the front pile and the back pile for the capped case is different, and both are different from that for the single pile. Unlike the case of free-head pile group, the cap in this case is seen to have a significant influence on the bending moment profiles. Thus, Positive and relatively large negative bending moments are developed along the upper portion of the front and back pile, respectively, due to the restraint provided by the cap. The negative moment is larger than the positive moment that was measured along the back pile at stationary soil layer, while the value of the bending moment for the front pile is almost zero along the lower portion of the front pile. Despite the developed negative bending moment, the position of the maximum bending moment remains essentially the same as that for the single pile.

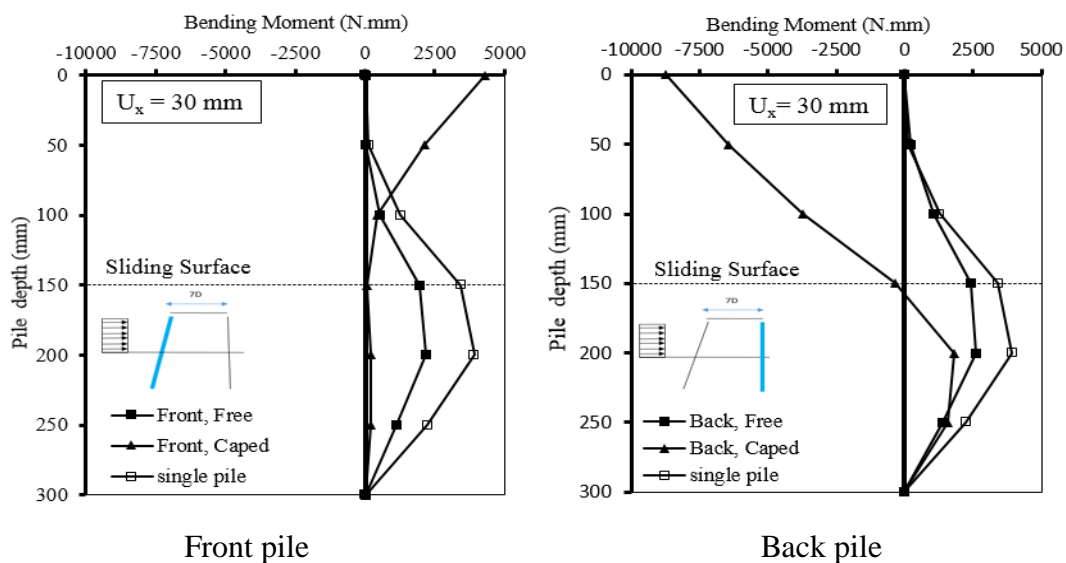


Fig. 5.18 Bending moments for free single vertical pile (standard test), free and capped two-batter pile, (BVF & BVL)

5.6 Group effect

In this section, pile group factors are first introduced to quantify the group effect. Then the pile group behaviour for the several configurations are analysed, focusing on comparison of the maximum bending moment, M_{\max} with that of the ‘standard’ single vertical pile test RSF16-0°.

5.6.1 Group factors

In order to assess the group effect of piles subjected to lateral soil movement, the critical pile responses of a pile within a group, such as the maximum bending moment, pile head deflection and limiting soil pressure (Chen and Poulos, 1997; Pan et al., 2002a) are compared with those of a single pile. Chen et al. (1997) have demonstrated that the group effect assessed in terms of measured maximum bending moment may be more reliable and consistent. In the present study, a group factor, F_m is introduced to quantify the group effect. This compares the absolute value of the maximum positive bending moment of a pile in a group with that of the ‘standard’ single pile at the same predetermined sliding depth ($L_m=150$ mm) and same amount of soil movement ($U_x=30$ mm), and is described by the following expression:

$$F_m = \frac{M_{g(\max)}}{M_{sv(\max)}} \quad (5.1)$$

Where:

F_m = group factor;

$M_{g(\max)}$ = absolute value of maximum bending moment for a pile in a group;

$M_{sv(\max)}$ = maximum bending moment of the ‘standard’ single vertical pile RSF16,0°.

5.6.2 Effect of pile groups arrangement on the group factors

In order to calculate the group factors, the measured maximum bending for the pile group tests were normalised by the measured $M_{sv(\max)} = 3950$ N.mm and for the ‘standard’ single pile TSF16,0°. Table 5.2 summarises the group factors obtained from the 10 pile group tests. The following characteristics have been noted:

- For the BVL arrangement, the group factors F_m decreases with the increasing batter angle β . Where, the group factor decreases about 20% and 14% as β increases from -10° to -20° for front and back pile, respectively.
- For the BBL of pile group, the F_m of the both piles depending on batter angle β . Where, the group factor increases about 77% and 8% as β increases from $\pm 10^\circ$ to $\pm 20^\circ$ for front and back pile, respectively.
- For the VBL of pile group, the F_m of the front piles also depending on the β , with the largest value of 0.40 being obtained at $\beta = -20^\circ$. Nevertheless, the F_m of the back pile decreases from 0.63 to 0.30 as the β increases from $+10^\circ$ to $+20^\circ$.
- For the VVL of pile group, it is found that the group factor F_m for the front and back pile are 0.38 and 0.44 for front and back pile, respectively.

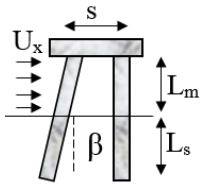
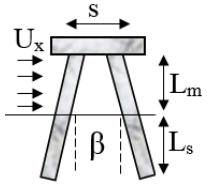
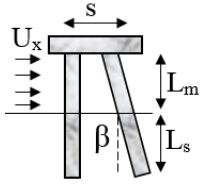
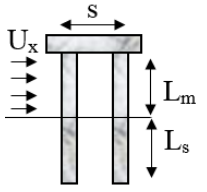
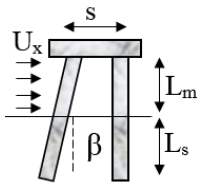
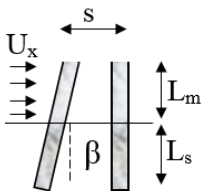
5.6.3 Effect of pile spacing on the group factors

The effect of pile spacing on the group factor F_m was investigated by conducting tests on the BVL of pile groups with $\beta = -10^\circ$, for three different spacings of 3D, 5D and 7D. Table 5.2 shows that the for both the front and back piles increases with the increasing spacing (s). F_m increases about 77 % from 0.31 to 0.55 and about 352% from 0.50 to 2.26 for the front and back piles, respectively, as the (s/D) increases from 3 to 7. This trend is consistent with that obtained by Miao et al. (2008), see Table 5.3. At the same pile spacing, values of F_m for the back piles are (1.6~4.10) times greater than those deduced for the front piles, depending on the pile spacing.

5.6.4 Effect of pile cap on the group factors

The effect of pile spacing on the group factor F_m was investigated by conducting tests on the BV of pile groups with $\beta = -10^\circ$, for the free-headed case (BVF) and the capped case (BVL), with $S/D = 7$. It can be seen that the group factors F_m of the front pile is same amount ($F_m = 0.55$) for the both head conditions. Nevertheless, the group factor F_m is very different for both cases, and the cap of piles in this case has a significant effect on F_m . Where, the F_m of the back pile is much larger for the capped case than for the free-headed case (see Table 5.2).

Table 5.2 Summary of group factors Pile

Test description		s/D	β	F_m			
				Front pile	Change %	Back pile	Change %
BVL		3	$-10^\circ, 0^\circ$	0.31	-	0.50	-
			$-20^\circ, 0^\circ$	0.25	-20	0.43	-14
BBL		3	$\pm 10^\circ$	0.22	-	0.32	-
			$\pm 20^\circ$	0.39	+77	0.34	+8
VBL		3	$0, +10^\circ$	0.35	-	0.63	-
			$0, +20^\circ$	0.40	+14	0.30	-30
VVL		3	$0^\circ, 0^\circ$	0.38	-	0.44	-
BVL		3	$-10^\circ, 0^\circ$	0.31	-	0.50	-
		5		0.35	+13	0.70	+49
		7		0.55	+77	2.26	+352
BVF		7	$-10^\circ, 0^\circ$	0.55	-	0.67	-

5.6.5 Group factors from previous study

Group effects on the lateral response of vertical piles to lateral soil movements have also been studied experimentally by Chen (1994), Chen et al. (1997) and Pan et al. (2002a) and numerically by Chen and Poulos (1997). The group effect was quantified by group factors. In their studies, the group factors were defined in terms of either maximum bending moment, M_{max} at the same amount of free-field soil movement (Chen, 1994) or limiting soil pressure, P_u (Chen and Poulos, 1997; Pan et al., 2002a; Miao et al., 2008). These group factors are summarised in Table 5.3.

Table 5.3 Summary of group factors from previous study

Soil type	Pile group		Pile head condition	Spacing S/D	F_m or F_p^*	Reference		
Sand	Two piles in a row		Free-head	2.5	0.81	Chen (1994)		
				5.0	0.88			
				7.5	0.98			
					Capped-head		2.5	0.72
							5.0	0.78
							7.5	0.84
	Two piles in a line	Front piles	Free-head	2.5	1.31			
				5.0	1.59			
				7.5	1.20			
				Capped-head	2.5		0.93	
					5.0		1.25	
					7.5		0.64	
			Back piles	Free-head	2.5		1.01	
					5.0		1.10	
					7.5		0.69	
		Capped-head	2.5	0.92				
			5.0	1.36				
			7.5	0.67				
Piles in one long row		Free-head	3.0	1.2	Chen and Poulos (1997)			
			4.0	1.1				
			8.0	1.0				
Clay	Two piles in a row		Head-tip-fixed	3.0	0.67	Pan et al. (2002a)		
	Two piles in a line	Front piles		5.0	0.81			
				3.0	0.77			
		Back piles		5.0	0.67			
				3.0	0.41			
	Four piles in a group 2x2			Head-tip-fixed	5.0		0.67	
			2.5		0.89	Miao et al. (2008)		
			5.0		0.41			
			2.5	0.98				
			5.0	0.68				

* Group factor $F_p = P_{ui}/P_{us}$, where $P_{ui} = P_u$ for a pile in the group; and $P_{us} = P_u$ for a single isolated vertical pile.

5.7 Summary

A series of laboratory tests has been carried out on 16 mm diameter model pile groups and the results have been discussed in this chapter. In the tests, the pile group of 2×1 with different arrangements have been considered, namely, VVL, BBL, VBL and BVL arrangement. Only the rectangular soil movement profile was investigated at this stage. The following conclusions can be drawn.

- Each pile in a group behaves differently, and the extent of the group effect on the lateral response of a pile in a group depends on a number of factors, including the arrangement of the pile in the group, the inclination angle of piles in the group, the pile spacing and the head fixity condition.
- A rigid cap has a significant effect on the pile response, which tends to reduce the positive bending moment, while developing a relatively large negative bending moment in the upper pile portion
- The $M_{+\max}$ and $M_{-\max}$ on front pile showed lower values compared to that on back pile for all pile group configurations.
- Batter pile groups with (BBL) configuration of $(-10^\circ, +10^\circ)$ offer more resistance to lateral soil movement compared to other pile group arrangements with the same pile spacing. This is confirmed by the development of higher bending moments in the back piles rather than the front piles. On the other hand, (VVL) configuration offered the least resistance.
- The bending moment profiles showed a double curvature on front and back piles within the capped piles group configuration, while a single curvature was the case for the uncapped pile group (free-head pile condition).
- The $M_{+\max}$ values recorded in the pile group were always lower than that of a single pile (standard test).
- The development of M_{\max} , shear force and soil reaction of each pile in a group with lateral soil movement (U_x), is similar to those of a single pile.
- Pile spacing have significant impact on the pile responses, in which the $M_{+\max}$ and $M_{-\max}$ increase with pile spacing increase.

Chapter 6

Three-Dimensional Finite Element Analysis

6.1 Introduction

Numerical methods such as finite element (FEM) and finite difference techniques (FDM) became popular due to drastic improvement of computing tools, which can conduct analysis of complex soil-structure interaction problems. Therefore, to better understand the mechanism of complicated soil-pile interaction, a series of three-dimensional finite element analyses were performed in this study. In the last two decades, there was a growing number of mature FEM and FDM commercial software in the existing market (e.g. DIANA, ABAQUS, PLAXIS and FLAC). Among those, PLAXIS and ABAQUS are widely used software in the geotechnical engineering and PLAXIS is excellent in dealing with the complex soil-pile interaction problem (Bingcan et al., 2010). Therefore, PLAXIS 3D Introductory geotechnical software was used for all analyses in this study. The same program was also used to conduct three-dimensional analysis of lateral loaded piles (e.g. Ong, 2008; Kahyaoglu et al., 2012a; Kelesoglu and Cinicioglu, 2010; Jeong et al., 2009; Nugroho and Prakoso, 2010; Ekici, 2013; Ekici and Huvaj, 2014; Al-abboodi et al., 2015).

The main purpose of this chapter is to investigate the ability of the existing PLAXIS 3D program using embedded pile model to predict the response of single batter piles and pile groups subjected to lateral soil movements. The procedure was validated by comparing the computed results with the testing programme results of this study which were described in Chapter 4 and Chapter 5. In addition, a parametric analysis was conducted to examine the influence of some input parameters on the batter pile behaviour, which had not been previously investigated in an experimental study. Variations in the factors such as roughness of the pile surface and material properties of moving soil and their effects were studied.

6.2 Description of the computer program

Information presented in this section is based on the PLAXIS 3D Reference Manual and the PLAXIS 3D Materials Manual (PLAXIS 3D, 2013).

PLAXIS 3D is a three-dimensional finite element analysis software designed to analyse the non-linear properties of soil and rock as well as soil-structure interaction problems such as excavations, foundations, embankments and tunnels. PLAXIS consists of two parts which are input and output program. Input program is used for the definition of the model and assignment of analysis properties. At the beginning of the input programme, project properties are asked from the user. Model boundaries in two horizontal directions (x and y) and unit system used in analyses are defined in this part. Input programme includes five main components which are soil, structures, mesh, water levels and staged construction. In soil mode, soil stratigraphy is assigned to the model by creating boreholes. In addition, ground water level of a specific point is defined also with boreholes. In structures mode, all kinds of geometric entities, structural elements and their configurations are assigned. In addition, boundary conditions; predefined displacement or loading of a point, line or a surface can be defined in this part. Both soil and structure modes include material sets option which is used for the definition of material properties of soil and structural elements. In mesh mode, geometry is divided into mesh elements with desired amount of fineness. After finalisation of all geometric entries, calculation stages are arranged in staged construction mode according to the purpose of the analysis. All geometric elements can be activated or deactivated for every stage. After setup of all stages, analysis can be conducted. PLAXIS 3D provides extensive ways for the documentation of the analysis results. Output program presents all numerical analysis results in variety of forms including curves, diagrams and tables. It mainly consists of the results of deformations and stresses. In addition, force results are presented for structural elements.

6.3 PLAXIS 3D Introductory limitations

PLAXIS 3D Introductory version is based on a software that has limitation compared to the Professional Version, those are listed below:

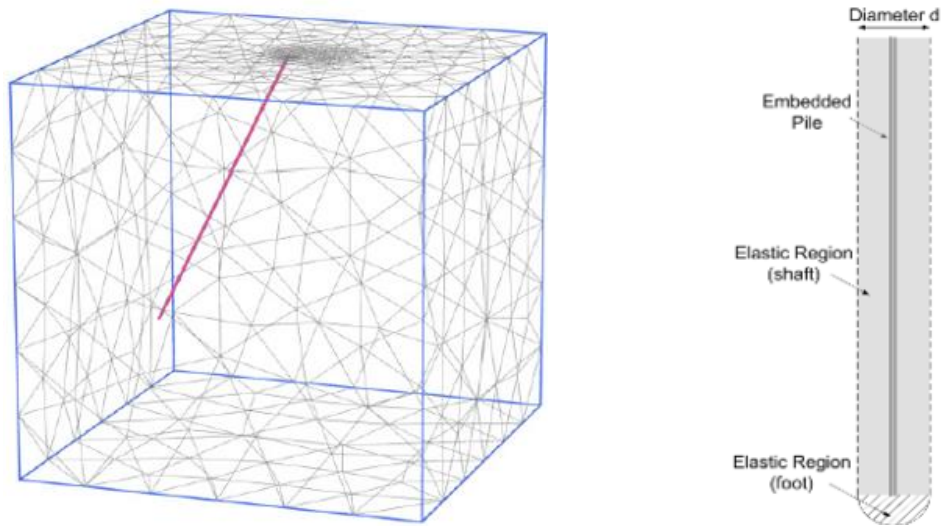
- Only one set of soil parameters can be used in each run calculation.
- Only three material models can be used to simulate the soil behaviour (Linear Elastic model, Mohar-Columbo model and Hardening Soil model).
- Only embedded piles feature can be used to model the piles.
- The number of calculation phases is limited to 5 phases.

However, the first limitation was already overcome due to the use of one soil type (sand) during the whole testing programme. Also, a Mohr-Coulomb model was used to represent the sand behaviour. Furthermore, batter piles are modelled by beam elements surrounded by special interface elements (known as embedded piles) rather than volume piles, to evaluate the embedded pile is able to simulate the pile behaviour in the situation of being subjected to lateral loading caused by soil movements. As for the last limitation, the number of available calculation phases was enough in this study.

6.4 PLAXIS embedded pile

Recently, PLAXIS has provided a special feature in pile modelling, namely embedded pile feature. Embedded pile is a pile composed of beam elements (e.g. 3-node elements with six degrees of freedom per node, 3 translations and 3 rotations) to model the pile itself, and embedded interface elements to model the interaction between the soil and pile. It can be embedded at any direction into existing finite element mesh of soil volume elements (Fig. 6.1a). According to the design of the embedded pile, volume is not taken into consideration. However, an elastic volume around the pile, whose dimension is like the pile diameter, is assumed (Fig. 6.1b). Unlike the embedded pile, volume pile can be generated and defined in the soil mode as a different material with certain dimensions and properties. Comparing the analytical results of embedded pile with that obtained by using volume pile in modelling a laterally loaded pile response showed a good agreement between them (Dao, 2011). It is important to mention that the calculation time and the number of elements required to analyse pile-soil interaction problems are sufficiently reduced by using embedded piles compared to using volume piles. This is mainly due to the complex meshing of the pile body and its interaction points with the surrounding soil when using volume pile. Another advantage of the embedded pile is that the output forces can be directly obtained, unlike the volume pile which is modelled as soil material.

However, one of the limitations of the embedded pile is that it does not take the method of installation into account, i.e. the change in soil density after the installation. Therefore, driven and displacement piles could be affected more than bored piles due to this limitation (Haryono, 2013).



a) Embedded pile with arbitrary direction b) Elastic region around embedded pile

Fig. 6.1. Schematic of embedded pile in 3D mesh and elastic zone around embedded pile (Brinkgreve et al., 2013)

6.5 Pile-soil interaction

After the mesh is generated, new “virtual” nodes are created inside existing soil volume elements (e.g. 10-node tetrahedral in PLAXIS) at position of the beam elements nodes (Fig. 6.2). Thus, the special interface forms a connection between the beam element nodes and these virtual nodes, and thus with all nodes of the soil volume element. The behaviour of the interaction of the pile and the soil at the shaft in axial direction is governed by elastic-plastic model, represented by spring and slide (see Fig. 6.3). On the other hand, the behaviour of the pile in lateral direction is only dictated by spring, which leads only to elastic. The interaction may involve a skin resistance (in unit of force per length) and a tip resistance (in unit of force) whose sum is considered as the bearing capacity of the embedded pile. For both the skin resistance and the tip resistance, a failure criterion is applied to distinguish between the interface elastic behaviour and the interface plastic behaviour. For elastic behaviour, small displacement differences occur within the interface (i.e. between the pile and the soil displacement, and for plastic behaviour permanent slip may occur.

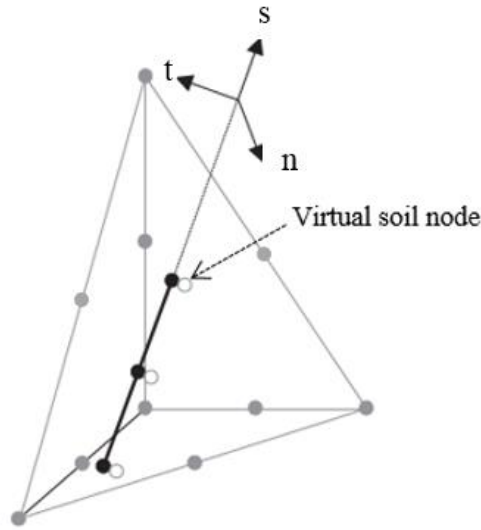


Fig. 6.2 Embedded pile element denoted by the solid line within a 10-node tetrahedral soil element (PLAXIS 3D, 2013)

The skin resistance of the interface is represented in Eq. (6.1):

$$\{t\}^{skin} = [K]^{skin} \cdot \{\Delta u_{rel}\}^{skin} \quad (6.1)$$

Where:

$\{t\}^{skin}$: force at the integration points;

$[K]^{skin}$: material stiffness matrix of the interface;

$\{\Delta u_{rel}\}^{skin} = u_p - u_s$: relative displacement vector between the soil and the pile.

Furthermore, the above equation can be represented in the three-dimensional local coordinate system (s, n, t) as in Eq. (6.2):

$$\begin{bmatrix} t_s \\ t_n \\ t_t \end{bmatrix} = \begin{bmatrix} K_s & 0 & 0 \\ 0 & K_n & 0 \\ 0 & 0 & K_t \end{bmatrix} \begin{bmatrix} u_n^p - u_n^s \\ u_s^p - u_s^s \\ u_t^p - u_t^s \end{bmatrix} \quad (6.2)$$

Where:

t_s : shear stress due to friction between pile and the soil.

t_n and t_t : normal stress due to lateral displacement of the pile.

K_s : elastic shear stiffness of the embedded interface element.

K_n and K_t : elastic normal stiffness of the embedded interface element in horizontal directions.

u_s^p : Pile movement in axial direction.

u_n^p, u_t^p : Pile movement in lateral direction.

u_s^s : soil movement in axial direction.

u_n^s, u_t^s : soil movement in lateral direction.

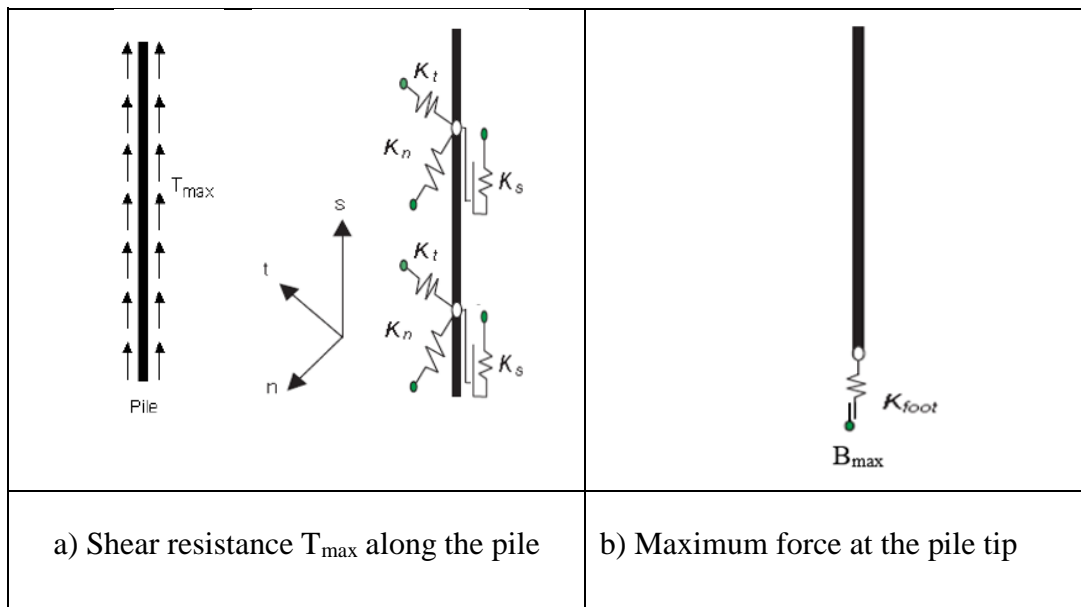


Fig. 6.3 Shear resistance and tip resistance (PLAXIS 3D, 2013)

According to PLAXIS 3D Reference manuals, 2013, interface stiffness in PLAXIS 3D are set by default at values given by the following equations.

$$K_s \gg G_{soil} \text{ and } K_n = K_t = \frac{2(1 - \nu_s)}{1 - 2\nu_s} K_s \quad (6.3)$$

$$G_{soil} = \frac{E_s}{2(1 + \nu_s)} \quad (6.4)$$

Where:

G_{soil} : the shear modulus of the soil,

E_s : Young 's modulus of soil,

ν_s : the poisson ratio of the soil.

Note that stiffness values are not user-defined values, but the values that are automatically set by PLAXIS 3D code, so the governing calibration factors for the model interface stiffness are the stiffness properties of the surrounding soil.

Fig. 6.3a gives a visualization of Eq. (6.1). It should be considered that the skin resistance T_{max} is defined as the capacity of the interface to sustain the shear force t_s along the pile (in axial direction of the pile). For elastic behaviour of the shaft, the shear force t_s at a particular point has to be smaller than the local skin resistance at that point T_{max} ($|t_s| < T_{\text{max}}$). Therefore, the plastic behaviour occurs if embedded pile $|t_s| \geq T_{\text{max}}$.

In addition to the skin resistance, the tip resistance is governed by a non-linear spring at the pile tip (Fig. 6.3b). The tip resistance presents the capacity against the maximum force acting at the interaction between the pile tip and the soil. It can be formulated in the equation (6.5) below.

$$0 \leq F_{\text{tip}} = K_{\text{tip}} \cdot (u_{\text{tip}}^p - u_{\text{tip}}^s) \leq F_{\text{max}} \quad (6.5)$$

Where:

F_{tip} : the force at the pile tip;

K_{tip} : the material stiffness matrix of the spring element at the pile tip;

$(u_{\text{tip}}^p - u_{\text{tip}}^s)$: the relative displacement vector between the soil and the pile at the foot.

It can be seen that the force at the pile tip F_{tip} is zero in case of pulling out (tension behaviour). The failure occurs when the force at the pile tip F_{tip} is equal to the maximum resistance at the pile tip in case of compression.

6.6 The influence of coefficient R_{inter} on the behaviour of the pile-soil interaction

Interface elements are automatically generated along embedded pile elements to model the soil-pile interaction (smooth to rough). Pile roughness is modelled by choosing a strength reduction factor for the interface (R_{inter}). This reduction factor relates the interface strength (wall friction and cohesion) to the soil strength (friction angle and cohesion). It should be taken into account that the skin resistance is the shear resistance of the interface in the axial direction of the pile, which is determined based on a “slide” between the pile and the soil. In PLAXIS, the skin resistance directly relates to the strength of the surrounding soil by the interface strength reduction factor R_{inter} , which is set up in the material data set of the soil. Therefore, R_{inter} reduces the soil shear strength parameters c and \emptyset into interface strength parameters c_{inter} and \emptyset_{inter} based on equations:

$$c_{inter} = R_{inter}c \quad (6.6)$$

$$\tan\emptyset_{inter} = R_{inter}\tan\emptyset \quad (6.7)$$

Where:

c_{inter} : cohesion of the embedded interface which is linked to the strength properties of the adjacent soil.

\emptyset_{inter} : friction angle (wall friction) of the embedded interface which is linked to the strength properties of the adjacent soil.

Consequently, R_{inter} can be used to control the “slide” between the pile and the soil in the axial direction of the pile. In other words, the value of R_{inter} gives an influence on the relative displacement between the pile and the soil when the pile is subjected to axial loading in s-direction (see Fig. 6.4). Dao (2011) pointed out that embedded pile option in PLAXIS 3D does not consider slide of the soil at the skin of pile in horizontal directions. Therefore, it may not give reliable results for laterally loaded piles having

smooth interaction surfaces. Thus, the nature of pile surface (rough or smooth) could play an essential role in the performance of laterally loaded piles simulated by embedded pile feature. However, it is not clear whether the embedded pile is suitable for modelling the response of "rough or smooth" piles subjected to lateral soil movement, which is the main objective of this study.

Table 6.1 presents some values proposed by Waterman (2006) for the value of R_{inter} .

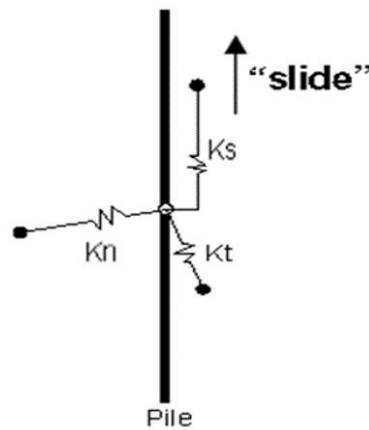


Fig. 6.4 Node model for the pile-soil interaction (Dao, 2011)

Table 6.1 Values for R_{inter} proposed by Waterman (2006)

Interaction type	R_{inter}
Sand / Steel	0.6 – 0.7
Clay / Steel	0.5
Sand / concrete	0.8 – 1.0
Clay / concrete	0.7 -1.0
Soil / Geogrid (interface may not be required)	1.0
Soil / Geotextile (foil, textile)	0.5 – 0.9

6.7 Skin resistance and base resistance (pile bearing capacity)

The total pile bearing capacity is given in terms of skin and base resistances as Eq. (6.8) (PLAXIS 3D Reference manual, 2013):

$$N_{\text{pile}} = B_{\text{max}} + \frac{1}{2} L_p (T_{\text{top,max}} + T_{\text{bot,max}}) \quad (6.8)$$

Where:

N_{pile} : pile bearing capacity (kN)

B_{max} : maximum base (foot) resistance (kN)

L_p : pile length (m)

$T_{\text{top,max}}$ and $T_{\text{bot,max}}$: maximum skin resistance (bearing capacity due to shaft friction) at pile head and pile tip, respectively, (kN/m).

In the current study, Meyerhof's method was followed to calculate the skin resistance and base resistance (Das, 2005).

The skin resistance (shaft friction capacity) (Q_f) of a pile embedded in a homogeneous sand is:

$$Q_f = A_f q_f \quad 6.9$$

Where:

$A_f = P_{\text{pile}} L_p$; effective surface area of the pile shaft, m^2 .

P_{pile} : Perimeter of pile cross-section, m.

q_f : Unit friction capacity at any depth z , kN/m^2 .

The unit friction resistance (capacity) q_f is:

$$q_f = K\sigma \tan\phi_{inter} \quad 6.10$$

Where:

K: lateral earth pressure coefficient.

σ : average vertical effective stress in a given layer, kN/m².

The base resistance (end bearing capacity) (Q_p) of the pile can be expressed as:

$$Q_p = A_p q_p \quad 6.11$$

Where:

A_p : is the area of pile tip.

q_p : unit base resistance (tip-bearing capacity), kN/m²

In sand soil, the unit base resistance q_p is:

$$q_p = q' N_q \quad 6.12$$

Where:

q' : is the effective stress at the level of pile tip.

N_q : is the bearing capacity factor, which is a function of soil friction angle and type of pile installation.

6.8 Finite element simulation of test results

In the following sections, three-dimensional analysis using PLAXIS 3D software was carried out to back analyse the model tests data. The numerical results are compared with the experimental measurements to test the ability of PLAXIS 3D program to predict the response of single batter piles and pile groups subjected to lateral soil movements. The results from PLAXIS 3D analyses are presented together with the results from the experimental tests, in terms of the five profiles, namely: 1) bending moment; 2) shear force; 3) soil reaction; 4) pile rotation and 5) pile deflection.

6.8.1 Material modelling

The accuracy of the FEM simulation depends significantly on the selection of appropriate material models to represent the soil, structure and soil-structure interaction. In the following section, the soil models, pile models and their interactions through interface elements are described.

6.8.1.1 Mohr-Coulomb model for sand soil

The Mohr-Coulomb model is widely used in finite element analysis of geotechnical engineering to simulate the non-linear behaviour of soil, due to its simplicity, sufficient accuracy, and reasonable number of model parameters (Ekici, 2013). Although it is well known that, the more advanced soil constitutive models can capture the nonlinear stress-strain behaviour of soils more accurately, they also require significant number of material model parameters to be input. For this reason, the Mohr-Coulomb model was selected for simulating the sand soil behaviour during passive loading of batter pile in this research study.

The Mohr-Coulomb model requires five parameters that are well known in most practical situations. The other two parameters, in addition to c , ϕ and ψ , are Young's modulus E and Poisson's ratio ν , based on Hooke's law for isotropic elastic material behaviour. In this study, the main soil parameters were determined from the laboratory test results or empirical equations. For the passive pile loading tests in this study, the soil loading condition is considered drained.

6.8.1.2 Sand properties

In the numerical studies, the following assumptions have been made regarding the input parameters of sand soil:

- Values of soil friction angle, \emptyset , were primarily selected based on laboratory direct shear test measurements for the sand material. The value of cohesion (c) for cohesionless soil ($c = 0$), is advised to use a small value of cohesion $c > 0.2$ kPa to avoid unrealistic results (PLAXIS 3D Material Models Manual, 2013). Therefore, a value of $c = 1.0$ kPa was adopted for sand in this study.
- The value of Strength Reduction Factor, R_{inter} , was estimated according to the Table 6.1.
- The Poisson's ratio ν_s was assumed to be 0.3 (Guo and Ghee, 2010) and unit weight of sand γ_s was based on average unit weight obtained from laboratory density testing.
- The selection of the dilatancy angle, ψ was based on Eq.(6.13), an approximation presented in the PLAXIS Materials Manual for granular soils (PLAXIS 3D, 2013):

$$\psi \approx \begin{cases} \emptyset - 30^\circ, & \text{for } \emptyset \geq 30^\circ \\ 0^\circ, & \text{for } \emptyset < 30^\circ \end{cases} \quad (6.13)$$

- The sand Young's modulus is determined by Eq.(6.14) which is suggested by Poulos (1989). The same equation was used by Chen (1994) for the same purpose.

$$E_s = m \cdot z \quad (6.14)$$

Where:

E_s : Young's modulus of sand soil in MPa,

m : is a proportional factor in MN/m³,

z : is the depth in m.

The proposed values of m for different densities of sand considering the installation

method of piles is illustrated in Table 6.2.

Table 6.2 Values of proportional factor (m), (Poulos, 1989)

Pile type	Sand classification	m (MN/m ³)
Driven pile	Loose	1.5
	Medium-dense	4.0
	Very dense	8.0
Bored pile	Loose	1.0
	Medium-dense	3.0
	Very dense	6.0

6.8.1.3 Modelling of pile and interface

In this study, the batter piles were modelled using the embedded pile option in PLAXIS 3D. As mentioned earlier, the embedded pile consists of beam elements with special interface elements that provide the interaction between the pile and the surrounding soil (pile bearing capacity).

6.8.1.4 Parameters of the embedded pile

In PLAXIS 3D, the embedded pile is defined in separate material data sets: the parameters for the beam and the parameters for the pile-soil interaction. Because of being considered as isotropic elastic pile, the pile is set up in linear elastic properties of a beam element which is presented in parameters of the Young Modulus E_p and the unit weight (γ_p) of pile material. Subsequently, geometric properties of the pile are defined in terms of both predefined shapes (Massive circular pile, Massive tube, Massive square pile) and real pile diameter which determines the elastic zone around the pile. Alternatively, a “user defined” type may be used to define the pile shape by means of pile’s cross section, (A_p) and Moments of inertia, (I_p). On the other hand, the properties of the pile-soil interaction are defined by skin resistance and base resistance (pile bearing capacity). These values are considered as input data rather than the result of Finite element calculation and can be calculated theoretically (see section 6.7).

6.8.2 Numerical analysis for standard test RSF16,0°

Three-dimension numerical analysis for model test RSF16,0° is detailed below, which include the following: three-dimension numerical geometry, boundary conditions, mesh size, element types and input parameters for soil and pile that used to analyse the standard test (RSF16, 0°) as well as numerical results.

6.8.2.1 3D Geometry and Boundary Conditions

For the numerical analysis of model tests, the geometry and boundary conditions corresponded to the dimensions and conditions of the testing box (shear box) that was used in the experimental tests. Subsequently, the model geometry can be created with dimensions of 60 mm in both x and y directions, and 70 mm in z direction. The soil is assumed to have two layers (stable and moving), and same material (sand) was used for both. The top boundary of the soil layer is at $z = 0$, and the bottom boundary of the soil layer is at $z = 70$ mm. Once the soil block is identified, the soil properties can be assigned to it. The soil is modelled with the Mohr-Coulomb model as mentioned previously. The next step is to create the structure phase, where the pile is inserted into the soil mass through the “create embedded pile” function. The embedded pile is located at the (30, 30, 0) of the coordinate system with the pile head at the ground surface. The embedded pile has 300 mm long with an outer diameter $D = 16$ mm and a wall thickness $t = 1.2$ mm.

Boundary surface fixities of the model were determined to simulate the behaviour of a laterally moving soil above a stable ground. For this purpose, standard surface boundary conditions of PLAXIS 3D (in all direction) were applied to the stable soil. The bottom surface of the geometry model was fixed in all three directions, x, y and z (Fig. 6.5). Also, both faces parallel to the yz-plane were fixed in the x direction; the other faces parallel to the xz-plane were fixed in the y direction, whereas surface boundaries of moving ground were redefined with surface prescribed displacement property. Movement in y direction is prevented and z direction is allowed for all surfaces. In x direction, an amount of uniformly distributed prescribed displacement (U_x) was defined on the left and right-side surface of the model. For ground surface, the model boundary is considered free in all directions (Table 6.3).

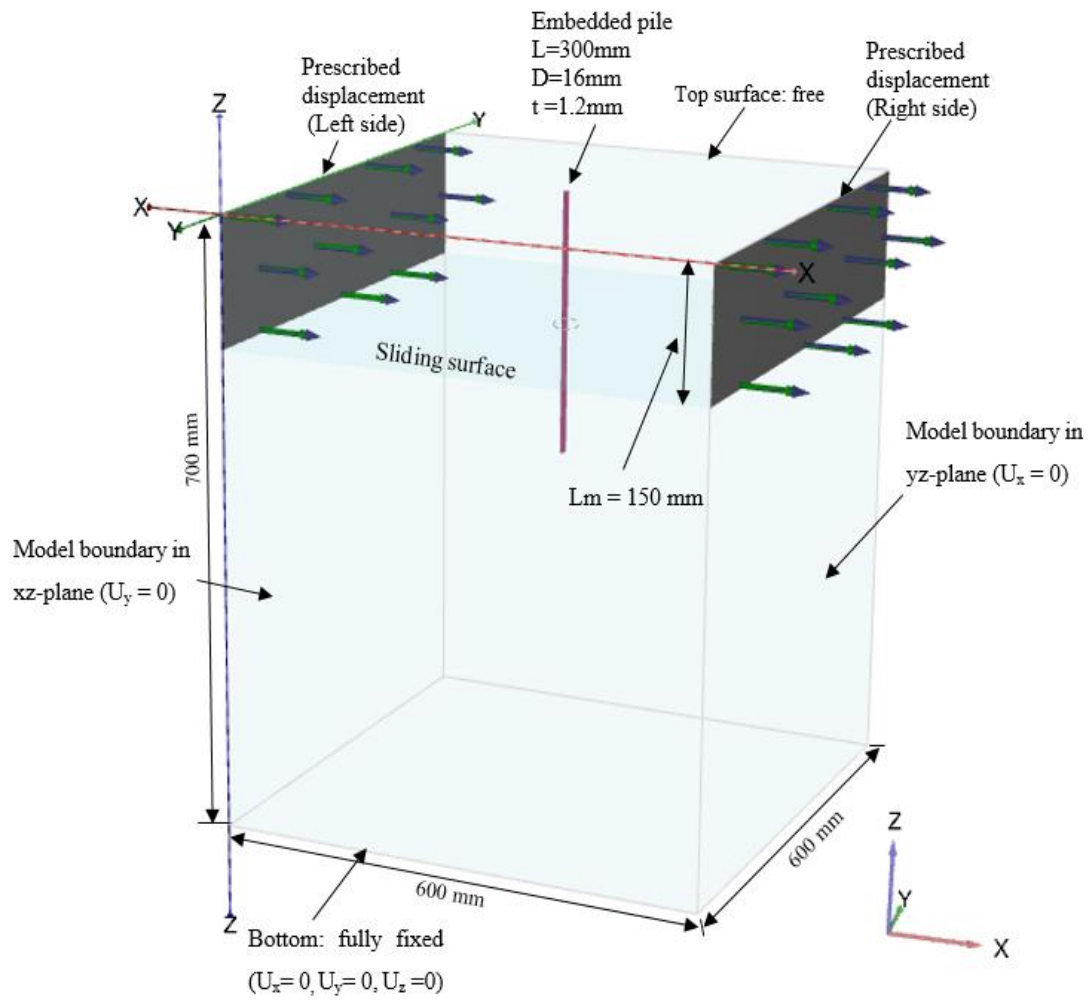


Fig. 6.5 3D geometry and boundary conditions for standard test

Table 6.3 Surface boundary fixities for moving ground

Surface		x direction	y direction	z direction
Moving ground	Front side	Free	Free	Free
	Rear side	Free	Free	Free
	Right side	Prescribed displacement (U_x)	Free	Free
	Left side	Prescribed displacement (U_x)	Free	Free

6.8.2.2 Summary of the input parameters used to analyse standard test

Table 6.4 and 6.5 show a summary of the input parameters for soil and pile that used to analyse the standard test (RSF16, 0). These parameters were used in all PLAXIS 3D analyses performed in this chapter, unless stated otherwise. It is worth mentioning that R_{inter} value (i.e., 0.95) has been adopted in the present study based on a previous research conducted by Al-abboodi (2017).

Table 6.4 Sand soil properties in PLAXIS 3D

Parameter		Value	Unit
Material model		Mohr-Coulomb	-
Drainage type		Drained	-
Unit weight	γ_s	15.2	kN/m ³
Young's modulus (standard)	E_s	1200	kN/m ²
Friction angle	ϕ	38	deg.
Dilatancy angle	ψ	8	deg.
Cohesion	c	1	kN/m ²
Poisson's ratio	ν_s	0.3	-
Strength reduction factor of the interface, sand/rough pile	R_{inter}	0.95	-
Lateral earth pressure coefficient at rest	K_o	0.38	-

Table 6.5 Pile properties in PLAXIS 3D

Parameter		Value	Unit
Material type		Aluminium	-
Predefined pile type		Circular tube	-
Diameter	D	16×10^{-3}	m
Wall thickness	t	1.2×10^{-3}	m
Pile area	A_p	5.579×10^{-5}	m ²
Moment of inertia	I_p	1.538×10^{-8}	m ⁴
Young's modulus	E_p	65×10^6	kN/m ²
Unit weight	γ_p	27.5	kN/m ³
Max. skin resistance at the pile top	$T_{top, max}$	0	kN/m
Max. skin resistance at the pile bottom	$T_{bot, max}$	0.9×10^{-1}	kN/m
Max. base resistance	B_{max}	0.1	kN

6.8.2.3 Mesh generation

Once the geometry modelling process is complete, calculations are proceeded which consist of the generation of meshes and definition of the construction stages. The defined geometry must be divided into finite elements in order to perform a FEM calculation. A mesh is a composition of finite elements that can be created in mesh mode. In PLAXIS 3D, a fully automatic generation of finite elements meshes is allowed. A 10–node tetrahedral element is used to model the soil which is available in PLAXIS 3D. This element is formulated in three-dimensional space with three degrees of freedom per node. This type of elements provides the second order interpolation of displacements. To calculate the numerical integration over the element volume, PLAXIS program uses the Gaussian integration method with 4 sample points. The numbers and positions of nodes and the integration points in such elements are shown in Fig 6.6.

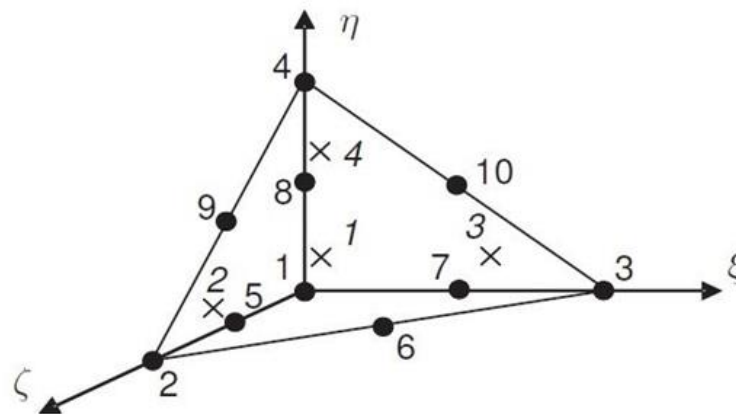


Fig. 6.6 Typical 3D soil element (10-Node Tetrahedrons) used in the model
(PLAXIS 3D Reference Manual, 2013)

6.8.2.4 Calculation process

A calculation process in PLAXIS is divided into calculation phases. In the first calculation phase, the initial stress field for the initial geometry configuration is calculated using k_0 procedure calculation type. After this initial phase, the second phase was implemented by activating the embedded batter pile. After that, the prescribed soil displacement is applied. The PLAXIS calculation phases were summarized as in Table 6.6.

Table 6.6 Calculation phases

Phase	Analysis type	Elements	Activated	Value
Initial	K ₀	Surrounding soil	✓	-
		Left/Right prescribed displacements	✗	-
		Embedded pile	✗	-
1	Plastic drained	Surrounding soil	✓	-
		Left/Right prescribed displacements	✓	U _x = 20mm
		Embedded pile	✓	-

6.8.2.5 Evaluation of Mesh Generation

In PLAXIS 3D, the mesh coarseness provides a significant influence on the calculation results. Therefore, before systematically investigating the factors affecting the pile-soil interaction behaviour, mesh generation effect on the computational results was studied as it is necessary in order to establish correct model of the problem. Typically, meshes should be generated fine enough to obtain accurate results and coarse enough to avoid excessive amount of calculation times. PLAXIS 3D have five standard finite element mesh generation options. These are very coarse, coarse, medium, fine and very fine meshes. Other than these standard options, desired amount of mesh fineness and local refinement for a specific volume or structural object can be provided by changing the fineness factor that is defined for all geometric entries.

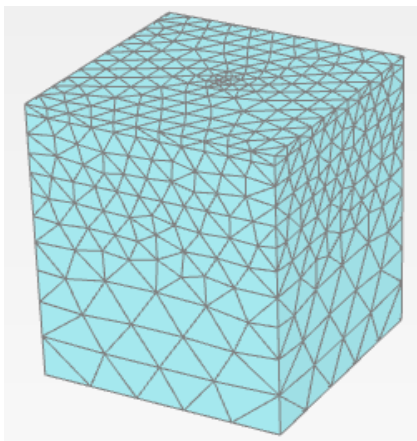
Standard mesh generation alternatives were investigated in the next section. Optimum mesh elements were decided by studying their effects on deformations and structural forces for pile at U_x = 20 mm. Boundary size and surface fixity conditions determined in section 6.8.2.1 were used in the analyses. In addition, same material properties were assigned to the models for moving soil, stable soil and the pile (Table 6.4 and 6.5). Fig. 6.5 shows the model illustration of embedded pile and soil for mesh evaluation analyses.

6.8.2.6 Effect of mesh density

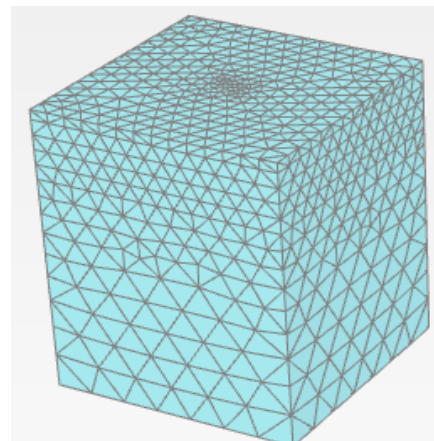
Four mesh densities were created to study the effect of the mesh density on the pile response. The meshes details are:

- Very coarse mesh, in Fig. 6.7(a): 5720 elements and 8810 nodes,
- Coarse mesh, in Fig. 6.7(b): 10854 elements and 16354 nodes,
- Medium mesh, in Fig. 6.7(c): 36209 elements and 51938 nodes,
- Fine mesh, in Fig. 6.7(d): 49701 elements and 70650 nodes.

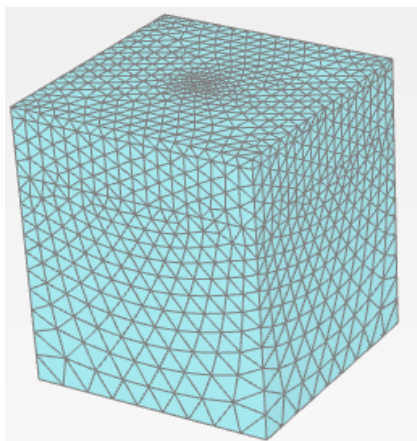
The results of this investigation for different mesh density are summarised in Table 6.7. It was observed that calculation time of different mesh density is highly variable. It is absolute that calculation time drastically increases from coarse meshes to fine meshes. In mesh evaluation study, very coarse and coarse mesh analyses lasted around 5-15 minutes, medium meshes around 80 minutes, fine mesh around 170 minutes for these indicated material types and conditions.



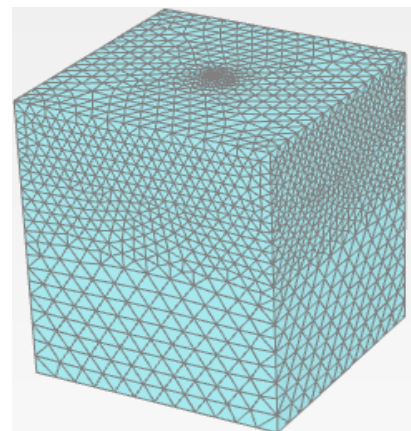
(a) Very coarse mesh



(b) Coarse mesh



(c) Medium mesh



(d) Fine mesh

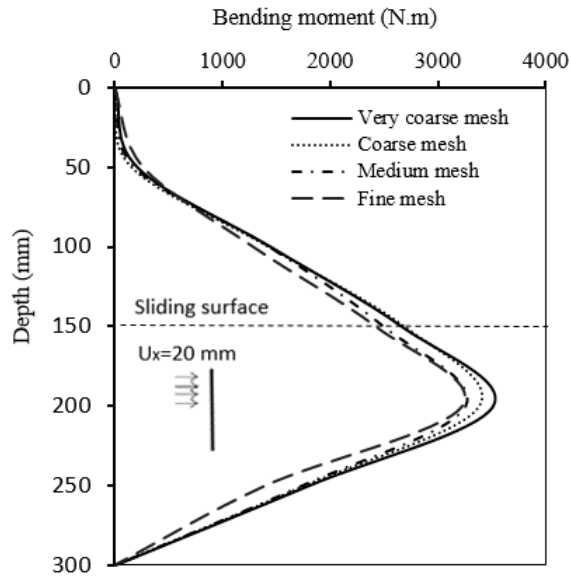
Fig. 6.7 Different densities of mesh coarseness generated in PAXIS 3D

Table 6.7 Results for different densities of mesh generation

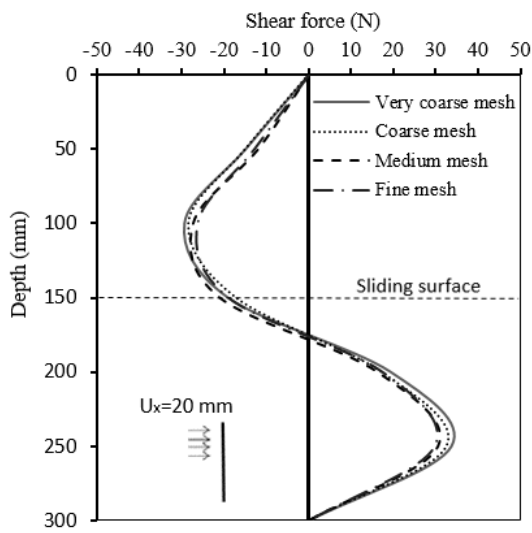
Mesh fineness	Pile Deflection at ground surface (mm)	Maximum bending moment in the pile (N.mm)	Maximum shear force in the pile (N)	Running time (minute)
Very coarse	8.02	3510	34.21	5
Coarse	8.46	3387	31.76	15
Medium	9.79	3251	30.35	80
Fine	9.92	3243	30.15	170

Deformations and structural forces of the pile were compared for implemented mesh generation densities. In analyses, pile deflection at ground surface, bending moment and shear force profiles through pile length were almost identical but only their maximum values were different, as shown in Fig. 6.8 (a, b and c). Pile head deflection, because of the prescribed soil displacement, was observed to increase generally from very coarse meshes to fine meshes. However, there is no significant variation in values. In addition, Maximum bending moment (M_{max}) and shear force (F_{max}) in the pile decreased from coarse to fine meshes. Maximum bending moments differ up to 9%, maximum shear forces differ up to 14% from very coarse mesh to fine mesh generation.

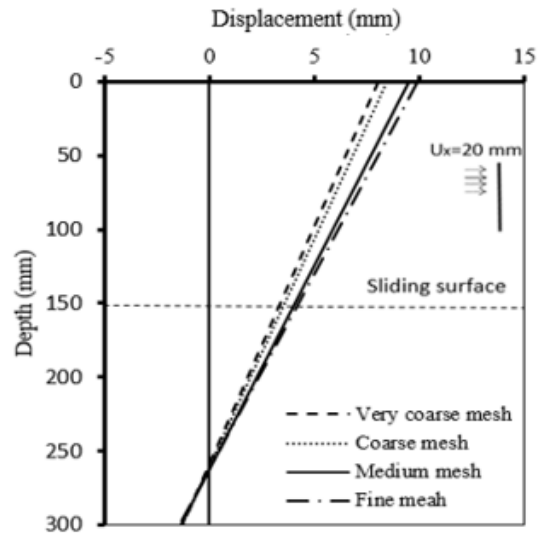
In conclusion, it is determined that medium mesh generation has sufficient degree of fineness and it gives enough numerical accuracy for the scope of parametric analyses. Displacement and structural forces of pile generally differ less than 2% with medium mesh generation and fine mesh generation. The comparison shows that the medium mesh requires less solution time and generates a smaller file size, while it has a similar degree of accuracy to that of the denser mesh. For this reason, the medium mesh could be selected as optimum mesh generation element and it was adopted for all later models



(a) Bending moment



(b) Shear force profile



(c) Pile deflection

Fig. 6.8 The effect of mesh density on the pile response

6.8.3 Numerical results for standard test RSF16,0°

The numerical and the measured results for the "standard" single vertical pile test (RSF16, 0°) are presented in Fig. 6.9 and Fig. 6.10. Fig. 6.9 (a) shows the bending moment profiles at two different soil surface displacements, namely $U_x = 10$ mm and $U_x = 30$ mm. The predicted profile agrees fairly well with that measured for $U_x = 30$ mm, but the theory overestimates the maximum bending moment for $U_x = 10$ mm by about 16 % (against the measured), although the distribution shape and the position of the maximum is very well predicted. Fig. 6.9 (b) plots the predicted and the measured maximum bending moments against the soil displacement (U_x). It shows that the theory tends to overestimate the measured value with an increasing soil surface displacement up to a value of about 17 mm and thereafter the theory underestimates the maximum moment. The largest overestimation and underestimation of maximum bending moment are about 16 % and 9 % (against the measured), respectively.

The predicted shear force, soil reaction, pile inclination angle and the pile deflection are shown in Fig. 6.10, together with those obtained from model tests. The predicted shear force and the soil reaction are seen to be in good agreement with the measured ones. On the other hand, the pile inclination angle and the pile deflection profiles are seen to be predicted fairly well for $U_x = 10$ mm, but are overestimated for $U_x = 30$ mm.

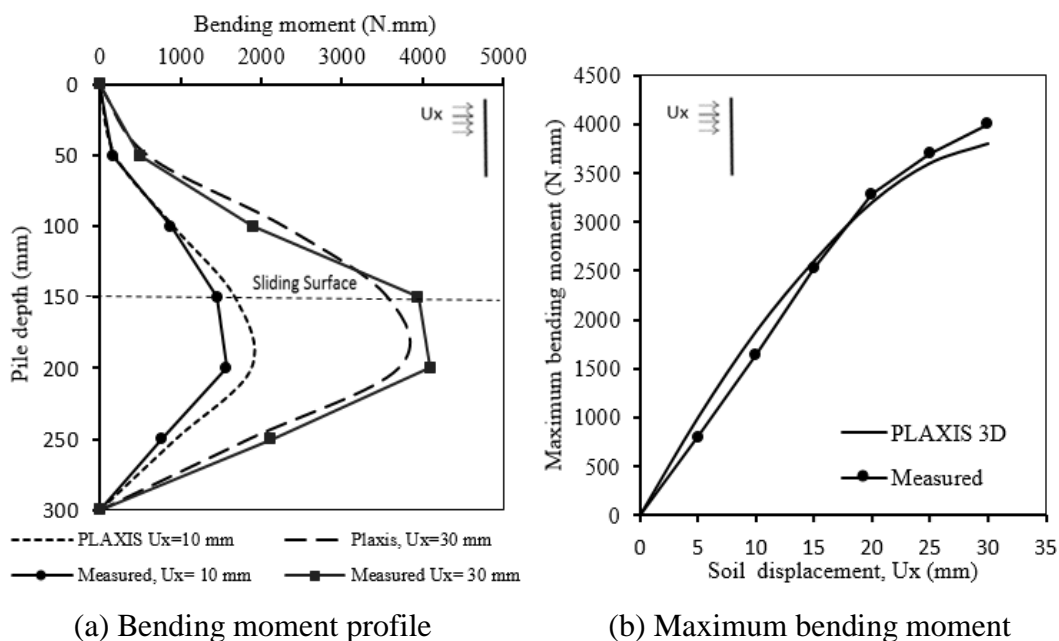
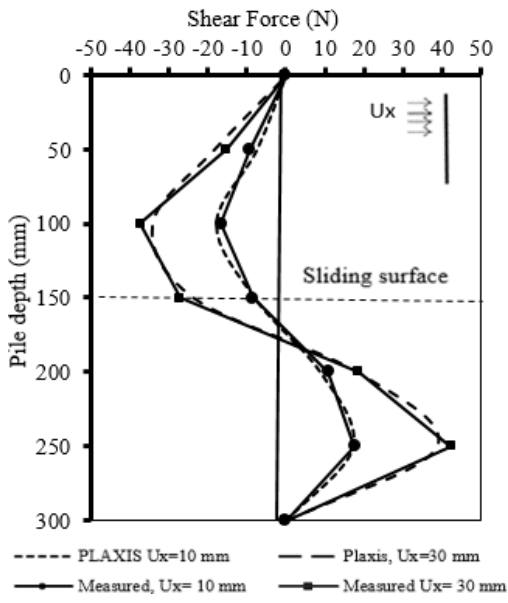
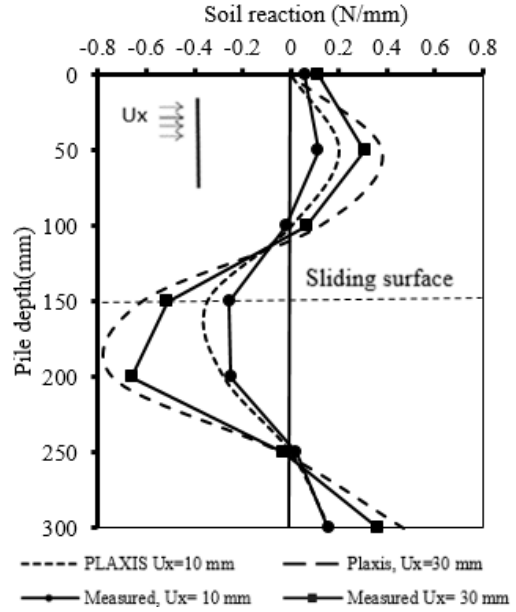


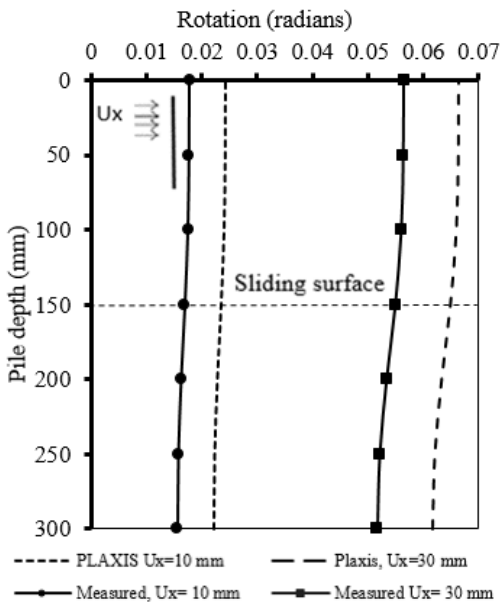
Fig. 6.9 Predicted and measured bending moments for the standard single vertical pile test (RSF16, 0°)



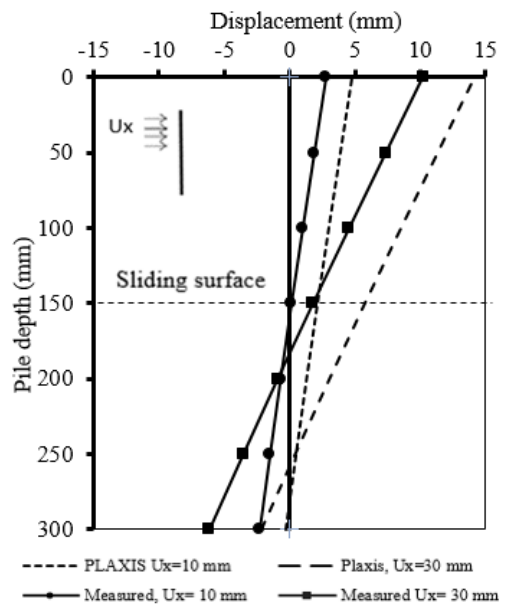
(a) Shear force profile



(b) Soil reaction profile



(c) Pile inclination angle profile



(d) Pile deflection profile

Fig. 6.10 Predicted and measured pile responses for the standard test (RSF16, 0°)

6.8.4 Numerical analysis of test RSL16, 0°

A similar 3D numerical analysis was carried out for test (RSL16, 0°). The numerical analysis was performed on the same pile (16 mm in diameter) under the same conditions as that of the standard test (RSF16, 0°), except that the pile head was fixed against rotation and displacement. The input parameters used in the PLAXIS 3D model can be seen in Table 6.4 and 6.5. Fig. 6.11 shows the predicted and the measured bending moment profiles for the fixed head single pile test for two soil surface displacements (i.e. $U_x = 10$ mm and $U_x = 30$ mm). Although the shapes of the predicted and measured profiles are quite similar (including the positions of the maximum positive and negative bending moments), the theory seems to overestimate the maximum negative moments, and either underestimate or overestimate the maximum positive moments, depending on the soil movement value.

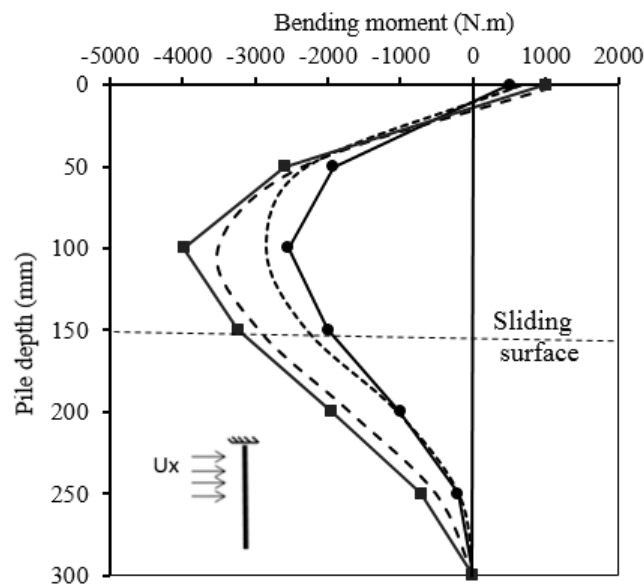


Fig. 6.11 Predicted and measured bending moments for the fixed-headed single vertical pile test

6.8.5 Numerical analysis of test (RSF20, 0°) and (RSF25, 0°)

Two PLAXIS 3D analyses were performed to compare results with the experimental test (RSF20, 0°) and (RSF25, 0°). The predicted bending moment profiles at the soil displacement (U_x) of 30 mm for 20 mm and 25 mm diameter single vertical piles are shown in Fig. 6.12. The theory predicts the maximum moment very well for the 20 mm diameter pile, but apparently underestimates the maximum moment for the 25 mm diameter pile by about 17% (against the measured).

The underestimation for the 25 mm diameter pile may be partly attributed to an increased soil density after the pile installation which was not considered in the numerical prediction as mentioned previously (see section 6.4). According to the experimental results in section 4.6, the M_{max} increases as the sand density increases. Therefore, using a higher value for density (γ_s) for the input into the analysis would certainly increase predicted maximum bending moment.

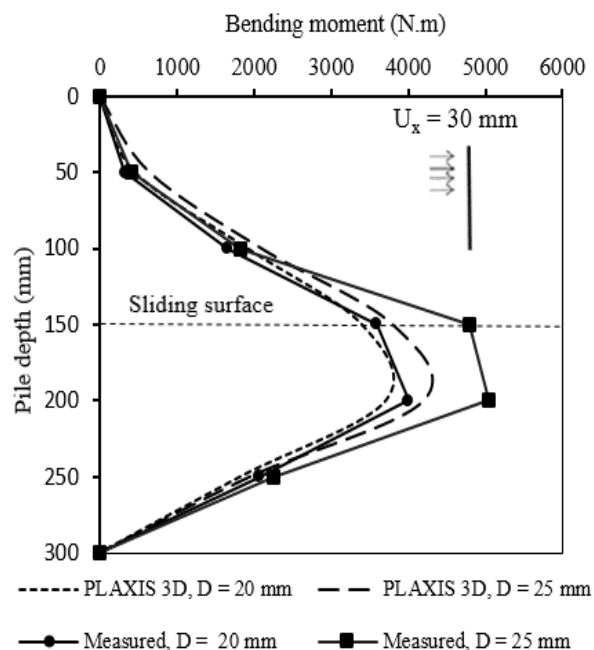


Fig. 6.12 Predicted and measured bending moments for 20 mm and 25 mm diameter single vertical pile tests

6.9 Numerical analysis for the batter pile group tests

To test the capability of PLAXIS in predicting the response of each pile in a group with different batter angles, two numerical analyses were carried out, namely test VVL and BBL. The embedded depth of piles in both cases is 300 mm. The properties of the soil and piles used in the group analysis were the same as those used earlier in the single pile analysis (see Table 6.4 and 6.5). Table 6.8 summarises the input parameters for pile cap used to analyse those tests. The size, geometry and boundary conditions of pile groups models were the same of these used in the standard model (RSF16, 0°). The numerical results are compared with the experimental measurements to evaluate the accuracy and reliability of 3D FEM in simulating batter pile groups subjected to lateral soil movements.

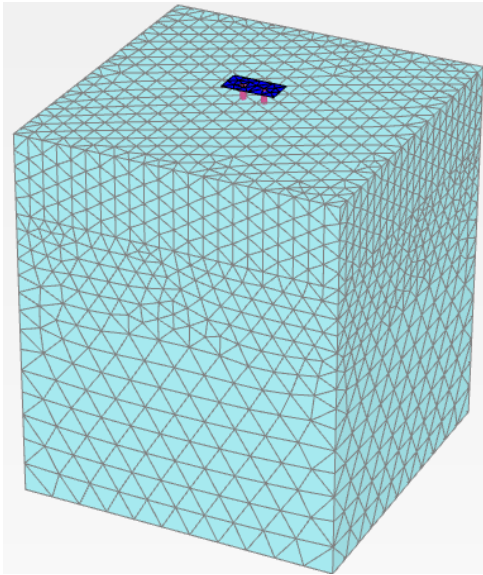
Table 6.8 Summary of pile cap input parameters used in PLAXIS 3D

Parameter		Value	Unit
Material type		Aluminium	-
Dimensions	-	0.2×0.2	m
Thickness	t	25×10^{-3}	m
Young's modulus	E_{cap}	65×10^6	kN/m ²
Unit weight	γ_{cap}	27.5	kN/m ³

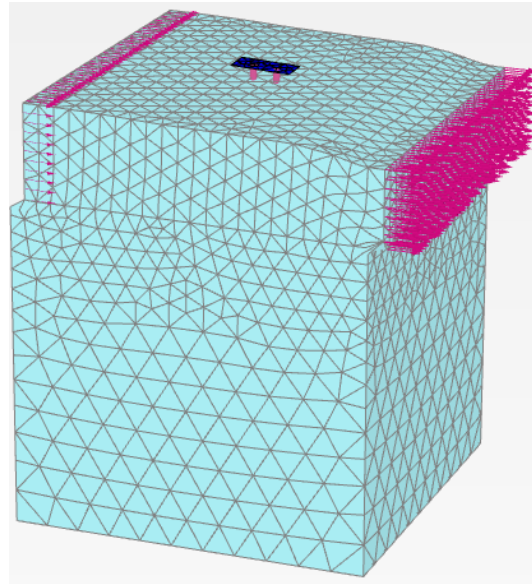
6.9.1 Numerical analysis of test VVL

The PLAXIS 3D analyse was performed to compare with the results obtained from the model test VVL, where $\beta = 0^\circ$ and $s = 3D$ (see Table 5.1). The geometry of the model is shown in Fig. 6.13. The 3D finite element mesh and the typical deformed mesh after FEM analysis are also shown in Fig. 6.14. Fig. 6.15 shows a visualisation of the bending moment, shear force, pile deflection and soil reaction profiles for the front and back piles at the end of FEM analysis at $U_x = 30$ mm. The predicted and the measured results for the VVL test (at $U_x = 30$ mm) are presented in Fig. 6.16.

Generally, the trend of the all predicted profiles computed numerically were in good agreement with those obtained from the model tests. The positions of maximum and

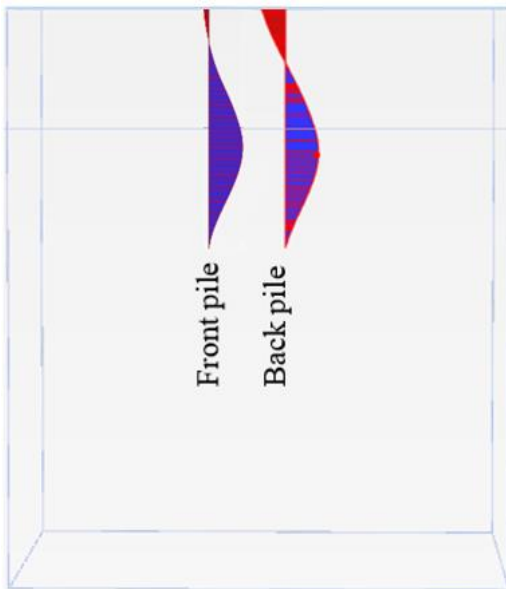


(a) Typical mesh generation of the model

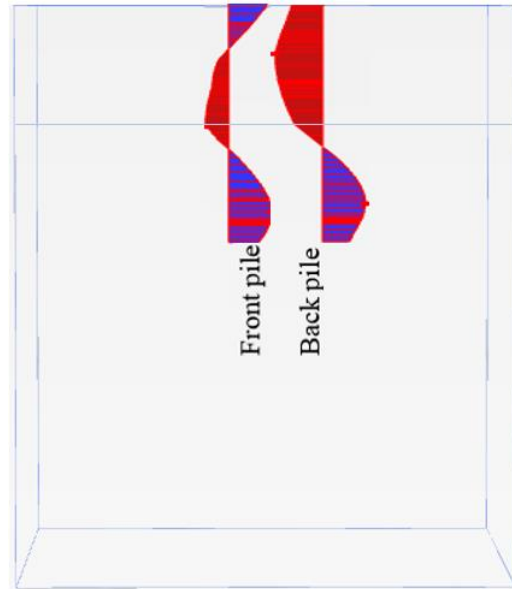


(b) Deformed mesh after analysis

Fig. 6.14 PLAXIS 3D mesh before and after FEM analysis



(a) Bending moment



(b) Shear force

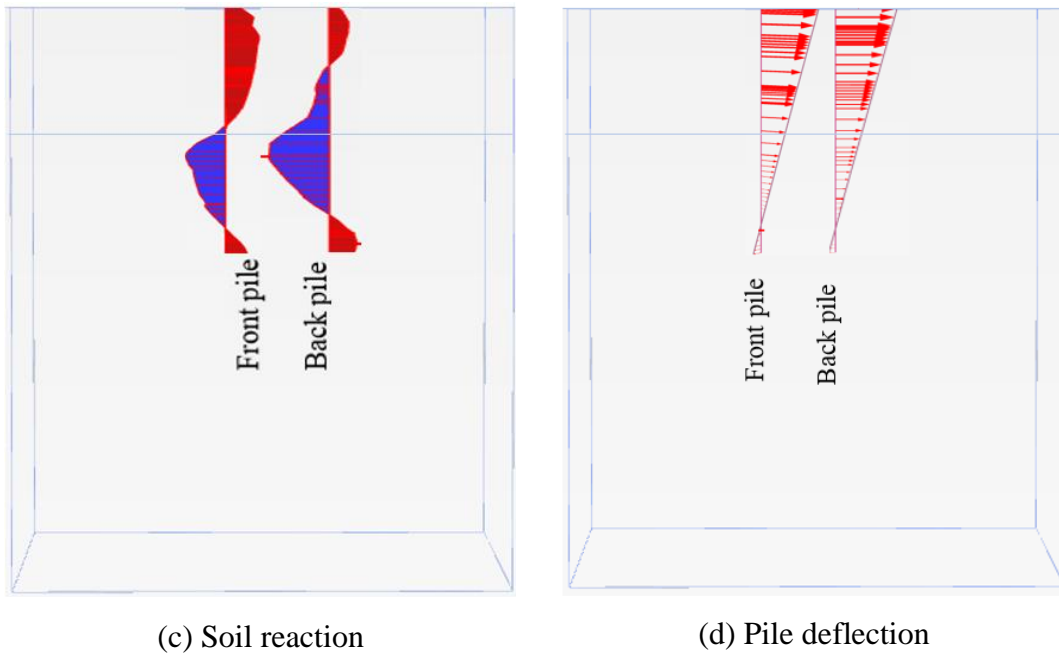
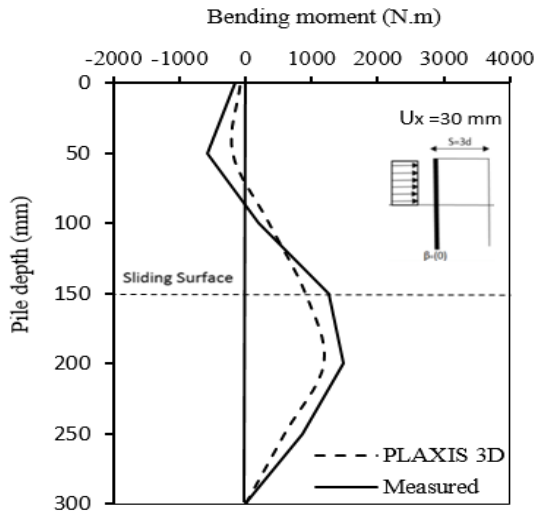
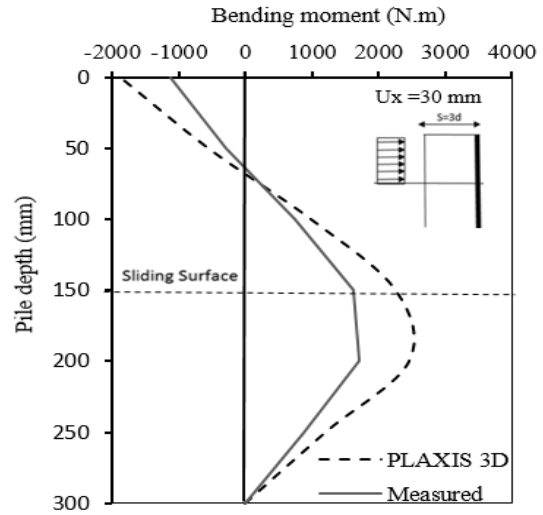


Fig. 6.15 Visualization of pile responses at the end of analysis, $U_x = 30$ mm

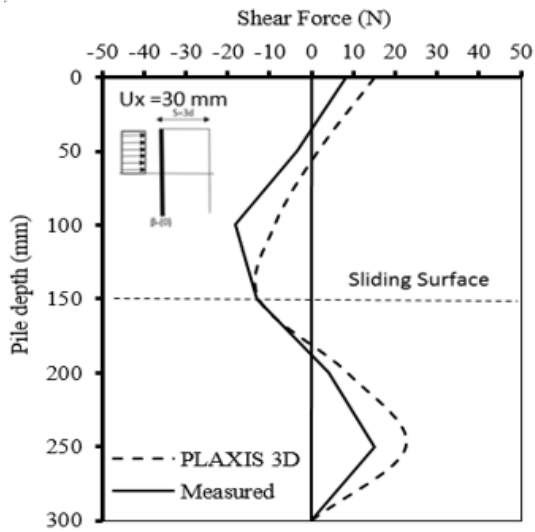
On the other hand, shear force and soil reaction distributions of the front and back piles were observed to be well predicted by PLAXIS. However, numerical results of shear force and soil reaction were, generally, noticed to be overestimated compared to shear force and soil reaction values obtained from the experimental results. The difference was in its maximum at the pile head as well as tip. Fig. 6.16 (c and d) shows 45 % and 40 % difference in the pile head shear force. Similarly, the computed soil reaction at the pile head was 52 % and 43% higher than that obtained from the model test for the front and back pile, respectively. However, the difference was 32 % and 40 % under the sliding surface for the front and back pile respectively (Fig. 6.16(e) and (f)). Fig. 6.16 (g and h) describes the lateral deflections of piles achieved from model tests and PLAXIS analysis. Generally, both cases have resulted in a rigid response of piles with rotation points close to the pile tip. The pile deflection profiles for both piles showed the PLAXIS 3D results are higher than that from the model test for the entire length of the pile. For example, the predicted pile deflection at the soil surface was 6.2 mm, while the measured value was 3.1 mm.



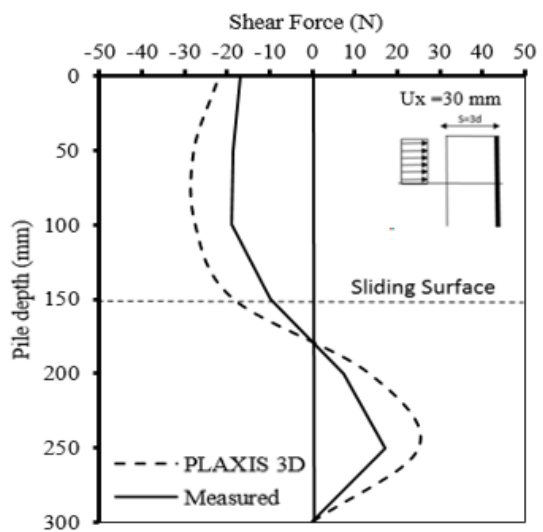
(a) Bending moment profile of front pile



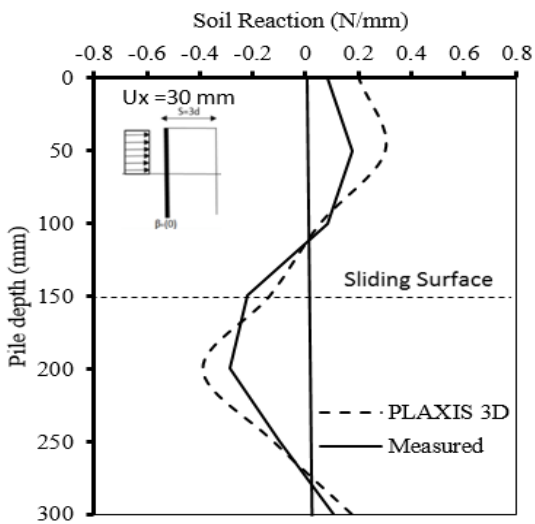
(b) Bending moment profile of back pile



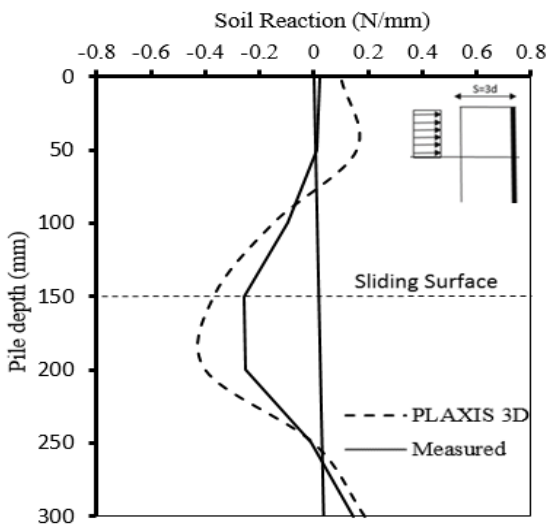
(c) Shear force profile of front pile



(d) Shear force profile of back pile



(e) Soil reaction profile of front pile



(f) Soil reaction profile of back pile

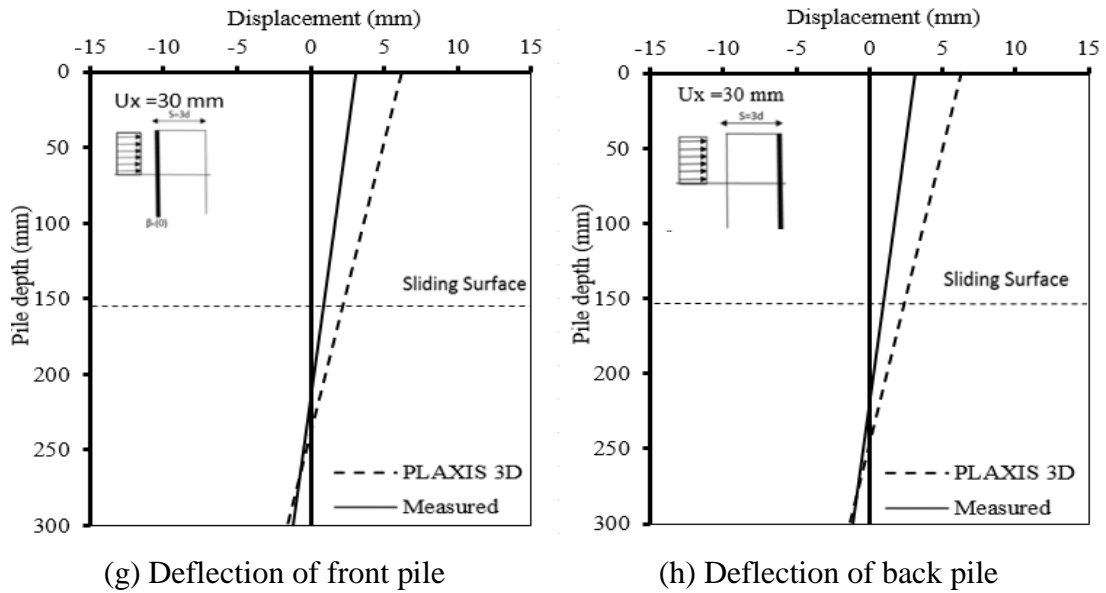


Fig. 6.16 Measured versus predicted piles responses of test VVL at $U_x = 30$ mm, $s=3D$

6.9.2 Numerical analysis of test BBL

After a reasonable comparison of PLAXIS in simulating the behaviour of passively loaded vertical pile group ($s = 3D$), the comparison was extended to batter pile group. As discussed in Chapter 5 (section 5.3.2), changing pile inclination angles of the pile groups have caused significant differences in the response of piles. Therefore, it is important to check the validity of PLAXIS to capture this response under a complex soil-pile interaction system. Thus, additional PLAXIS analyses performed to compare with the experimental test BBL, where $\beta = \pm 10^\circ$ and $s = 3D$. The adopted 3D model for test BBL is shown in Fig. 6.17. Pile responses in terms of bending moment, shear force, soil reaction and lateral displacement are shown in Fig. 6.18.

As shown in Fig. 6.18 (a), the numerical analysis prediction of the shape of bending moment profile was in a good agreement. The position of the maximum positive bending moment at the front and back pile heads were consistent with those measured. However, despite this similarity in moments at pile heads, bending moments calculated along the pile length had lower values for front pile. On the other hand, numerical maximum negative bending moment (M_{-max}) and the maximum positive bending (M_{+max}) for the back pile were 42 % and 28% higher than the measured value, respectively.

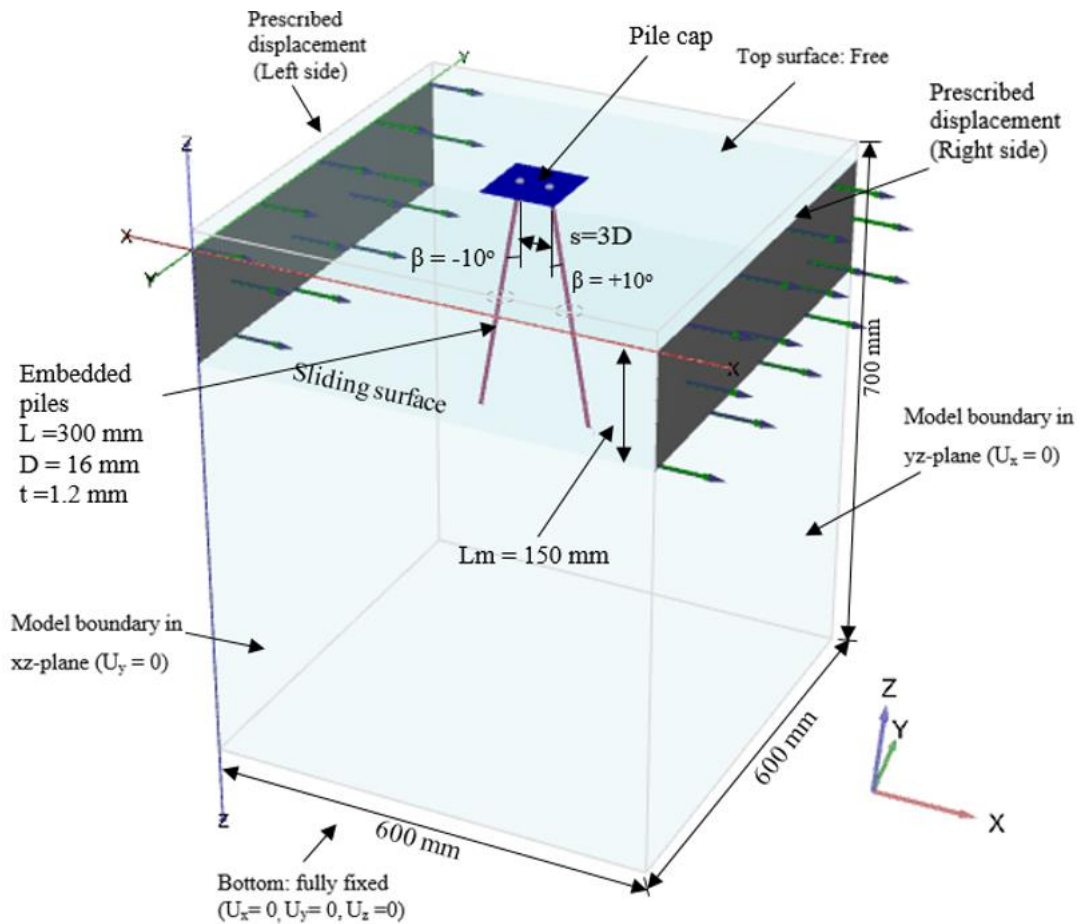
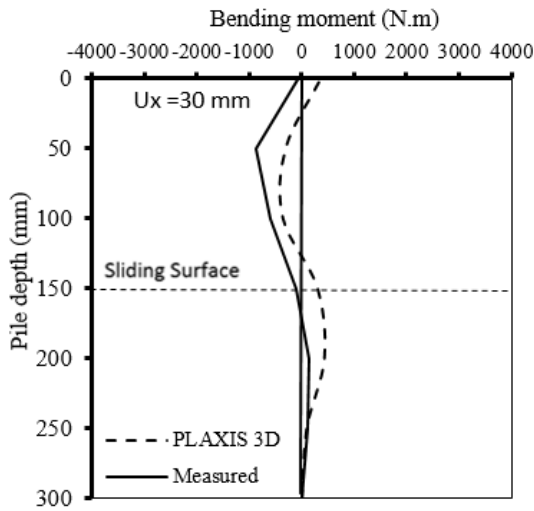


Fig. 6.17 The geometry of a 3D FEM analysis for test BBL, $\beta = \pm 10^\circ$

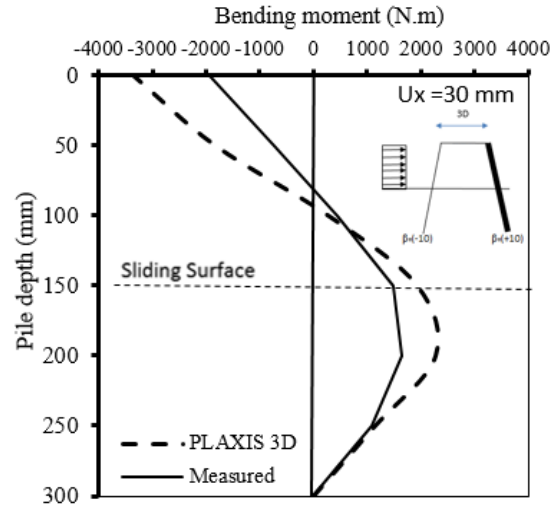
Fig. 6.18 (c and d) indicates that shear force diagrams predicted using PLAXIS have followed the experimental profiles with a tendency of their values to be higher than those measured. In this context, the numerical shear forces were about 33 % and 41 % higher than the measured shear forces at the front and back pile heads respectively.

The shape of soil reaction distributions of both piles was observed to be well predicted compared to those obtained from model tests (Fig. 6.18 e and f). However, soil reaction values predicted in the back pile showed a better match with the experimental data compared to those deduced in the front pile. The latter recorded a difference of 95 % between the two cases lower sliding surface, while the difference was only 13 % in the back pile.

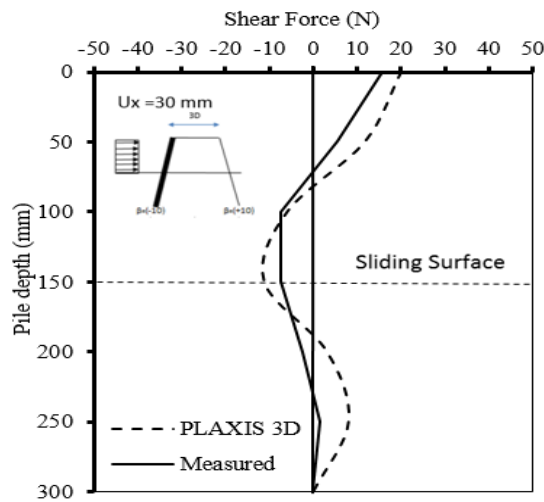
As expected, an overestimation of the predicted lateral pile deflection compared to the test data can be seen in Fig. 6.18 (g and h). The difference in lateral pile head displacement was 95% between the two procedures.



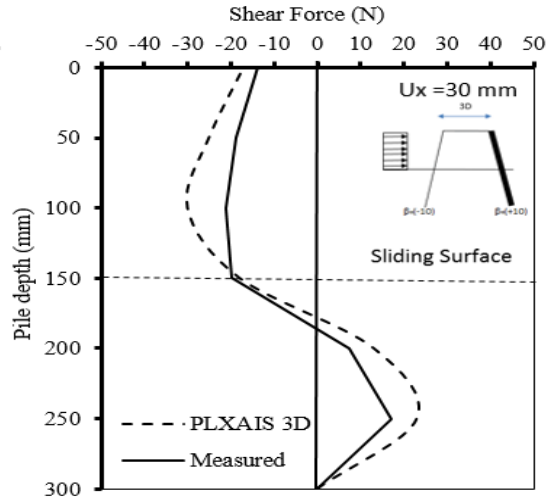
(a) Bending moment profile of front pile



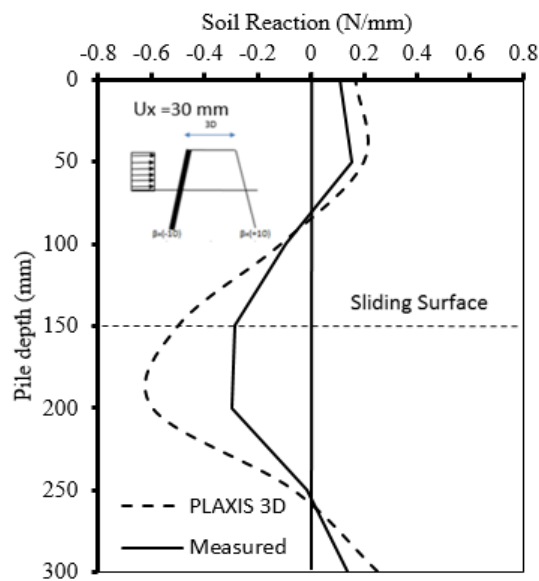
(b) Bending moment profile of back pile



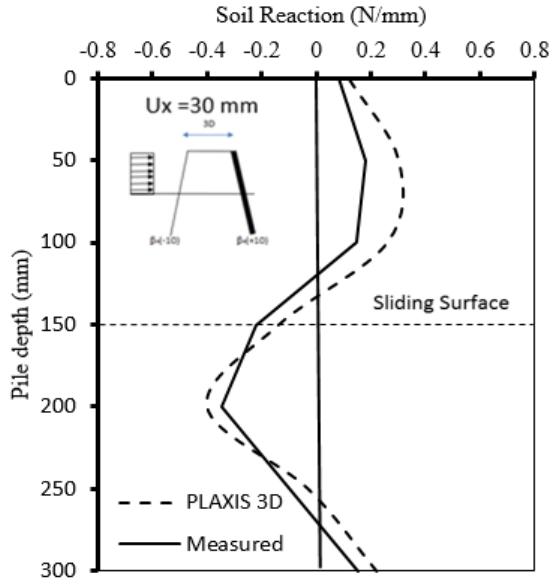
(c) Shear force profile of front pile



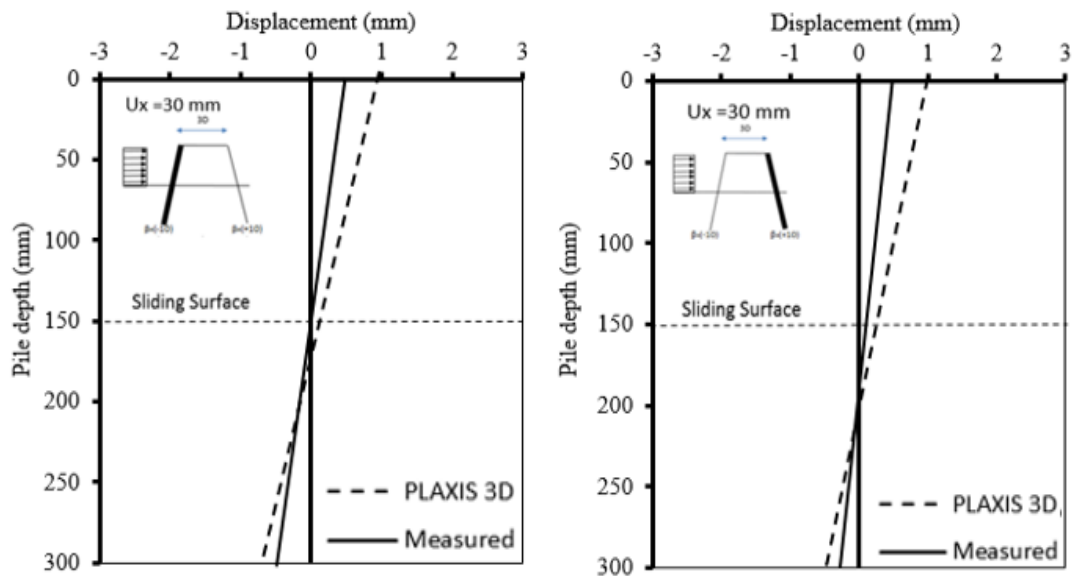
(d) Shear force profile of back pile



(e) Soil reaction profile of front pile



(f) Soil reaction profile of back pile



(g) Deflection of front pile

(h) Deflection of back pile

Fig. 6.18 Measured Vs. predicted piles responses of test BBL ($\beta = \pm 10^\circ$) at $U_x = 30$ mm, $s=3D$

6.10 Parametric studies

Parametric studies were performed to examine the effects of various soil and pile parameters on the passive pile behaviour. The numerical analyses were carried out for standard PLAXIS 3D (shown in Fig. 6.5) and the material properties used were as described in Section 6.8.2.2). The soil parameters varied included the soil elastic modulus E_s , dilatancy angle ψ , friction angle ϕ , and the soil-pile interface R_{inter} , while for the pile, the effect of pile shape was evaluated. The values of these parameters are shown in Table 6.9.

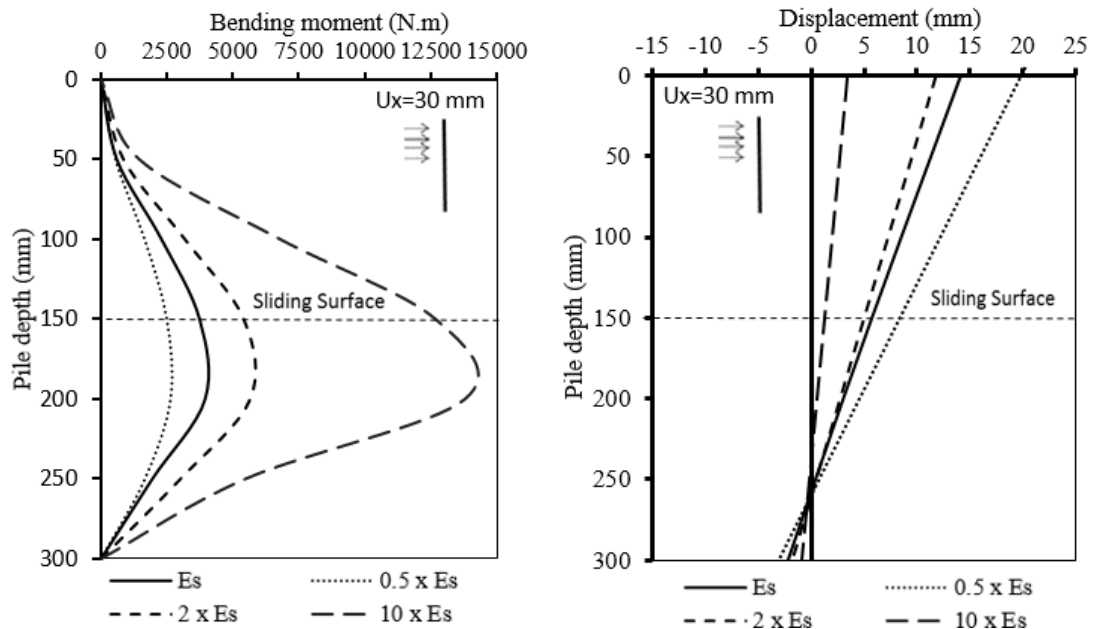
In order to simplify the parametric study, the effect of any parameter is investigated while the other parameters are being fixed, e.g. the influence of elasticity modulus is investigated by changing its value while keeping the values of other parameters constant. The results being presented, mainly, in terms of the bending moment and the pile deflection profiles, at $U_x = 30$ mm.

Table 6.9 Different sand properties used in parametric study

Parameter		Value	Unit
Sand:			
Young's modulus	E_s	$0.5 \times E_s = 600$ $2 \times E_s = 2400$ $10 \times E_s = 12000$	KPa
Friction angle	ϕ	30, 45	deg.
Dilatancy angle	ψ	0, 15	deg.
Strength reduction factor of the interface	R_{inter}	0, 0.5, 1	-
Pile:			
Pile cross-section	-	Square	-

6.10.1 Effect of Young's modulus

To examine the influence of soil elastic modulus on the lateral response of a passive pile, additional analyses were carried out using three values for $E_s = 600$, 2400 and 12000 kPa, respectively. The bending moment and pile deflection profiles for all three cases are plotted in Fig. 6.19. Fig. 6.19 (a) shows that, by increasing the E_s of the standard model ($E_s = 1200$ kPa) to 10 times, the bending moments along the pile increase most notably at a depth of 200 mm. However, the change in Young's modulus value within the range of $0.5 \times E_s$ to $10.0 \times E_s$ did not change the shape of moment profiles. Similar findings were also reported by Ghee (2011) and Al-abboodi (2017) in their finite element analyses. As expected, when the pile is embedded in a stiffer soil ($10 \times E_s$), the deflection of the pile reduces to approximately 84.5 % from that obtained from the least stiff soil ($0.5 \times E_s$). However, the variation of the soil elastic modulus does not affect the depth of the rotation point greatly.



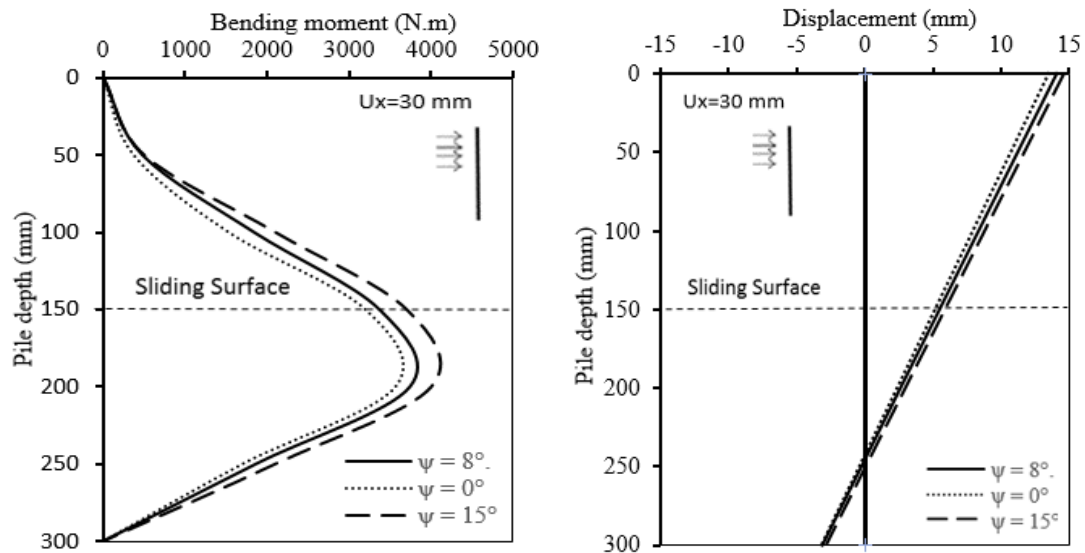
(a) Bending moment profile of pile

(b) Deflection of pile

Fig. 6.19 The effect of Young's modulus on the pile response

6.10.2 Effect of dilatancy angle of sand

Two additional dilatancy angles of $\psi = 0^\circ$ and 15° were investigated for the effect of the dilatancy angle of sand on the lateral response of a passive pile. The computed results, using the standard model with different dilatancy angles of sand, are shown in Fig. 6.20. As shown in Fig. 6.20(a), an increase in ψ , from 0° to 15° , leads to an increase of 15 % on the maximum bending moment. However, the shape of moment profile remained the same. Also, the location of maximum bending moment (M_{\max}) for both values appear to be at a depth of 200 mm. It is also observed that the value of the lateral displacement at the pile head in the case of $\psi = 0^\circ$ is around 10 % less than in the case of $\psi = 15^\circ$. The dilatancy angle has little influence on the M_{\max} and maximum pile deflection. Similar findings were also reported by Ghee (2009) and Shaia (2013) in their finite element analyses.



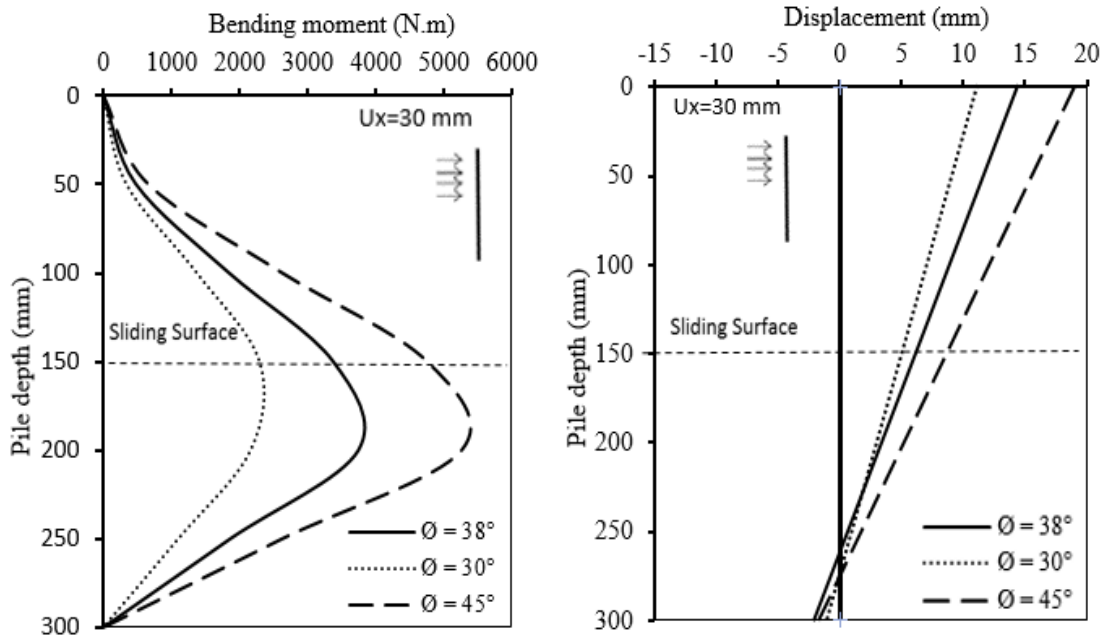
(a) Bending moment profile of pile

(b) Deflection of pile

Fig. 6.20 The effect of dilatancy angle of sand on the pile response

6.10.3 Effect of soil friction angle

To examine the influence of the soil friction angle on the lateral behaviour of passively loaded pile, two analyses were carried out for $\phi = 30^\circ$ and $\phi = 45^\circ$, respectively, in addition to 38° that was used to analysis the standard model (RSF16, 0). As shown in Fig. 6.21(a), increasing ϕ from 30° to 38° leads to an increase of about 60 % in the maximum bending moment. Increasing ϕ to 45° has caused a further increase in maximum bending moment of around 40 % compared to that calculated when $\phi = 38^\circ$. Similar results have been found by Ghee and Guo (2011) in their finite element analyses. The same behaviour was obtained in the pile head deflection but with different increasing rates i.e. 28 % and 35 % respectively, as shown in the Fig. 6.21(b).



(a) Bending moment of pile

(b) Deflection of pile

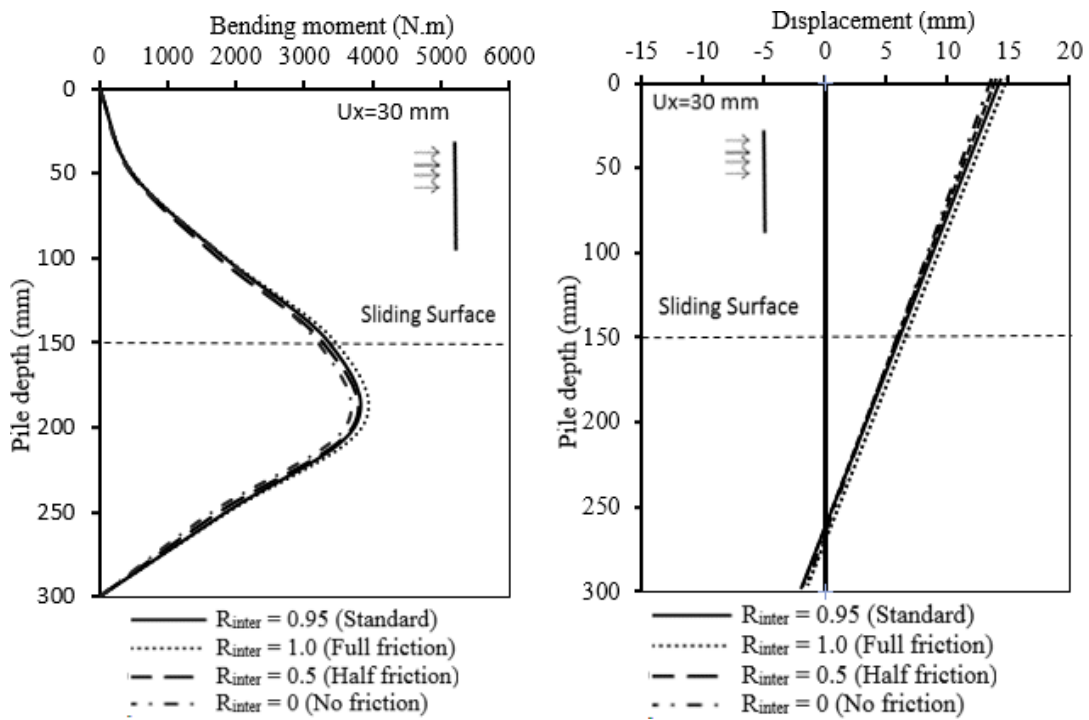
Fig. 6.21 The effect of soil friction angle on the pile response

6.10.4 Effect of strength reduction factor (R_{inter})

To examine the influence of the friction coefficient at the soil-pile interface, R_{inter} was decreased from the value of 1.0 to 0.5 and 0, i.e. representing full friction (rough), half friction and zero friction (smooth), respectively. The results of the analyses in terms of the bending moment and the pile deflection profiles, with different R_{inter} values, are shown in Fig. 6.22.

Regarding the shape of the bending moment profile, as shown in Fig. 6.22(a), the effect of R_{inter} is minimal with three curves almost identical. In other words, there is 3 % difference between zero and full friction, and minimal difference between half and full friction. Besides, the lateral displacement of the pile has not changed much with increasing R_{inter} values. Therefore, it can be concluded that the embedded pile shows a very good performance in modelling piles with “rough” shaft surface and to have an overestimation in modelling piles with “smoother” shaft surfaces, where relative displacement is expected to be high. This is because the embedded pile does not

consider the relative displacement effect ‘slide’, which is used to model pile-soil interaction, in the horizontal directions (see section 6.6). As a result, the upper pile portions almost displaced laterally a similar value of the surrounding soil as if they were bonded together. This is in contrary to reality, where the relative displacement increases as the smoothness of the pile shaft surface increases. Subsequently, this caused the pile lateral deformation to be overestimated. Similar results (using PLAXIS 3D) have also been reported by Dao (2011) using similar interface elements to investigate the behaviour of laterally loaded piles. This may be one of the limitations of PLAXIS.



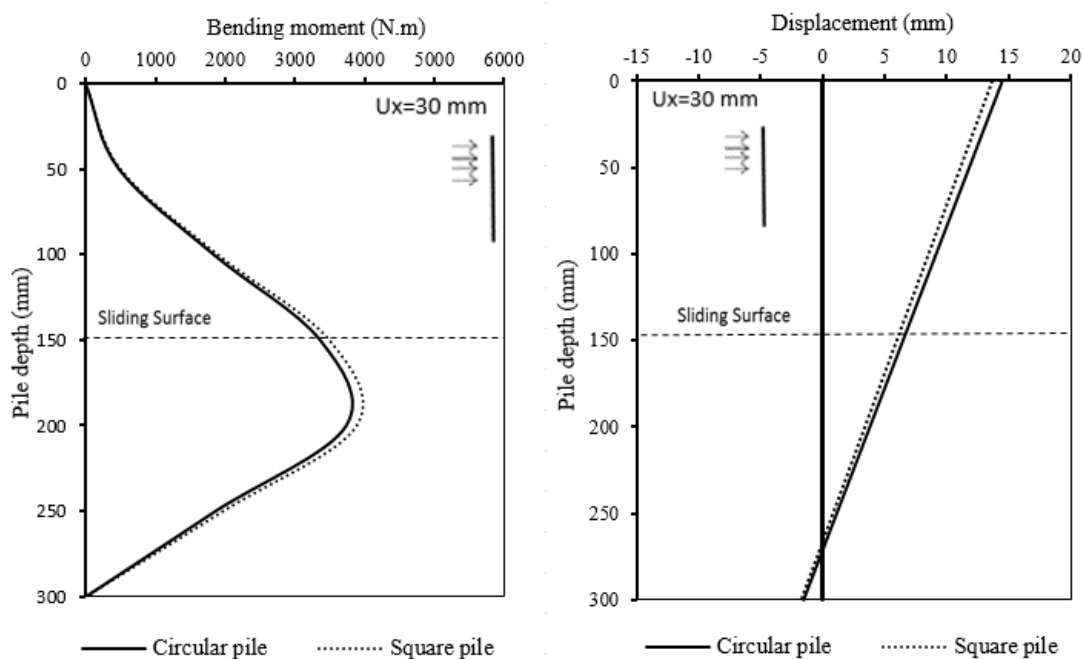
(a) Bending moment of pile

(b) Deflection of pile

Fig. 6.22 Effect of strength reduction factor (R_{inter}) on the pile response

6.10.5 Effect of pile cross-sectional

To investigate the effects of pile shape on the lateral response of a passive pile, a new analysis was performed on a square pile with a width 16 mm and a wall thickness 1.8 mm instead of the circular pile in the standard model RSF16, 0. The results of the analyses in terms of the bending moment and the pile deflection profiles, additional to the result of the standard model are shown in Fig. 6.23. Bending moment profile was very similar to that of the standard test (with the circular pile). The value of maximum bending moment for a single square pile was 5 % higher than that for a single circular pile. This was close to the results that have been found by Broms (1964) and Miao (2005) in their model tests with different pile cross-section. Whereas, the computed maximum deflection (located at the pile head) of the single circular pile was 8% higher than that of the single square pile. In conclusion, the square pile was found to exhibit stiffer behaviour and provide a fairly higher soil resistance than a circular pile. The present results were reasonable compared with this by Miao (2005).



(a) Bending moment of pile

(b) Deflection of pile

Fig. 6.23 Effect of pile cross-sectional on the pile response

6.10.6 Effect of L_m/L_s on batter pile response with different values of batter angles (β)

A further study investigated the effect the L_m/L_s ratios on the batter pile response with different values of batter angle (β), which was not investigated experimentally in Chapters 4. Five models using the 16 mm diameter pile, $L = 300$ mm and $\beta = 0^\circ, \pm 10^\circ$ and $\pm 20^\circ$ were analysed on different ratios of L_m/L_s (Table 6.5). All the PLAXIS 3D models used the same standard input parameters (shown previously in Table 6.4 and 6.5).

Table 6.10 PLAXIS 3D models with ($\beta = 0^\circ, \pm 10^\circ$ and $\pm 20^\circ$) at different ratio of L_m/L_s

Moving

Pile length (mm)	Moving layer, L_m (mm)	Stable layer L_s (mm)	Ratio, L_m/L_s
300	50	250	0.2
300	100	200	0.5
300	150	150	1.0
300	200	100	2.0
300	250	50	5.0

The bending moment profiles from all the PLAXIS 3D models, as stated in Table 6.10, are presented in Fig. 6.24, respectively. Generally, the shape of the bending moment profiles shows a single curvature at $L_m \leq 150$ mm, and changes to a double curvature at $L_m/L_s = 200/100$. Finally, at $L_m/L_s = 250/50$, the bending moment profile shows a single curvature shape with the M_{-max} of -3600 N.mm at the depth of 150 mm. In summary, for a fixed pile length, by increasing the L_m/L_s (from 0.2 to 5.0), the M_{+max} and M_{-max} change, but did not exceed +3700 N.mm and -3600 N.mm, respectively. However, the pile may not be stable when $L_m/L_s > 150/150$, due to the excessive pile deflection (> 32 mm or 2D) as shown on the deflection profiles of the pile in Fig. 6.24(b).

The mode (translation, rotation or combination of both) of the deflection profiles changes as the L_m/L_s increases. The maximum pile deflection, located at the surface, also increases with L_m/L_s ratio. At $L_m/L_s = 100/200$, the soil movement is more than the pile deflection at the soil surface. Therefore, at this ratio, the soil starts to slide past the pile surface. Starting from L_m/L_s of about 200/100, the pile begins to “rip” through the

soil at the stable layer (L_s), as the soil movement increases (the pile deflection mode consists of initial rotation, follows by translation as U_x increases).

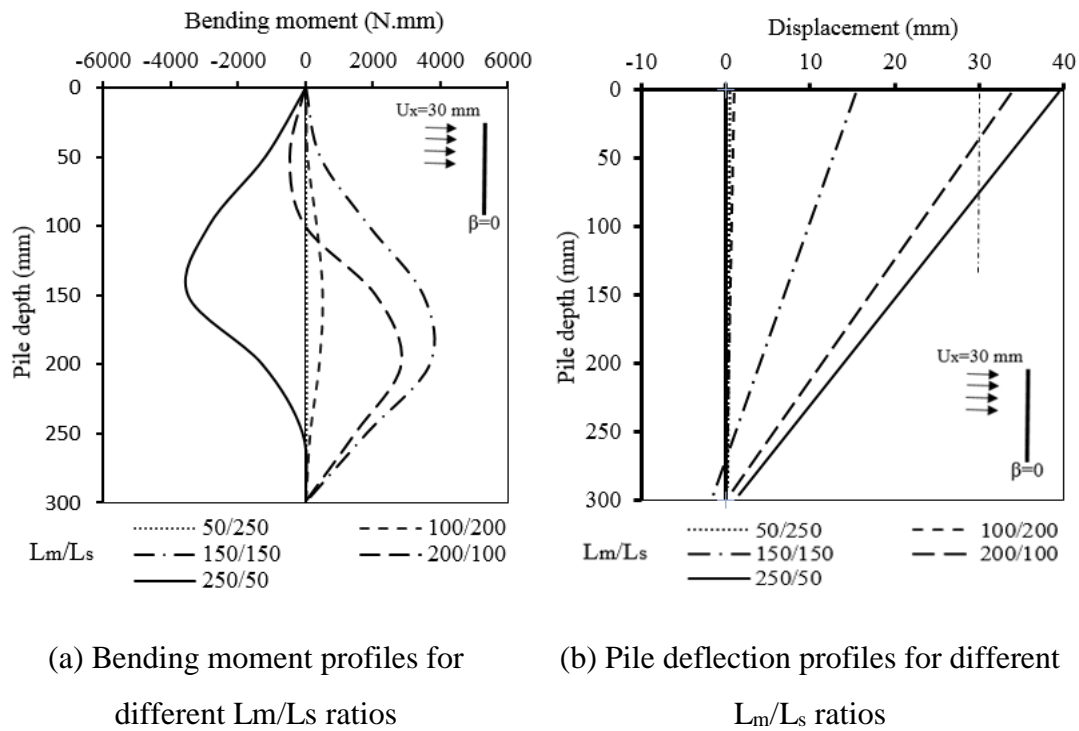


Fig. 6.24 Response of the 16 mm diameter pile with different L_m/L_s ratio

The PLAXIS 3D results for the maximum bending moment against L_m/L_s for several batter angles ($\beta = 0^\circ, \pm 10^\circ$ and $\pm 20^\circ$) and soil displacements ($U_x = 10, 20, 30$ and 40 mm) are shown in Fig. 6.25. For all value of β , there is a unique profile, where the peak value of M_{+max} was constant at $L_m/L_s = 150/150$ and increases as the U_x increases. Beyond $L_m/L_s > 1.0$, M_{+max} starts to reduce and becomes zero at the L_m/L_s of approximately 5, while the M_{-max} starts to increase, and becomes negative as the L_m/L_s increases further (> 1).

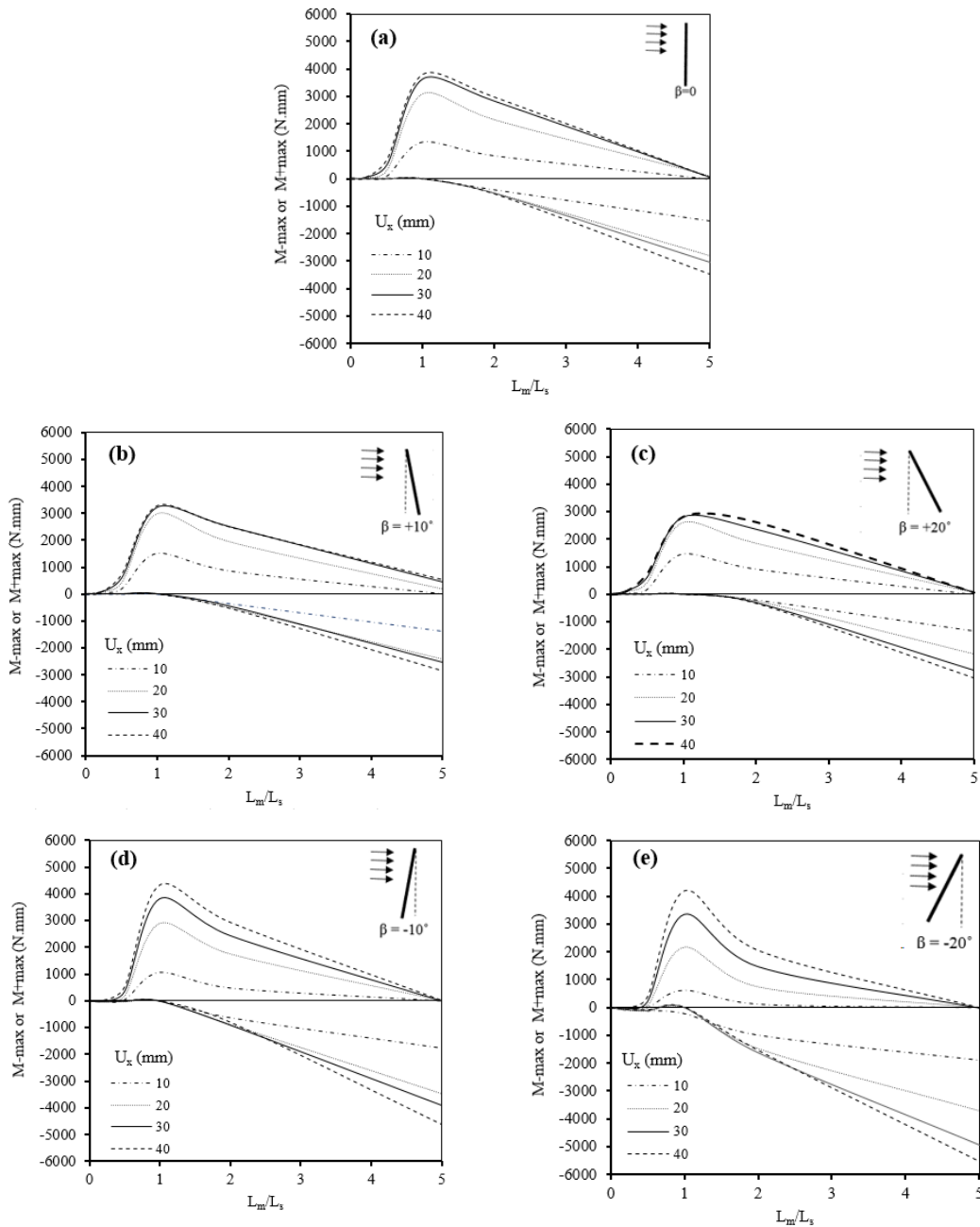


Fig. 6.25 Variation of maximum bending moment with L_m/L_s for different values of soil displacement at: (a) $\beta=0^\circ$, (b) $\beta = +10^\circ$, (c) $\beta = +20^\circ$, (d) $\beta = -10^\circ$, (e) $\beta = -20^\circ$

6.11 Limitations of PLAXIS program

The comparison between experimental and predicted results revealed some differences in response. The differences were more pronounced when comparing the lateral deformations of piles in which an overestimation of the predicted results was obtained. A number of limitations might be the reason behind these differences. Software limitations and suggestions to improve the current PLAXIS software can be drawn

below:

- The "embedded pile" does not consider the relative displacement occurred between the soil and piles in the lateral direction. This makes the simulation of "smooth" passive piles, in which the relative pile-soil displacement in horizontal directions is a key parameter, not a suitable choice especially when pile displacement is required. Therefore, the "slide" in the horizontal directions should be developed for the improved embedded pile simulation model in further research.
- The change in sand density after the installation of pile group is not considered and cannot be simulated in PLAXIS with the option of embedded pile. A procedure to consider the effect of pile installation method should be developed to improve embedded pile properties.
- Input data in terms of soil Young's modulus, soil dilatancy angle and parameters of pile bearing capacity have been calculated theoretically. This could have an impact on the numerical results.

6.12 Summary

In this chapter, the PLAXIS 3D program was used to predict the results from the experimental work reported in Chapters Four and Five. An elastic-perfectly plastic Mohr-Coulomb model was used to describe the sand behaviour. The pile was modelled using "embedded pile" approach. In this approach, the pile is represented by linear beam elements, while soil-pile interaction along the pile shaft and at the pile tip is described by special interface elements. Firstly, the effect of mesh generation was evaluated, and the three-dimensional medium density of mesh generation was seen to provide sufficient accuracy for the scope of this study. After that, the back analysis has been conducted on a number of model tests including parameters such as pile head fixity (free and fixed head), pile diameter and pile groups arrangement and inclination, two types of pile group configuration, namely, VVL and BBL with $\beta = 0^\circ$ and $\beta = \pm 10^\circ$, respectively. The results from the analyses show the following key findings:

- For single batter pile tests, PLAXIS 3D predicted bending moments well for the free-headed 16 mm and 20 mm diameter single pile tests but seemed to overestimate the results of the free-headed 25 mm diameter pile test. In addition,

the agreement between predicted and measured maximum bending moments for the fixed headed pile seemed to be less satisfactory, although the position of the maximum bending moment was predicted very well by the theory.

- For the batter pile group tests, the general trend of the four predicted profiles deduced numerically (bending moment, shear force, soil reaction and lateral deflection) of piles were in good agreement with those obtained experimentally.
- In all results of the analyses, the shape of the bending moment, shear force, soil reaction, pile rotation and deflection profiles from the PLAXIS 3D were in good agreement to that obtained from the experimental results.

A parametric study has been performed to investigate the effects of various soil-pile parameters on behaviour of batter piles subjected to passive loading due to lateral soil movement. The following conclusions can be drawn:

- Friction angle is a significant influence factor on the lateral response of batter piles. According to the results, when soil friction angle increases, the lateral deflection of the pile and maximum bending moment increases.
- In contrast, it is observed that the dilatancy angle (ψ) and pile shape had little effect on the lateral behaviour of batter piles.
- Young's modulus of the sand (E_s) had a considerable effect on the behaviour of the pile. It is found that increasing soil Young's modulus has caused an increase in bending moments and a decrease in lateral displacement of piles.
- Strength reduction factor (R_{inter}) of the interface around the embedded pile shaft has no influence on both bending moments along the pile and pile displacements.
- The mode of the deflection profiles changed as the L_m/L_s increased. The maximum pile deflection, located at the surface, increased with the L_m/L_s ratio. Beyond the $L_m/L_s > 200/100$, the maximum pile deflection at the surface exceeded the applied U_x .
- Regardless of the batter angle value (β), M_{max} peaked at L_m/L_s close to unity for different values of soil displacement (U_x).

Chapter 7

Conclusions and Recommendations for Future Work

7.1 Conclusions

In this thesis, experimental and numerical studies have been conducted to investigate the behaviour of batter piles and pile groups embedded in sand when subjected to lateral soil movements. Detailed conclusions have been presented in the previous chapters, and the major findings are summarised below.

7.1.1 Experimental work

A specially designed laboratory apparatus was utilized to perform a series of experimental tests on single batter piles and pile groups in sand, with some piles being instrumented with strain gauges to measure bending moments in the pile.

Single batter pile tests

The following conclusions were drawn for the single batter piles subjected to two soil movement profiles (rectangular and triangular). From the test results, the effects of a number of parameters on the batter pile response were identified. It has been identified that:

- The bending moment profile for free-headed piles was generally found to be more-or-less a parabolic curve, with a zero value at both pile head and pile tip and a maximum value at the proximity of the interface between the upper moving layer and the lower stable layer (section 4.3.1).
- The value of the maximum bending moment induced in the vertical pile was found to be dependent on the ratio of the pile embedded length in the upper moving soil layer (L_m) and the lower stable soil layer (L_s), and it was concluded that it might reach its peak value when the values of L_m and L_s were similar (section 4.3.2).
- Regardless of the soil movement profile (rectangular or triangular), pile batter angle has shown a substantial effect on the behaviour of pile. The bending moment of the “negative” batter pile ($\beta = -10^\circ$ and -20°) increases as the batter

angle increases. In contrast, the bending moment of the “positive” batter pile ($\beta = +10^\circ$ and $+20^\circ$) decreases as the batter angle increases. The bending moment of the negative batter pile was larger than that of the vertical pile and positive pile (section 4.3.3 & 4.4).

- The maximum bending moment, M_{\max} induced by the lateral load from soil movement is approximately linearly related to the maximum shear force, F_{\max} and can be evaluated by $M_{\max} = \alpha F_{\max} L$, with $\alpha = 1/3$, regardless of the magnitude of soil movement and batter pile inclination β (section 4.3.3).
- For all values of (β), the shape of the bending moment profile was a single curvature when batter piles subjected to rectangular or triangular soil movement profile (section 4.3.3 & 4.4).
- The ultimate soil pressure P_u for single batter piles ranged from 3.5 to 5.2 Rankine passive pressure P_p at moving layer L_m and (2.4 to 3.4) P_p at stable layer L_s , depending on the value of batter angle β (section 4.3.4.1 & 4.3.4.1).
- Pile responses in terms of bending moment and soil reaction increased as the distance to the source of lateral loading decreased when the value of $\beta = 0^\circ$ and -10° (section 4.3.5).
- For the fixed-headed pile, the shape of the bending moment profile was different from that for the free-headed piles, with negative bending moment developed at pile head and positive bending moment along the middle portion of the pile. As compared with the case of free-headed piles, the maximum positive bending moment for the fixed-headed pile was smaller because of the negative bending moment developed at the head (section 4.3.6).
- The bending moment was found to increase with increasing pile diameter, and the maximum bending moment appeared to normalise in terms of pile diameter and pile stiffness (section 4.3.7).
- For single batter piles subjected to triangular profile of soil movement, pile response in terms of bending moment increased as sand density increases (section 4.5).
- For all values of (β), the shape of the bending moment profile was a single curvature when batter piles subjected to rectangular or triangular soil movement profile (section 4.6).
- Bending moment and deformations developed along the pile length due to rectangular soil movement were higher compared to those in triangular profile

(section 4.6).

Pile group tests

A series of laboratory tests were carried out on a pile group of 2×1 with different arrangements. Only the rectangular soil movement profile was investigated for the pile group tests. Several parameters were varied in the group tests, namely: the arrangement of the pile in the group, the inclination angle of piles in the group, the pile spacing and the head fixity condition to investigate the lateral behaviour of a pile in a group. By varying these parameters, general trends were identified from the response of the two instrumented piles within the pile group.

The findings from a comparison between the different pile group arrangements showed that:

- Each pile in a group behaves differently, and the extent of the group effect on the lateral response of a pile in a group depends on a number of factors, including the arrangement of the pile in the group, the inclination angle of piles in the group, the pile spacing and the head fixity condition (section 5.3, 5.4, 5.5 & 5.6.1).
- Batter pile groups with (BBL) configuration of $(-10^\circ, +10^\circ)$ offer more resistance to lateral soil movement compared to other pile group arrangements with the same pile spacing. This is confirmed by the development of higher bending moments in the back piles rather than the front piles. On the other hand, (VVL) configuration offered the least resistance (section 5.3.2).
- A rigid cap has a significant effect on the pile response, which tends to reduce the positive bending moment while developing a relatively large negative bending moment in the upper pile portion (section 5.5).
- The bending moment profiles showed a double curvature on front and back piles within the capped piles group configuration, while a single curvature was the case for the uncapped pile group (section 5.5).
- The $M_{+\max}$ values recorded in the pile group were always lower than that of a single pile (section 5.3.2, Fig. 5.14).
- Pile spacing have a significant impact on its response to loading, at which the $M_{+\max}$ and $M_{-\max}$ increase when pile spacing increase (section 5.4).

7.1.2 Numerical work

The finite element program PLAXIS 3D with "embedded pile" concept was used to predict the experimental results from both single batter pile tests and pile group tests. It has been identified that:

- The numerical predictions for single piles and pile groups were generally in good agreement in terms of the shape of the bending moment, shear force, soil reaction, and pile deflection profiles (section 6.8.3, 6.8.4 & 6.8.5).
- The position of the maximum bending moment was very well predicted in all cases, even for the cases where the agreement between the predicted and the measured maximum bending moment was not as satisfactory (section 6.8.3, 6.8.4 & 6.7.5).
- In all analyses, PLAXIS 3D over predicted the pile deflection obtained from the experimental tests (section 6.8.3, 6.9.1 & 6.9.2).
- The parametric study, performed on a standard model, indicated that the Young's modulus and friction angle of the sand had a significant effect on the magnitude of the maximum bending moment and deflection of the pile (section 6.10.1 & 6.10.3).
- The dilatancy angle (ψ), and pile shape had little effect on the lateral behaviour of piles (section 6.10.2 & 6.10.5).
- The strength reduction factor (R_{inter}) at the soil-pile interface had no influence on response of the pile (section 6.10.4).
- The deflection mode of the pile changed with an increase in L_m/L_s . Regardless of the batter angle value (β), the maximum bending moment peaks at the L_m/L_s ratio were close to unity for different values of soil displacement (section 6.10.6).

7.2 Suggestions for future research

Although considerable research work has already been done to investigate the behaviour of batter piles and pile groups subjected to lateral soil movement, however, there are still a number of areas which are not covered in the current research. Therefore, further research in the following areas is suggested:

Experimental work

- The present work may be extended to include tests for different pile material properties.
- Different soils may be used, such as clay.
- The present work may be extended to study the combined effect of vertical loading and passive lateral loading due to lateral soil movement on lateral batter pile response.
- More tests are required to investigate the responses of batter pile foundations under combined lateral load (active load) and soil movements (passive load).
- The investigation of the behaviour for batter pile groups in sandy soils with different arrangements, such as (2×2), deserves research.

Numerical work

- The existing PLAXIS 3D program with the option of embedded pile, appears to be reasonably powerful in general, however, currently the embedded pile model does not take into account the “slip”, which is used to model pile-soil interaction, in horizontal directions. This makes the embedded pile impossible to model the laterally loaded pile with “smooth” surface. Therefore, the “slip” in the horizontal directions should be developed for the improved embedded pile model in further research.
- Further analysis on single batter piles and pile groups subjected to triangular soil movement is worth investigating.
- Further analysis on batter piles subjected to soil movement in clay is useful.
- A comparison between the results of "embedded pile" and "volume pile" models is required.

7.3 Concluding remarks

The current thesis presents a study of the responses of batter piles and pile groups subjected to lateral soil movements. Indeed, from the current study, a better understanding of the mechanism of the batter pile behaviour under moving soil has been obtained. The laboratory model tests on single batter piles and pile groups identified the way the batter piles respond to a number of parameters. The numerical study helped

to predict the results from the experimental tests, illustrating the ability of the three-dimensional finite element program (PLAXIS 3D) to simulate the behaviour of the batter piles under lateral soil movements.

References

- Al-Abboodi, I., & Toma-Sabbagh, T. M. (2017). Effects of axial loads and soil density on pile group subjected to triangular soil movement. *International Journal of Environmental, Chemical, Ecological, Geological and Geophysical Engineering*, 11(3), 138-143.
- Al-Abboodi, I., Toma-Sabbagh, T. M., & Al-Jazaairry, A. (2015). Modelling the response of single passive piles subjected to lateral soil movement using PLAXIS. *International Journal of Engineering Research & Technology*, 4(3), 176-180.
- Ashford, S. A., Juirnarongrit, T., Sugano, T., & Hamada, M. (2006). Soil–pile response to blast-induced lateral spreading. I: field test. *Journal of Geotechnical and Geoenvironmental Engineering*, 132(2), 152-162.
- Barton, Y.O. (1982). *Laterally Loaded Model Piles in Sand: Centrifuge Tests and Finite Element Analyses*, PhD Thesis, University of Cambridge.
- Bing-can, H., Hao, C., Jing-song, Z., Cong-jun, W., Xin, Z., & Guo-jian, W. (2010). Nonlinear FEM analysis of bearing capacity and sedimentation of single pile in multi-layered soils. In *Proceedings of the International Conference on Computing in Civil and Building Engineering* (pp. 481-490).
- Bransby, M. F., & Springman, S. M. (1996). 3-D finite element modelling of pile groups adjacent to surcharge loads. *Computers and Geotechnics*, 19(4), 301-324.
- Bransby, M.F. & Springman, S.M. (1997). Centrifuge modelling of pile groups adjacent to surcharge loads. *Soils and Foundations*, 37(2), p. 39.
- Brinkgreve, R. B. J., Engin, E., & Swolfs, W. M. (2013). *PLAXIS 3D material models Manual*. Plaxis company, Delft, The Netherlands.
- Britto, A. M. (1990). CRISP90. *User's and programmer's guide*. Cited by Miao, L. F. (2005).
- Britto, A. M., & Gunn, M. J. (1987). *Critical state soil mechanics via finite elements*. Chichester: Ellis Horwood Ltd. Cited by Miao, L. F. (2005).

- Broms, B. B. (1964). Lateral resistance of piles in cohesionless soils. *Journal of the Soil Mechanics and Foundations Division, ASCE*, 90(3), 123–156.
- Byrne, B. W., McAdam, R., Burd, H. J., Houlsby, G., Martin, C., Zdravković, L., & Schroeder, F. C. (2015). New design methods for large diameter piles under lateral loading for offshore wind applications. In *3rd International Symposium on Frontiers in Offshore Geotechnics (ISFOG 2015), Oslo, Norway*, (pp. 10-12).
- Cai, F. & Ugai, K. (2003). Response of flexible piles under laterally linear movement of the sliding layer in landslides. *Canadian Geotechnical Journal*, 40(1), pp. 46–53.
- Carrubba, P., Maugeri, M., & Motta, E. (1989). Esperienze in vera grandezza sul comportamento di pali per la stabilizzazione di un pendio. *Proceedings of the XVII Convegno Nazionale di Geotecnica, Taormina, Italy*, 26-28. Cited by Miao, L. F. (2005).
- Chen, C.Y. & Martin, G.R. (2002). Soil - Structure interaction for landslide stabilizing piles. *Computers and Geotechnics*, 29(5), pp. 363–386.
- Chen, C.Y. & Tsai, C.X. (2014). Batter Pile Behaviour modelling using finite difference analysis. *Applied Mechanics and Materials*, 566, pp. 199–204.
- Chen, L. T., & Poulos, H. G. (1997). Piles subjected to lateral soil movements. *Journal of Geotechnical and Geoenvironmental Engineering, ASCE*, 123(9), 802-811.
- Chen, L.T., Poulos, H.G. & Hull, T.S. (1997). Model Tests on Pile Groups Subjected to Lateral Soil Movement. *Soil and Foundations Japanese Geotechnical Society*, 37(1), pp. 1–12.
- Choudhury, D., Shen, R. F., & Leung, C. F. (2008). *Centrifuge model study of pile group due to adjacent excavation*. Paper presented at *GeoCongress: Characterization, Monitoring and Modelling of GeoSystem*, Geotechnical Special Publication, ASCE, pp. 141–148.
- Chow, Y., 1996. Analysis of piles used for slope stabilization. *International journal for numerical and analytical methods in geomechanics*, 20(9), pp. 635–646.

- Cubrinovski, M., & Ishihara, K. (2007, June). Simplified analysis of piles subjected to lateral spreading: parameters and uncertainties. In *Proceedings of the 4th international conference on Earthquake Geotechnical Engineering-invited lectures, Paper* (Vol. 1385, pp. 1-12).
- Dao, T. P. T. (2011). *Validation of PLAXIS embedded piles for lateral loading*. Master of Science Thesis, Delft University, The Netherlands, pp. 113.
- D'Arezzo, F. B., Haigh, S. K., Ishihara, Y., Gaudin C., & White, D. (2014). *Modelling of jacked piles in centrifuge*. Paper presented at the 8th International Conference on Physical Modelling in Geotechnics (ICPMG2014), Perth, Australia.
- De Beer, E. E., & Wallays, M. (1972). *Forces induced in piles by unsymmetrical surcharges on the soil around the piles*. Paper presented at the 5th European Conference on Soil Mechanics and Foundations Engineering, Madrid, Spain.
- Ekici, A. (2013). *Three-dimensional finite element modelling for the laterally loaded passive pile behaviour*. Master of Science Thesis, Middle East Technical University, Ankara, Turkey, pp. 116.
- Ekici, A., & Huvaj, N. (2014). *Validation of 3D finite element solution for laterally loaded passive piles*. Paper presented at NUMGE 2014, the 8th European Conference on Numerical Methods in Geotechnical Engineering, Delft, The Netherlands.
- Ellis, E.A. & Springman, S.M. (2001). Modelling of soil structure interaction for a piled bridge abutment in plane strain FEM analyses. *Computer and Geotechnics*, 28, pp. 79–98.
- Ersoy & Yildirim (2014). Experimental Investigation of Piles Behaviour subjected to lateral soil movement. *Teknik Dergi*, 25(4), pp. 1827–1846.
- Esu, F., & D'Elia, B. (1974). Interazione terreno-struttura in un palo sollecitato da una frana tipo colata. *Rivista Italiana di Geotecnica*, 8(1), 27-38. Cited by Miao, L. F. (2005).
- Finno, R. J., Lawrence, S. A., Allawh, N. F., & Harahap, I. S. (1991). Analysis of performance of pile groups adjacent to deep excavation. *Journal of Geotechnical Engineering*, 117(6), 934-955.

- Gaaver, K.E. (2013). Uplift capacity of single piles and pile groups embedded in cohesionless soil. *Alexandria Engineering Journal*, 52(3), pp. 365–372.
- Gatmiri, B., Allahverdizadeh, P., & Abbasi, A. (2011). Numerical modelling of pile groups under lateral loading in sand. In *14 th Pan-Am CGS Geotechnical Conference*.
- Ghazavi, M., Ravanshenas, P. & Lavasan, A.A., 2014. Analytical and numerical solution for interaction between batter pile group. *KSCE Journal of Civil Engineering*, 18(7), pp. 2051–2063.
- Ghee, E.H. & Guo, W.D. (2011). FLAC^{3D} analysis on soil moving through piles. *International Symposium on Frontiers in offshore Geotechnics*, pp. 1–6.
- Ghee, E.H. (2009). The Behaviour of Axially Loaded Piles Subjected to Lateral Soil Movements. *PhD thesis, Griffith University*, pp. 431.
- Giannakou, A. et al. (2010). Seismic Behaviour of Batter Piles: Elastic Response. *Journal of Geotechnical and Geoenvironmental Engineering*, 136(9), pp. 1187–1199.
- Guo, W.D. and Ghee, E.H. (2006). Behaviour of axially loaded pile groups subjected to lateral soil movement. *Geotechnical Special Publication*, 153, p. 174.
- Hanna, A.M. & Afram, A. (1986). Pull-out capacity of single batter piles in sand: Reply. *Canadian Geotechnical Journal*, 23(3), pp. 387–392.
- Haryono, I. S. (2013). *Pile foundation and soil response to deep excavation*. MSc Thesis, Delft University, The Netherlands, pp. 186.
- Hazzar, L., Hussien, M. N. & Karray, M. (2015). 3D modelling laterally loaded batter piles in sand. *Conference, 68 Canadian geotechnical conferenc, Canada*.
- Hirani, K.R. & Verma, A.K. (2011). Lateral Load Carrying Capacity of Model Pile Groups. *National Conference on Recent Trends in Engineering & Technology*, (May), p. 13-14.
- Ilamparuthi, K., & Madhumathi, R. K. (2011). *Effect of ground movement on the performance of pile foundation*. Paper presented at the Indian Geotechnical Conference, Kochi, India.

- Ilyas, T., Leung, C.F., Chow, Y.K. and Budi, S.S. (2005). Closure to “Centrifuge Model Study of Laterally Loaded Pile Groups in Clay”. *Journal of Geotechnical and Geoenvironmental Engineering*, 131(10), pp. 1308-1308.
- Ito, T., & Matsui, T. (1975). Methods to estimate lateral force acting on stabilizing piles. *Soils and Foundations*, 18(4), 43-59.
- Ito, T., Matsui, T., & Hong, W. P. (1982). Extended design method for multi-row stabilising piles against landslides. *Soils and Foundations*, 22(1), 1-13.
- Jeong, S., Seo, D., & Kim, Y. (2009). Numerical analysis of passive pile groups in offshore soft deposits. *Computers and Geotechnics*, 36, 1164-1175.
- Jeong, S., Seo, D., Lee, J., & Park, J. (2004). Time-dependent behavior of pile groups by staged construction of an adjacent embankment on soft clay. *Canadian geotechnical journal*, 41(4), 644-656.
- Kahyaoglu, M. R. (2010). *A modelling study for load transfer mechanisms of slope stabilizing piles*. PhD Thesis, Dokuz Eylül University, Turkey, pp. 265.
- Kahyaoglu, M. R., Imancli, G., Onal, O., & Kayalat, A. S. (2012a). Numerical analyses of piles subjected to lateral soil movements. *KSCE Journal of Civil Engineering*, 16(4), 562-568.
- Kahyaoglu, M. R., Imancli, G., Ozturk, A. U., & Kayalar, A. S. (2009). Computational 3D finite element analyses of model passive piles. *Computational Materials Science*, 46(1), 193-202.
- Kalteziotis, N., Zervogiannis, H., Frank, R., Seve, G., & Berche, J. -C. (1993). *Experimental study of landslide stabilization by large diameter piles*. Paper presented at the International Symposium on Geotechnical Engineering of Hard Soils – Soft Rocks, Athens. A. A. Balkema, Rotterdam, the Netherlands.
- Karim, M. R. (2013). Behaviour of piles subjected to passive subsoil movement due to embankment construction – A simplified 3D analysis. *Computers and Geotechnics*, 53, 1–8.

- Karthigeyan, S., Ramakrishna, V. V. G. S. T., & Rajagopal, K. (2006). Influence of vertical load on the lateral response of piles in sand. *Computers and Geotechnics*, 33(2), 121-131.
- Khari, M., Kassim, K. A., & Adnan, A. (2013). An experimental study on pile spacing effects under lateral loading in sand. *The Scientific World Journal*, 2013, 1-8.
- Khari, M., Kassim, K. A., & Adnan, A. (2014). Development of p-y curves of laterally loaded piles. *The Scientific World Journal*, 2014, 1-8.
- Khudeira, S. (2010). Building collapse during construction. *Practice Periodical on Structural Design and Construction*, ASCE, 15(2), 99-100.
- Lee, C. & Chiang, K. (2007). Responses of single piles to tunneling-induced soil movements in sandy ground. *Canadian Geotechnical Journal*, 44, pp. 1224–1241.
- Leung, C. F., Chow, Y. K., & Shen, R. F. (2000). Behaviour of pile subject to excavation-induced soil movement. *Journal of Geotechnical and Geoenvironmental engineering*, ASCE, 126(11), 947–954.
- Leung, C. F., Lim, J. K., Shen, R. F. & Chow, Y. K. (2003). Behaviour of pile groups subject to excavation-induced soil movement. *Journal of Geotechnical and Geoenvironmental engineering*, ASCE, 129(1), 58–65.
- Leung, C.F. & Chow, Y.K. (2003). Piles subject to excavation-induced soil movement in clay. *Soil Mechanics and Geotechnical Engineering*, 2, pp. 777–782.
- Liang, F., Yu, F., & Han, J. (2013). A simplified analytical method for response of an axially loaded pile group subjected to lateral soil movement. *KSCE Journal of Civil Engineering*, 17(2), 368-376.
- Liyanapathirana, D. S., & Nishanthan, R. (2016). Influence of deep excavation induced ground movements on adjacent piles. *Tunnelling and Underground Space Technology*, 52, 168–181.
- Lv, F.R., Yin, J.M. & Jin, Y.H. (2011). Study on proportional relation-ship of lateral bearing capacity of batter pile by model experiments. *Procedia Engineering*, 16, pp. 8–13.

- Manoppo, F.J. (2010). Behaviour of the ultimate bearing capacity of single flexible batter pile under horizontal loads in homogenous sand. *Dinamika TEKNIK SIPIL*, 10(2), pp.116–119.
- Meyerhof, G.G. & Ranjan, G. (1972a). The Bearing Capacity of Rigid Piles Under Inclined Loads in Sand. I: Vertical Piles. *Canadian Geotechnical Journal*, 9(4), pp. 430–446.
- Meyerhof, G.G. & Ranjan, G. (1972b). The Bearing Capacity of Rigid Piles Under Inclined Loads in Sand. II: Batter Piles. *Canadian Geotechnical Journal*, 10, pp. 71–85.
- Meyerhof, G.G. & Yalcin, a. S. (1994). Bearing capacity of flexible batter piles under eccentric and inclined, loads in layered soil. *Canadian Geotechnical Journal*, 31(4), pp. 583–590.
- Meyerhof, G.G. & Yalcin, A.S. (1993). Behaviour of flexible batter piles under inclined loads in layered soil". *Canadian Geotechnical Journal*, 30, pp. 247–256 (1993).
- Miao, L. F. (2005). *Effects of lateral soil movements on piles*. PhD Thesis, Nanyang Technological University, Singapore, 243 pp.
- Miao, L.F. et al. (2006). Three-dimensional finite element analyses of passive pile behaviour. *International Journal for Numerical and Analytical Methods in Geomechanics*, 30(7), pp. 599–613.
- Murthy, V. N. S. (1965). Behaviour of batter piles embedded in sand subjected to lateral loads, PhD Thesis, Indian Institute of Technology, Kharagpur, India. (Cited by Ghazavi, M., Ravanshenas, P. & Lavasan, A.A., 2014).
- Ng, C. W. W., Wei, J., Poulos, H., & Liu, H. (2017). Effects of multipropped excavation on an adjacent floating pile. *Journal of Geotechnical and Geoenvironmental Engineering, ASCE*, 143(7).
- Nugroho, A. H., & Prakoso, W. A. (2010). *Behaviour of single pile subjected to lateral soil movement due to wall supported excavations*. Paper presented at Development of Geotechnical Engineering in Civil Works and Geo-Environment Conference, Yogyakarta, Indonesia.

- Ong, D. E. L. (2004). *Pile behaviour subject to excavation-induced soil movement in clay*. PhD Thesis, National University of Singapore, Singapore, 275 pp.
- Ong, D. E. L. (2008). *Benchmarking of FEM technique involving deep excavation, pile soil interaction and embankment construction*. Paper presented at (IACMAG), the 12th International Conference of International Association for Computer Methods and Advances in Geomechanics, Goa, India.
- Ong, D. E. L., Leung, C. F., & Chow, Y. K. (2003). *Piles subject to excavation-induced soil movement in clay*. Paper presented at the 13th European Conference on Soil Mechanics and Geotechnical Engineering, Prague, Czech Republic.
- Pan, J. L., Goh, A. T. C., Wong, K. S., & Teh, C. I. (2002a). Ultimate soil pressures for piles subjected to lateral soil movements. *Journal of Geotechnical and Geoenvironmental Engineering*, 128(6), 530-535.
- Pan, J., Goh, A., Wong, K., & Selby, A. (2002b). Three-dimensional analysis of single pile response to lateral soil movements. *International Journal for Numerical and Analytical*, 26(8), 747–758.
- Pathak, B., Abu-Farsakh, M., Yu, X., & Alshibli, K. (2011). Interpretation of lateral load test of batter pile group using high order polynomials curve fitting. In *Geo-Frontiers 2011: Advances in Geotechnical Engineering* (pp. 152-161).
- Poulos, H. G. & Davis, E. H. (1980). *Pile foundation analysis and design*. New York: John Wiley & Sons.
- Poulos, H. G. (1973). Analysis of piles in soil undergoing lateral movement. *Journal of Soil Mechanics and Foundation Engineering Division, ASCE*, 99, 391-406.
- Poulos, H. G. (1989). Pile behaviour – theory and application. *Geotechnique*, 39(3), 365-415.
- Poulos, H. G. (1995). Design of reinforcing piles to increase slope stability. *Canadian Geotechnical Journal*, 32(5), 808–818.
- Poulos, H. G. (2006). Raked piles Virtues and drawbacks. *Journal of geotechnical and geoenvironmental engineering*, 132(6), 795-803.

- Poulos, H. G., Chen, L. T., & Hull, T. S. (1995). Model tests on single piles subjected to lateral soil movement. *Soils and Foundation*, 35(4), pp. 85-92.
- Prabha, S.M. & Boominathan, A. (2010). Static and cyclic lateral response of batter piles in clay. *Physical Modelling in Geotechnics*, pp.971–977.
- Qin, H. (2010). *Response of pile foundations due to lateral force and soil movement*. PhD Thesis, Griffith University, Australia, 471 pp.
- Rahimi, M.R. & Bargi, K. (2010). Efficient arrangement of batter piles of a pile-supported wharf in sand. *Electronic Journal of Geotechnical Engineering*, 15 G, pp. 1–10.
- Rajashree, S.S. & Sitharam, T.G. (2001). Nonlinear finite-Element modelling of batter piles under lateral load. *Journal of Geotechnical and Geoenvironmental Engineering*, 127(7), pp. 604–612.
- Randolph, M. F. (1981). The response of flexible piles to lateral loading. *Geotechnique*, 31(2), 247-259.
- Ranjan, G., Ramasamy, G. & Tyagi, R.P. (1980). lateral response of batter piles in clay. *Indian Geotechnical Journal*, 10(2), pp. 135–142.
- Rao, S. Narasimha, Veeresh, C. & Shankaranarayana, G.V.S. (1994). Behaviour of model batter piles soft clays. *Geotechnical Eng., Jl. South East Asian geotechnical Society, Bangkok*, Vol. 25, No.2, pp. 37 – 46.
- Reese, L. C., Van Impe, W. F., & Holtz, R. D. (2002). Single piles and pile groups under lateral loading. *Applied Mechanics Reviews*, 55, B9.
- Shaia, H. (2013). *Behaviour of Fibre Reinforced Polymer Composite Piles: Experimental and Numerical Study* (PhD dissertation, The University of Manchester (United Kingdom)).
- Singh, T., & Arora, V. K. (2017). Influence of pile inclination on batter pile groups subjected to lateral loading in sand. In *Proceedings of 29th research world international conference, Las Vegas, USA, 16th–17th March*.

- Smethurst, J. A., & Powrie, W. (2007). Monitoring and analysis of the bending behaviour of discrete piles used to stabilise a railway embankment. *Geotechnique*, 57(8), 663-677.
- Springman, S. M., Ng, C. W. W., & Ellis, E. A. (1994). Centrifuge and analytical studies of full height bridge abutment on piled foundation subjected to lateral loading. Technical Report. Cambridge University Engineering Department.
- Tsuchiya, T., Kakurai, M., Yamashita, K., and Hamada, J. (2001). Large-scale laminar shear box for lateral pile load tests with ground displacements. *International Journal of Physical Modelling in Geotechnics*, 2, 43-51.
- Viggiani, C. (1981). *Ultimate lateral load on piles used to stabilize landslides*. Paper presented at the 10th International Conference on Soil Mechanics and Foundation Engineering (ICSMFE), Stockholm, Sweden
- Wang, L., Zheng, G. & Ou, R. (2014). Finite element analysis of couple effect of soil displacement and axial load on single inclined pile. *Journal of Central South University*, 21(9), pp. 3656–3664.
- Waterman, D. (2006), “*Structural elements and excavations*”, Presentation in CG1 Chile.
- White, D. J., Thompson, M. J., Suleiman, M. T., & Schaefer, V. R. (2008). Behaviour of slender piles subject to free-field lateral soil movement. *Journal of Geotechnical and Geoenvironmental Engineering, ASCE*, 134(4), 428-436.
- Yoon, B. S., & Ellis, E. A. (2009). Centrifuge modelling of slope stabilisation using a discrete pile row. *Geomechanics and Geoengineering: An International Journal*, 4(2), 103-108.
- Zhang, L., McVay, M.C. & W. Lai Peter (1999). Centrifuge modelling of laterally loaded single batter piles in sands. *Canadian Geotechnical Journal*, 36(6), pp. 1074–1084.
- Zhang, L.M., McVay, M.C., Han, S.J., Lai, P.W. and Gardner, R. (2002). Effects of dead loads on the lateral response of batter pile groups. *Canadian Geotechnical Journal*, 39(3), pp. 561-575.

Appendix A
Single Pile Test Results

Test number	RSF16, 0	Density kN/m ³	15.2	Batter angle (β) (degree)	0
Pile-head condition)	Free-head	Soil moving Profile	rectangular		
Moving layer, L_m (mm)	150	Stable layer, L_s (mm)	150	Diameter (mm)	16

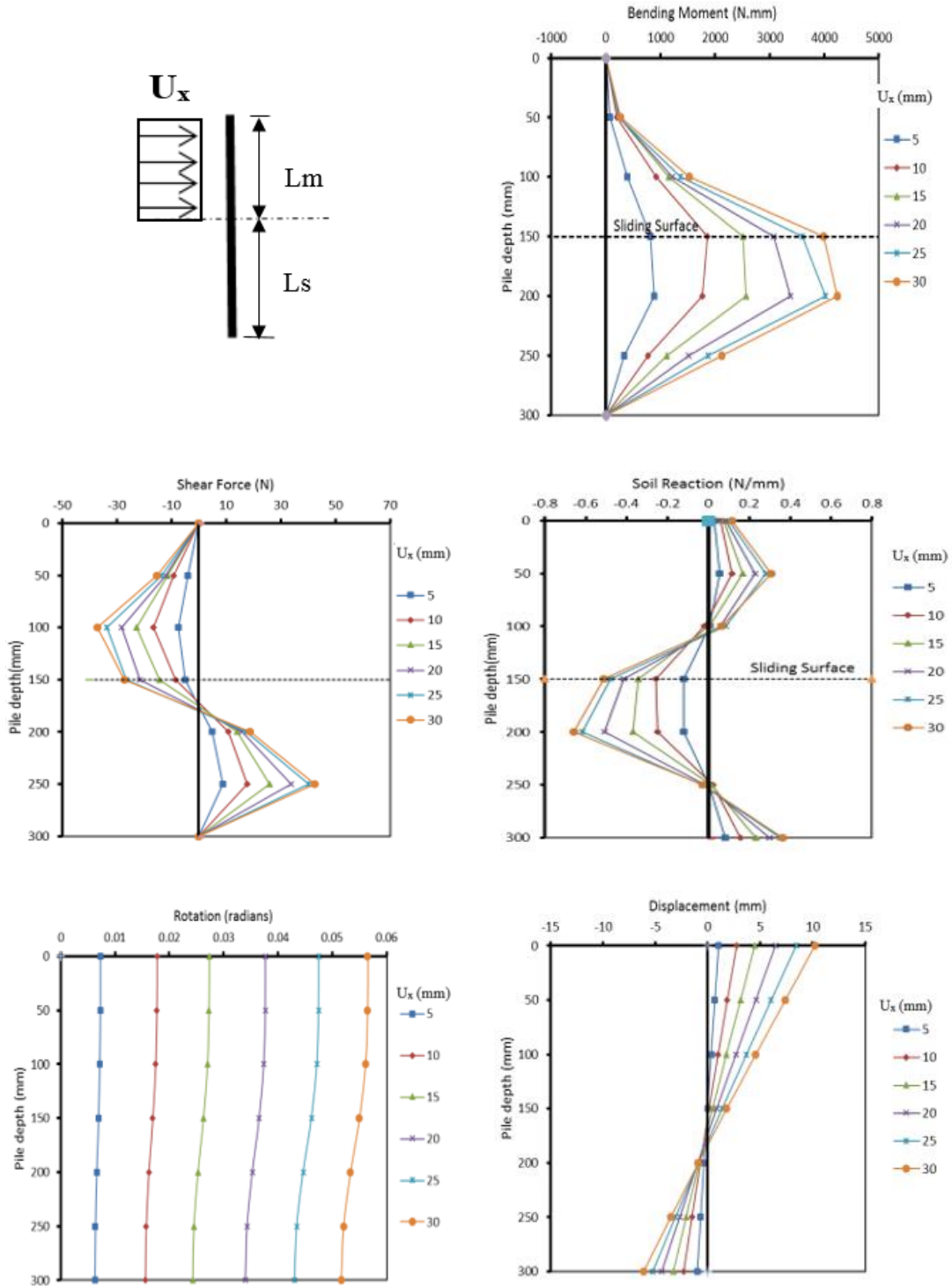


Fig. A.1 Single batter pile response, test (RSF16, 0°), $d_s = 300$ mm

Test number	RSF16, 0	Density kN/m ³	15.2	Batter angle (β) (degree)	0
Pile-head condition)	Free-head	Soil moving Profile	rectangular		
Moving layer, L_m (mm)	150	Stable layer, L_s (mm)	50	Diameter (mm)	16

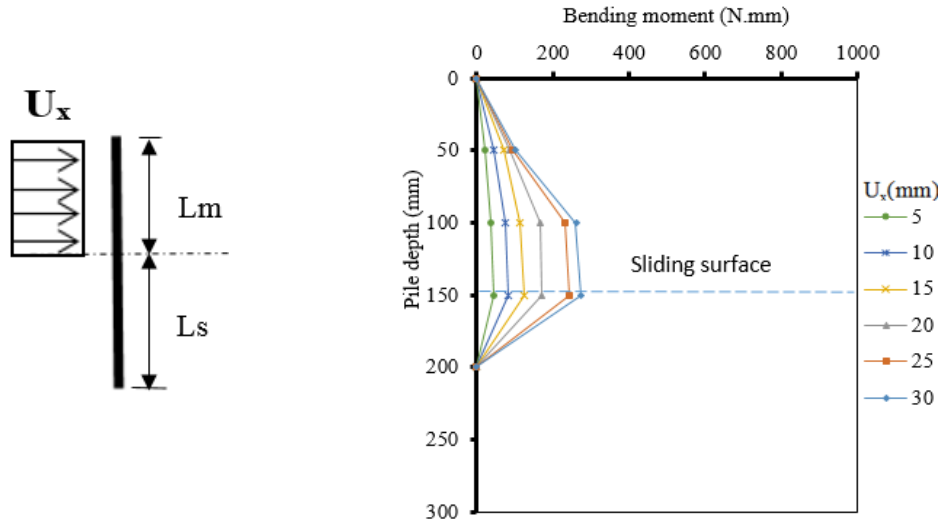


Fig. A.2 Single batter pile response, test (RSF16, 0°)

Test number	RSF16, 0	Density kN/m ³	15.2	Batter angle (β) (degree)	0
Pile-head condition)	Free-head	Soil moving Profile	rectangular		
Moving layer, L_m (mm)	150	Stable layer, L_s (mm)	75	Diameter (mm)	16

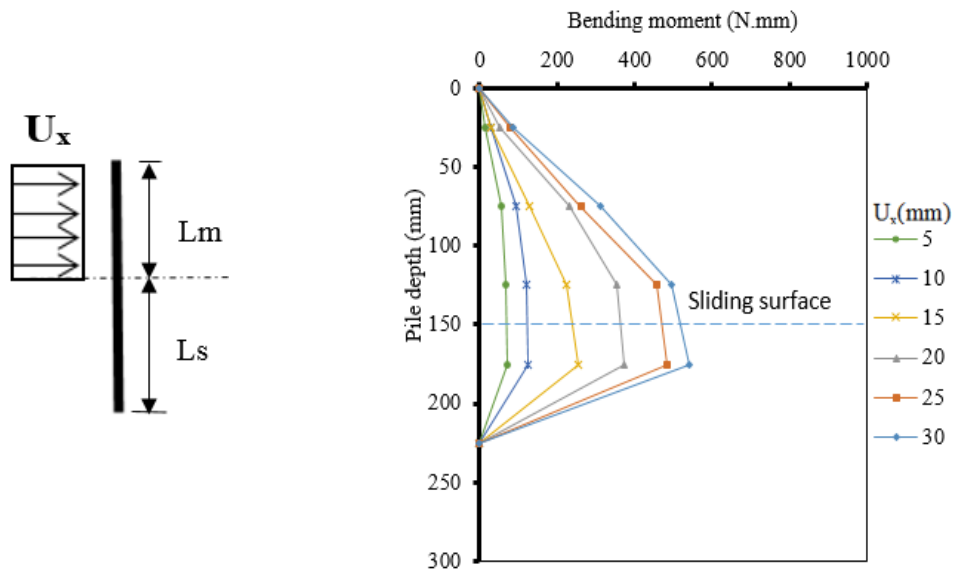


Fig. A.3 Single batter pile response, test (RSF16, 0°)

Test number	RSF16, 0	Density kN/m ³	15.2	Batter angle (β) (degree)	0
Pile-head condition)	Free-head	Soil moving Profile	rectangular		
Moving layer, L_m (mm)	150	Stable layer, L_s (mm)	100	Diameter (mm)	16

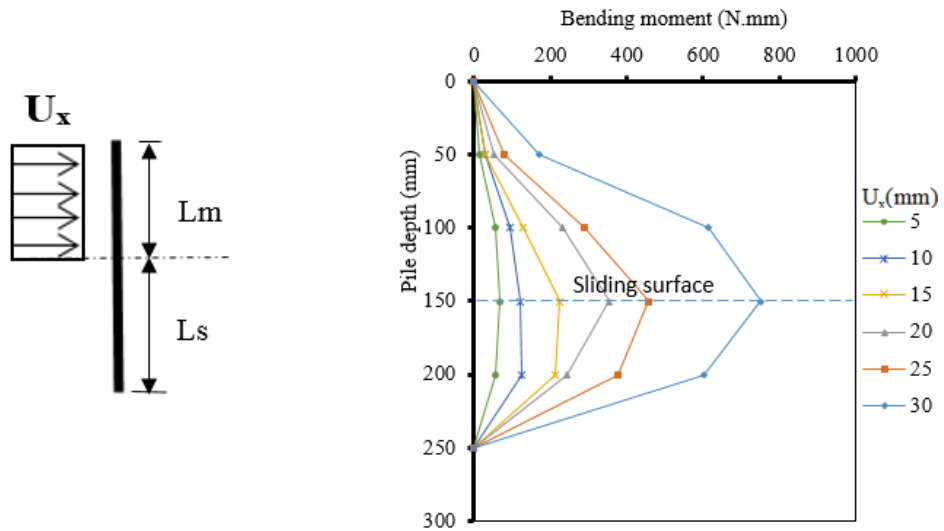


Fig. A.4 Single batter pile response, test (RSF16, 0°)

Test number	RSF16, 0	Density kN/m ³	15.2	Batter angle (β) (degree)	0
Pile-head condition)	Free-head	Soil moving Profile	rectangular		
Moving layer, L_m (mm)	150	Stable layer, L_s (mm)	125	Diameter (mm)	16

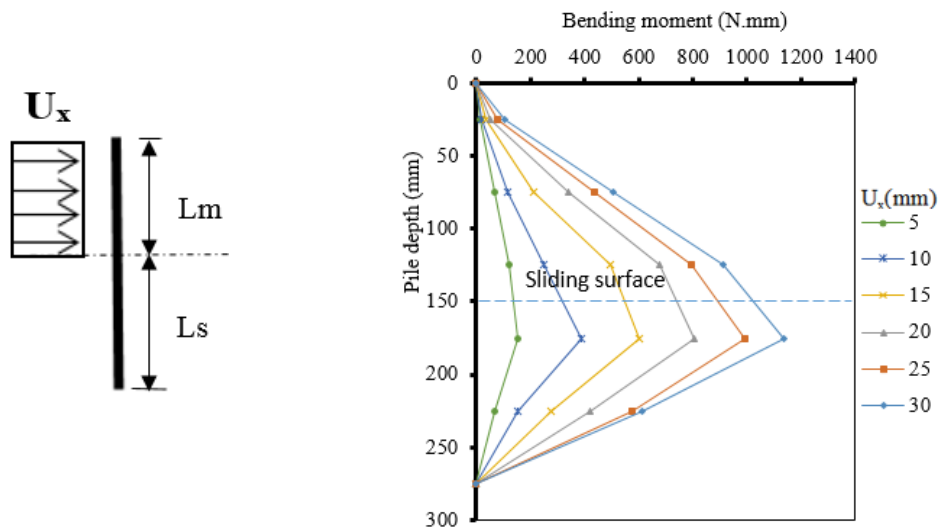


Fig. A.5 Single batter pile response, test (RSF16, 0°)

Test number	RSF16, 0	Density kN/m ³	15.2	Batter angle (β) (degree)	0
Pile-head condition)	Free-head	Soil moving Profile	rectangular		
Moving layer, L_m (mm)	125	Stable layer, L_s (mm)	150	Diameter (mm)	16

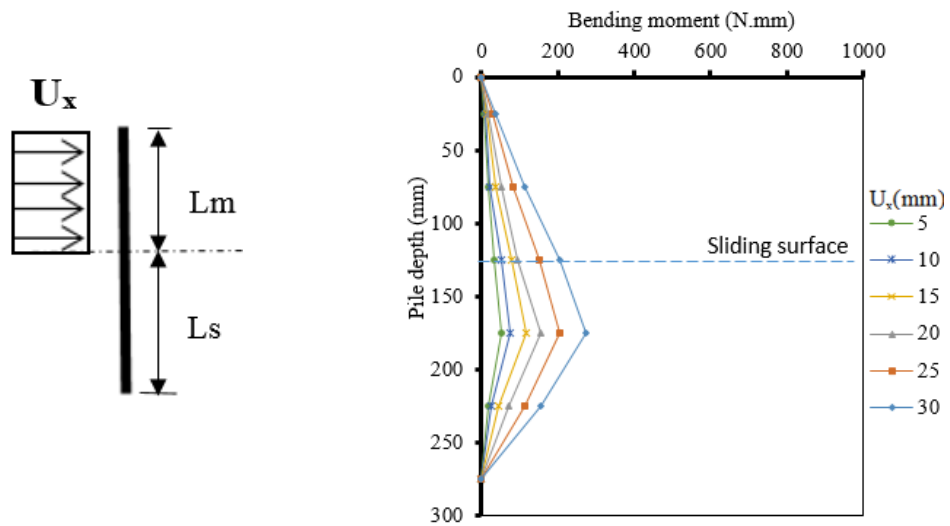


Fig. A.6 Single batter pile response, test (RSF16, 0°)

Test number	RSF16, +10	Density kN/m ³	15.2	Batter angle (β) (degree)	+10
Pile-Head condition)	Free-head	Soil moving Profile	rectangular		
Moving layer, L_m (mm)	150	Stable layer, L_s (mm)	150	Diameter (mm)	16

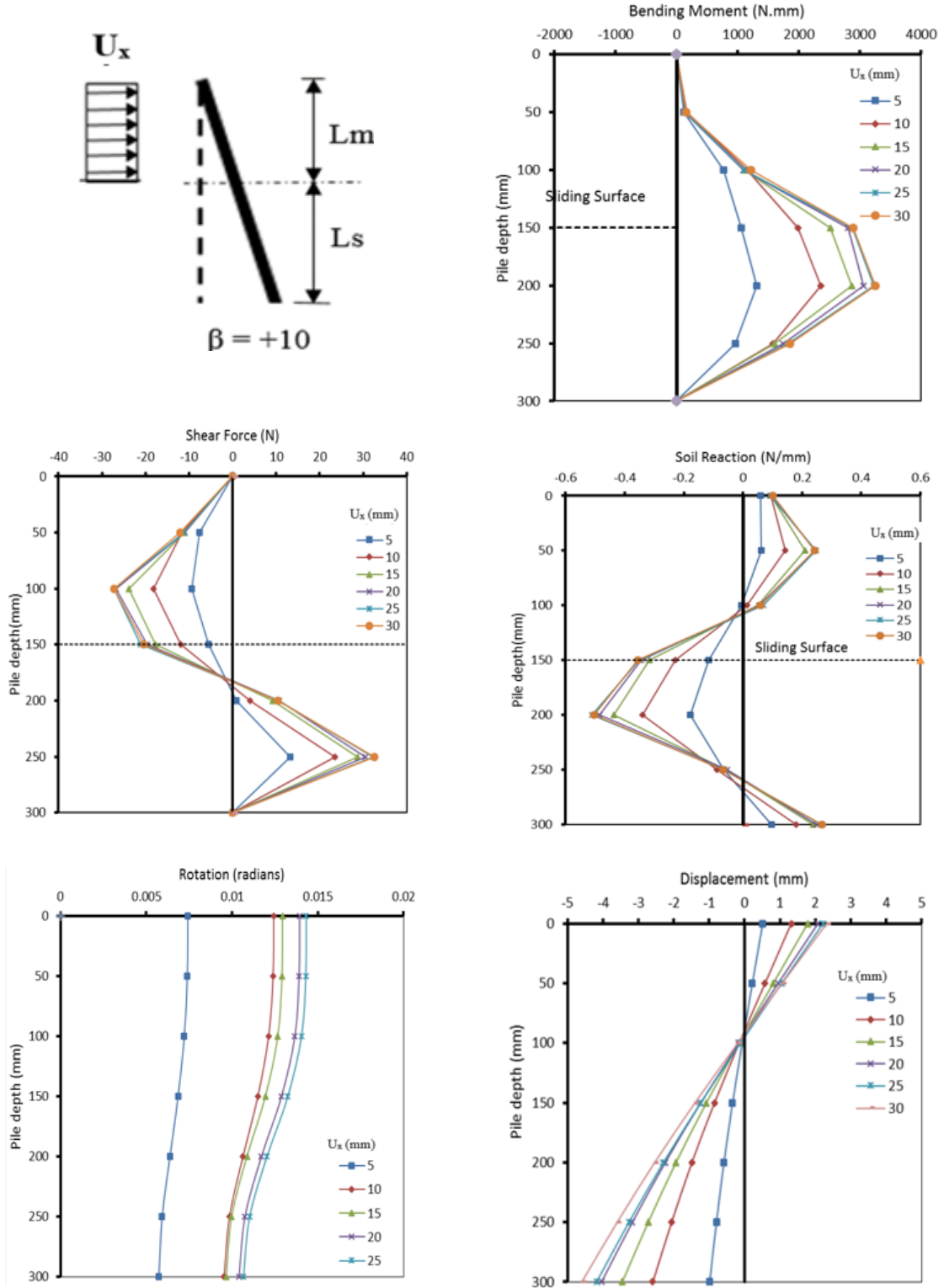


Fig. A.7 Single batter pile responses of test RSF16, +10°

Test number	RSF16, +20	Density KN/m ³	15.2	Batter angle (β)	+20
Pile-head condition)	Free-head	Soil moving Profile	rectangular	(degree)	
Moving layer, L_m (mm)	150	Stable layer, L_s (mm)	150	Diameter (mm)	16

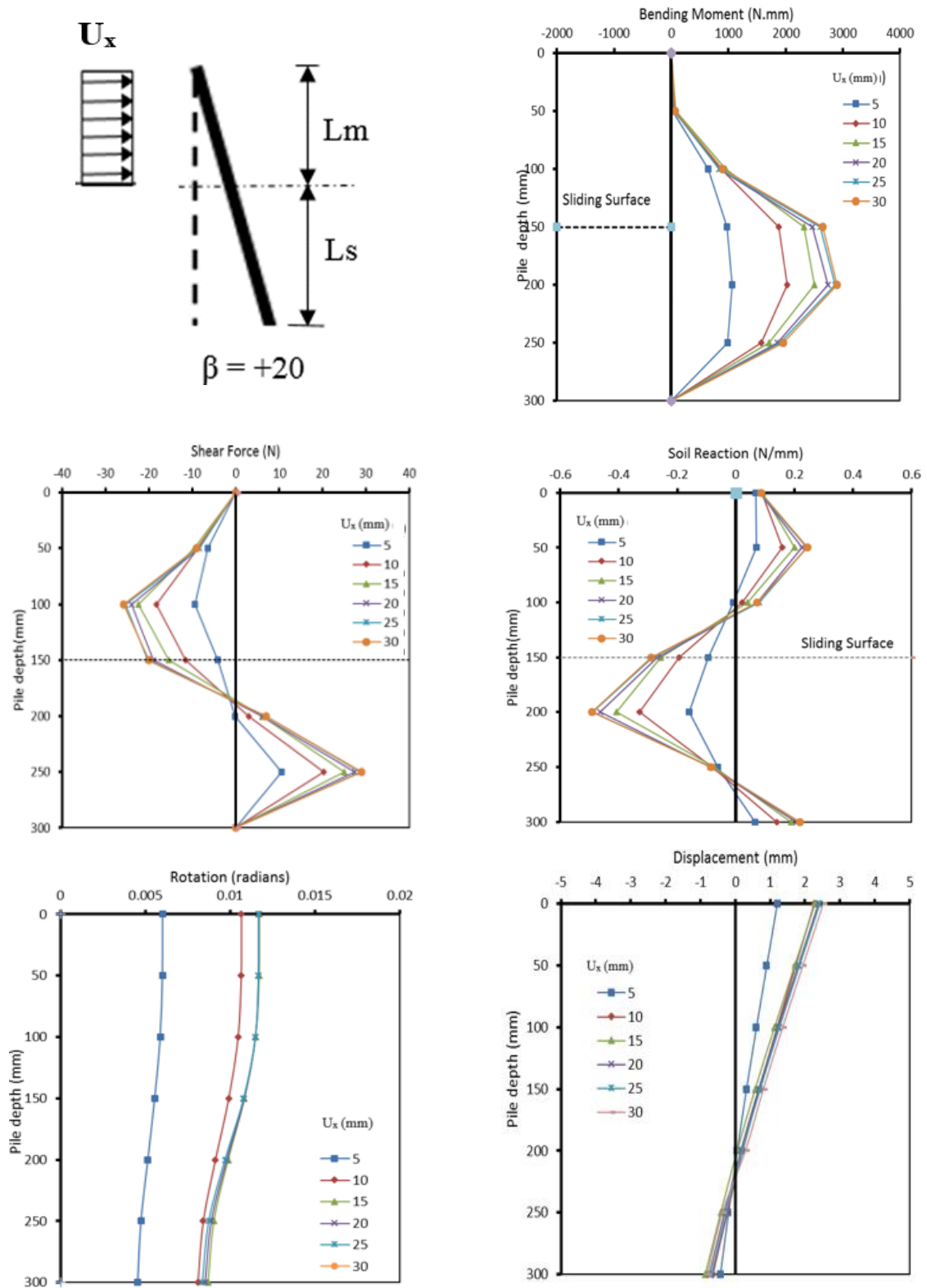


Fig. A.8 Single batter pile response, test (RSF16, +20°)

Test number	RSF16, -10	Density kN/m ³	15.2	Batter angle (β) (degree)	-10
Pile-head condition)	Free-head	Soil moving Profile	rectangular		
Moving layer, L_m (mm)	150	Stable layer, L_s (mm)	150	Diameter (mm)	16

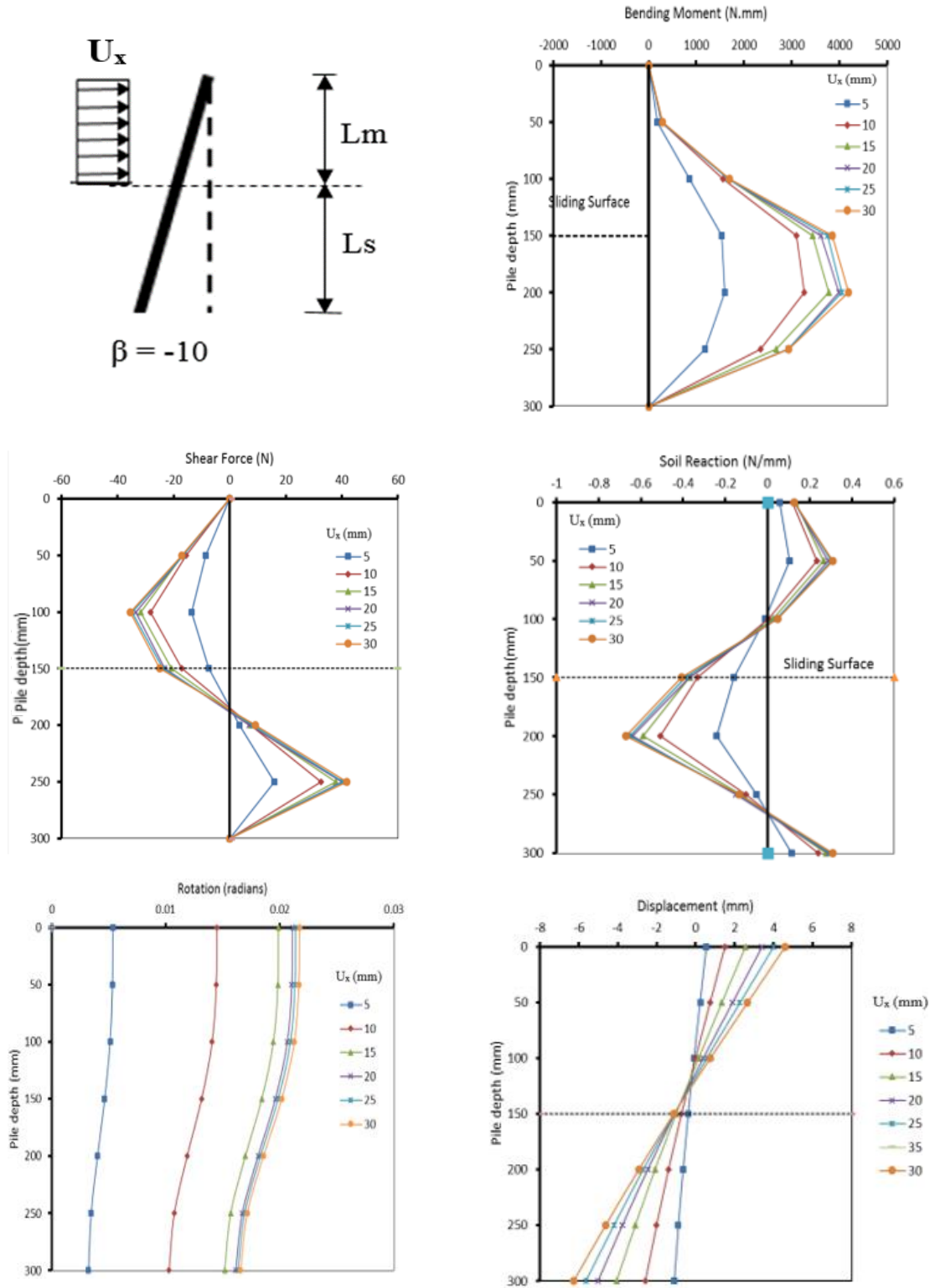


Fig. A.9 Single batter pile response, test (RSF16, -10°)

Test number	RSF16, -20	Density kN/m ³	15.2	Batter angle (β)	-20
Pile-head condition)	Free-head	Soil moving Profile	rectangular	(degree)	
Moving layer, L_m (mm)	150	Stable layer, L_s (mm)	150	Diameter (mm)	16

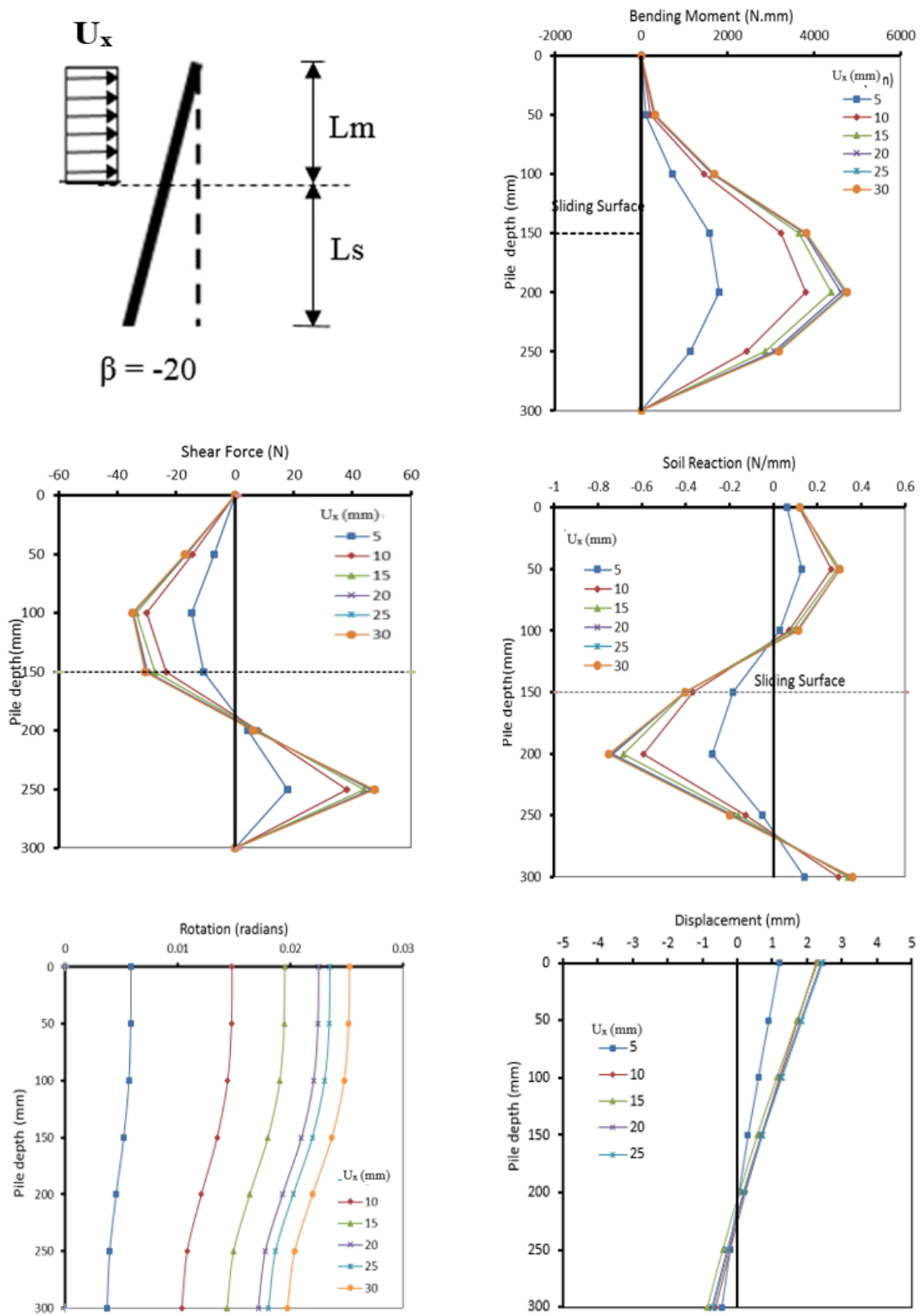


Fig. A.10 Single batter pile response, test (RSF16, -20°)

Test number	RSF16, 0	Density kN/m^3	15.2	Batter angle (β) (degree)	0
Pile-Head condition)	Free-head	Soil moving Profile	rectangular		
Moving layer, L_m (mm)	150	Stable layer, L_s (mm)	150	Diameter (mm)	16

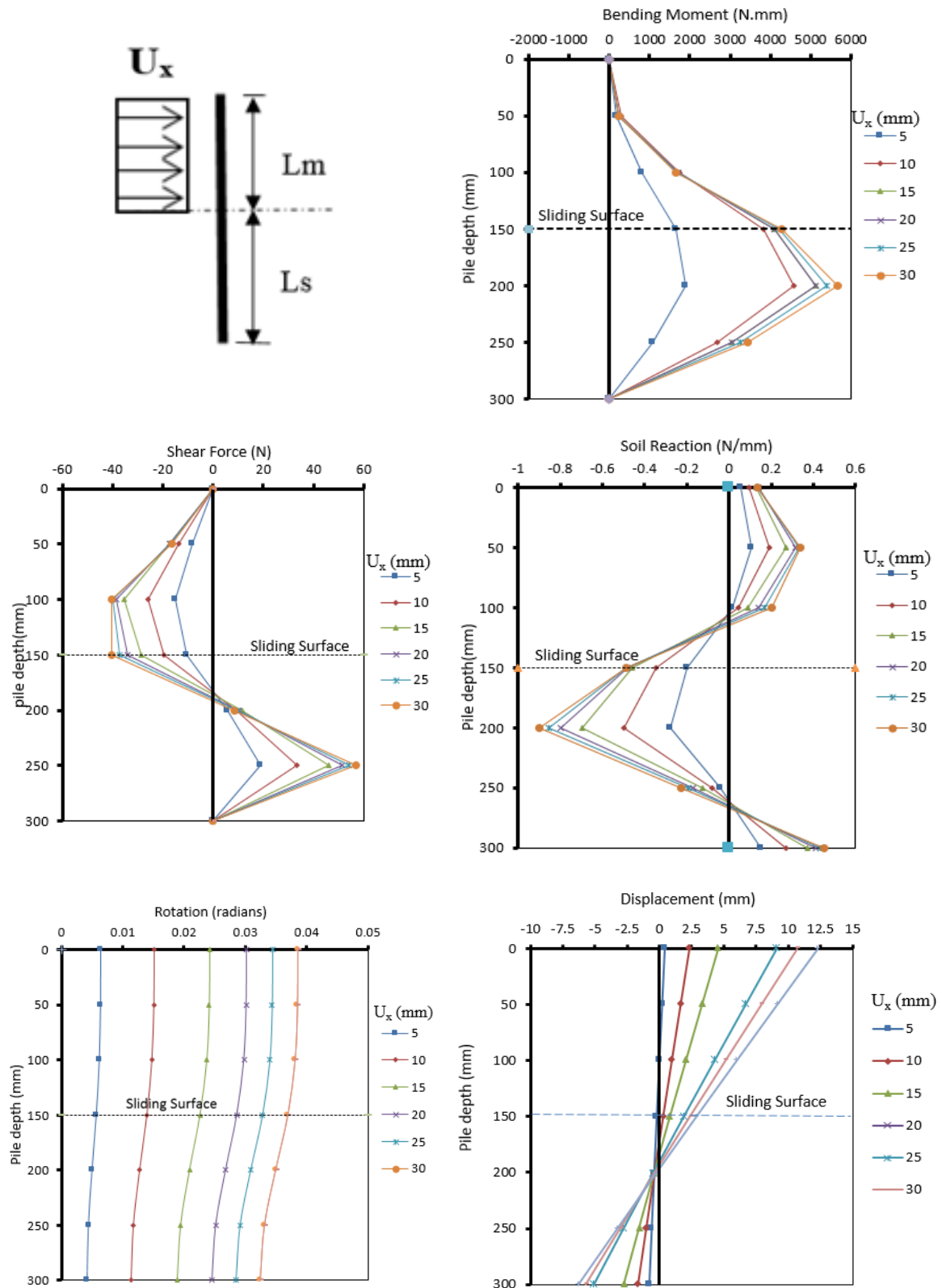


Fig. A.11 Single batter pile responses of test RSF16, 0° , $d_s=200$ mm

Test number	RSF16, 0	Density kN/m ³	15.2	Batter angle (β) (degree)	0
Pile-Head condition)	Free-head	Soil moving Profile	rectangular		
Moving layer, L_m (mm)	150	Stable layer, L_s (mm)	150	Diameter (mm)	16

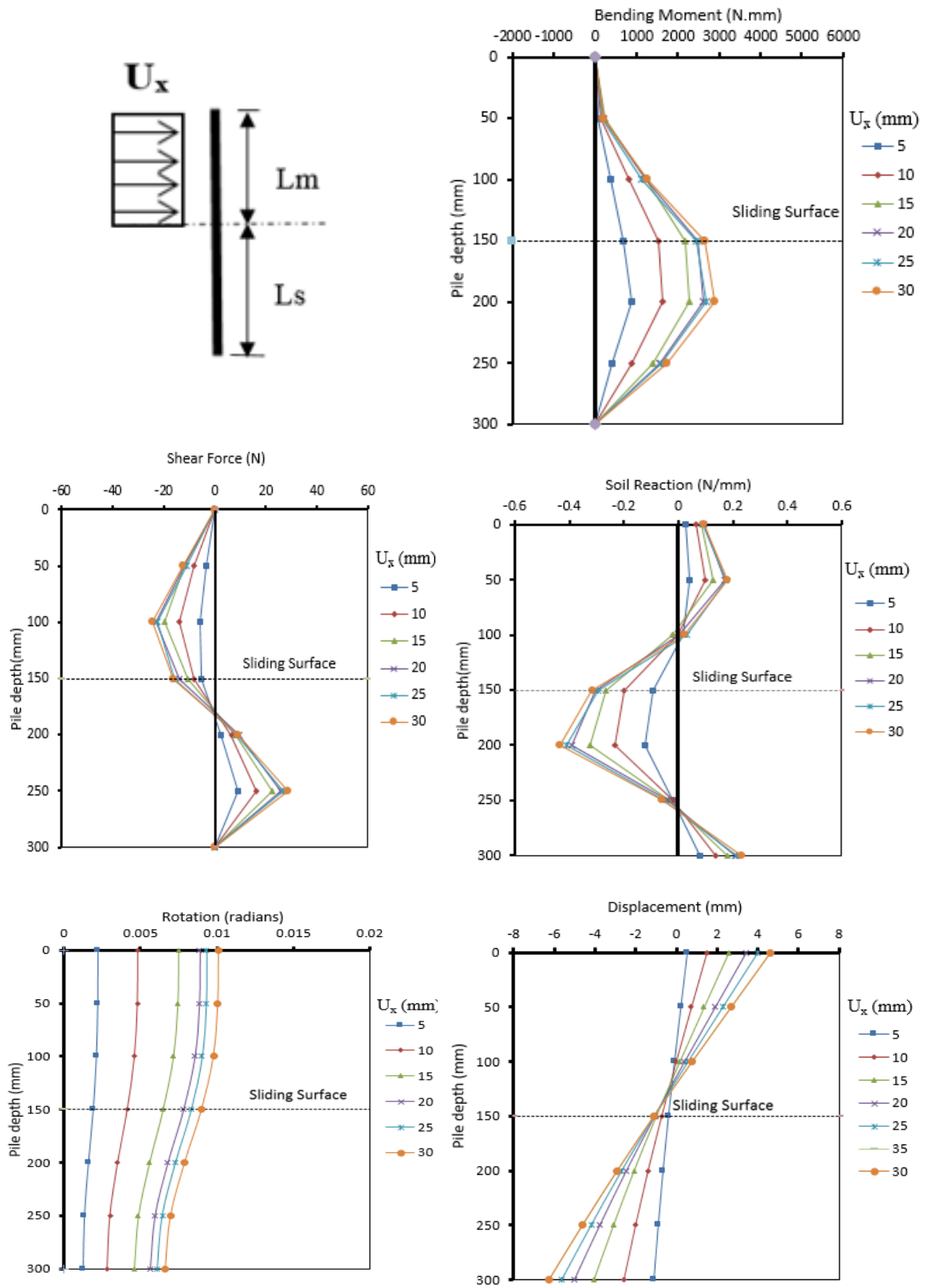


Fig. A.12 Single batter pile responses of test RSF16, 0°, $d_s = 400$ mm

Test number	RSF16, +10	Density kN/m ³	15.2	Batter angle (β) (degree)	+10
Pile-Head condition)	Free-head	Soil moving Profile	rectangular		
Moving layer, L_m (mm)	150	Stable layer, L_s (mm)	150	Diameter (mm)	16

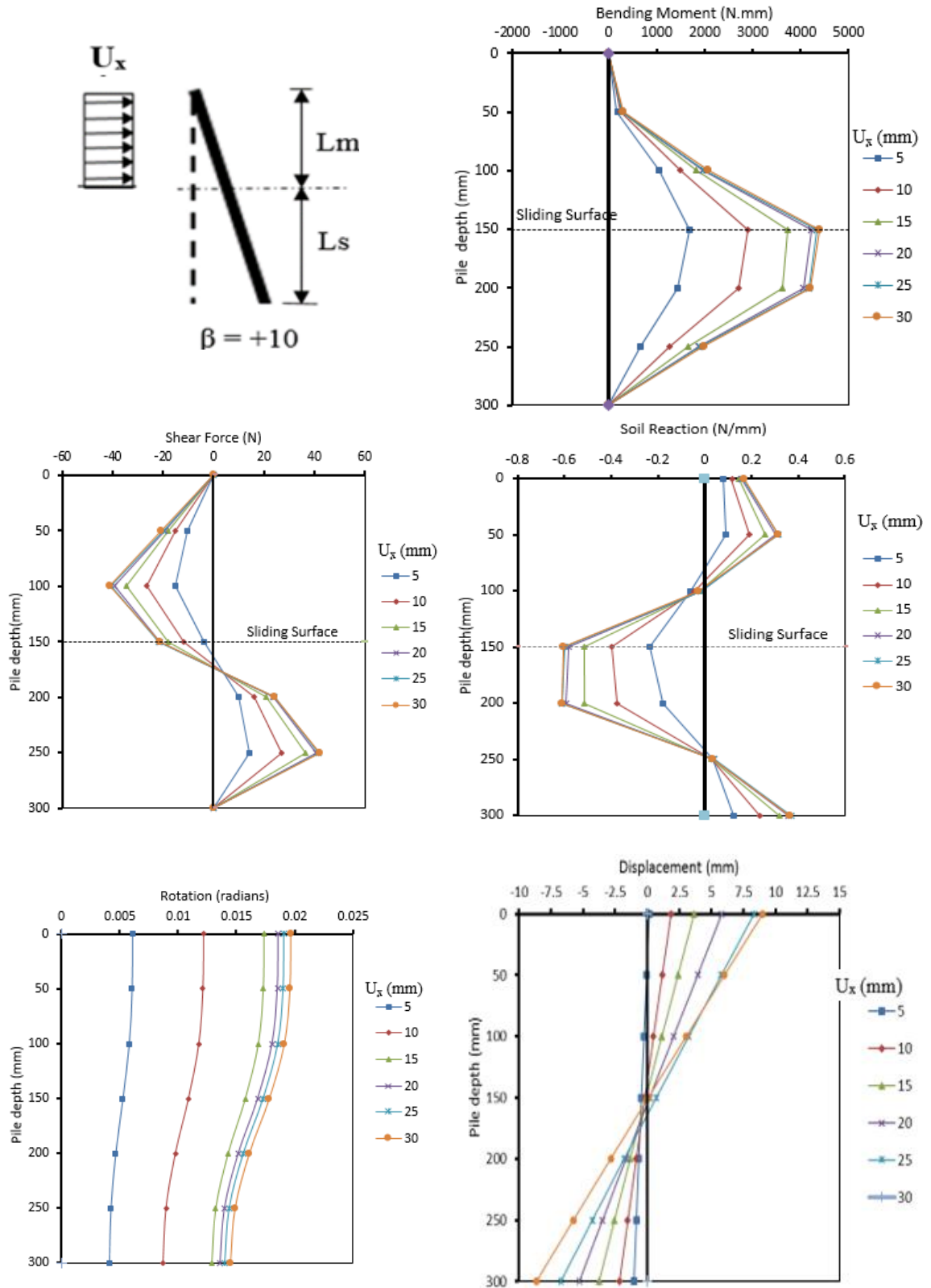


Fig. A.13 Single batter pile responses of test RSF16, +10°, $d_s = 200$ mm

Test number	RSF16, +10	Density kN/m ³	15.2	Batter angle (β) (degree)	+10
Pile-Head condition)	Free-head	Soil moving Profile	rectangular		
Moving layer, L_m (mm)	150	Stable layer, L_s (mm)	150	Diameter (mm)	16

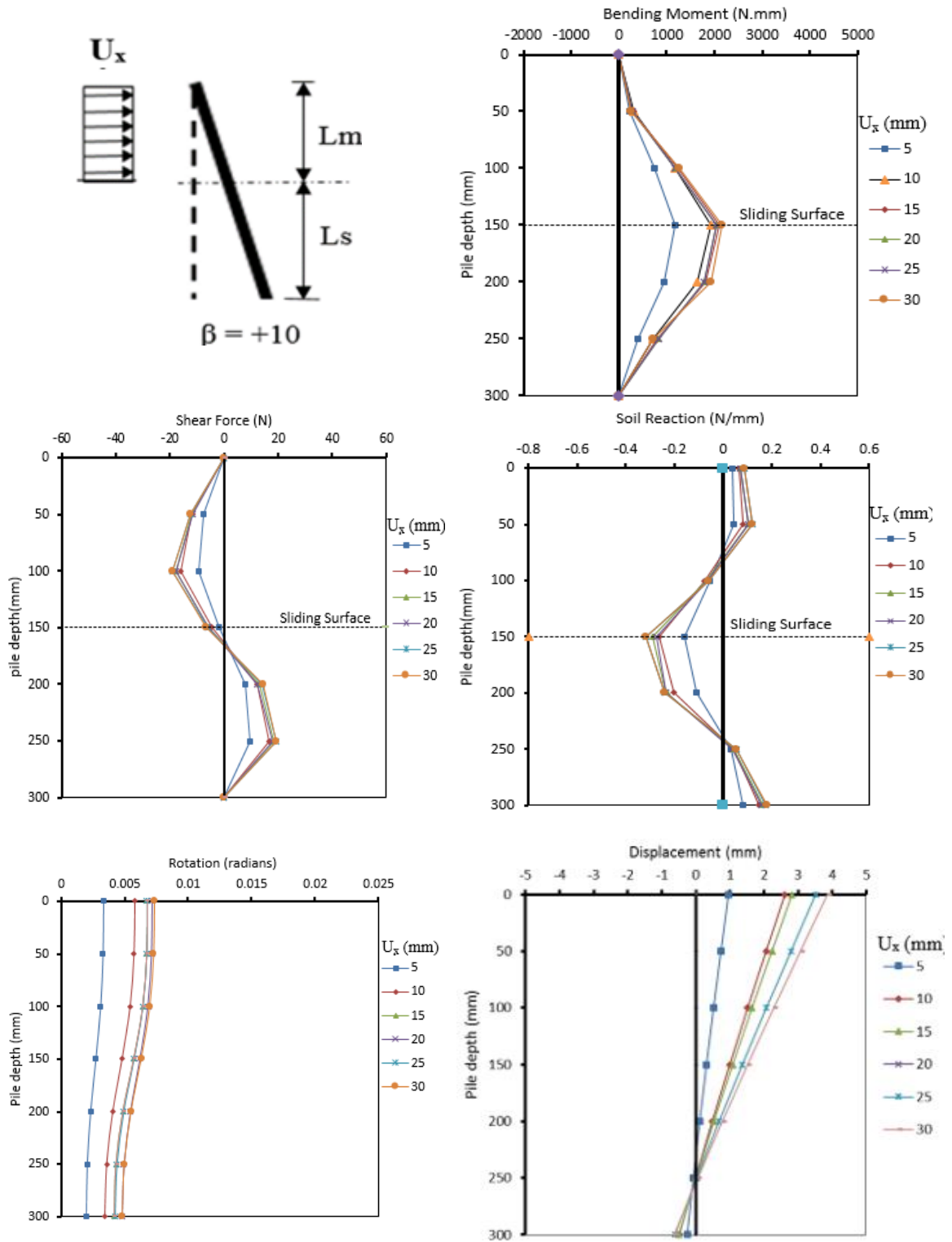


Fig. A.14 Single batter pile responses of test RSF16, +10°, $d_s = 400$ mm

Test number	RSL16, 0	Density kN/m ³	15.2	Batter angle (β) (degree)	0
Pile-head condition)	Fixed-head	Soil Moving Profile	rectangular		
Moving layer, L _m (mm)	150	Stable layer, L _s (mm)	150	Diameter (mm)	16

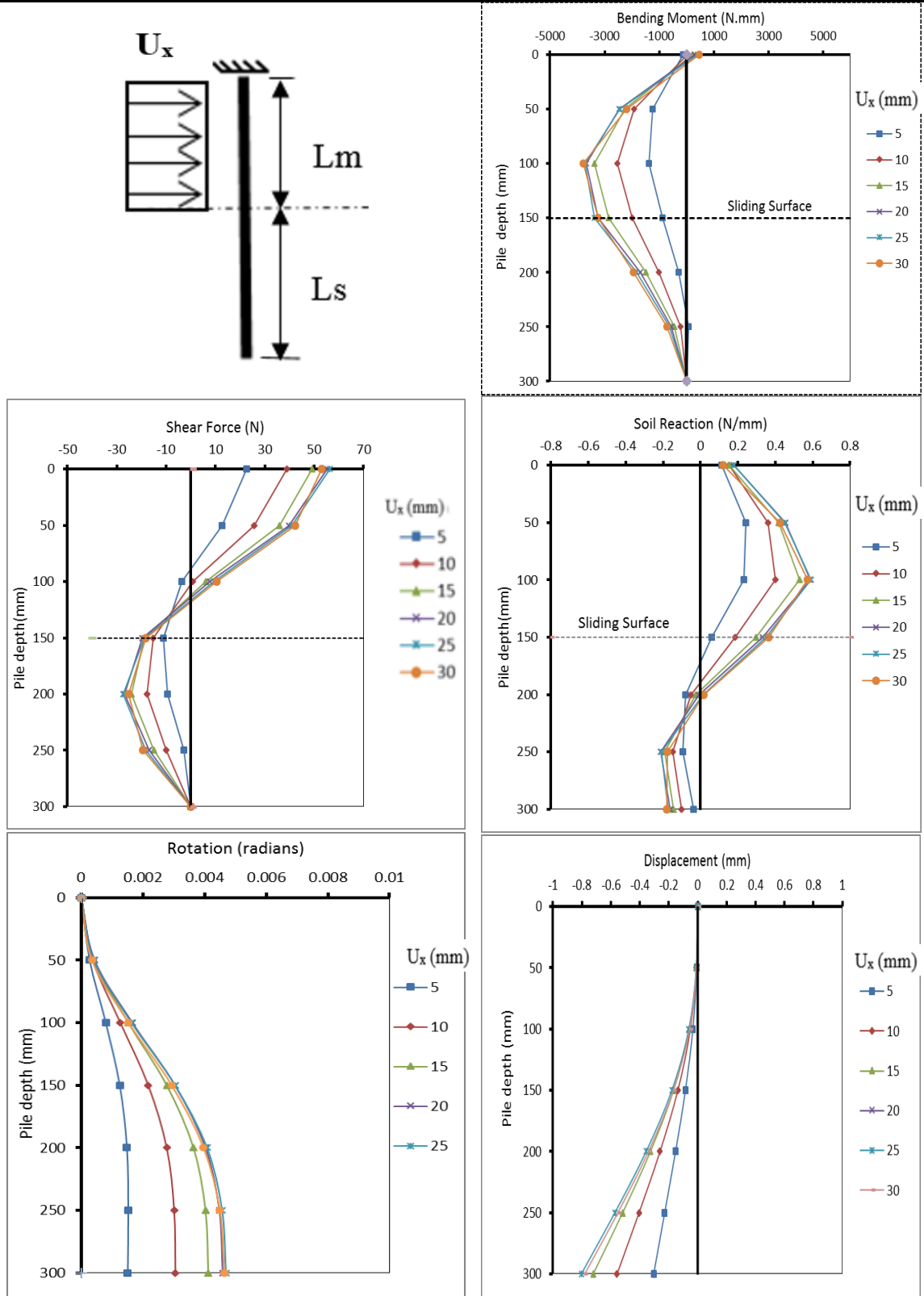


Fig. A.15 Single batter pile response, test (RSL16, 0°)

Test number	RSL16, +10	Density kN/m ³	15.2	Batter angle (β) (degree)	+10
Pile-head condition)	Free-head	Soil moving Profile	rectangular		
Moving layer, L _m (mm)	150	Stable layer, L _s (mm)	150	Diameter (mm)	20

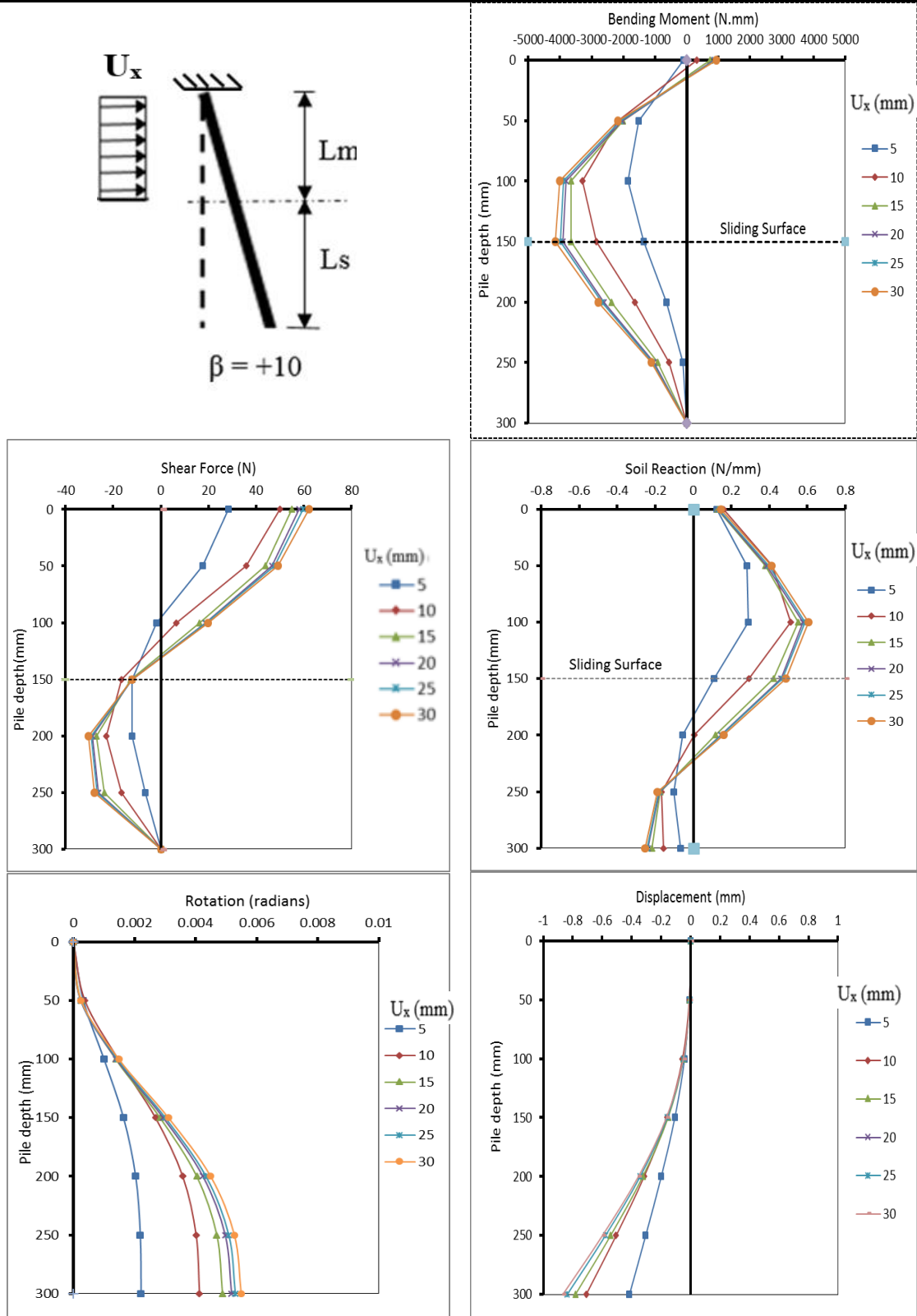


Fig. A.16 Single batter pile response, test (RSL16, +10°)

Test number	RSL16, +20	Density kN/m ³	15.2	Batter angle (β) (degree)	+20
Pile-head condition)	Fixed-head	Soil moving Profile	rectangular		
Moving layer, L _m (mm)	150	Stable layer, L _s (mm)	150	Diameter (mm)	16

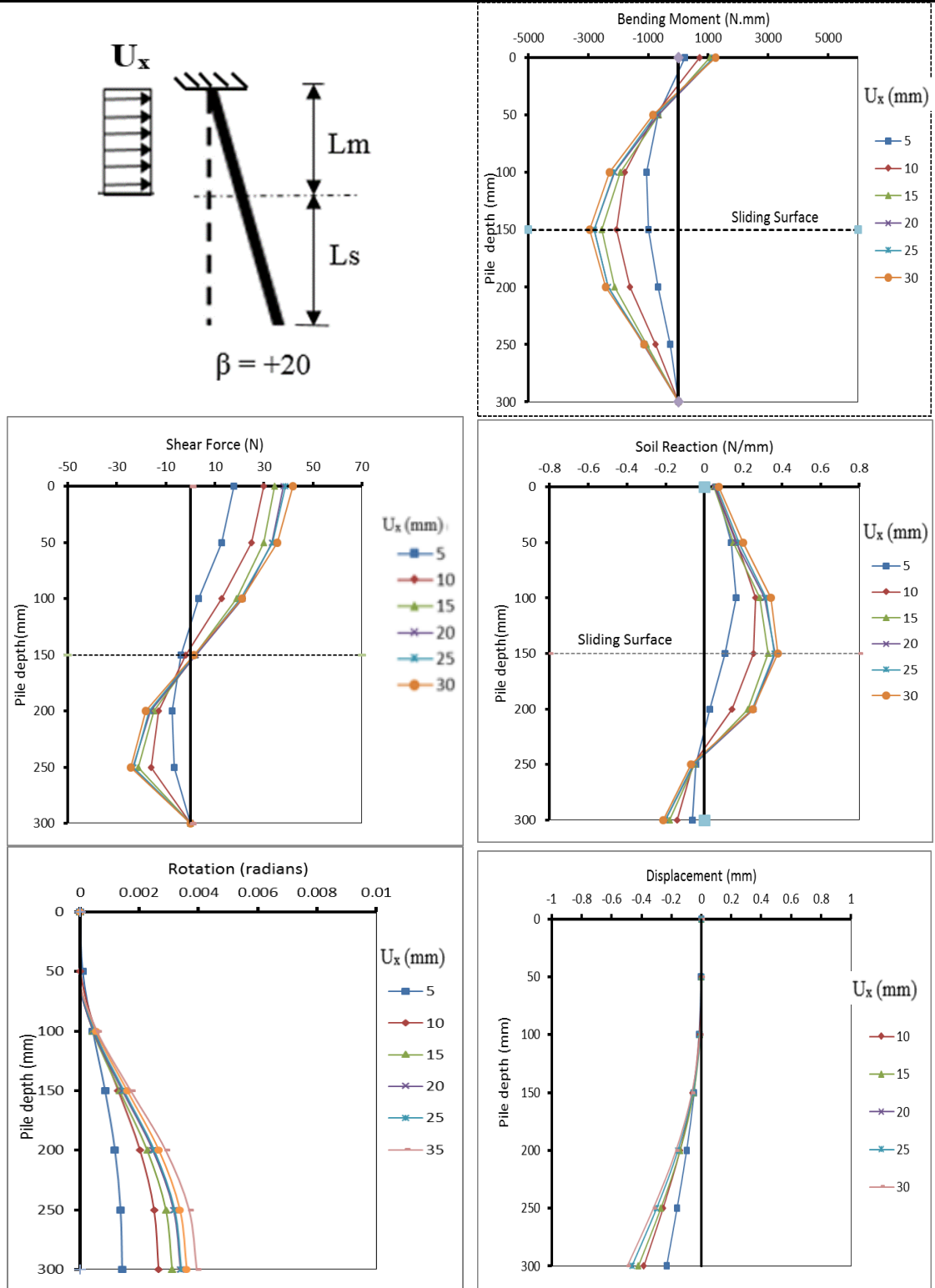


Fig. A.17 Single batter pile response, test (RSL16, +20°)

Test number	RSL16, -10	Density kN/m ³	15.2	Batter angle (β) (degree)	-10
Pile-head condition)	Fixed-head	Soil moving Profile	rectangular		
Moving layer, L _m (mm)	150	Stable layer, L _s (mm)	150	Diameter (mm)	16

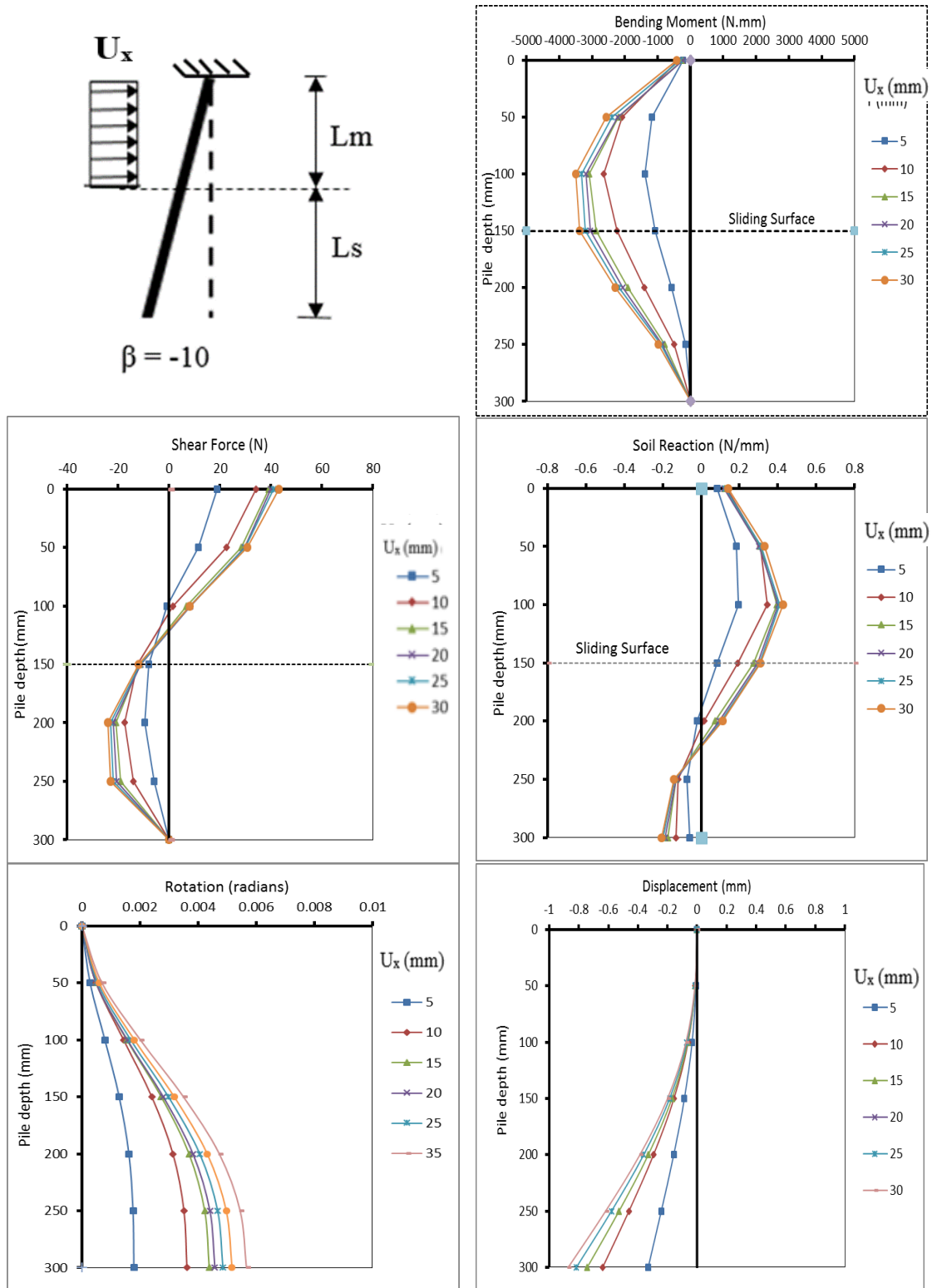


Fig. A.18 Single batter pile response, test (RSL16, -10°)

Test number	RSL16, -20	Density kN/m ³	15.2	Batter angle (β) (degree)	-20
Pile-head condition)	Fixed-head	Soil Moving Profile	Triangular		
Moving layer, L _m (mm)	150	Stable layer, L _s (mm)	150	Diameter (mm)	16

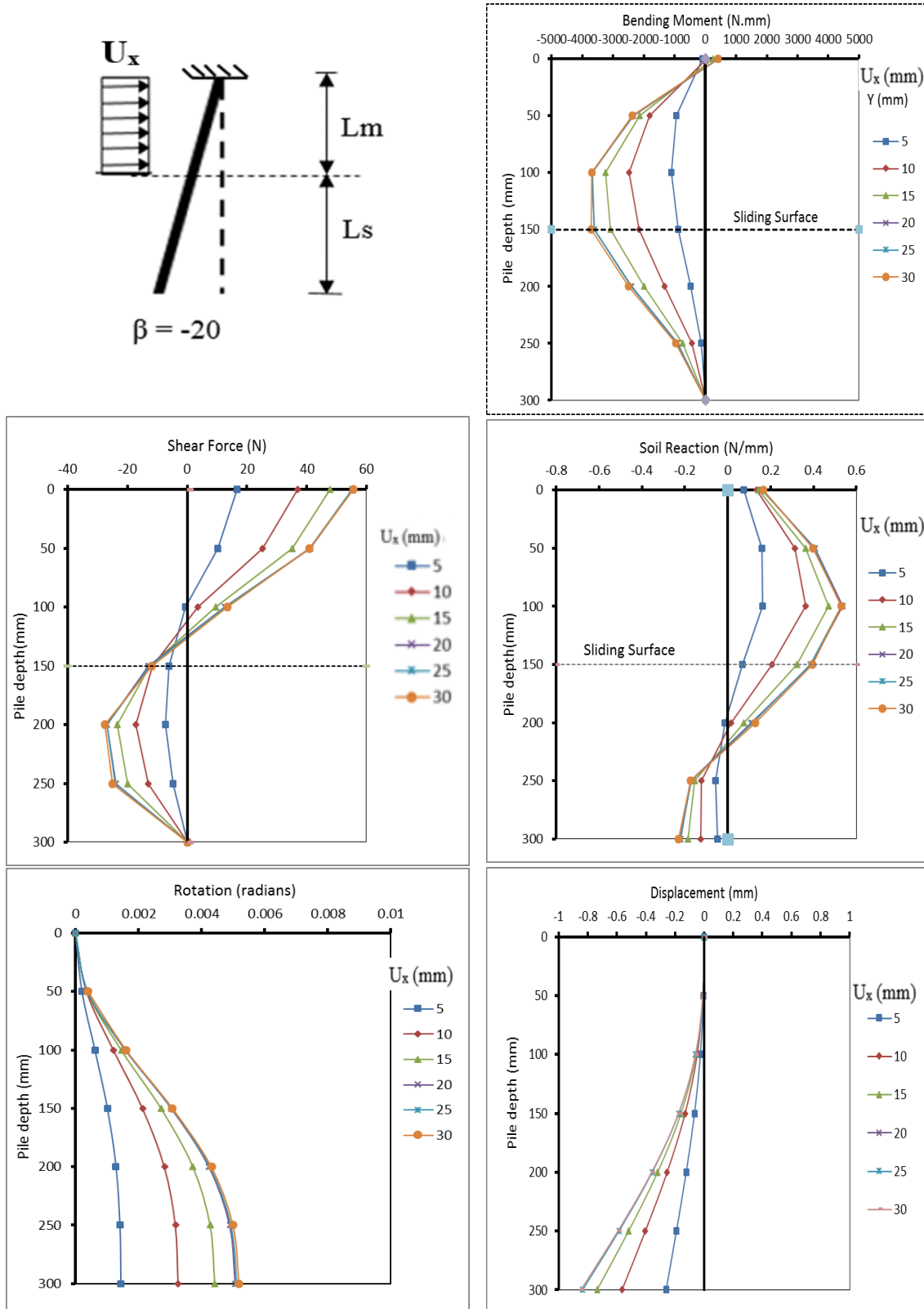


Fig. A.19 Single batter pile response, test (RSL16, -20°)

Test number	RSF20, 0	Density kN/m ³	15.2	Batter angle (β) (degree)	0
Pile-head condition)	Free-head	Soil moving Profile	rectangular		
Moving layer, L_m (mm)	150	Stable layer, L_s (mm)	150	Diameter (mm)	20

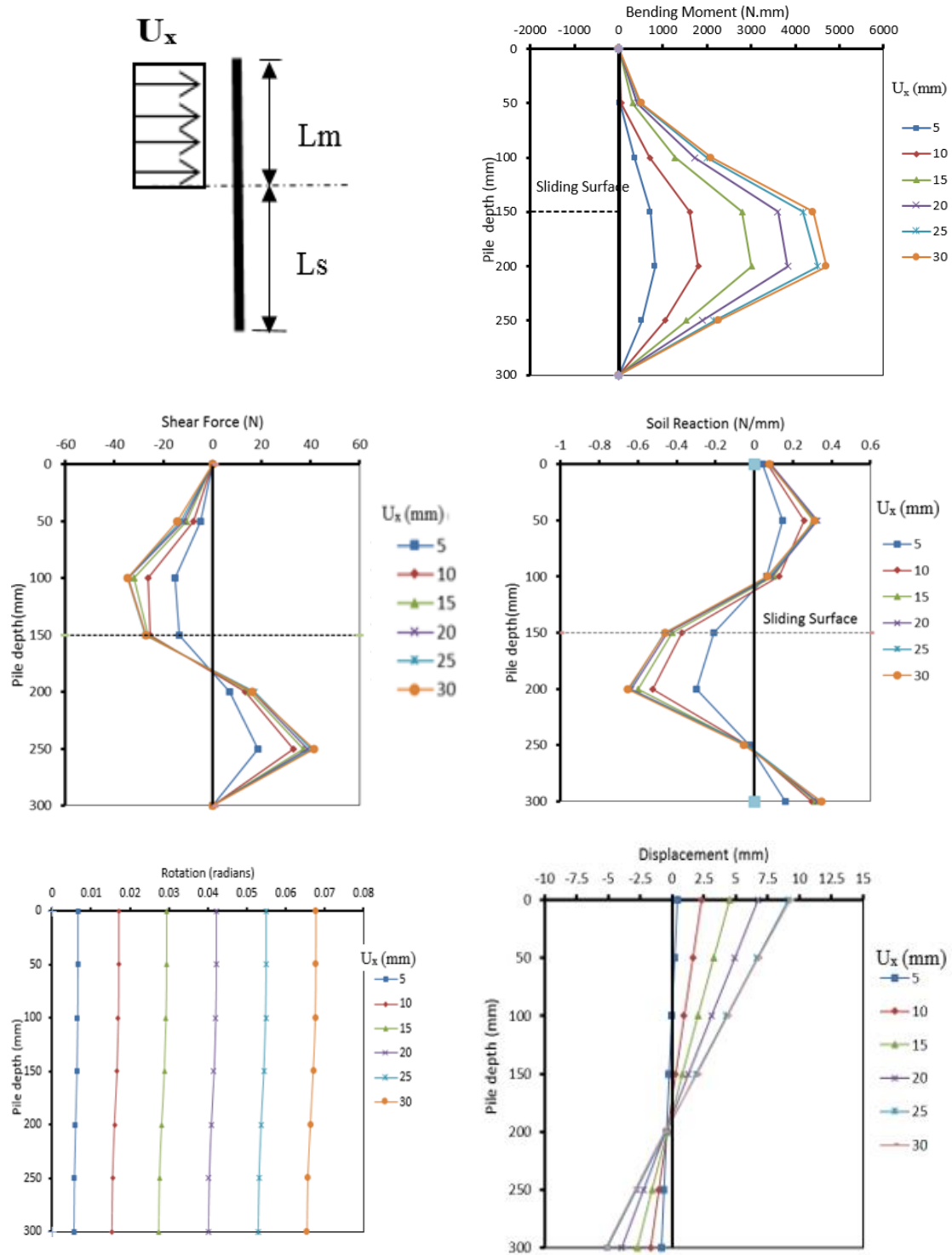


Fig. A.20 Single batter pile response, test (RSF20, 0°)

Test number	RSF20, +10	Density kN/m ³	15.2	Batter angle (β) (degree)	+10
Pile-head condition)	Free-head	Soil moving Profile	rectangular		
Moving layer, L_m (mm)	150	Stable layer, L_s (mm)	150	Diameter (mm)	20

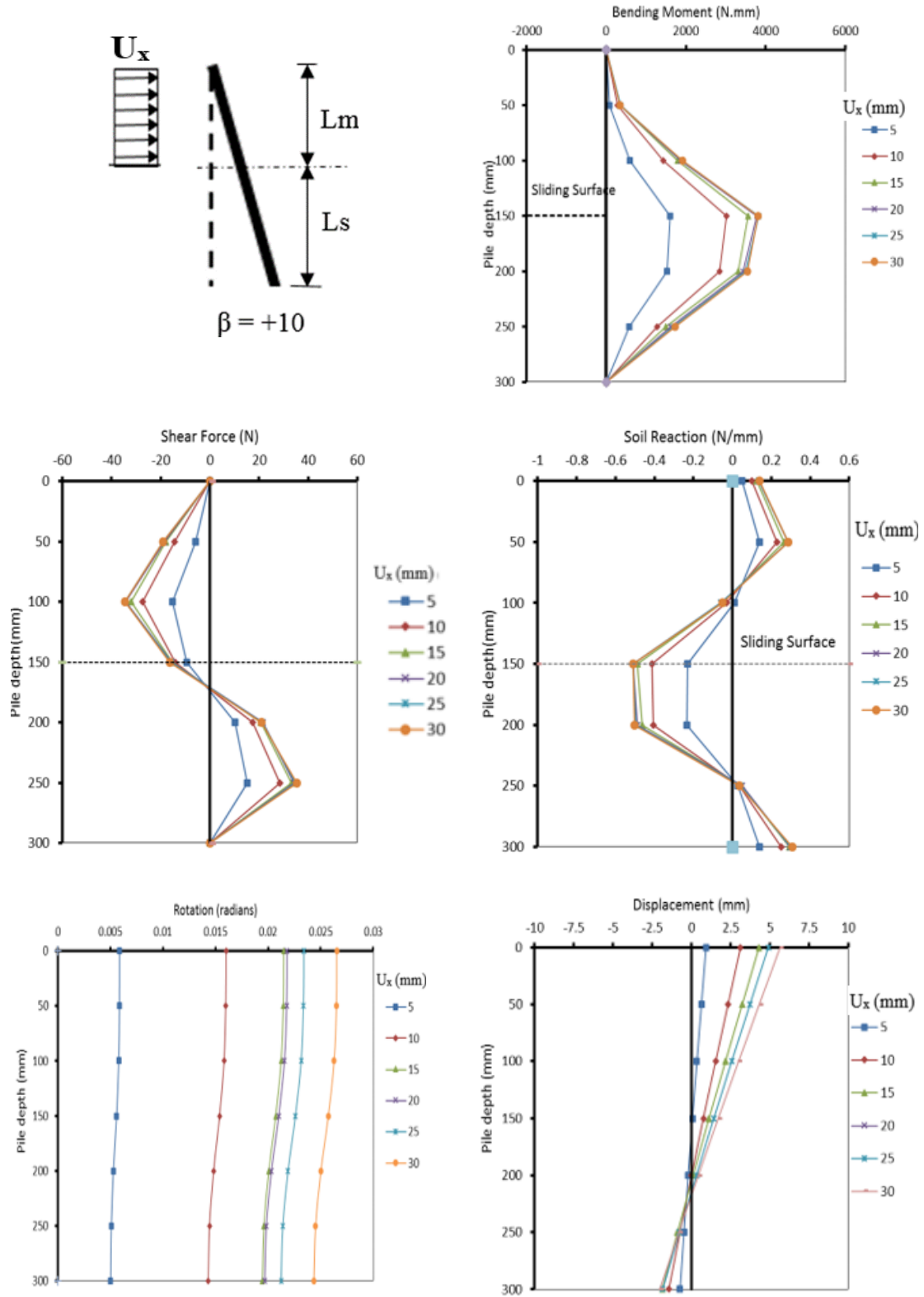


Fig. A.21 Single batter pile response, test (RSF20, +10°)

Test number	RSF20, +20	Density kN/m ³	15.2	Batter angle (β) (degree)	+20
Pile-head condition)	Free-head	Soil moving Profile	rectangular		
Moving layer, L_m (mm)	150	Stable layer, L_s (mm)	150	Diameter (mm)	20

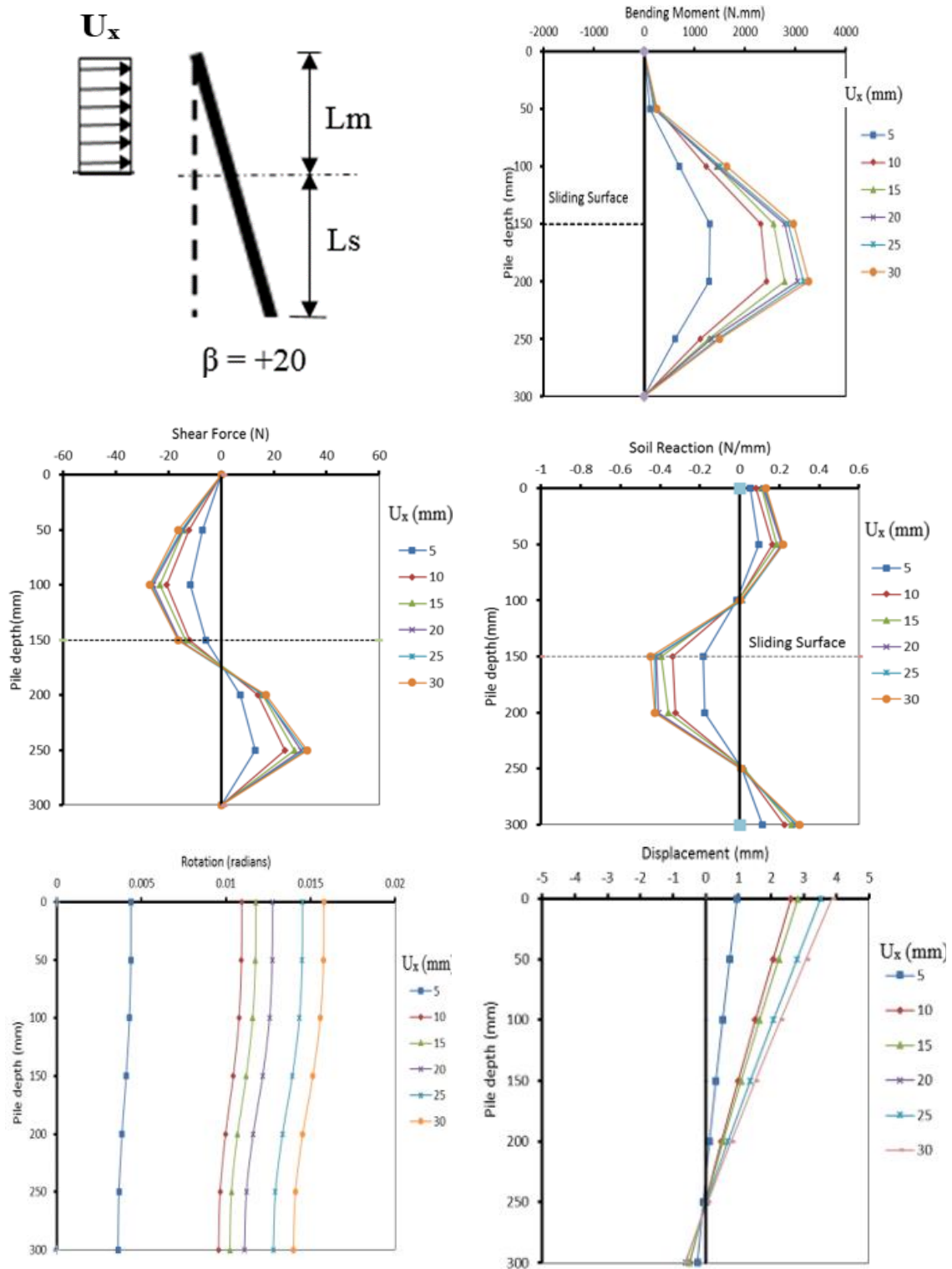


Fig. A.22 Single batter pile response, test (RSF20, +20°)

Test number	RSF20, -10	Density kN/m ³	15.2	Batter angle (β)	-10
Pile-head condition)	Free-head	Soil moving Profile	rectangular	(degree)	
Moving layer, L_m (mm)	150	Stable layer, L_s (mm)	150	Diameter (mm)	20

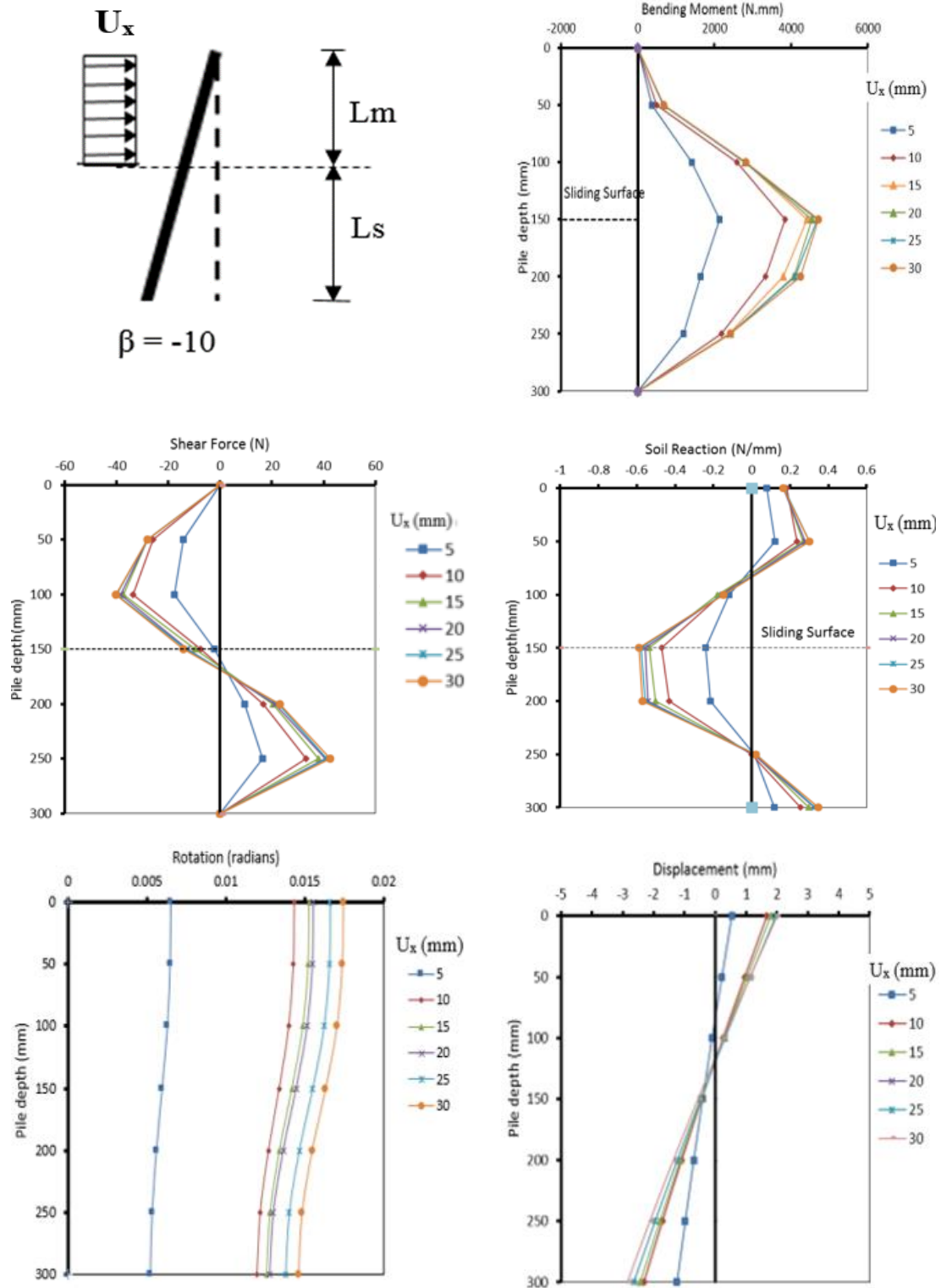


Fig. A.23 Single batter pile response, test (RSF20, -10°)

Test number	RSF20, -20	Density kN/m ³	15.2	Batter angle (β) (degree)	-20
Pile-head condition)	Free-head	Soil moving Profile	rectangular		
Moving layer, L_m (mm)	150	Stable layer, L_s (mm)	150	Diameter (mm)	20

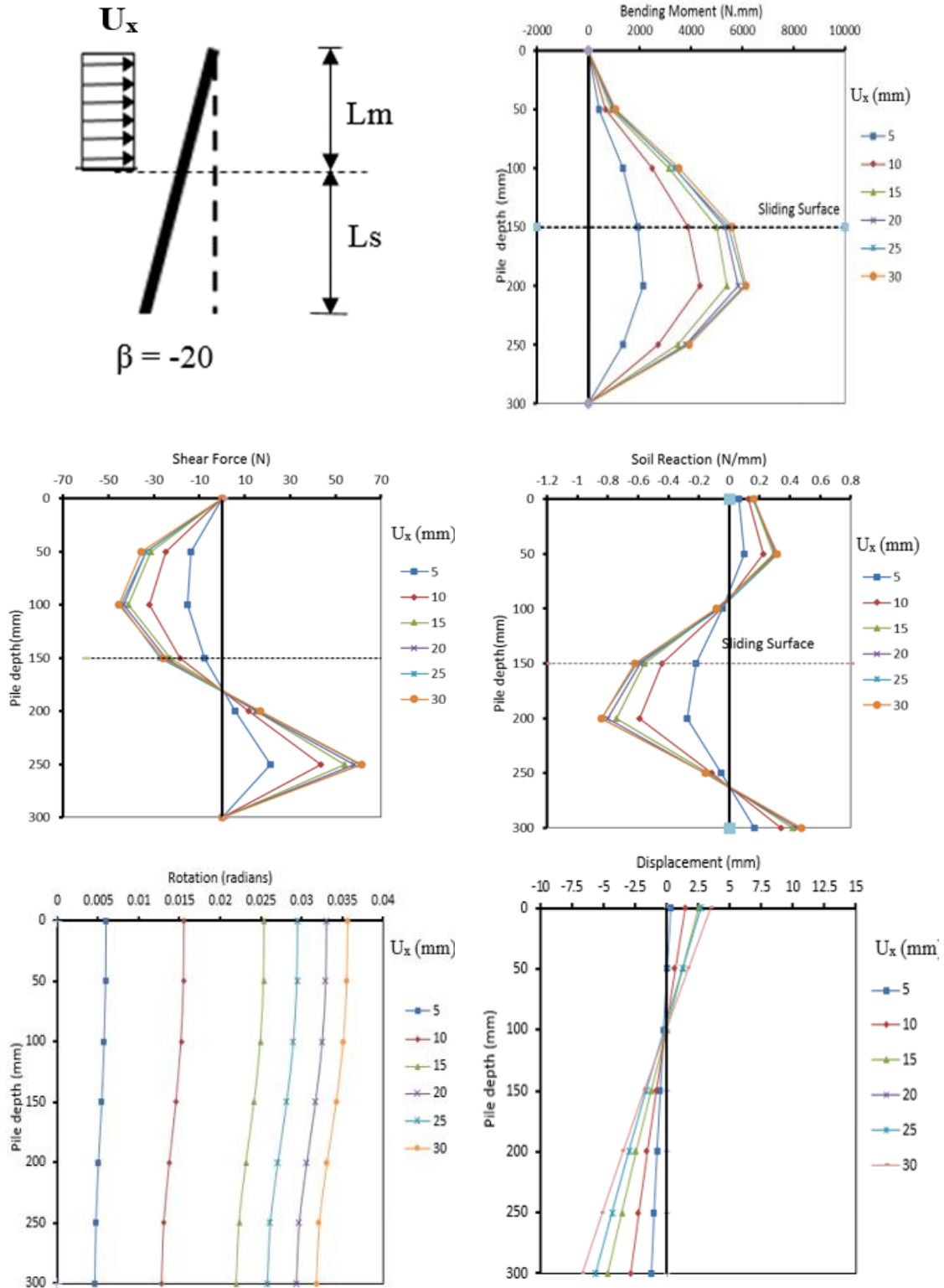


Fig. A.24 Single batter pile response, test (RSF20, -20°)

Test number	RSF25, 0	Density kN/m ³	15.2	Batter angle (β) (degree)	0
Pile-head condition)	Free-head	Soil moving Profile	rectangular		
Moving layer, L_m (mm)	150	Stable layer, L_s (mm)	150	Diameter (mm)	25

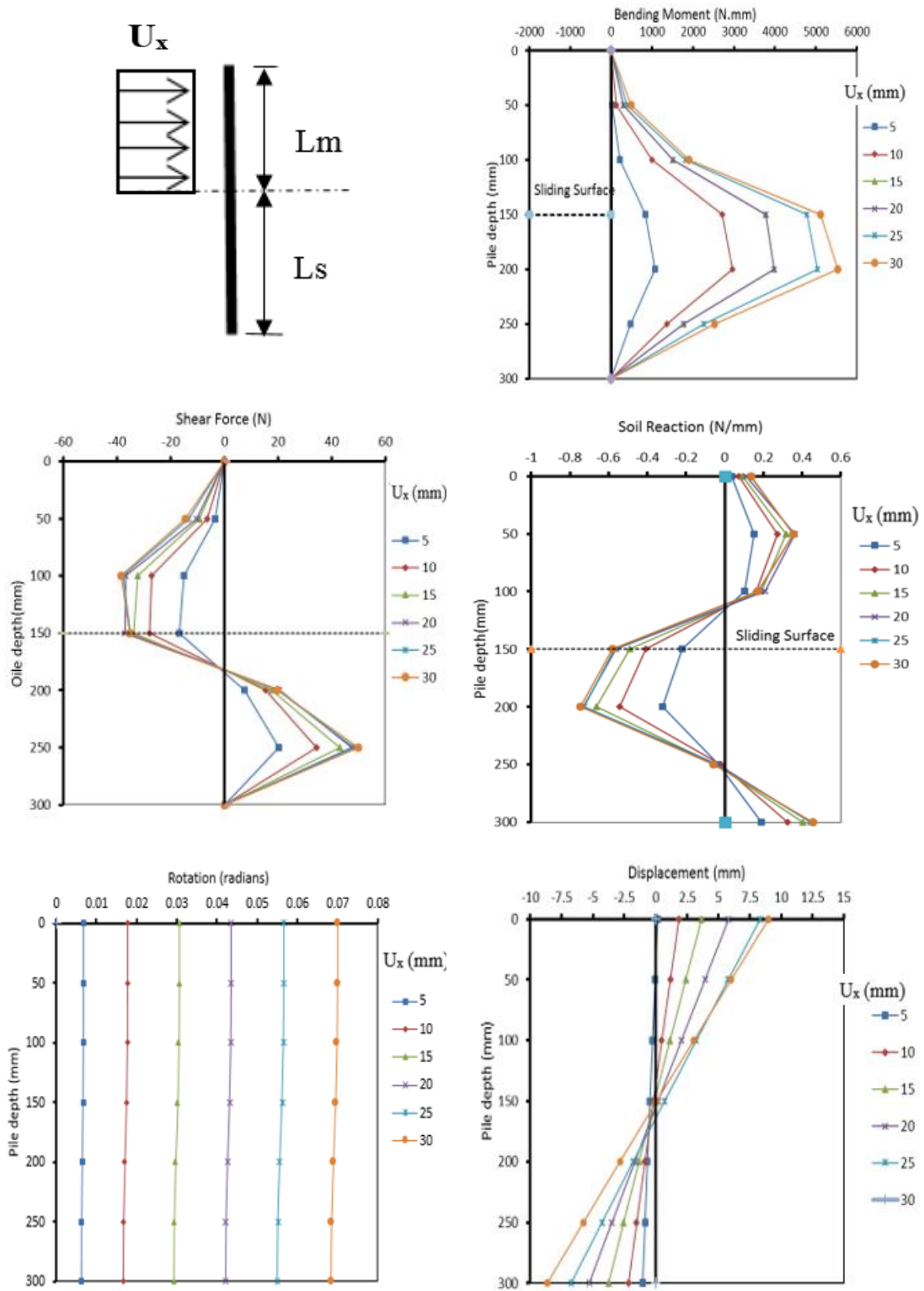


Fig. A.25 Single batter pile response, test (RSF25, 0°)

Test number	RSF25, +10	Density kN/m ³	15.2	Batter angle (β) (degree)	+10
Pile-head condition)	Free-head	Soil moving Profile	rectangular		
Moving layer, L_m (mm)	150	Stable layer, L_s (mm)	150	Diameter (mm)	25

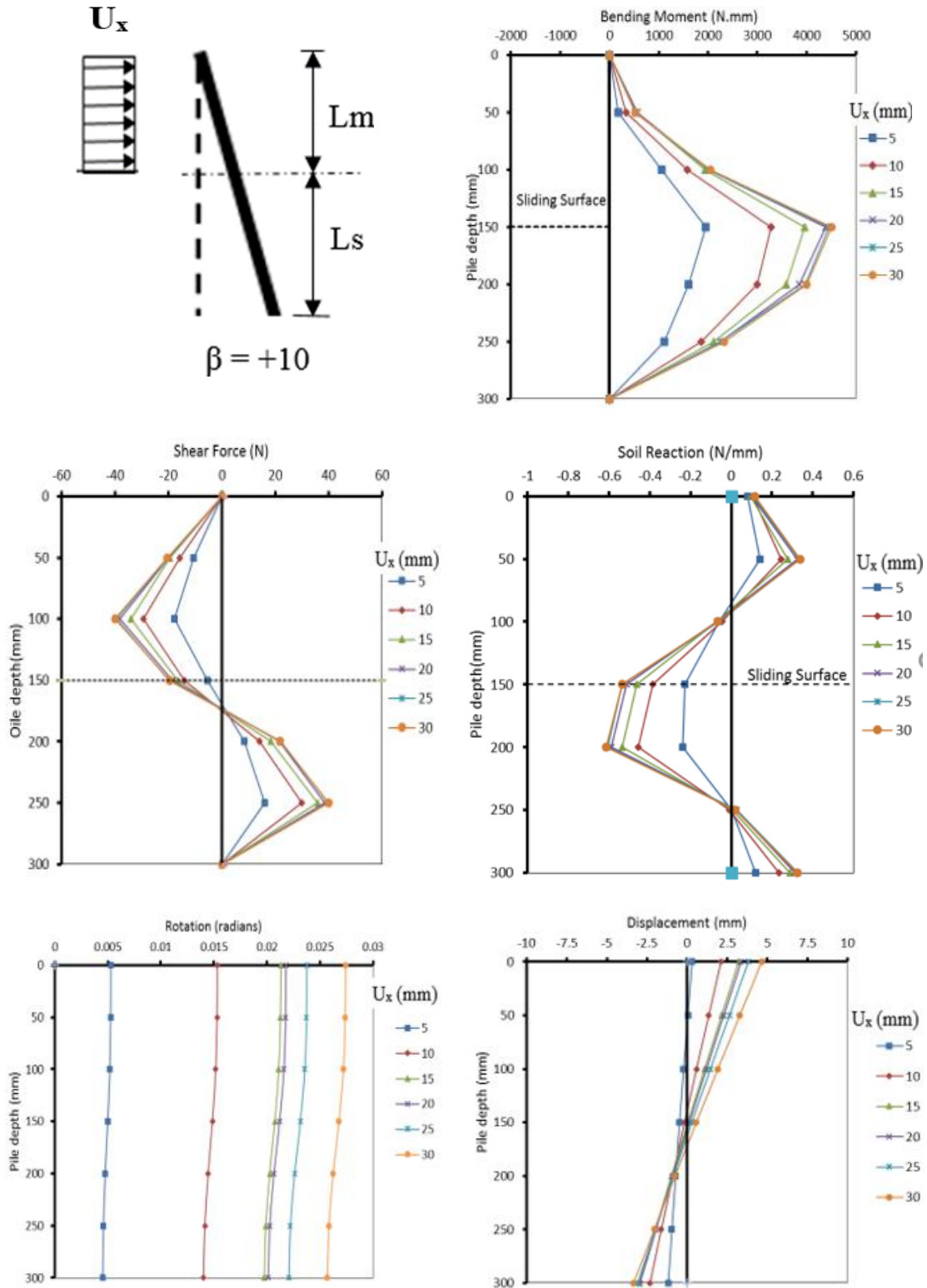


Fig. A.26 Single batter pile response, test (RSF25, +10°)

Test number	RSF25, +20	Density kN/m ³	15.2	Batter angle (β) (degree)	+20
Pile-head condition)	Free-head	Soil moving Profile	rectangular		
Moving layer, L _m (mm)	150	Stable layer, L _s (mm)	150	Diameter (mm)	25

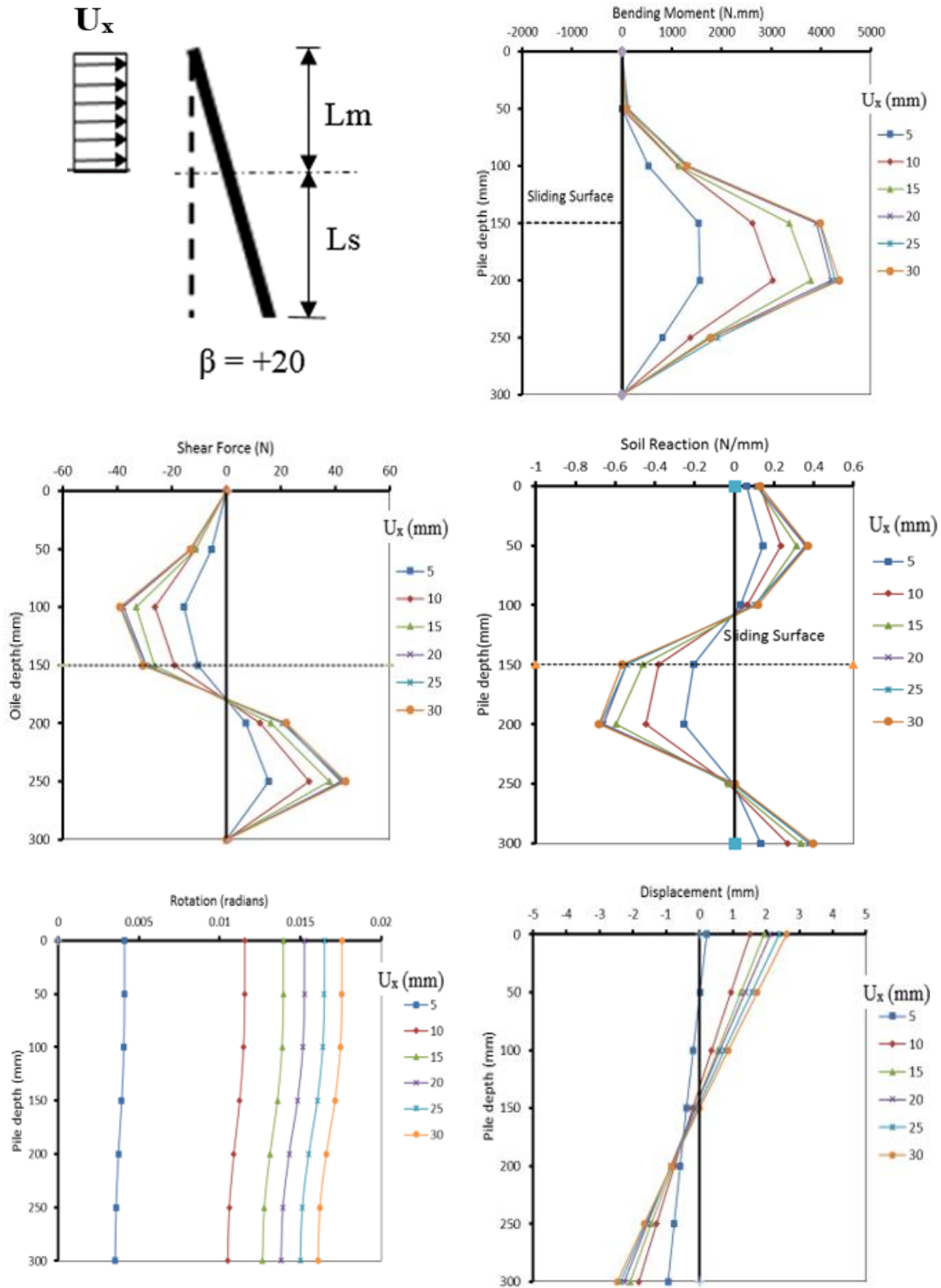


Fig. A.27 Single batter pile response, test (RSF25, +20°)

Test number	RSF25, -10	Density kN/m ³	15.2	Batter angle (β) (degree)	-10
Pile-head condition)	Free-head	Soil moving Profile	rectangular		
Moving layer, L_m (mm)	150	Stable layer, L_s (mm)	150	Diameter (mm)	25

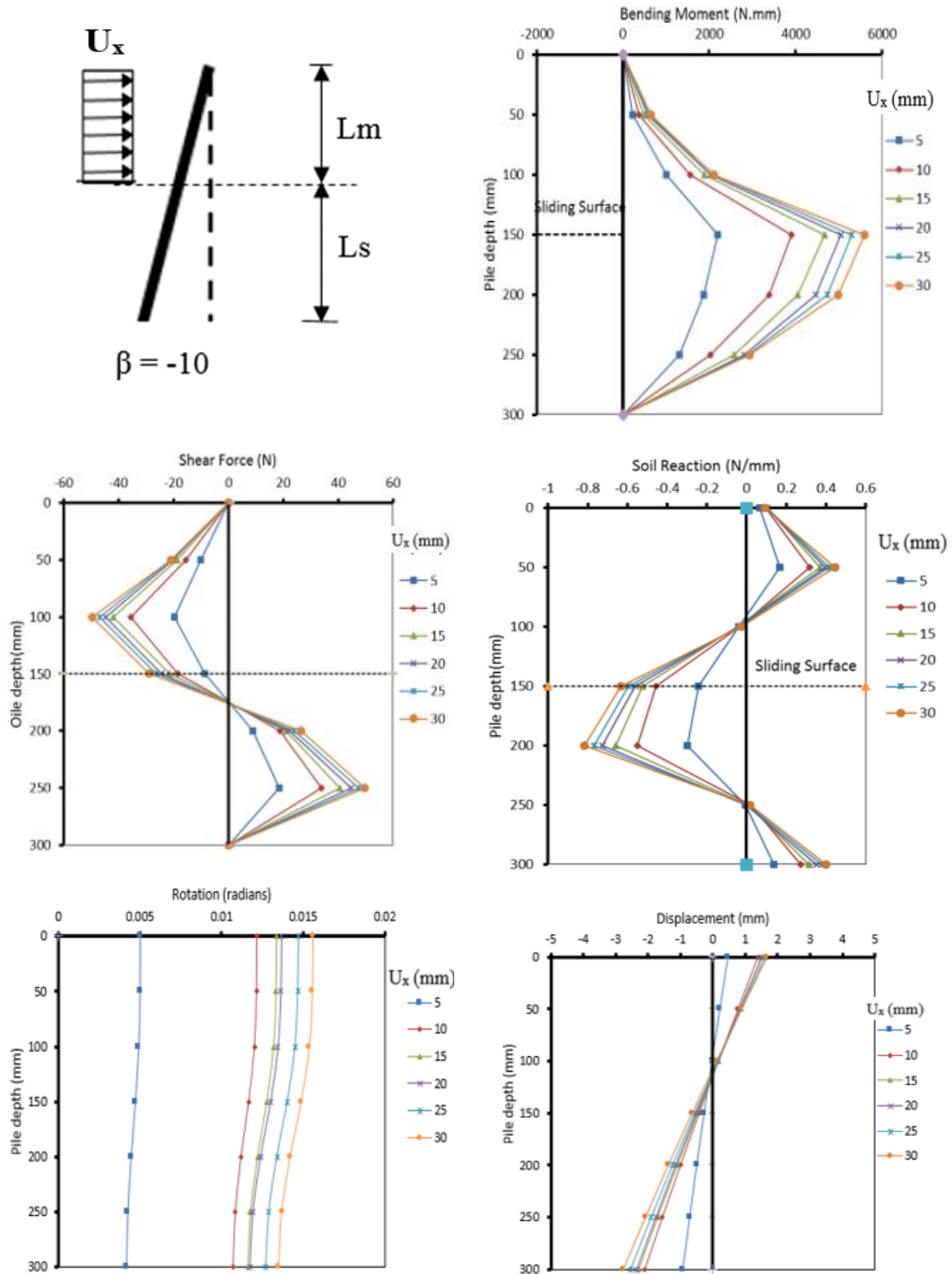


Fig. A.28 Single batter pile response, test (RSF25, -10°)

Test number	RSF25, -20	Density kN/m ³	15.2	Batter angle (β) (degree)	-20
Pile-head condition)	Free-head	Soil moving Profile	rectangular		
Moving layer, L_m (mm)	150	Stable layer, L_s (mm)	150	Diameter (mm)	25

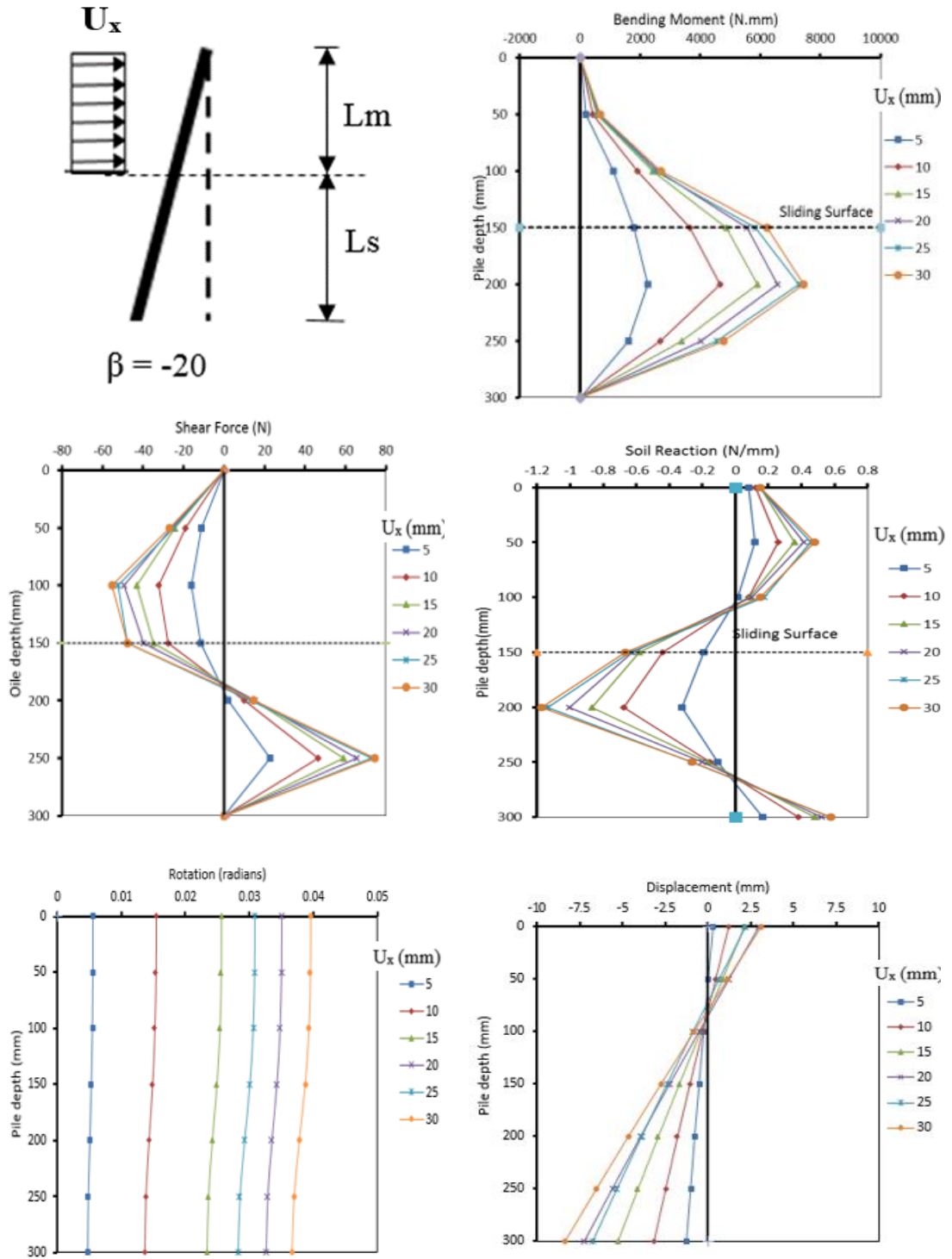


Fig. A.29 Single batter pile response, test (RSF25, -20°)

Test number	TSF16, 0	Density kN/m^3	14.7	Batter angle (β) (degree)	0
Pile-head condition)	Free-head	Soil moving Profile	Triangular		
Moving layer, L_m (mm)	150	Stable layer, L_s (mm)	150	Diameter (mm)	16

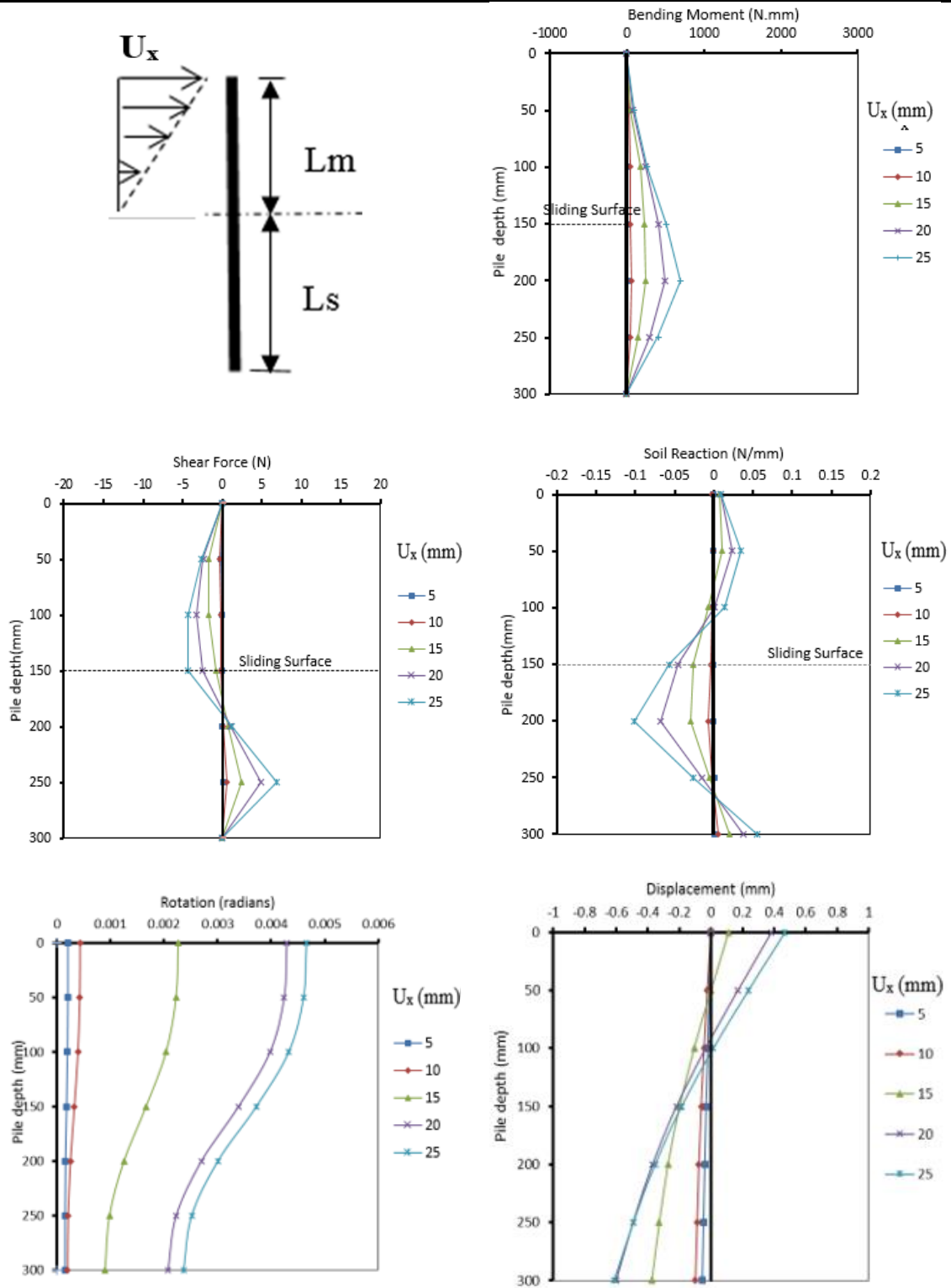


Fig. A.30 Single batter pile response, test (TSF16, 0°)

Test number	TSF16, +10	Density kN/m ³	14.7	Batter angle (β) (degree)	+10
Pile-head condition)	Free-head	Soil moving Profile	Triangular		
Moving layer, L_m (mm)	150	Stable layer, L_s (mm)	150	Diameter (mm)	16

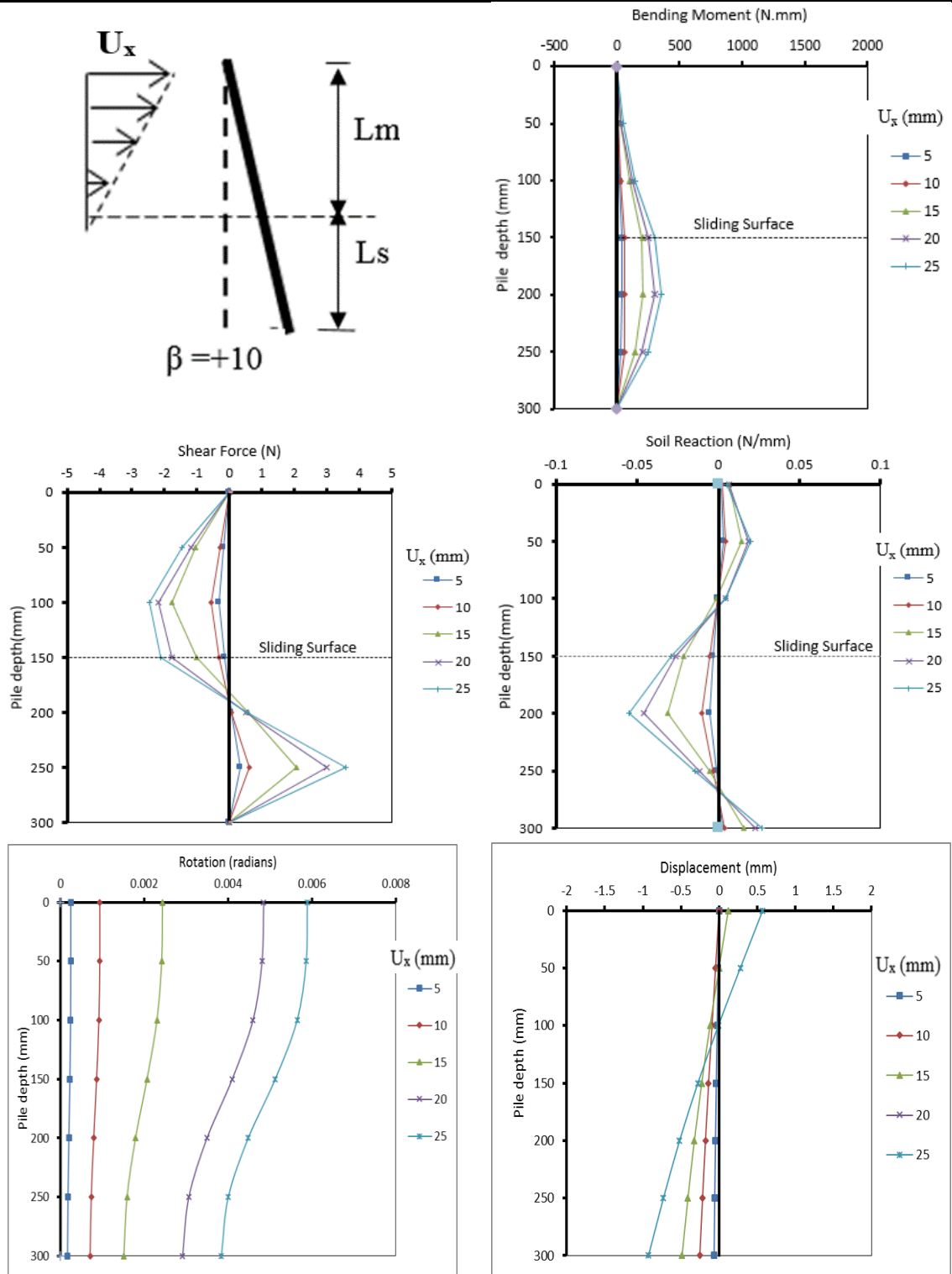


Fig. A.31 Single batter pile response, test (TSF16, +10°)

Test number	TSF16, +20	Density kN/m ³	14.7	Batter angle (β) (degree)	+20
Pile-head condition)	Free-head	Soil moving Profile	Triangular		
Moving layer, L_m (mm)	150	Stable layer, L_s (mm)	150	Diameter (mm)	16

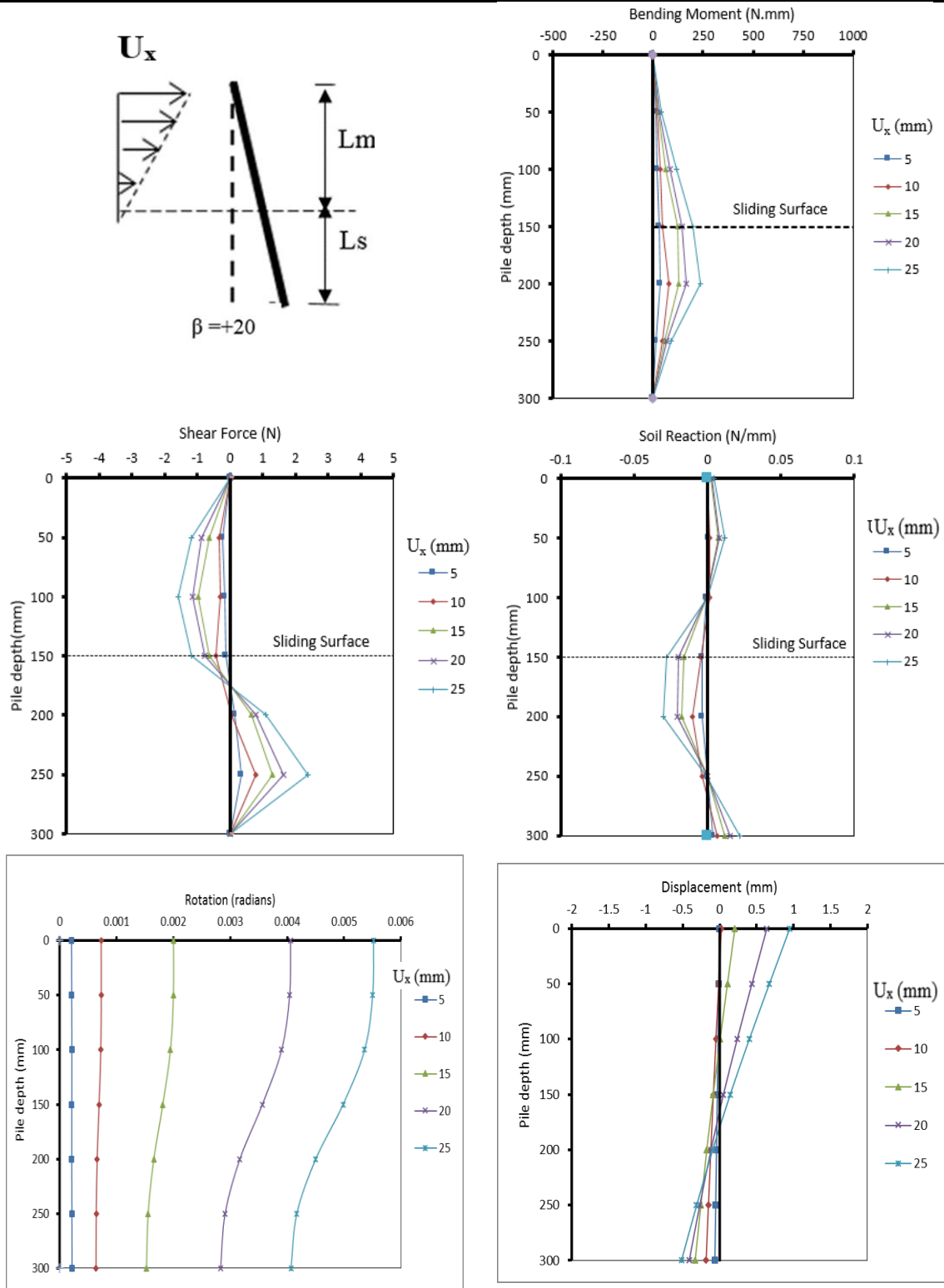


Fig. A.32 Single batter pile response, test (TSF16, +20°)

Test number	TSF16, -10	Density kN/m ³	14.7	Batter angle (β) (degree)	-10
Pile-head condition)	Free-head	Soil moving Profile	Triangular		
Moving layer, L_m (mm)	150	Stable layer, L_s (mm)	150	Diameter (mm)	16

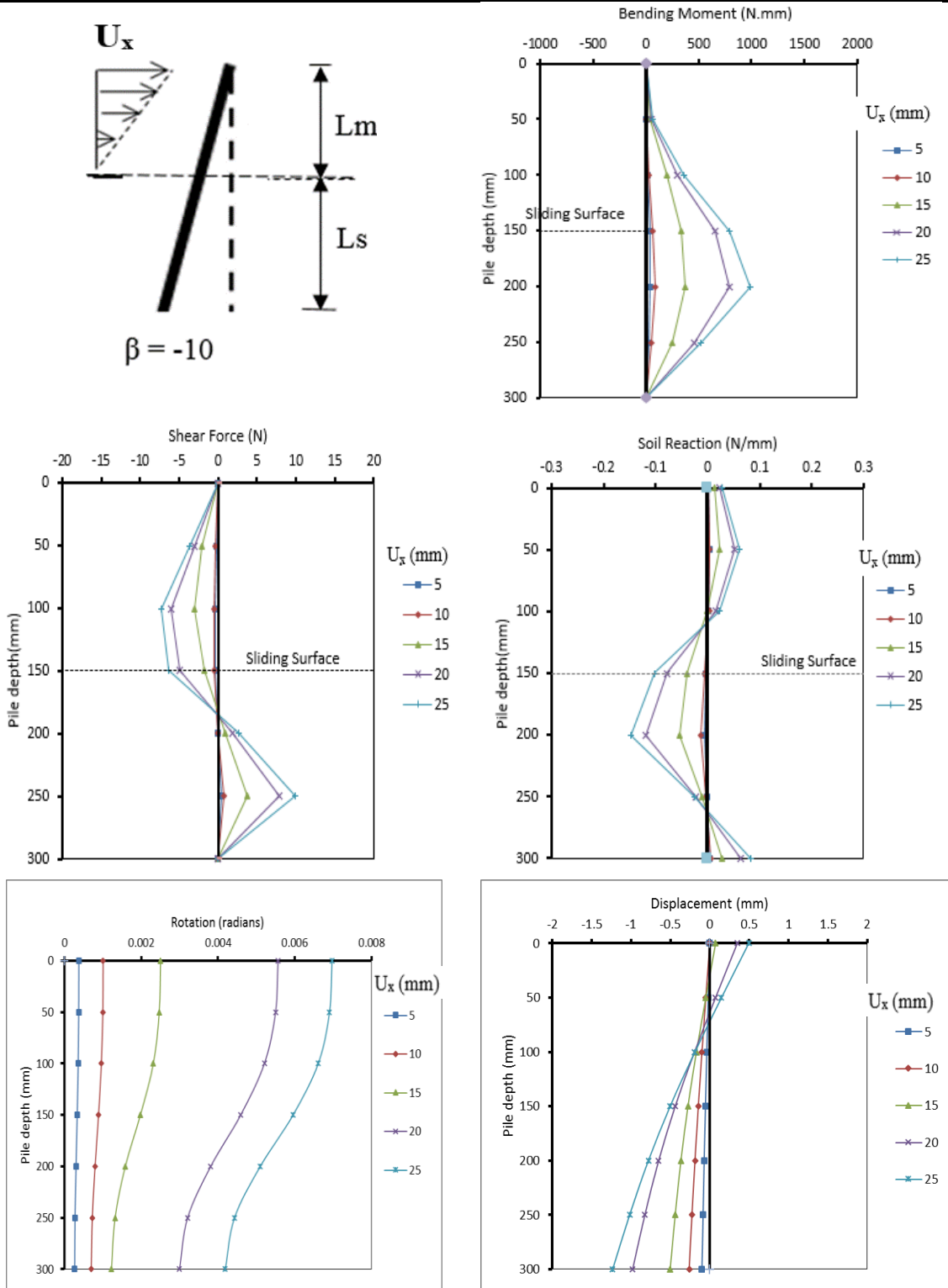


Fig. A.33 Single batter pile response, test (TSF16, -10°)

Test number	TSF16, -20	Density kN/m ³	14.7	Batter angle (β) (degree)	-20
Pile-head condition)	Free-head	Soil moving Profile	Triangular		
Moving layer, L_m (mm)	150	Stable layer, L_s (mm)	150	Diameter (mm)	16

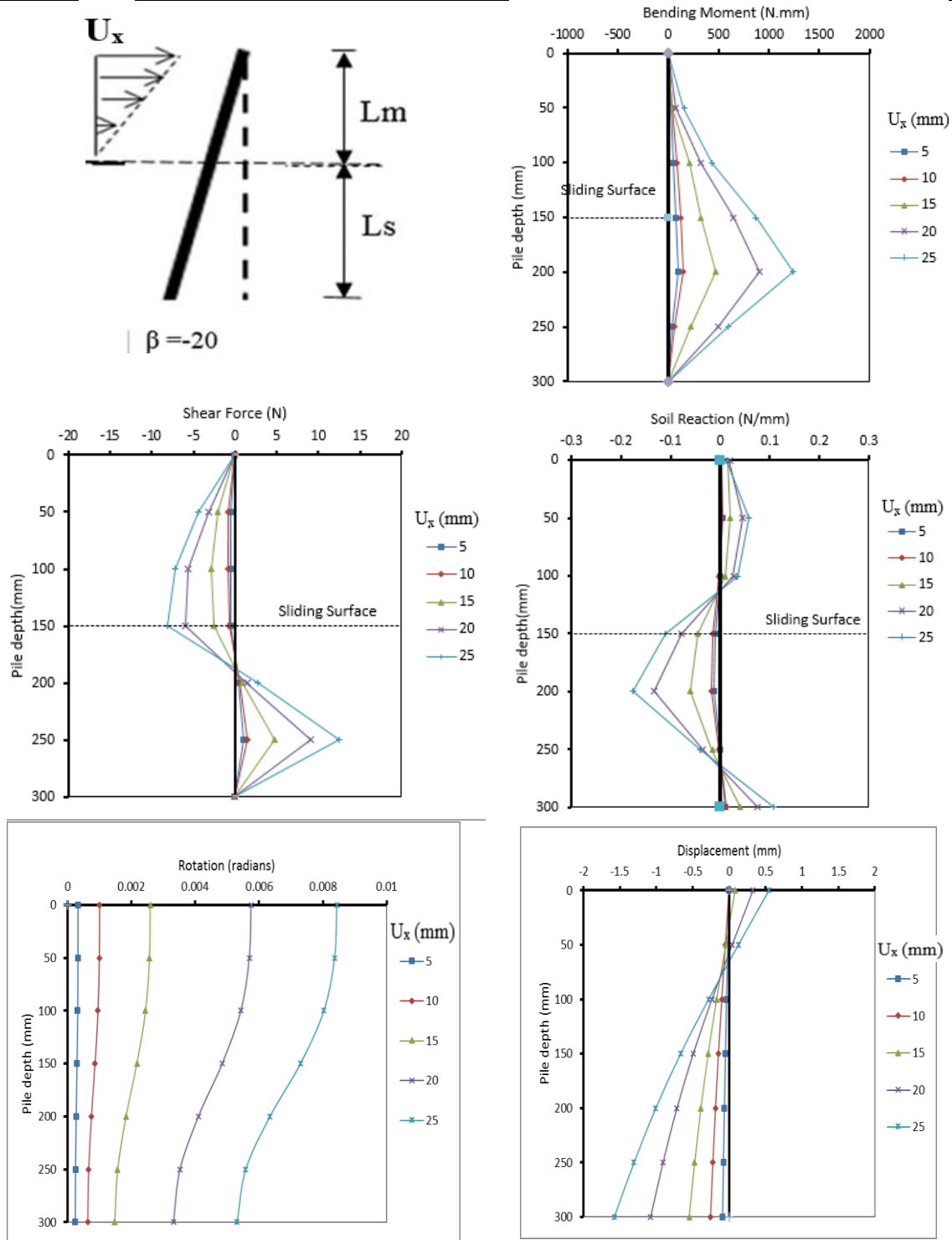


Fig. A.34 Single batter pile response, test (TSF16, -20°)

Test number	TSF16, 0	Density kN/m ³	15.2	Batter angle (β) (degree)	0
Pile-head condition)	Free-head	Soil moving Profile	Triangular		
Moving layer, L_m (mm)	150	Stable layer, L_s (mm)	150	Diameter (mm)	16

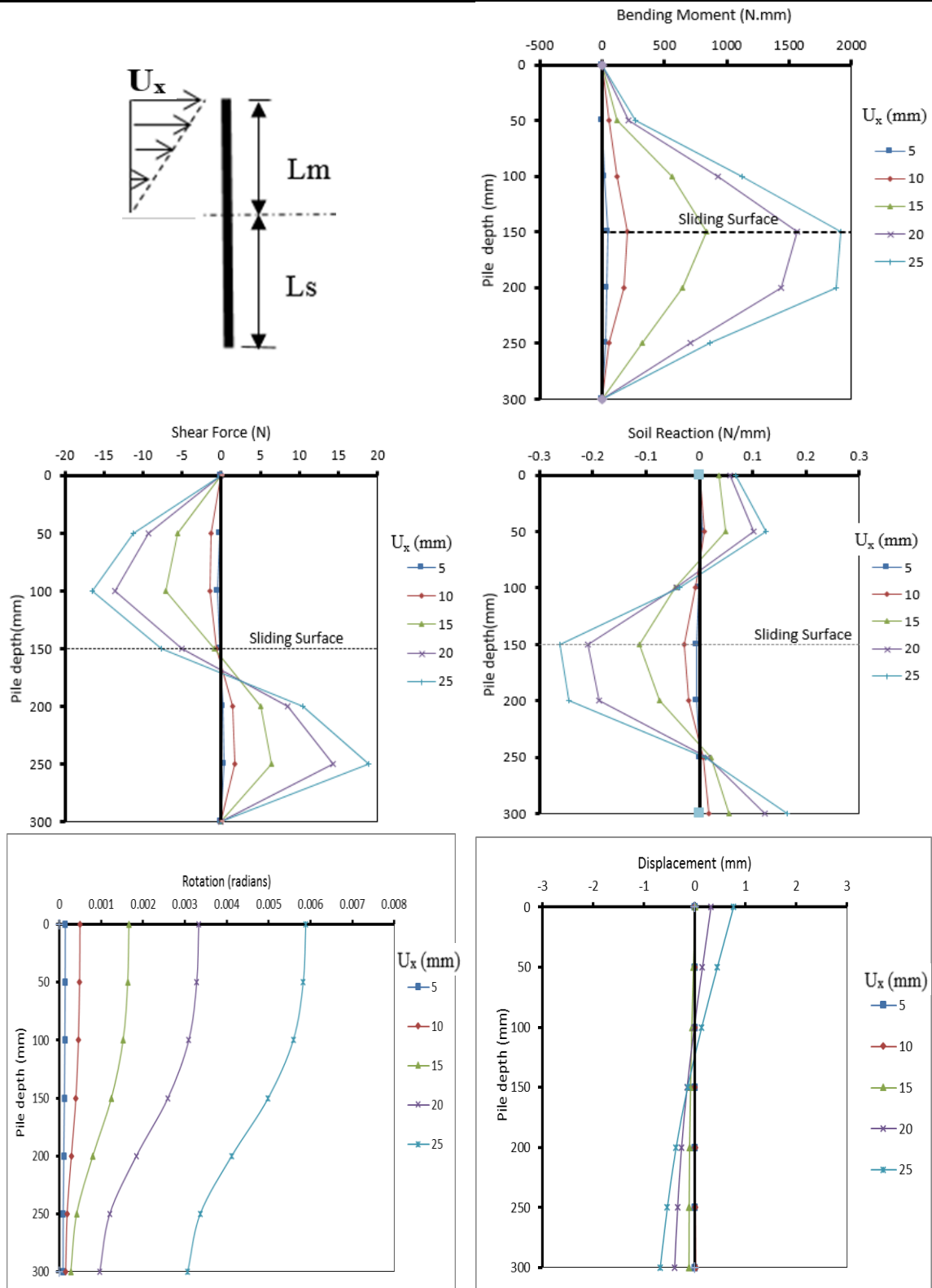


Fig. A.35 Single batter pile response, test (TSF16, 0°)

Test number	TSF16, +10	Density kN/m ³	15.2	Batter angle (β)(degree)	+10
Pile-head condition)	Free-head	Soil moving Profile	Triangular		
Moving layer, L _m (mm)	150	Stable layer, L _s (mm)	150	Diameter (mm)	16

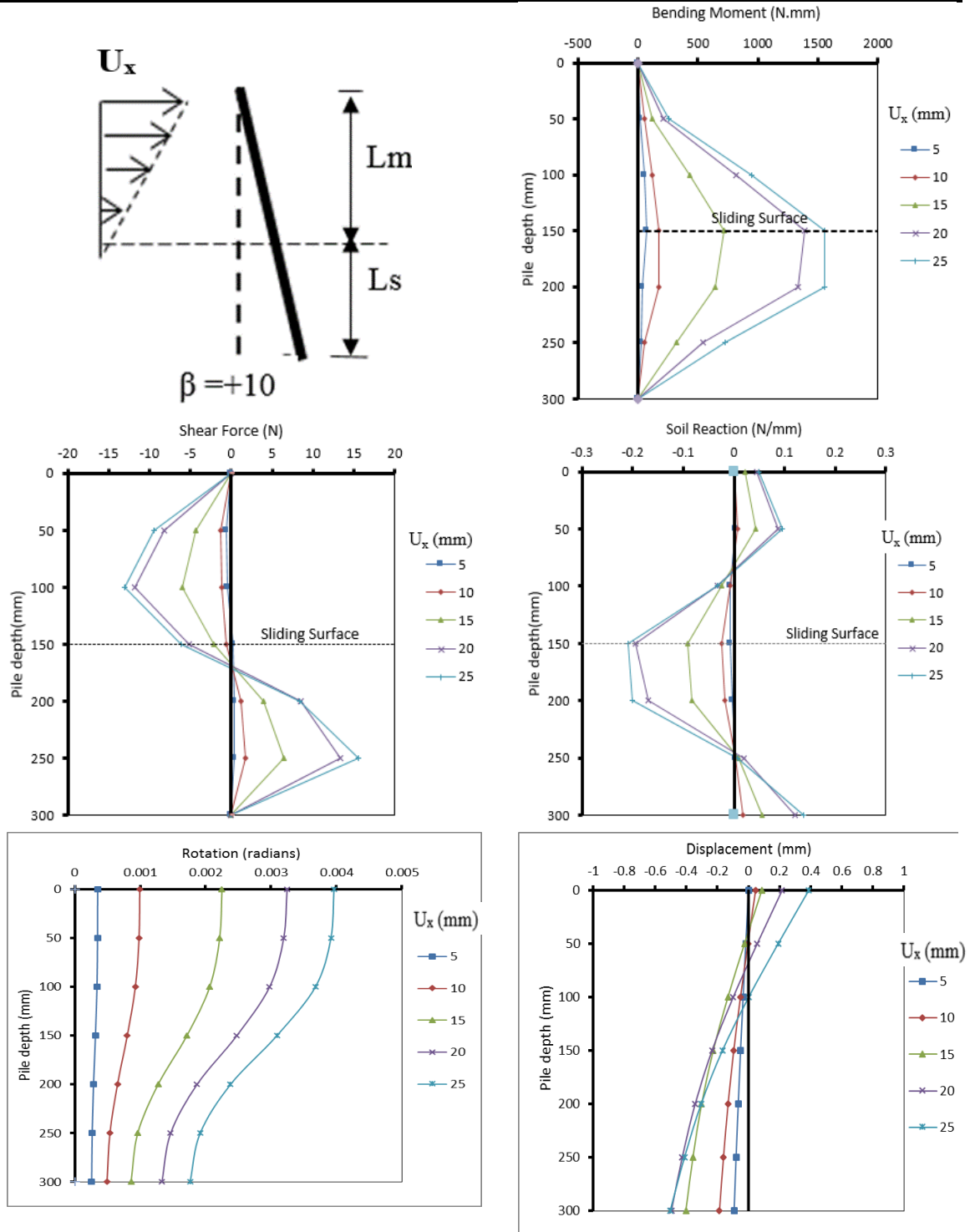


Fig. A.36 Single batter pile respons2, test (TSF16, +10°)

Test number	TSF16, +20	Density kN/m ³	15.2	Batter angle (β) (degree)	+20
Pile-head condition)	Free-head	Soil moving Profile	Triangular		
Moving layer, L_m (mm)	150	Stable layer, L_s (mm)	150	Diameter (mm)	16

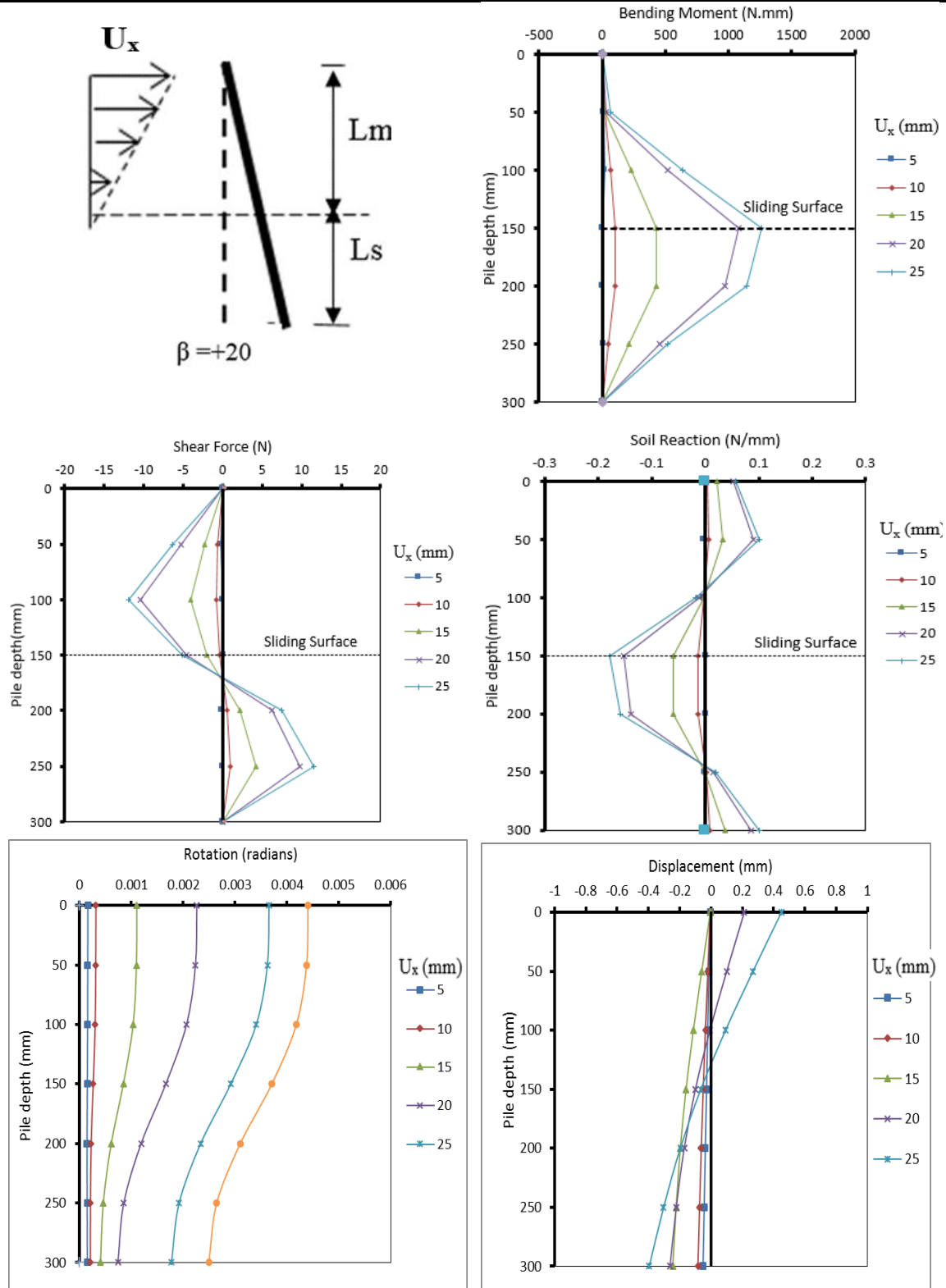


Fig. A.37 Single batter pile response, test (TSF16, +20°)

Test number	TSF16, -10	Density kN/m ³	15.2	Batter angle (β) (degree)	-10
Pile-head condition)	Free-head	Soil moving Profile	Triangular		
Moving layer, L_m (mm)	150	Stable layer, L_s (mm)	150	Diameter (mm)	16

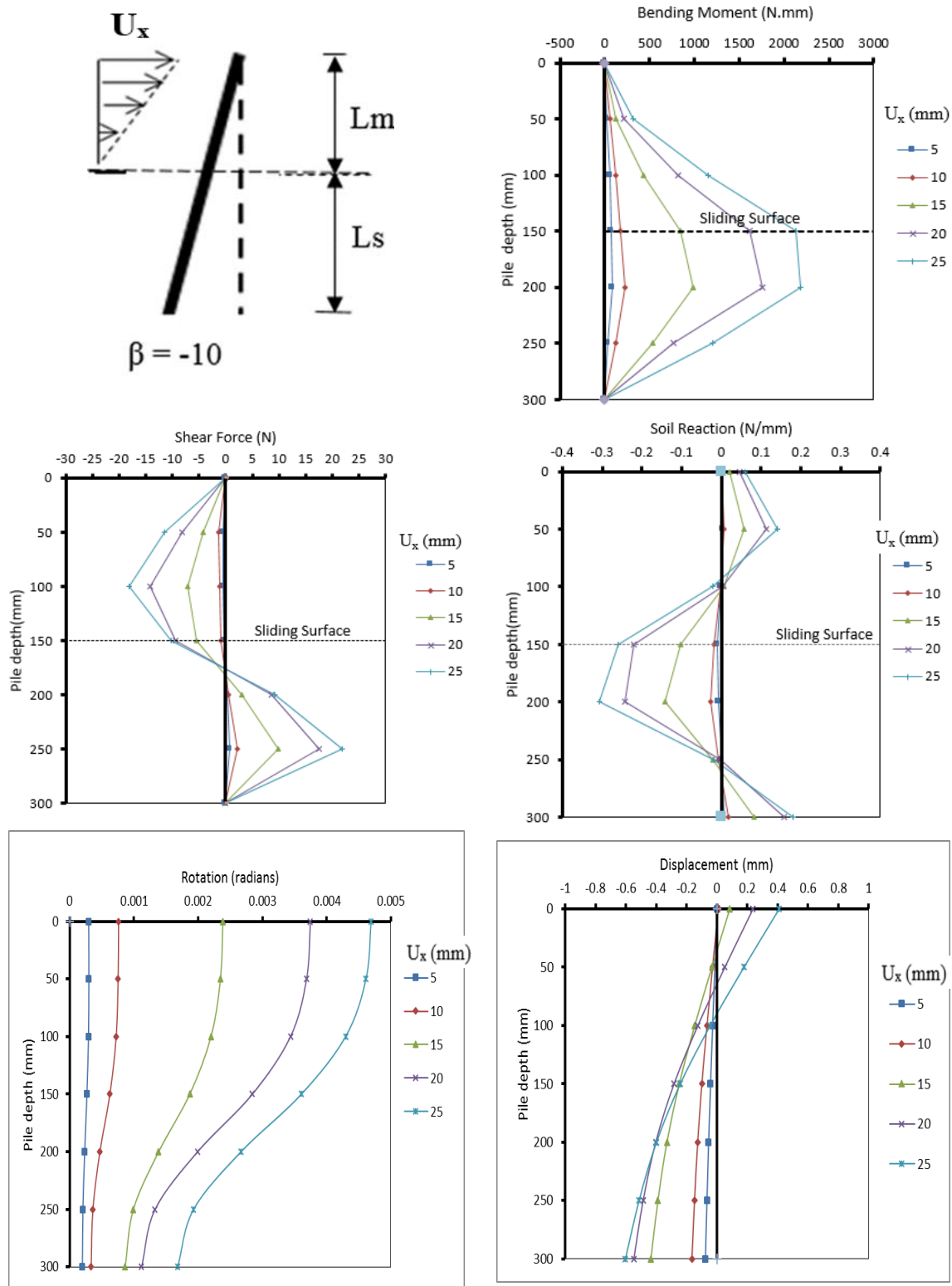


Fig. A.38 Single batter pile response, test (TSF16, -10°)

Test Number	TSF16, -20	Density KN/m ³	15.2	Batter angle (β) (degree)	-20
Pile-Head condition)	Free-head	Soil Moving Profile	Triangular		
Moving layer, Lm (mm)	150	Stable layer, Ls (mm)	150	Diameter (mm)	16

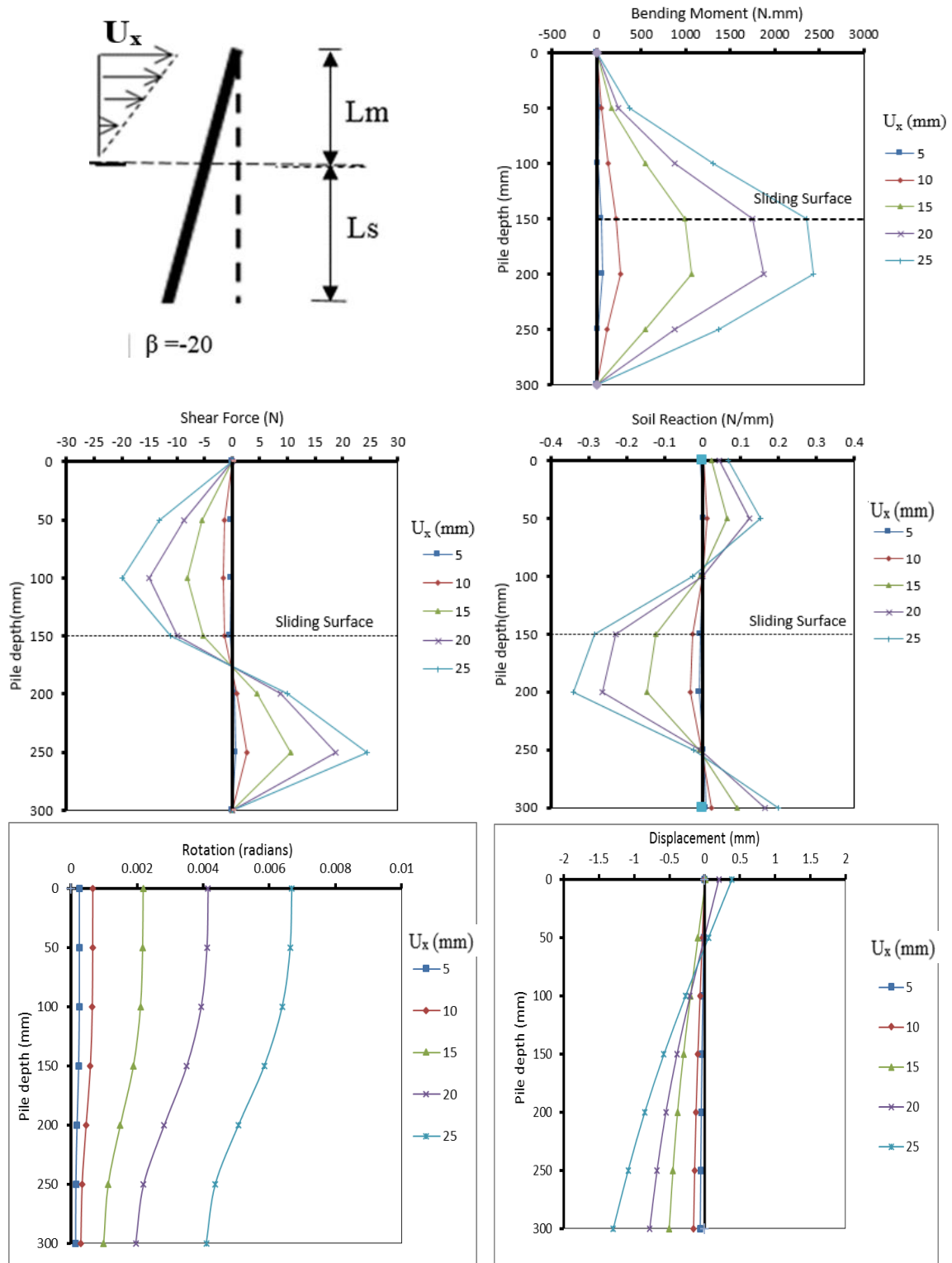


Fig. A.39 Single batter pile response, test (TSF16, -20°)

Test Number	TSF16, 0	Density KN/m ³	15.7	Batter angle (β) (degree)	0
Pile-Head condition)	Free-head	Soil Moving Profile	Triangular		
Moving layer, Lm (mm)	150	Stable layer, Ls (mm)	150	Diameter (mm)	16

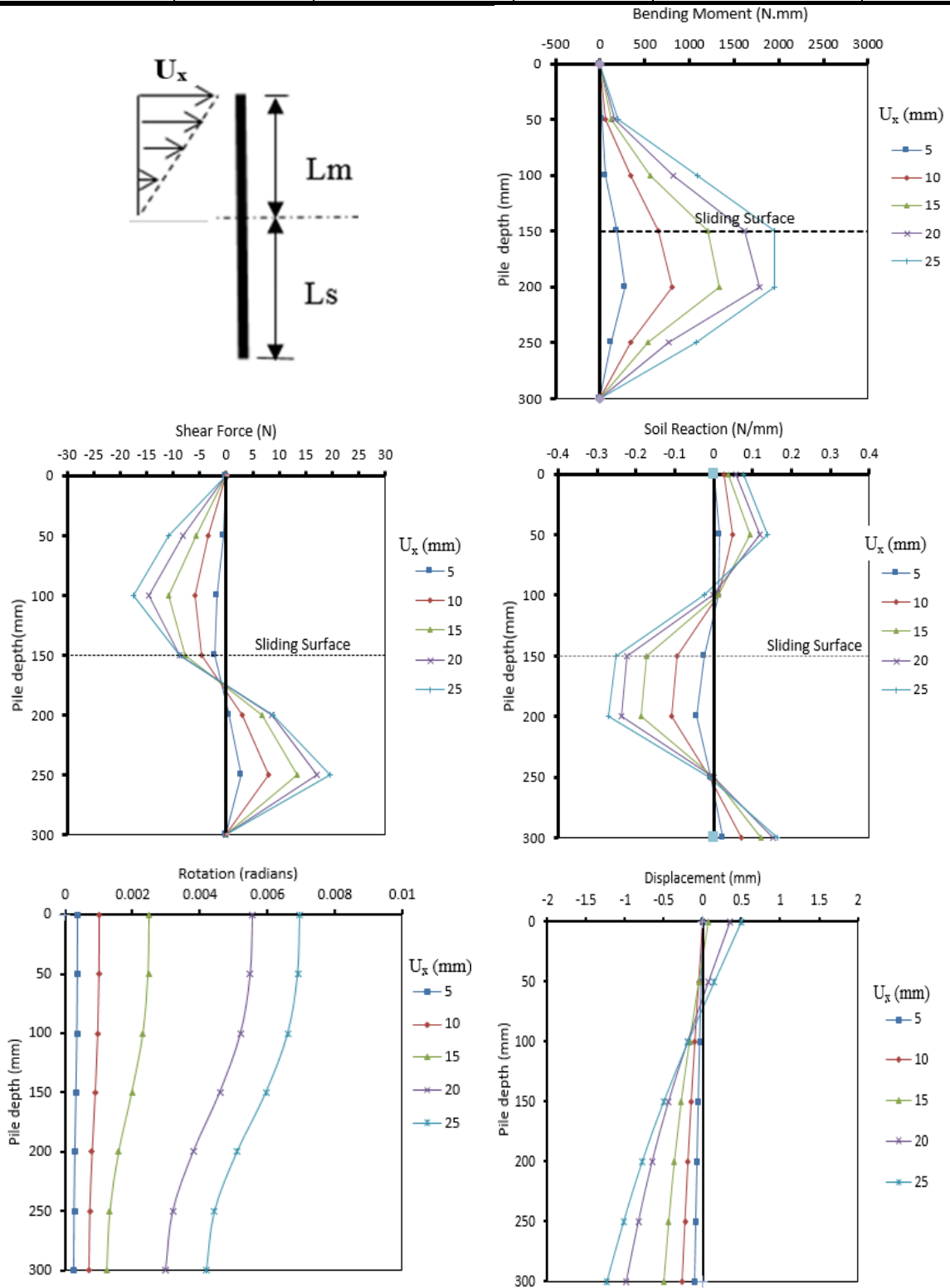


Fig. A.40 Single batter pile response, test (TSF16, 0°)

Test Number	TSF16, +10	Density KN/m ³	15.7	Batter angle (β) (degree)	+10
Pile-Head condition)	Free-head	Soil Moving Profile	Triangular		
Moving layer, L _m (mm)	150	Stable layer, L _s (mm)	150	Diameter (mm)	16

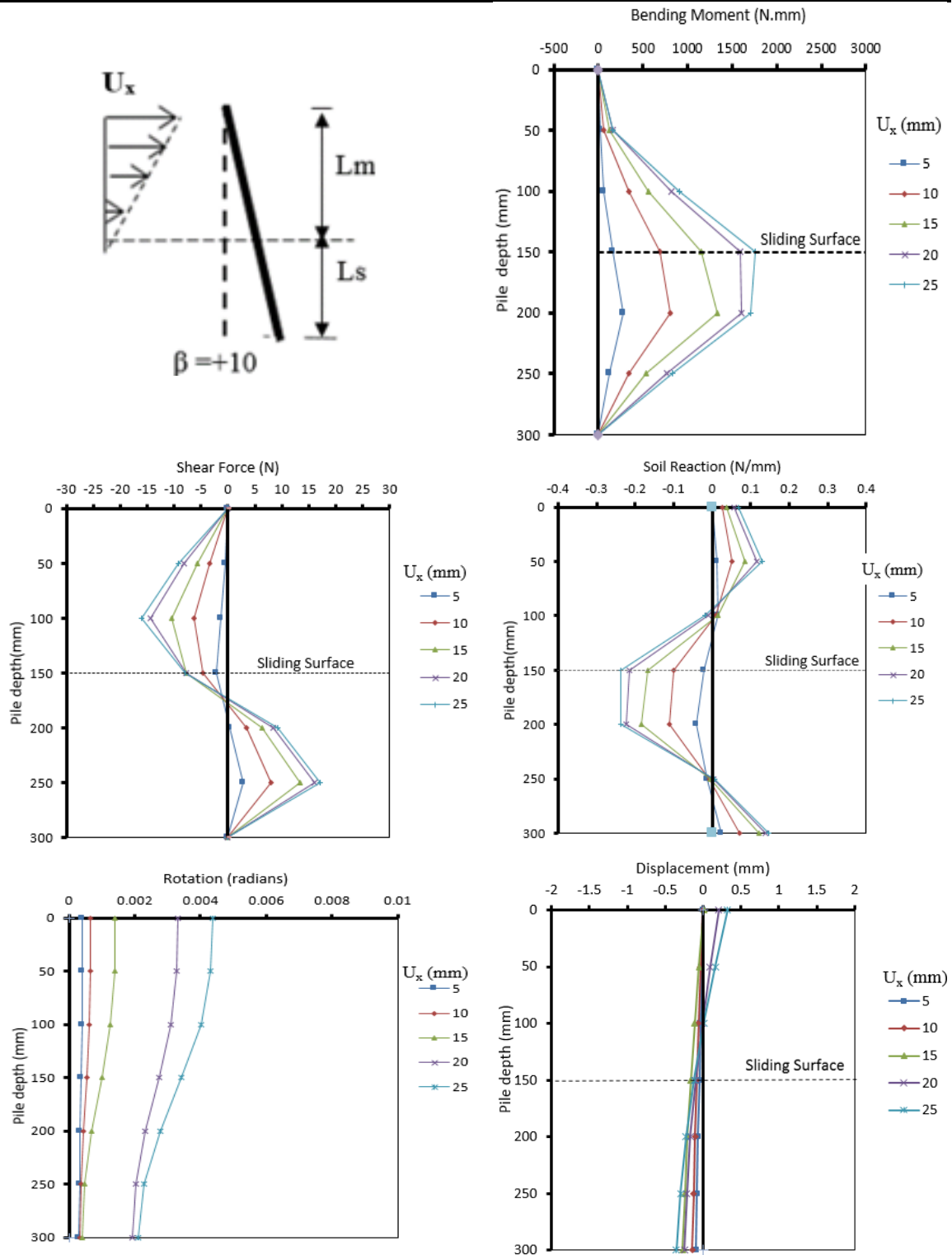


Fig. A.41 Single batter pile response, test (TSF16, +10°)

Test Number	TSF16, +20	Density KN/m ³	15.7	Batter angle (β) (degree)	+20
Pile-Head condition)	Free-head	Soil Moving Profile	Triangular		
Moving layer, Lm (mm)	150	Stable layer, Ls (mm)	150	Diameter (mm)	16

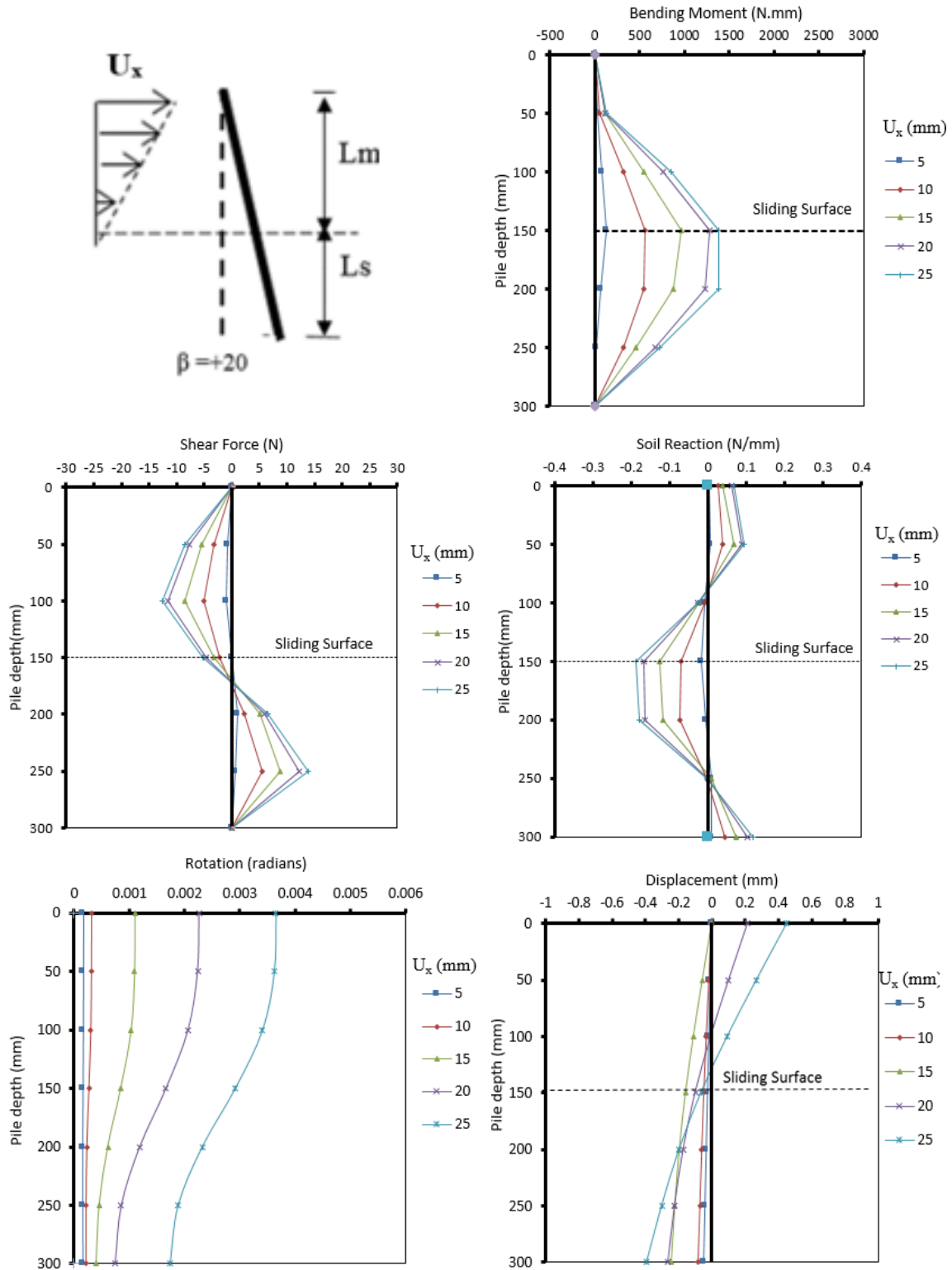


Fig. A.42 Single batter pile response, test (TSF16, +20°)

Test Number	TSF16, -10	Density KN/m ³	15.7	Batter angle (β) (degree)	-10
Pile-Head condition)	Free-head	Soil Moving Profile	Triangular		
Moving layer, Lm (mm)	150	Stable layer, Ls (mm)	150	Diameter (mm)	16

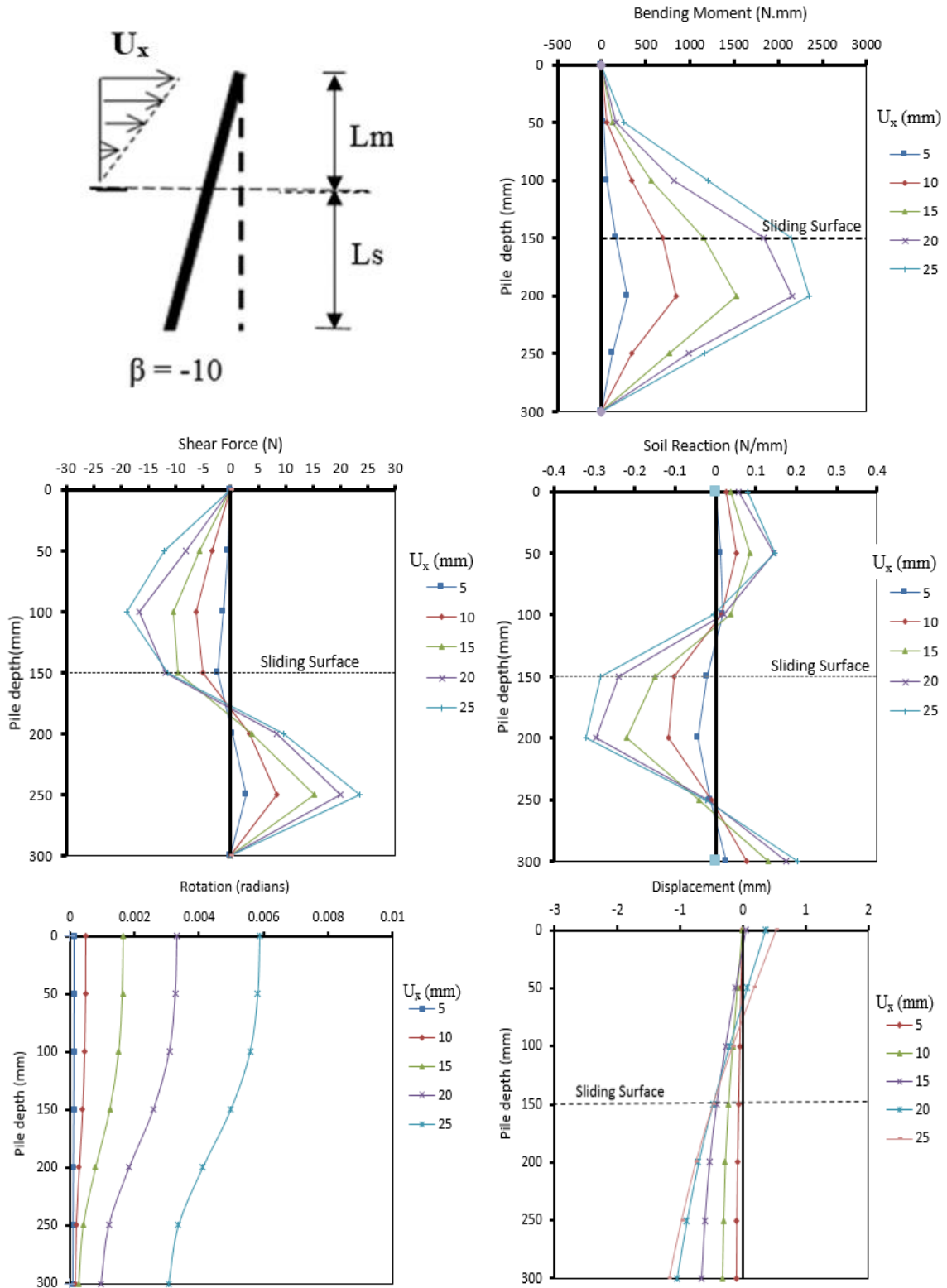


Fig. A.43 Single batter pile response, test (TSF16, -10°)

Test Number	TSF16, -20	Density KN/m ³	15.7	Batter angle (β) (degree)	-20
Pile-Head condition)	Free-head	Soil Moving Profile	Triangular		
Moving layer, Lm (mm)	150	Stable layer, Ls (mm)	150	Diameter (mm)	16

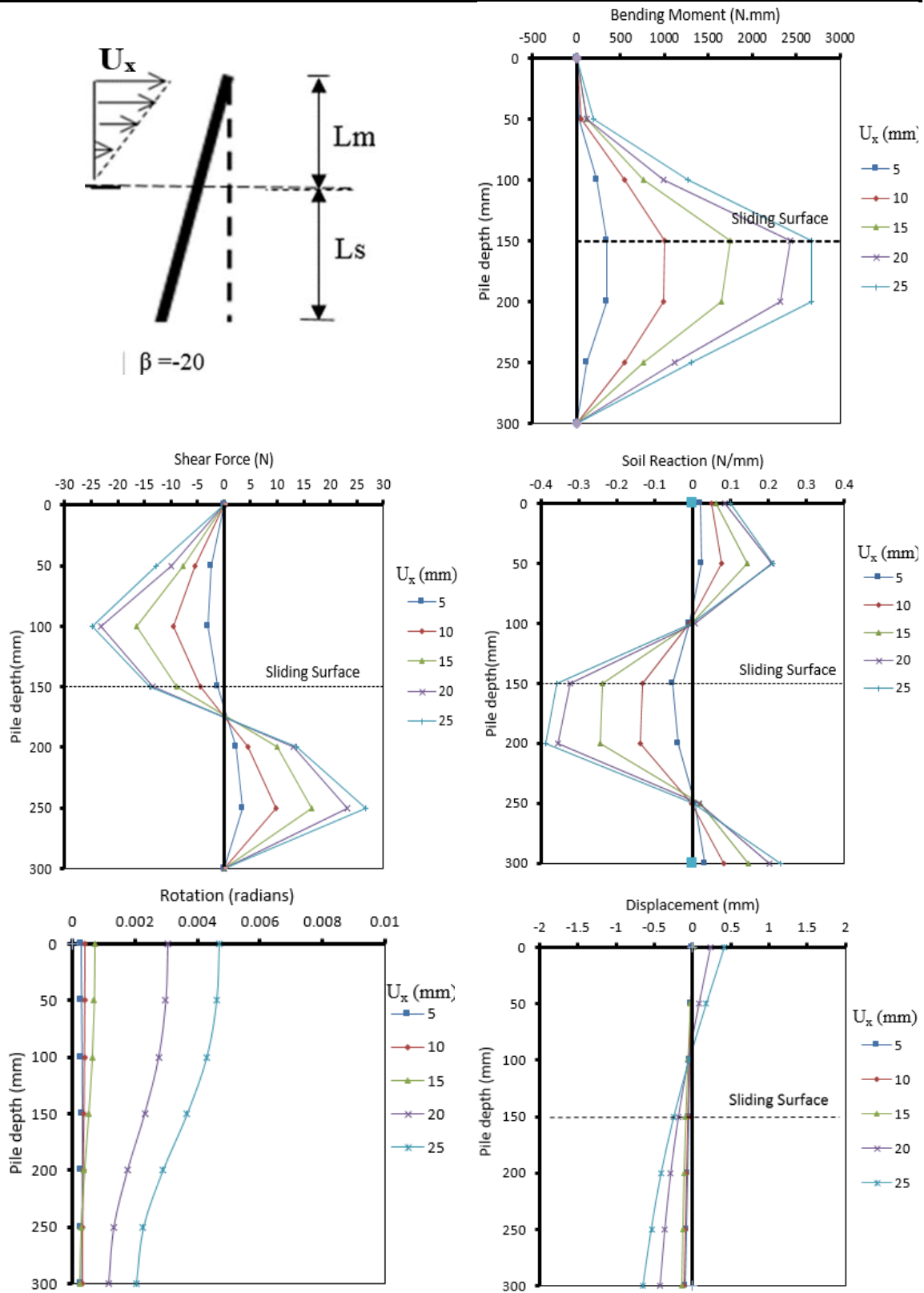


Fig. A.44 Single batter pile response, test (TSF16, -20°)

Appendix B
Pile Group Test Results

Test Number	VVL	Density kN/m ³	15.2	Batter angle (β) (degree)	0
Pile-Head condition)	Capped	Soil Moving Profile	rectangular		
Moving layer, Lm (mm)	150	Stable layer, Ls (mm)	150	Diameter (mm)	16

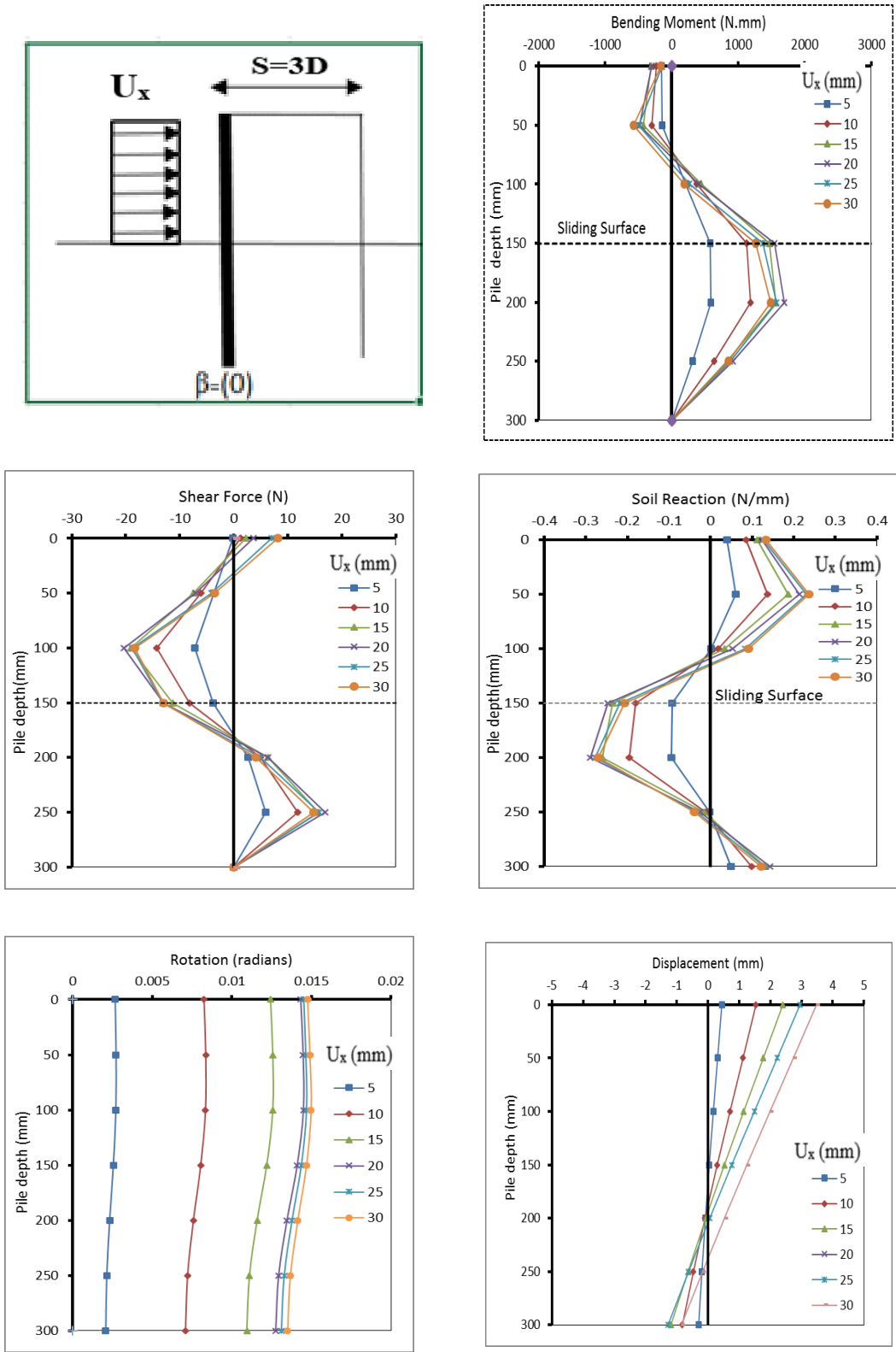


Fig. B.1a Response front pile, test (VVL)

Test Number	VVL	Density kN/m ³	15.2	Batter angle (β) (degree)	0
Pile-Head condition)	Capped	Soil Moving Profile	rectangular		
Moving layer, Lm (mm)	150	Stable layer, Ls (mm)	150	Diameter (mm)	16

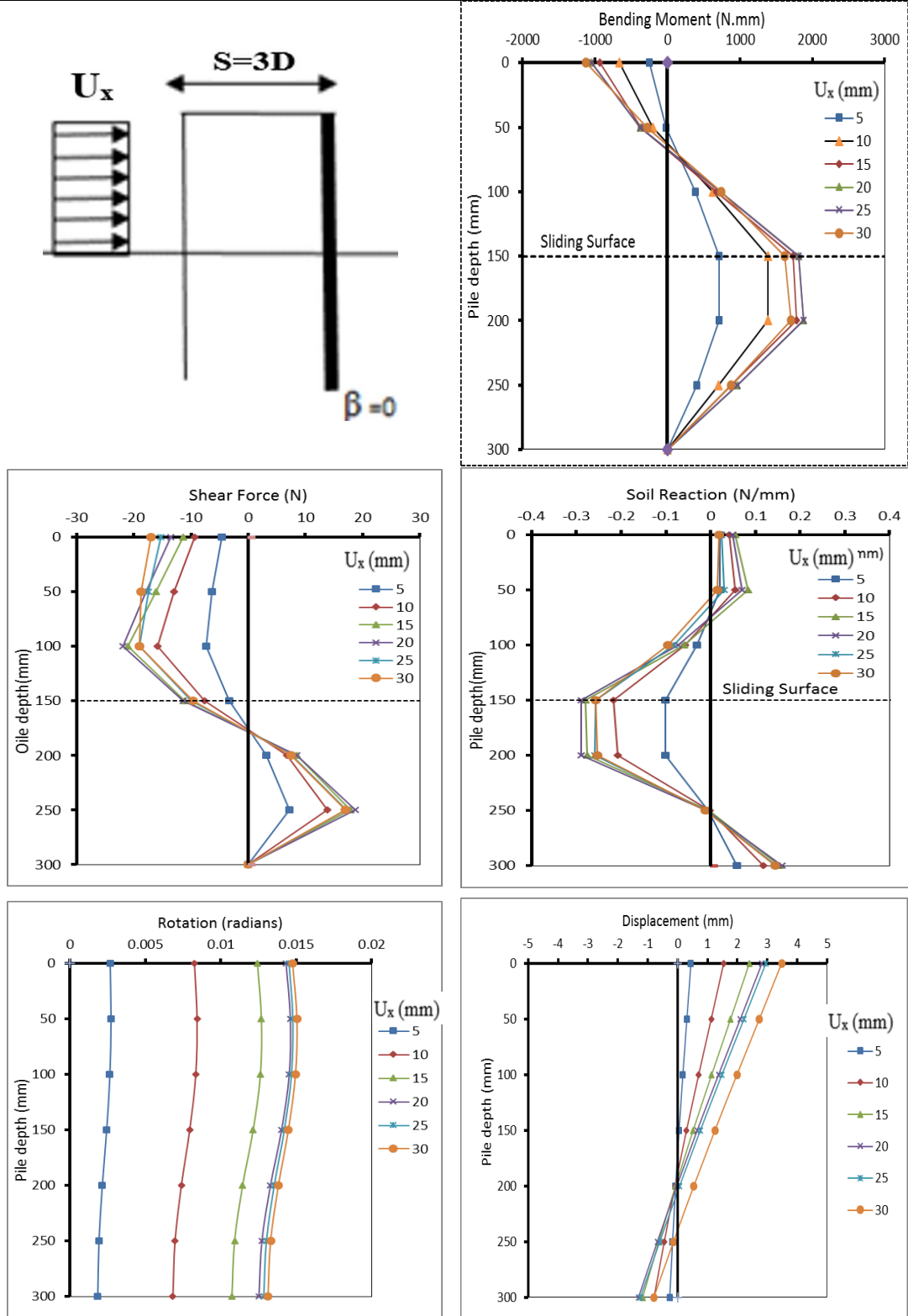


Fig. B.1b Response of back pile, test (VVL)

Test Number	VBL	Density kN/m ³	15.2	Batter angle (β) (degree)	+10
Pile-Head condition)	Capped	Soil Moving Profile	rectangular		
Moving layer, Lm (mm)	150	Stable layer, Ls (mm)	150	Diameter (mm)	16

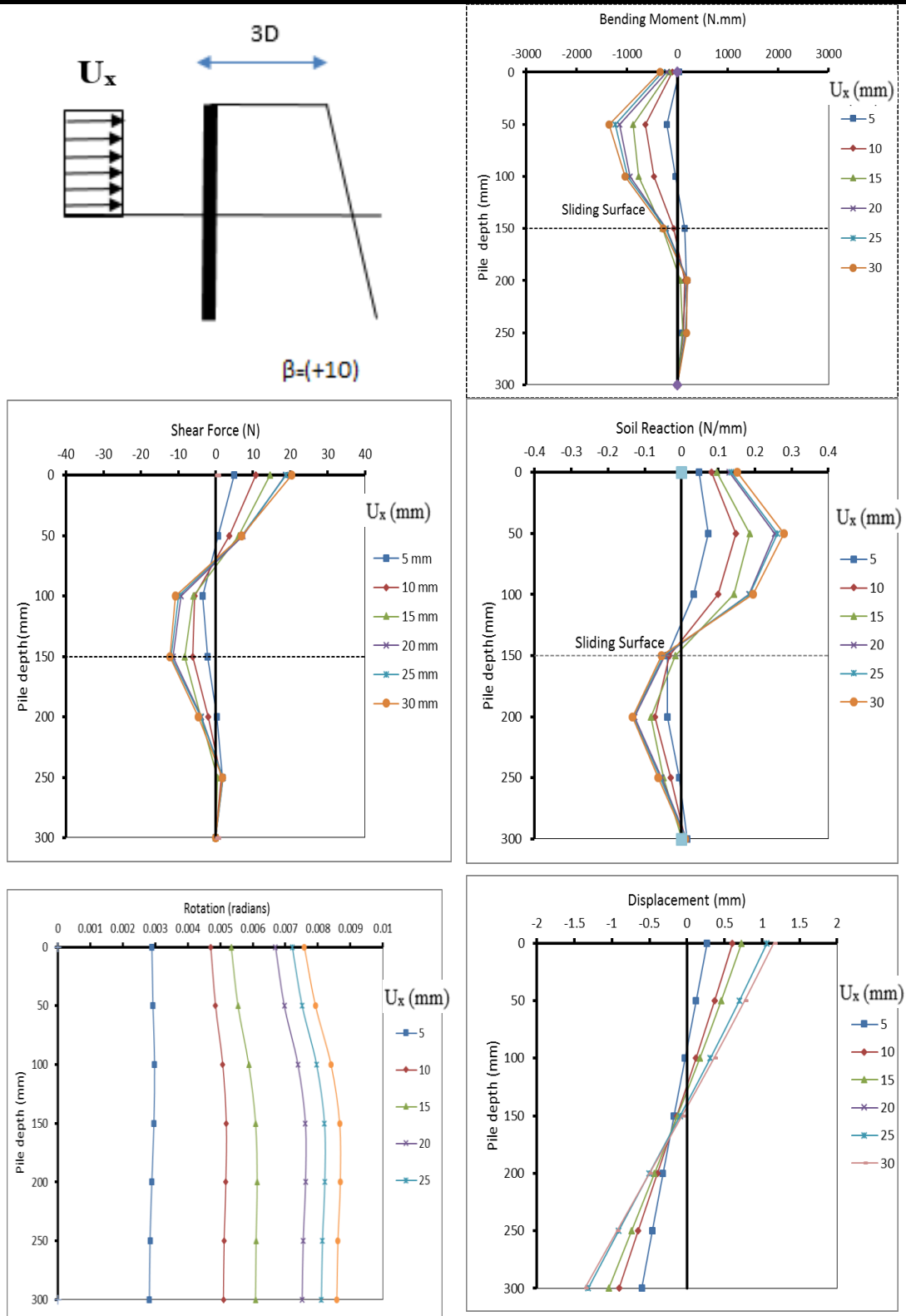


Fig. B.2a Response of front pile, test (VBL), $\beta = +10^\circ$

Test Number	VBL	Density kN/m ³	15.2	Batter angle (β) (degree)	+10
Pile-Head condition)	Capped	Soil Moving Profile	rectangular		
Moving layer, Lm (mm)	150	Stable layer, Ls (mm)	150	Diameter (mm)	16

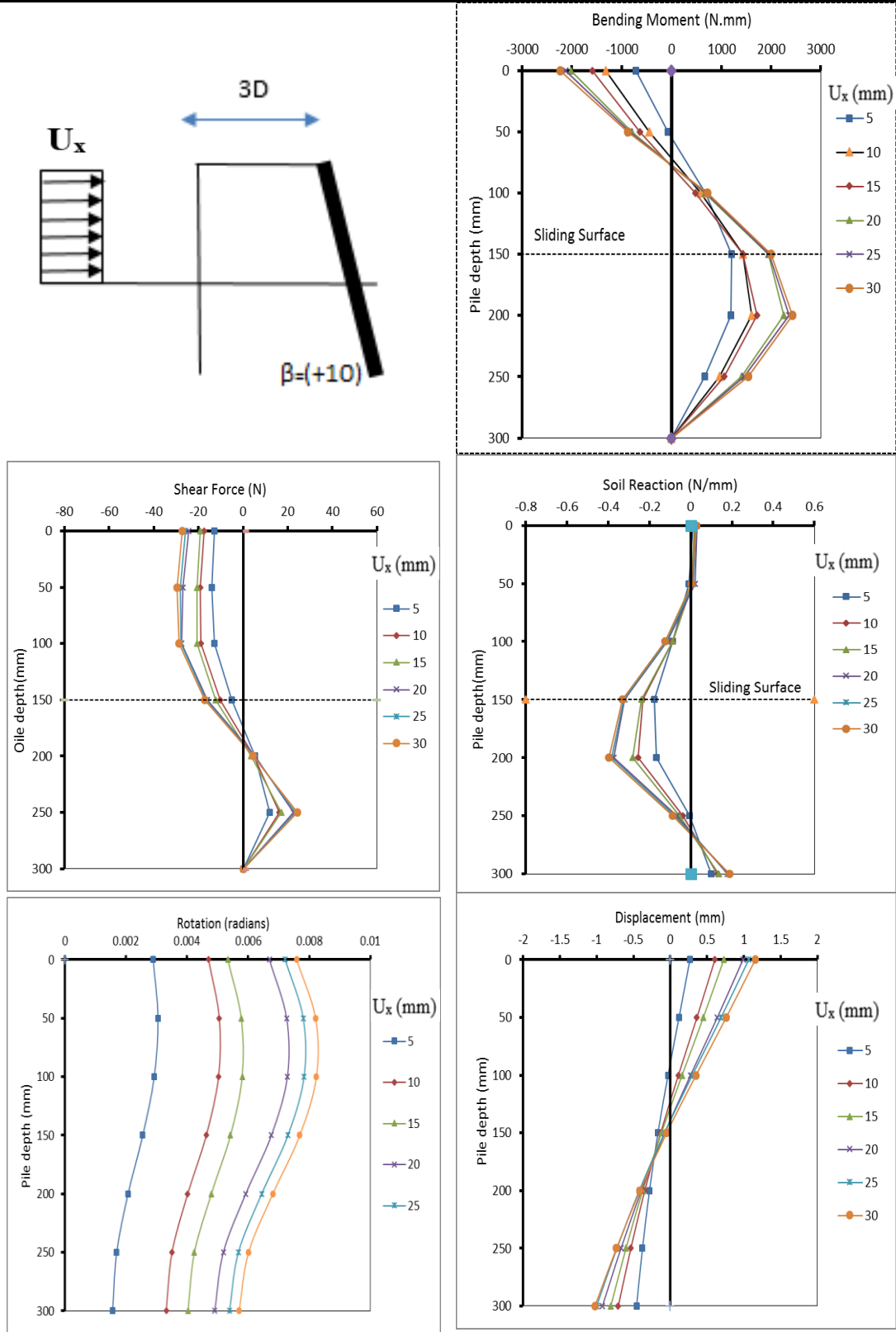


Fig. B.2b Response of back pile, test (VBL), $\beta = +10^\circ$

Test Number	VBL	Density kN/m ³	15.2	Batter angle (β) (degree)	+20
Pile-Head condition)	Capped	Soil Moving Profile	rectangular		
Moving layer, Lm (mm)	150	Stable layer, Ls (mm)	150	Diameter (mm)	16

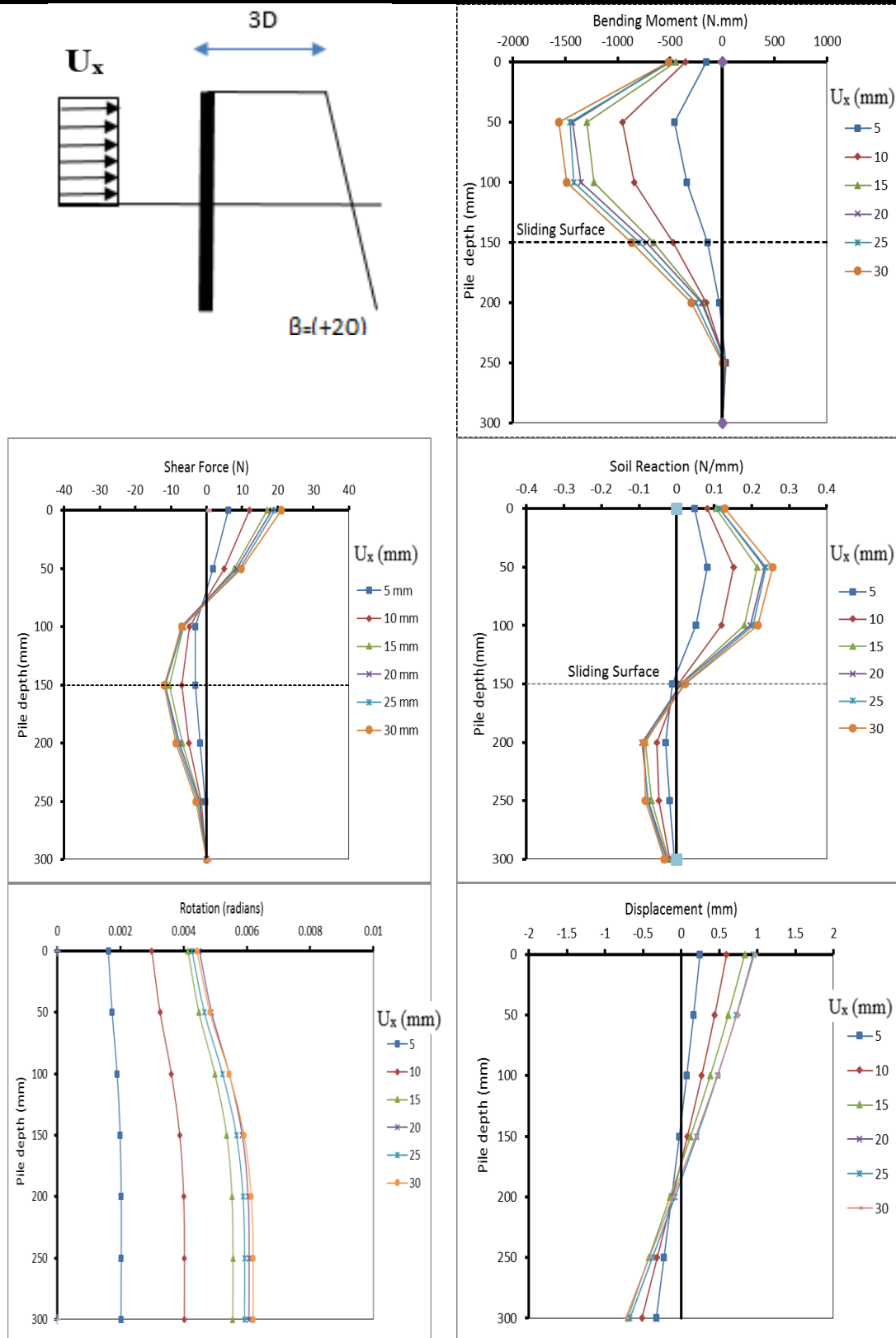


Fig. B. 3a Response of front pile, test (VBL), $\beta = +20^\circ$

Test Number	VBL	Density kN/m ³	15.2	Batter angle (β) (degree)	+20
Pile-Head condition)	Capped	Soil Moving Profile	rectangular		
Moving layer, Lm (mm)	150	Stable layer, Ls (mm)	150	Diameter (mm)	16

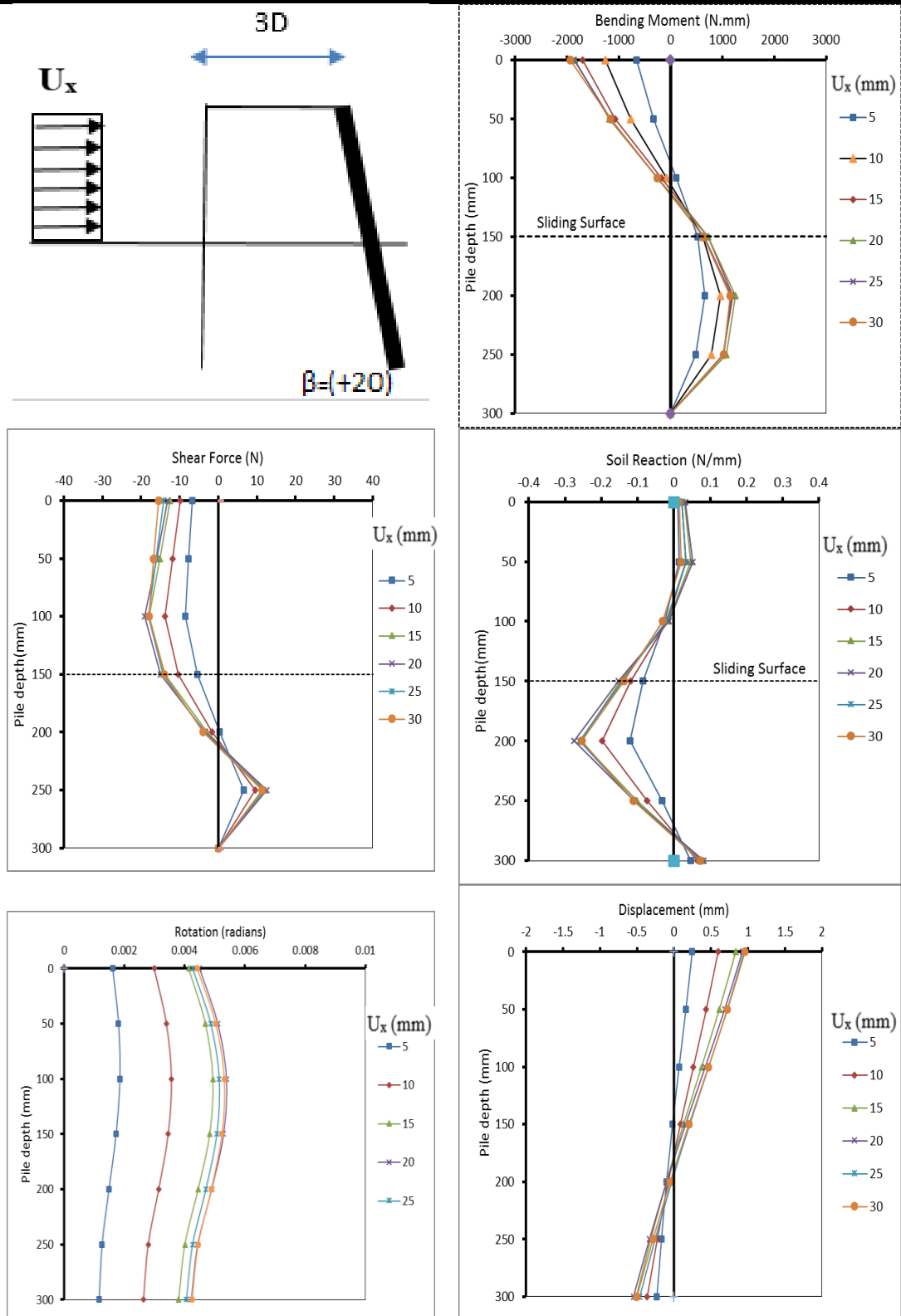


Fig. B.3b Response of back pile, test (VBL), $\beta = +20^\circ$

Test Number	BBL	Density kN/m ³	15.2	Batter angle (β) (degree)	± 10
Pile-Head condition)	Capped	Soil Moving Profile	rectangular		
Moving layer, Lm (mm)	150	Stable layer, Ls (mm)	150	Diameter (mm)	16

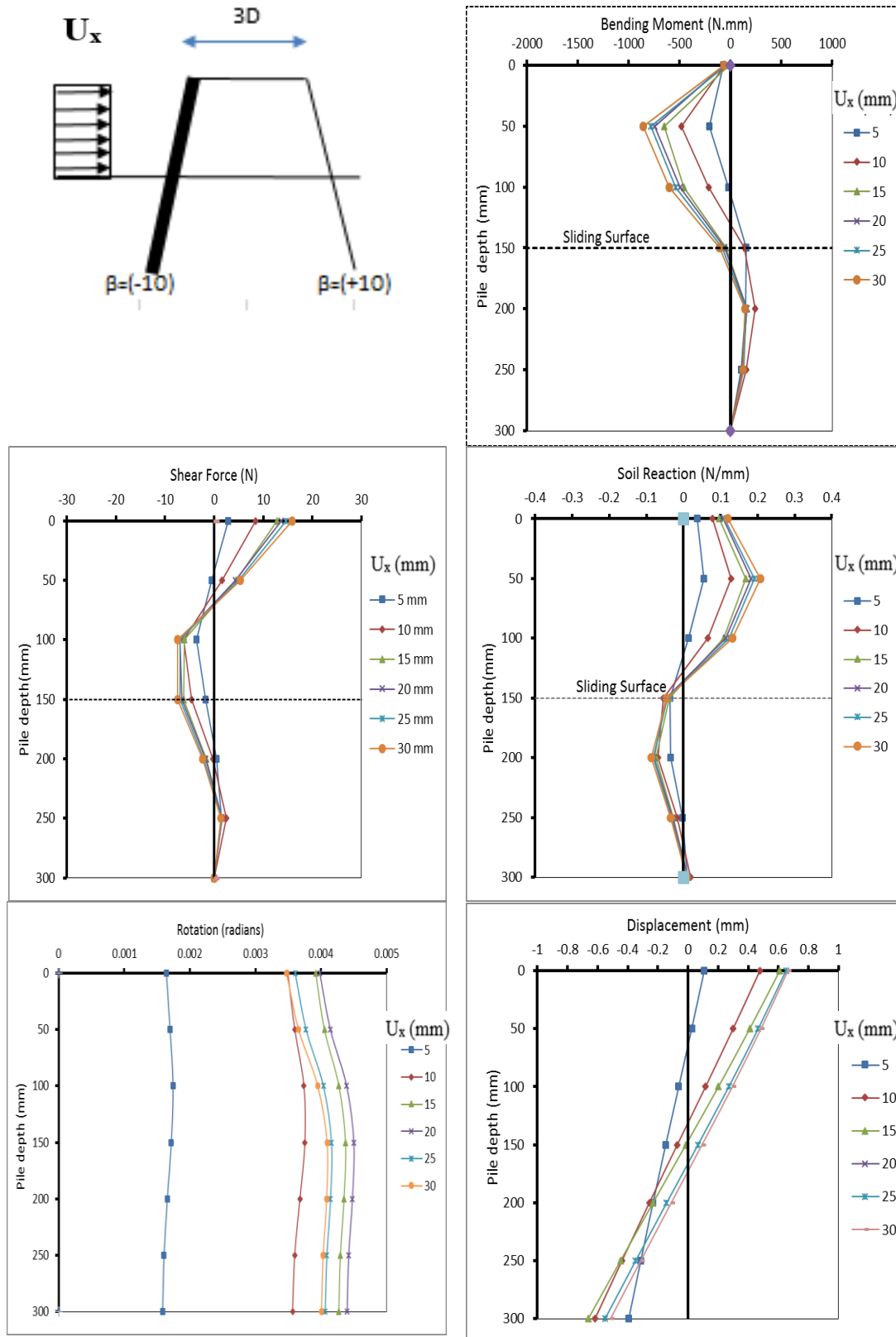


Fig. B.4a Response of front pile, test (BBL), $\beta = -10^\circ, +10^\circ$

Test Number	BBL	Density kN/m ³	15.2	Batter angle (β) (degree)	± 10
Pile-Head condition)	Capped	Soil Moving Profile	rectangular		
Moving layer, Lm (mm)	150	Stable layer, Ls (mm)	150	Diameter (mm)	16

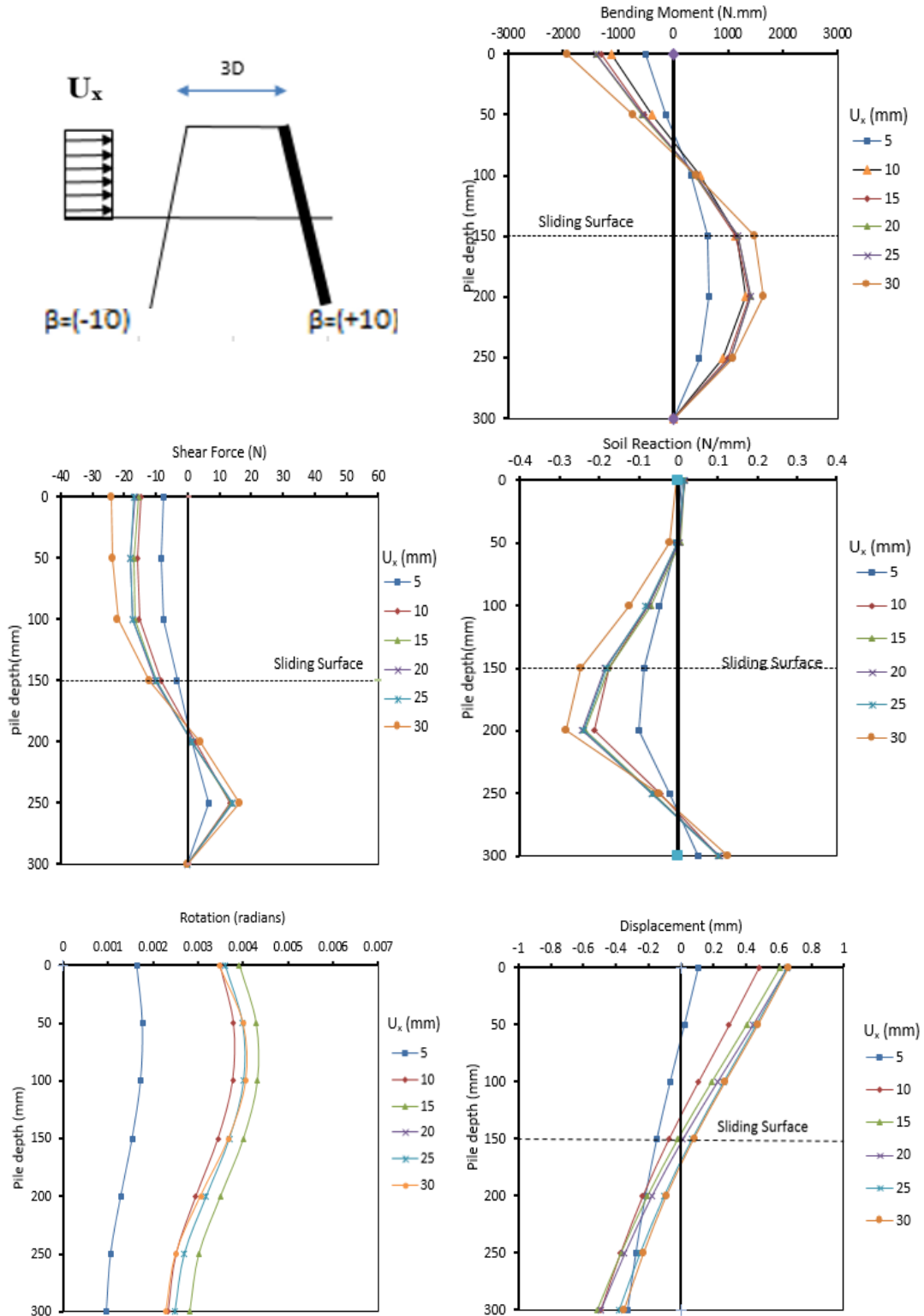


Fig. B.4b Response of back pile, test (BBL), $\beta = -10^\circ, +10^\circ$

Test Number	BBL	Density kN/m ³	15.2	Batter angle (β) (degree)	± 20
Pile-Head condition)	Capped	Soil Moving Profile	rectangular		
Moving layer, L _m (mm)	150	Stable layer, L _s (mm)	150	Diameter (mm)	16

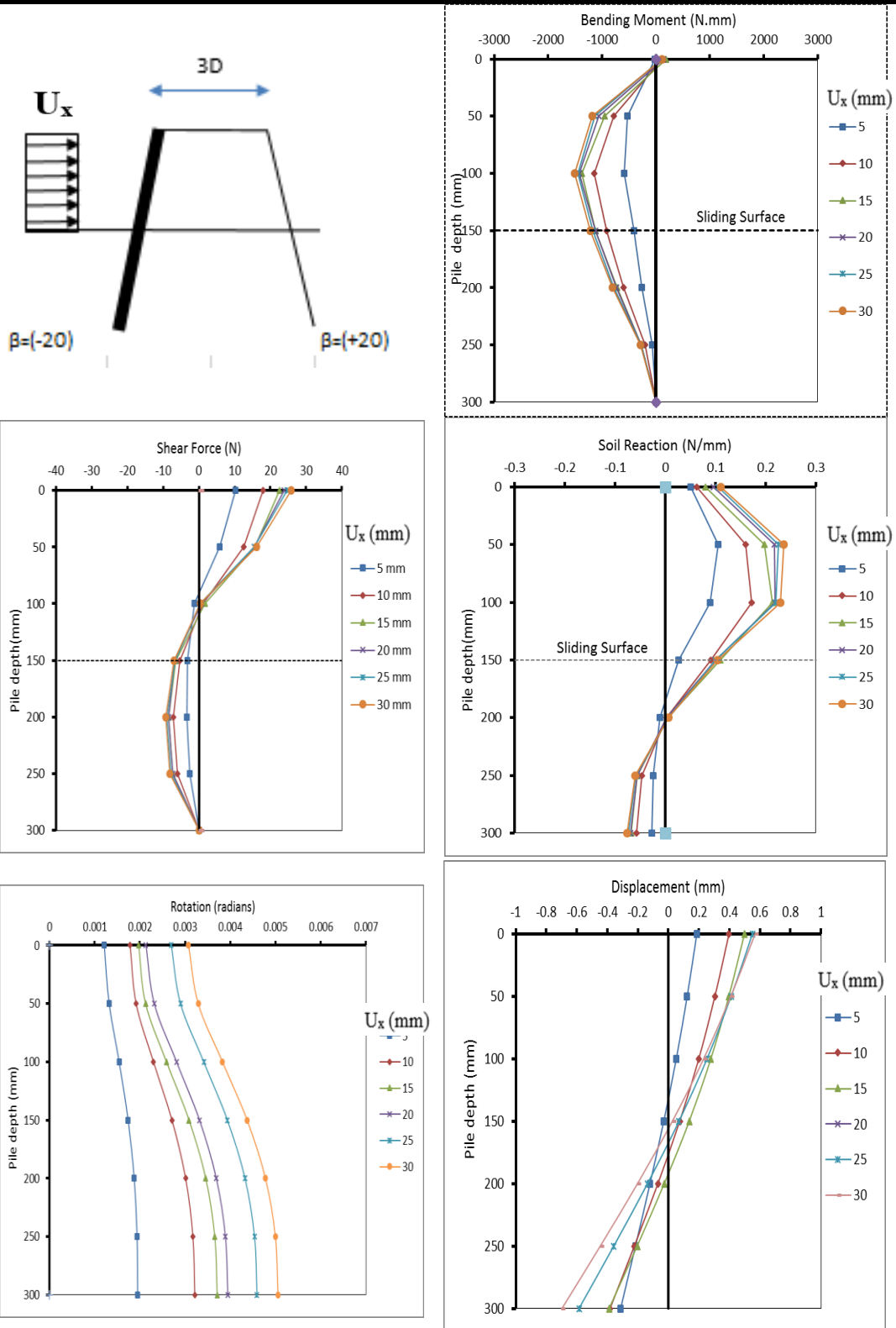


Fig. B.5a Response of front pile, test (BBL), $\beta = -20^\circ, +20^\circ$

Test Number	BBL	Density kN/m ³	15.2	Batter angle (β) (degree)	± 20
Pile-Head condition)	Capped	Soil Moving Profile	rectangular		
Moving layer, Lm (mm)	150	Stable layer, Ls (mm)	150	Diameter (mm)	16

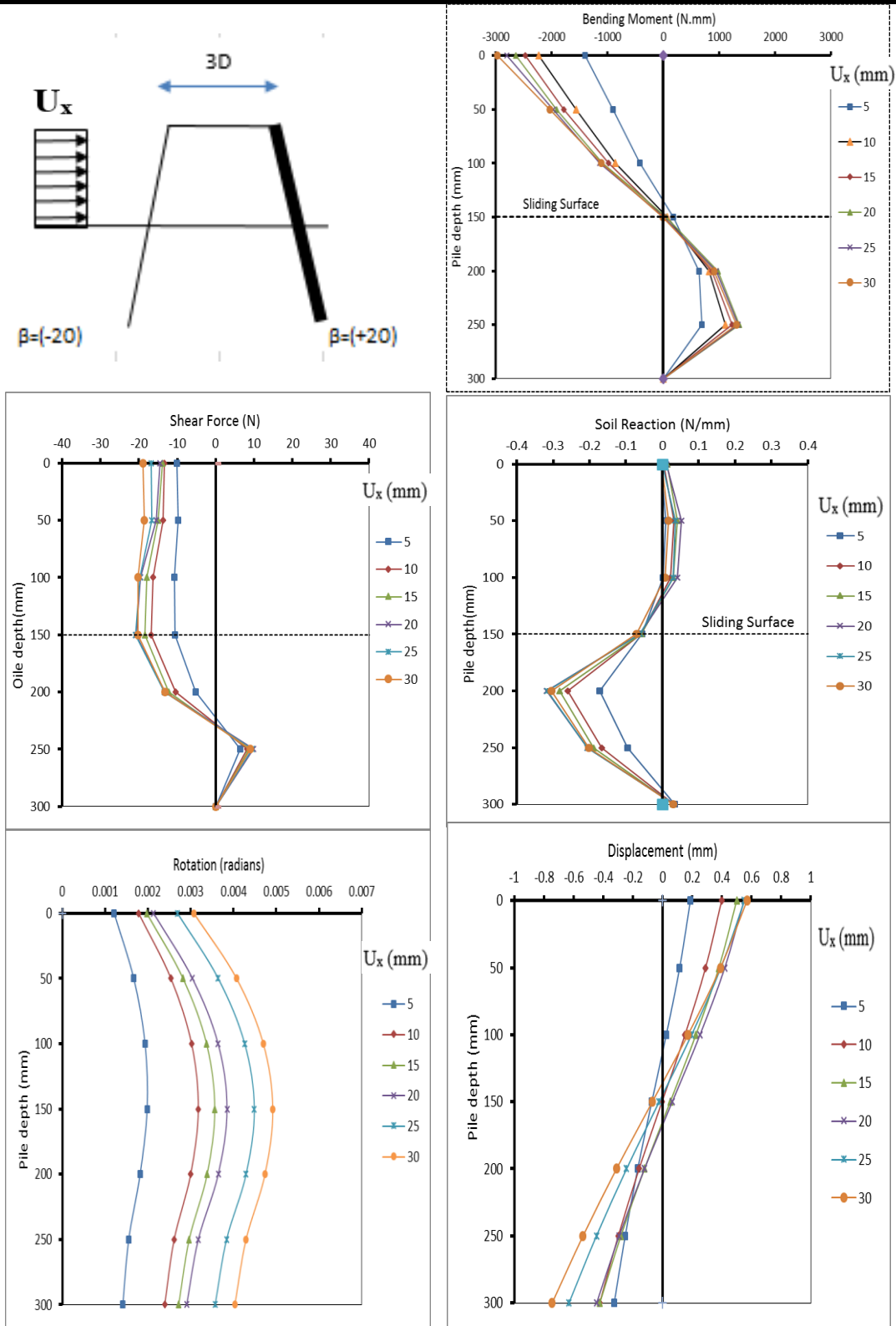


Fig. B.5b Response of back pile, test (BBL), $\beta = -20^\circ, +20^\circ$

Test Number	BVL	Density kN/m ³	15.2	Batter angle (β) (degree)	-10
Pile-Head condition)	Capped	Soil Moving Profile	rectangular		
Moving layer, Lm (mm)	150	Stable layer, Ls (mm)	150	Diameter (mm)	16

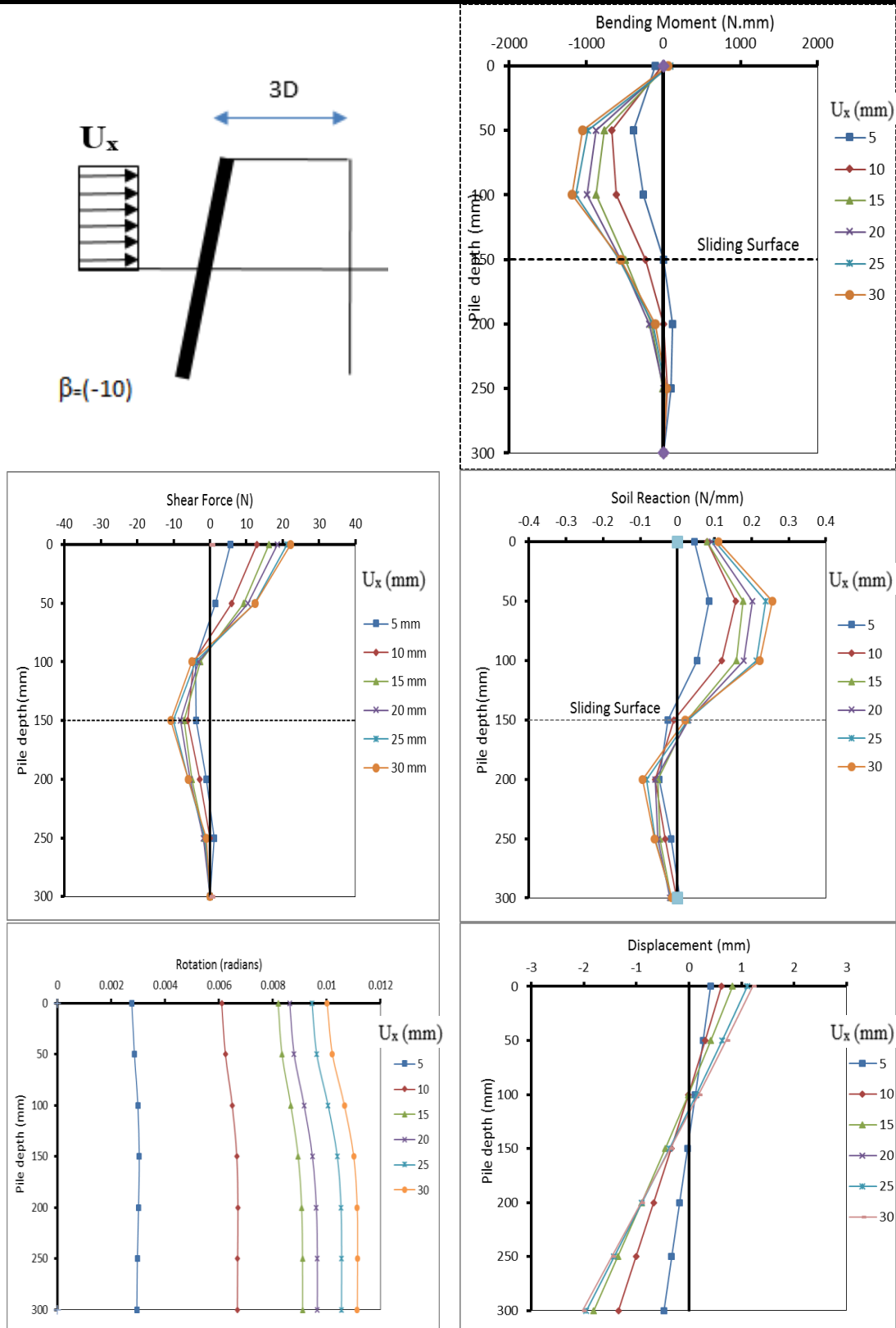


Fig. B.6a Response of front pile, test (BVL), $\beta = -10^\circ$

Test Number	BVL	Density kN/m ³	15.2	Batter angle (β) (degree)	-10
Pile-Head condition)	Capped	Soil Moving Profile	rectangular		
Moving layer, Lm (mm)	150	Stable layer, Ls (mm)	150	Diameter (mm)	16

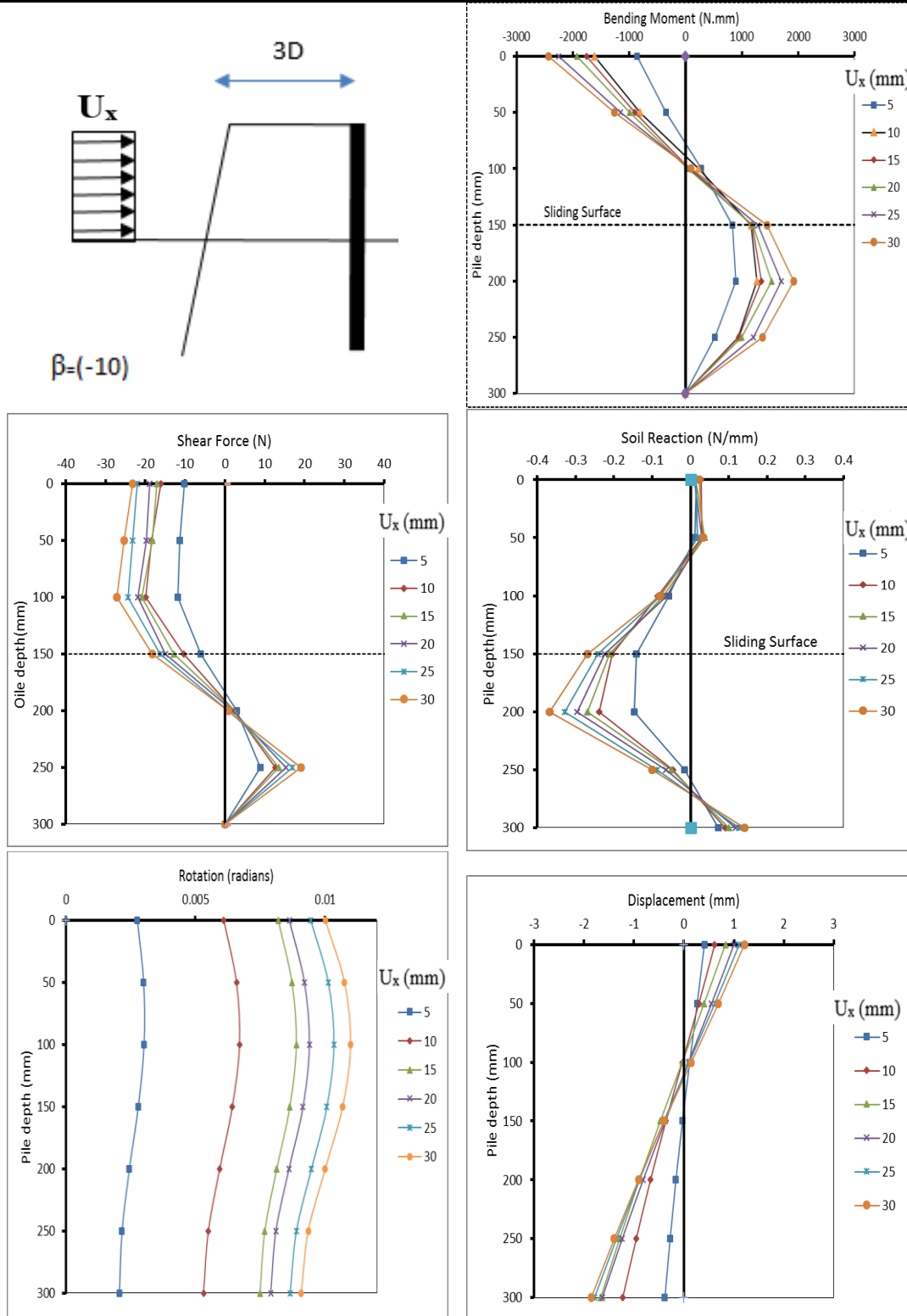


Fig. B.6b Response of back pile, test (BVL), $\beta = -10^\circ$

Test Number	BVL	Density kN/m ³	15.2	Batter angle (β) (degree)	-20
Pile-Head condition)	Capped	Soil Moving Profile	rectangular		
Moving layer, Lm (mm)	150	Stable layer, Ls (mm)	150	Diameter (mm)	16

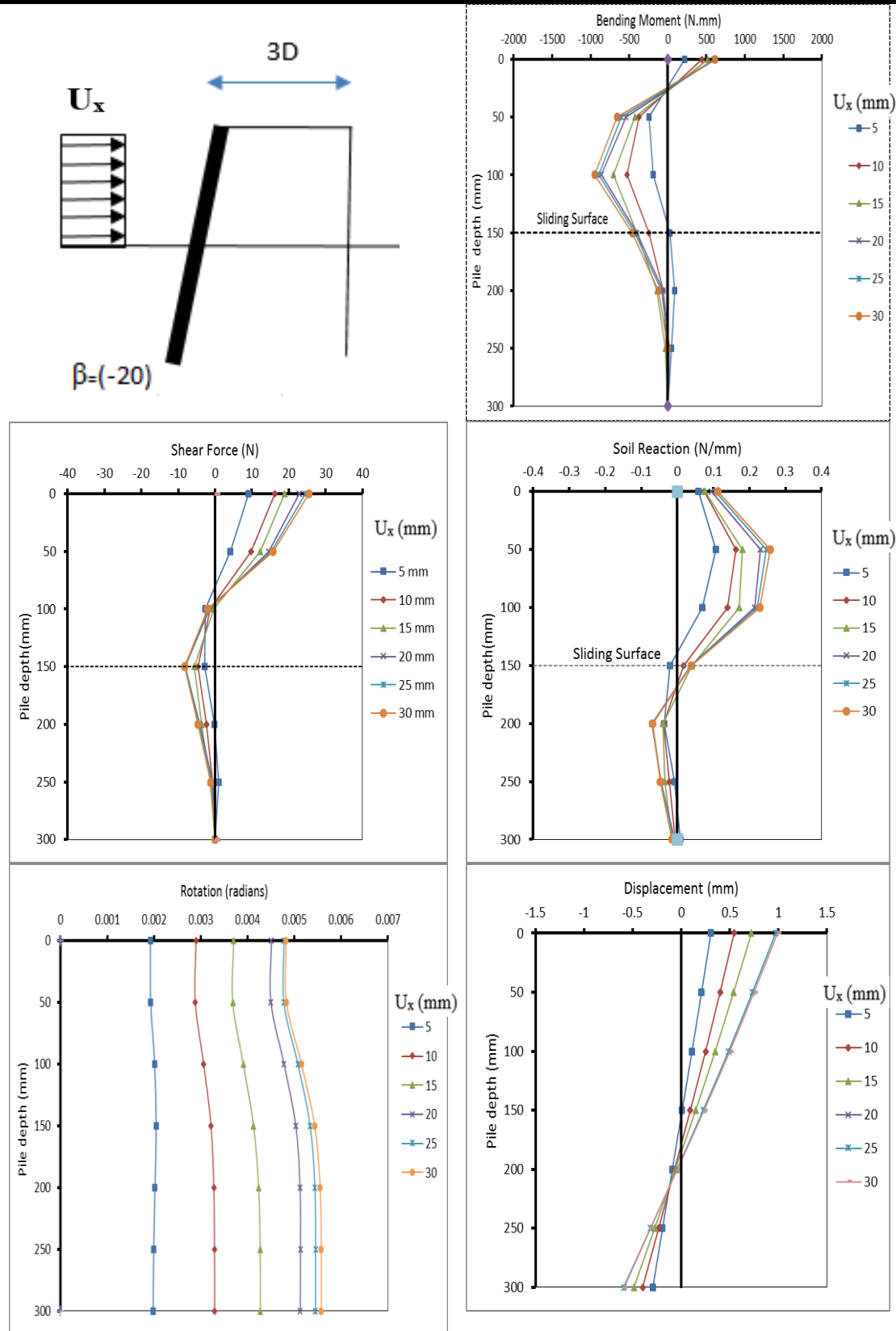


Fig. B.7a Response of front pile, test (BVL), $\beta = -20^\circ$

Test Number	BVL	Density kN/m ³	15.2	Batter angle (β) (degree)	-20
Pile-Head condition)	Capped	Soil Moving Profile	rectangular		
Moving layer, L _m (mm)	150	Stable layer, L _s (mm)	150	Diameter (mm)	16

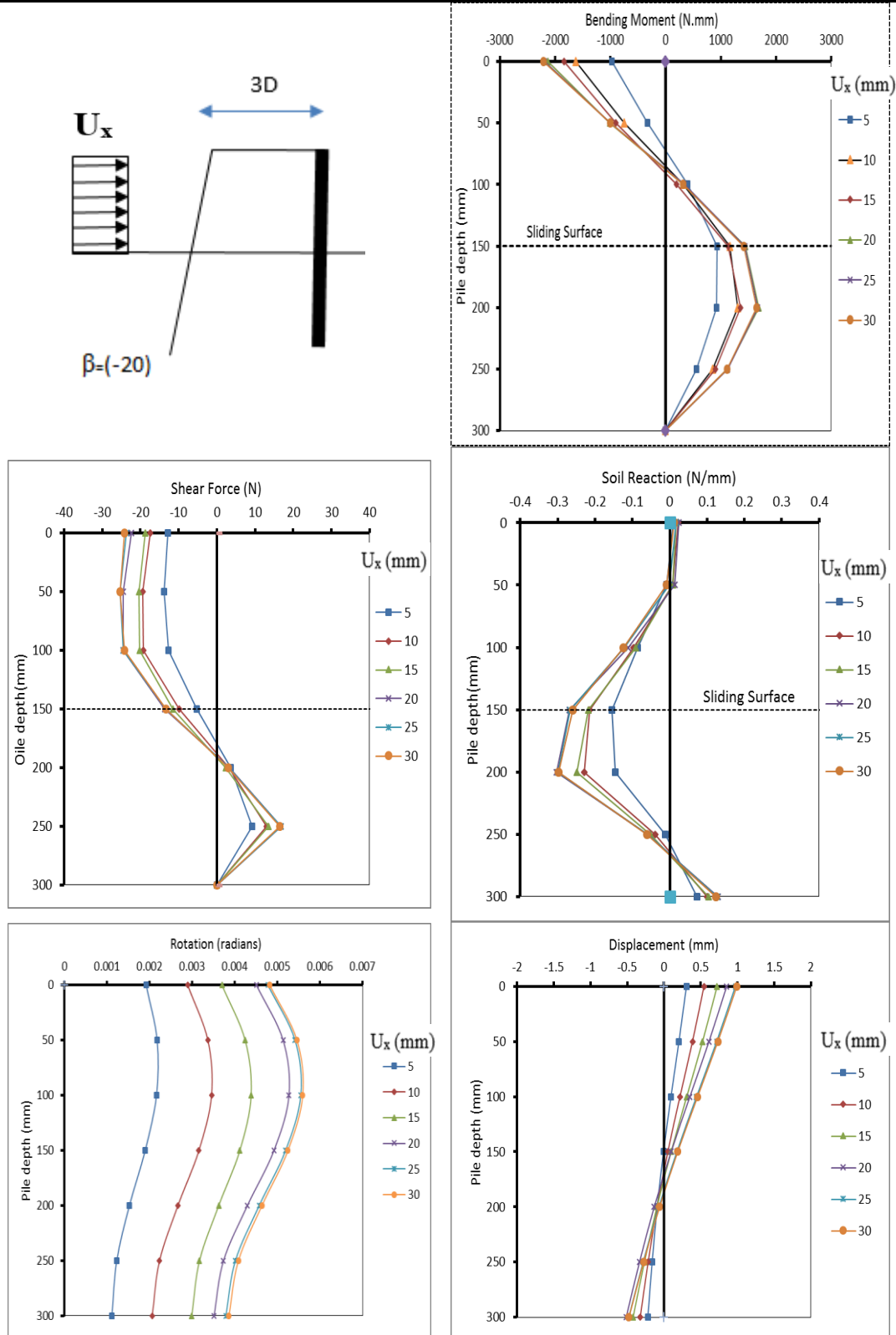


Fig. B.7b Response of back pile, test (BVL), $\beta = -20^\circ$

Test Number	BVL	Density kN/m ³	15.2	Batter angle (β) (degree)	-10
Pile-Head condition)	Capped	Soil Moving Profile	rectangular		
Moving layer, Lm (mm)	150	Stable layer, Ls (mm)	150	Diameter (mm)	16

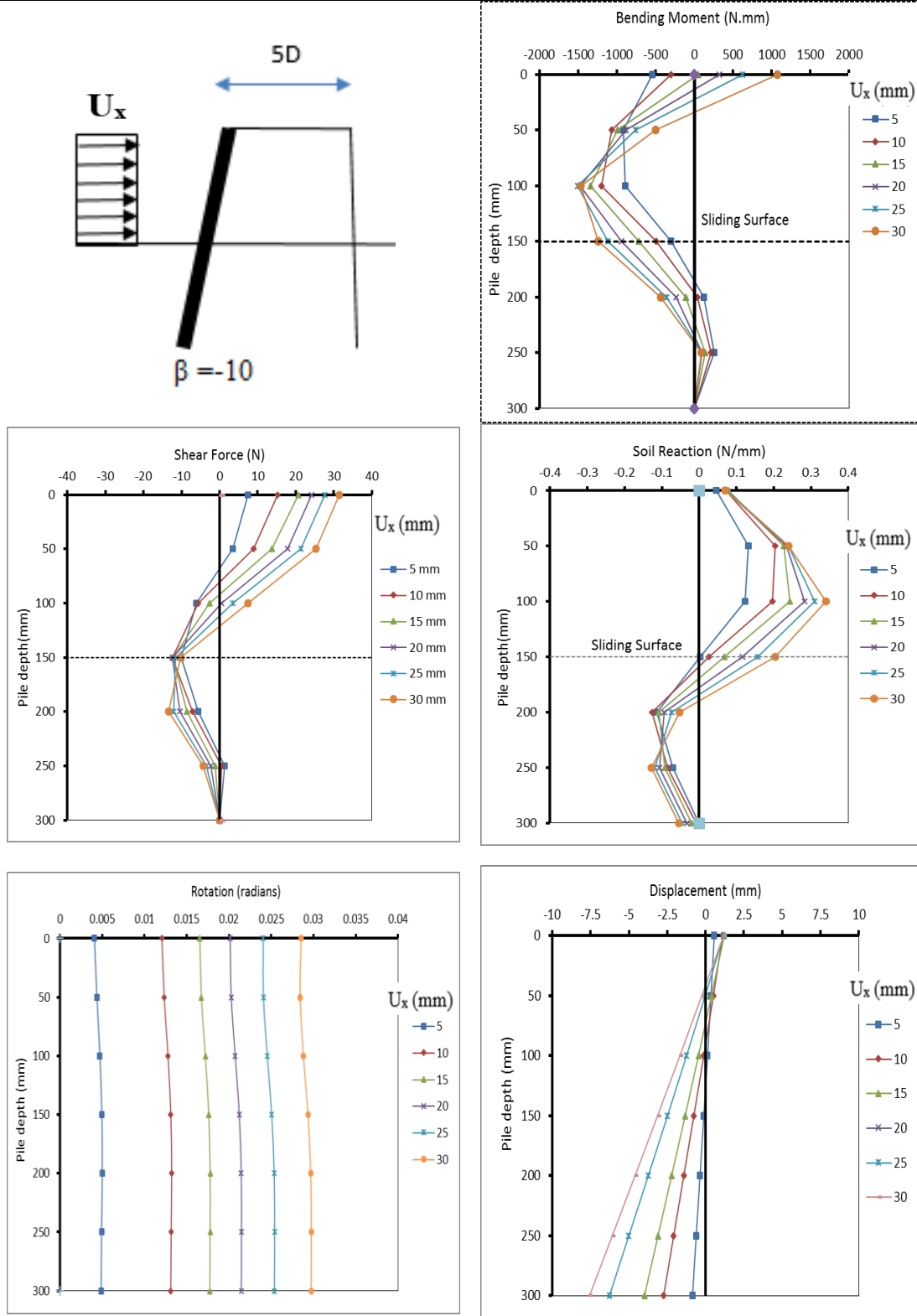


Fig. B.8a Response of front pile, test (BVL), $\beta = -10^\circ$

Test Number	BVL	Density kN/m ³	15.2	Batter angle (β) (degree)	-10
Pile-Head condition)	Capped	Soil Moving Profile	rectangular		
Moving layer, Lm (mm)	150	Stable layer, Ls (mm)	150	Diameter (mm)	16

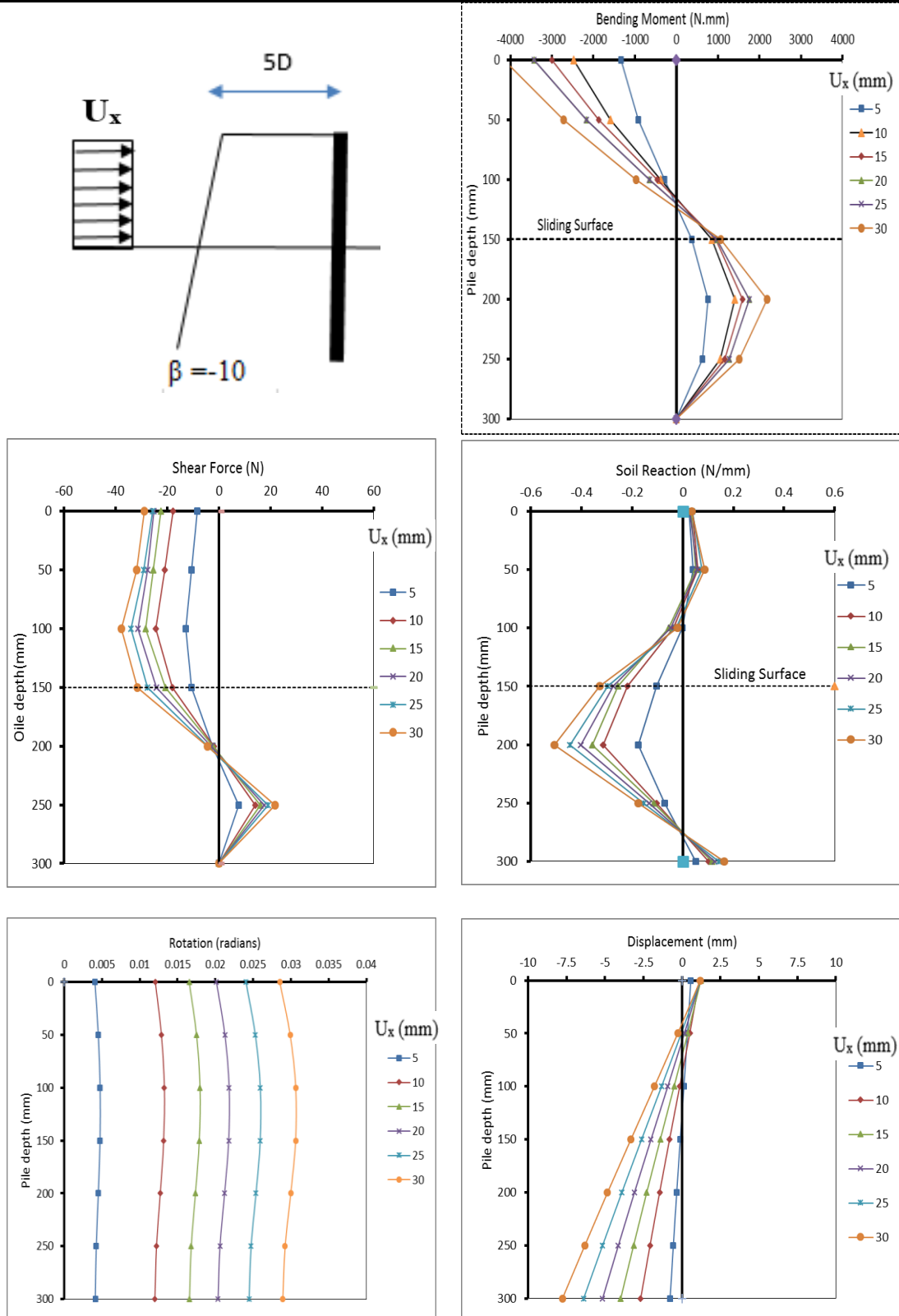


Fig. B.8b Response of back pile, test (BVL), $\beta = -10^\circ$

Test Number	BVL	Density kN/m^3	15.2	Batter angle (β) (degree)	-10
Pile-Head condition)	Capped	Soil Moving Profile	rectangular		
Moving layer, L_m (mm)	150	Stable layer, L_s (mm)	150	Diameter (mm)	16

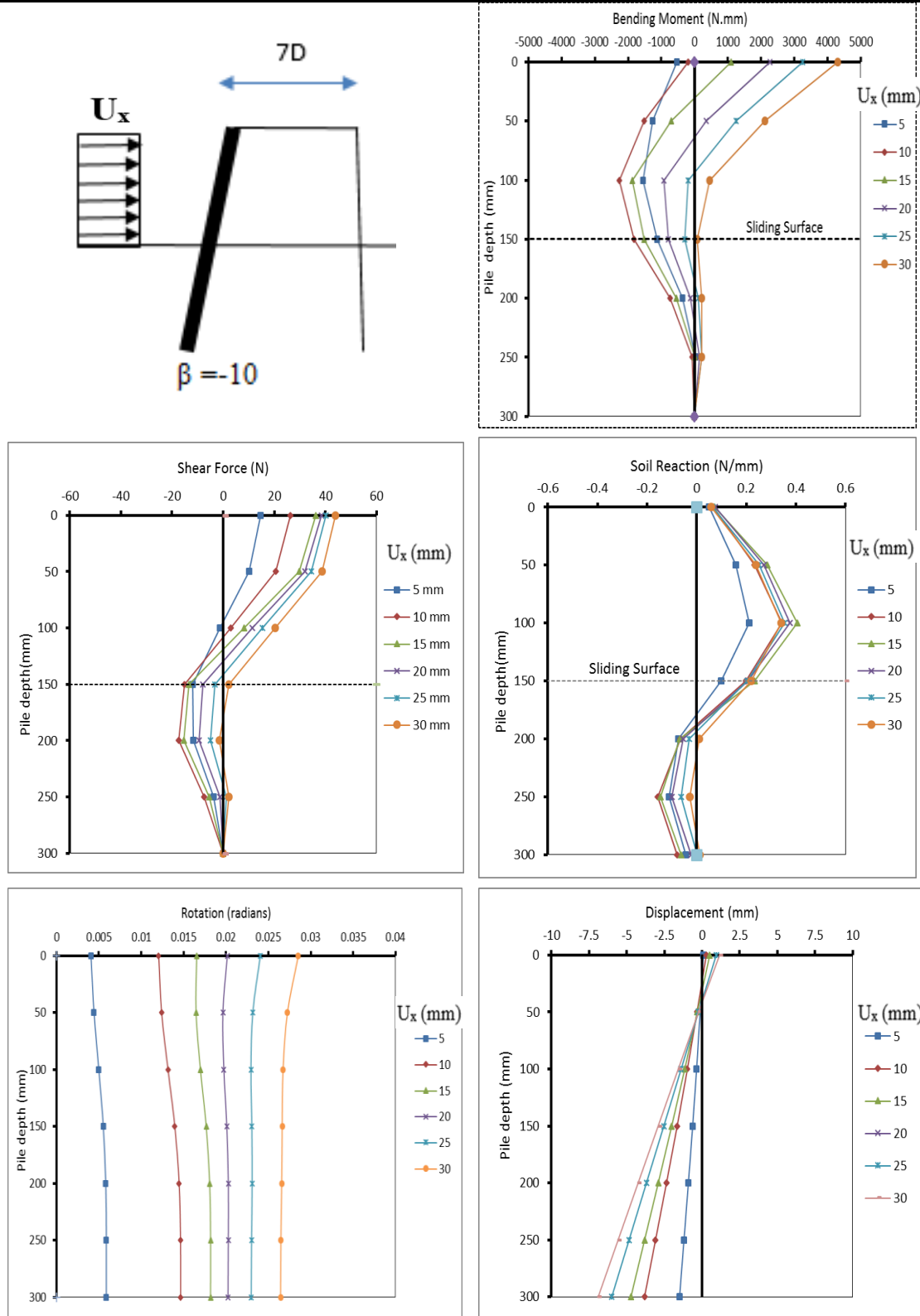


Fig. B.9a Response of front pile, test (BVL), $\beta = -10^\circ$

Test Number	BVL	Density kN/m ³	15.2	Batter angle (β) (degree)	-10
Pile-Head condition)	Capped	Soil Moving Profile	rectangular		
Moving layer, Lm (mm)	150	Stable layer, Ls (mm)	150	Diameter (mm)	16

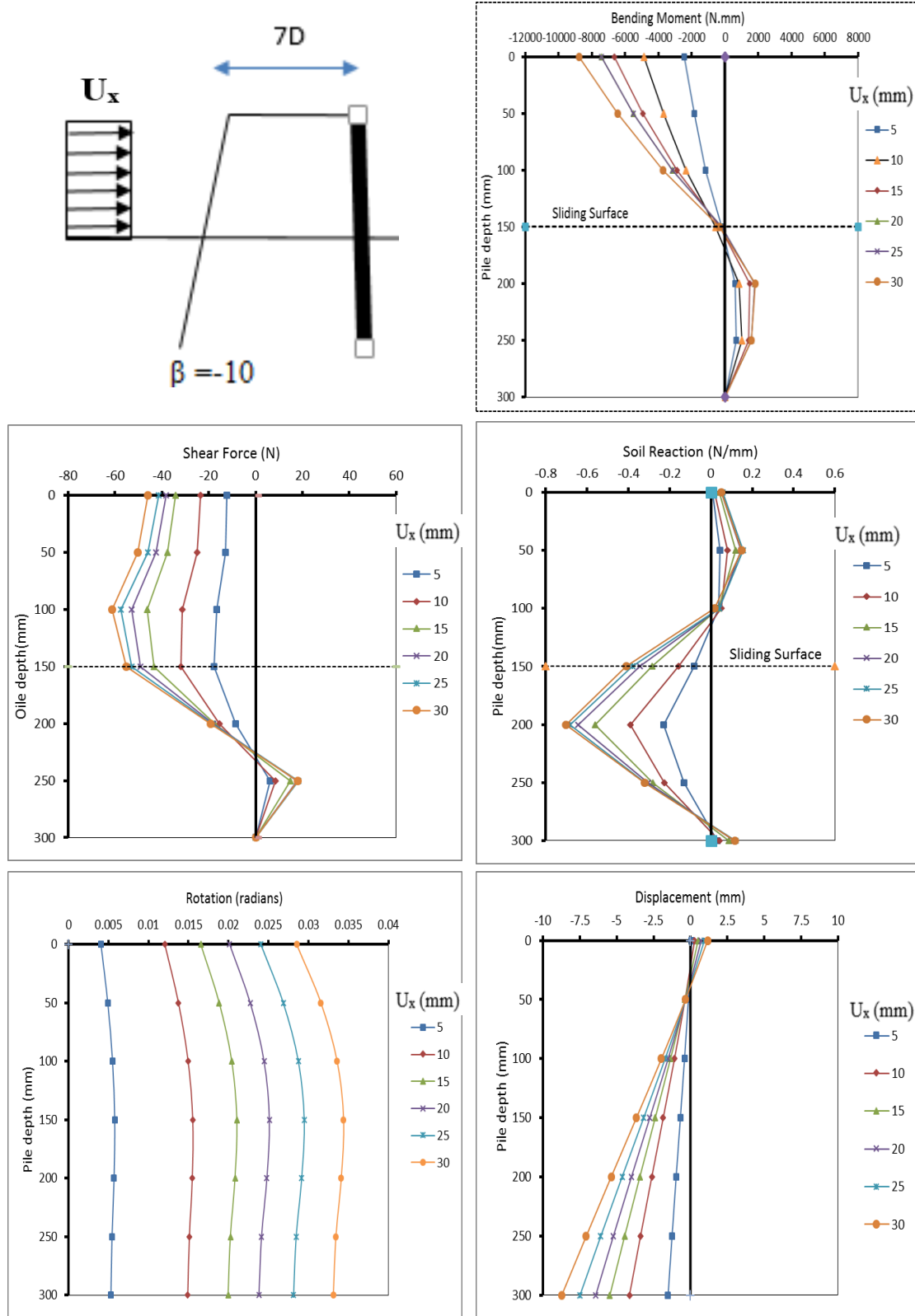


Fig. B.9b Response of back pile, test (BVL), $\beta = -10^\circ$

Test Number	BVF	Density kN/m ³	15.2	Batter angle (β) (degree)	-10
Pile-Head condition)	No cap	Soil Moving Profile	rectangular		
Moving layer, Lm (mm)	150	Stable layer, Ls (mm)	150	Diameter (mm)	16

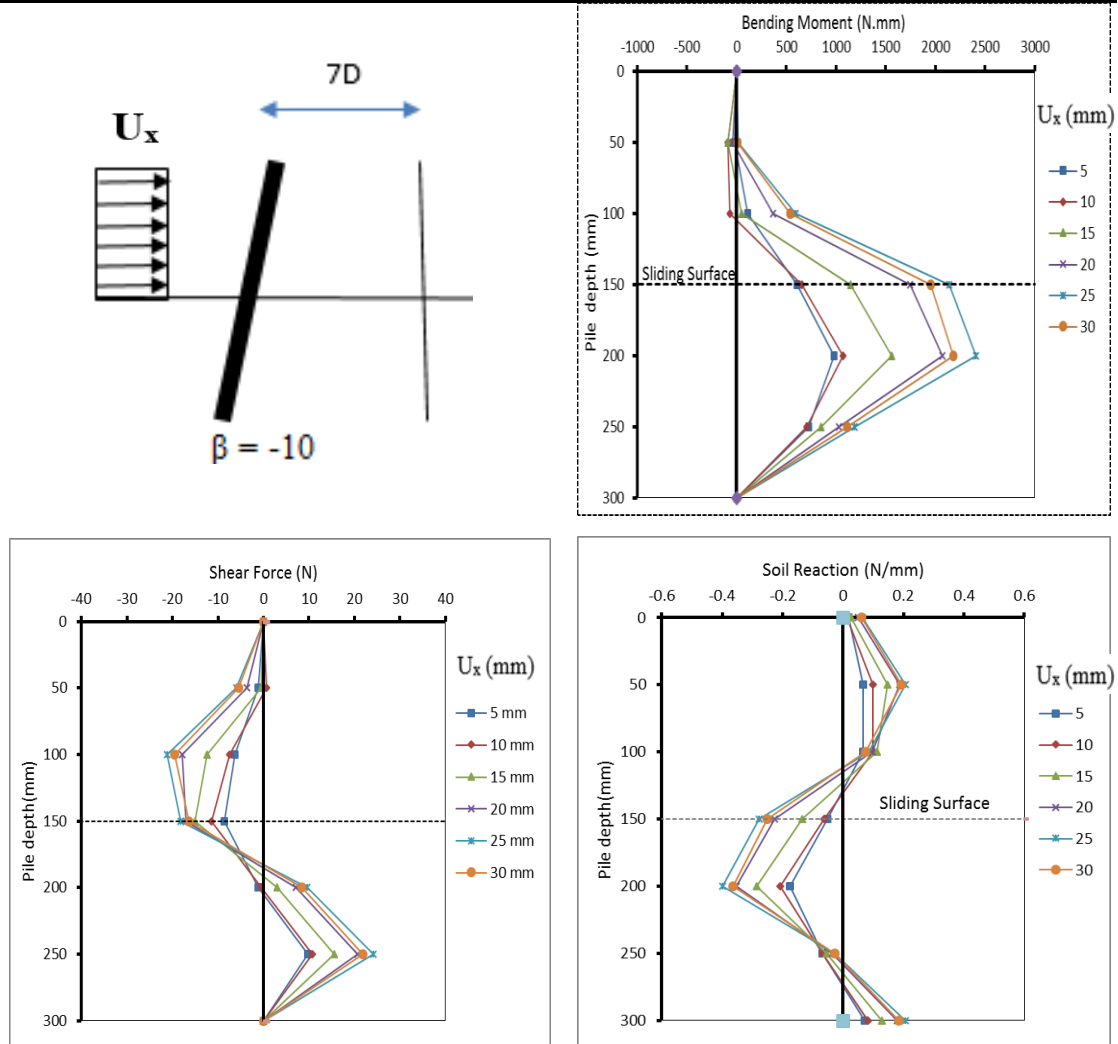


Fig. B.10a Response of front pile, test (BVF), $\beta = -10^\circ$

Test Number	BVF	Density kN/m ³	15.2	Batter angle (β) (degree)	-10
Pile-Head condition)	No cap	Soil Moving Profile	rectangular		
Moving layer, Lm (mm)	150	Stable layer, Ls (mm)	150	Diameter (mm)	16

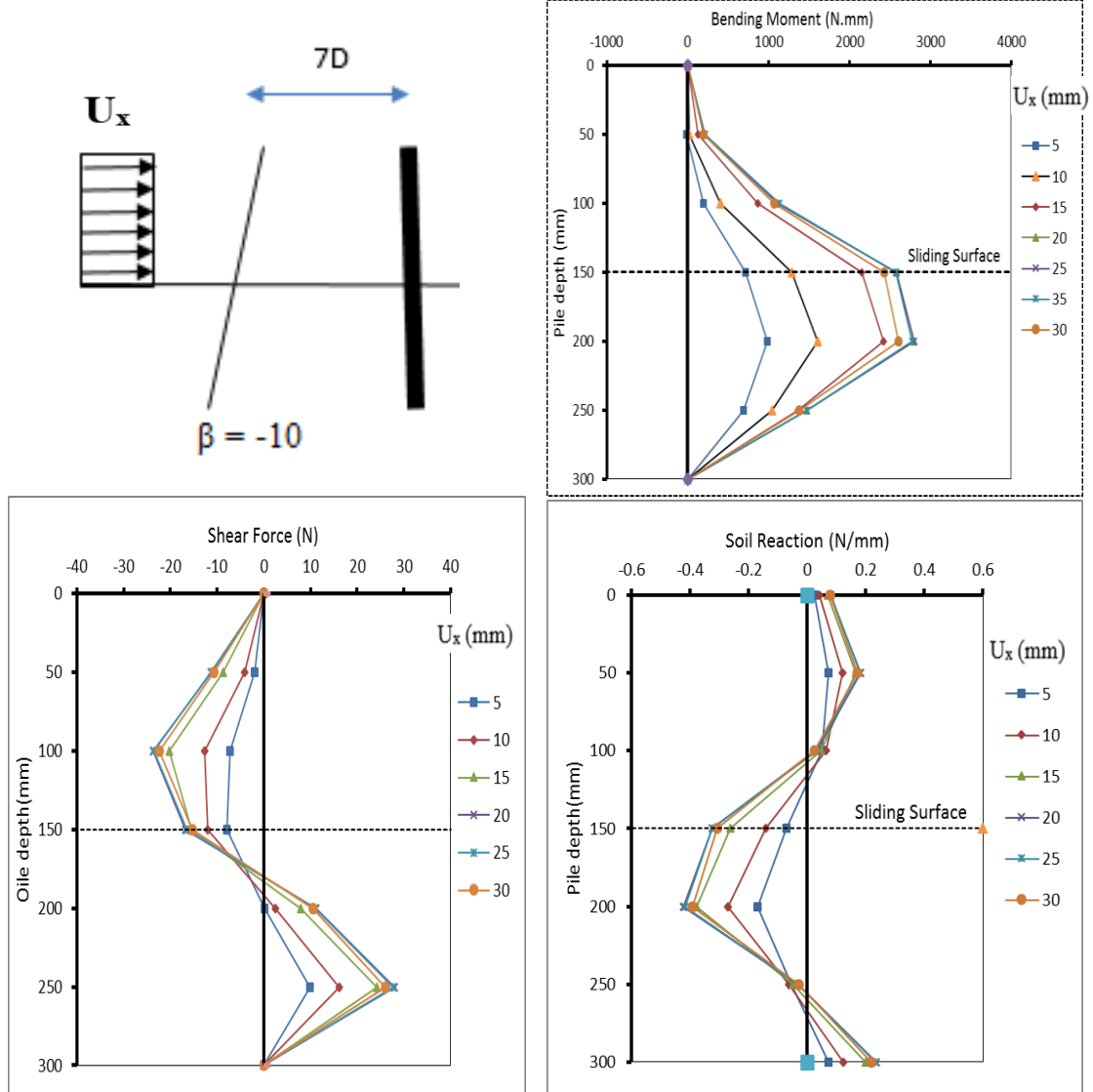


Fig. B.10b Response of back pile, test (BVF), $\beta = -10^\circ$